

**Characterizing the role of Inter Alpha Trypsin Inhibitor Heavy Chain 2
and Slit2/Robo1 in malignant brain tumor invasion**

By

Tamra Werbowetski

Department of Neurology and Neurosurgery

McGill University

July, 2005

A thesis submitted to McGill University in partial
fulfillment of the requirements
of the Degree of Doctor of Philosophy

©Tamra Werbowetski, 2005



Library and
Archives Canada

Bibliothèque et
Archives Canada

Published Heritage
Branch

Direction du
Patrimoine de l'édition

395 Wellington Street
Ottawa ON K1A 0N4
Canada

395, rue Wellington
Ottawa ON K1A 0N4
Canada

Your file *Votre référence*
ISBN: 978-0-494-25284-0
Our file *Notre référence*
ISBN: 978-0-494-25284-0

NOTICE:

The author has granted a non-exclusive license allowing Library and Archives Canada to reproduce, publish, archive, preserve, conserve, communicate to the public by telecommunication or on the Internet, loan, distribute and sell theses worldwide, for commercial or non-commercial purposes, in microform, paper, electronic and/or any other formats.

The author retains copyright ownership and moral rights in this thesis. Neither the thesis nor substantial extracts from it may be printed or otherwise reproduced without the author's permission.

AVIS:

L'auteur a accordé une licence non exclusive permettant à la Bibliothèque et Archives Canada de reproduire, publier, archiver, sauvegarder, conserver, transmettre au public par télécommunication ou par l'Internet, prêter, distribuer et vendre des thèses partout dans le monde, à des fins commerciales ou autres, sur support microforme, papier, électronique et/ou autres formats.

L'auteur conserve la propriété du droit d'auteur et des droits moraux qui protègent cette thèse. Ni la thèse ni des extraits substantiels de celle-ci ne doivent être imprimés ou autrement reproduits sans son autorisation.

In compliance with the Canadian Privacy Act some supporting forms may have been removed from this thesis.

Conformément à la loi canadienne sur la protection de la vie privée, quelques formulaires secondaires ont été enlevés de cette thèse.

While these forms may be included in the document page count, their removal does not represent any loss of content from the thesis.

Bien que ces formulaires aient inclus dans la pagination, il n'y aura aucun contenu manquant.


Canada

Abstract

Malignant brain tumors such as glioblastoma multiforme (GBM) and medulloblastoma are among the most devastating of cancers and their extensive infiltration into normal brain tissue leads to recurrence and poor patient prognosis. This thesis focuses on negative regulators of malignant brain tumor invasion in three-dimensional collagen gel matrices. We observed a chemorepellent effect in co-cultures of glioma spheroids where C6 and U251 glioblastoma cells are repelled by a secreted chemotropic molecule produced by the adjacent spheroid. In addition, the inhibitory effect of glioma conditioned medium on implanted C6 and U251 spheroids suggests that a chemorepellent effect may be accompanied by an inhibitory kinetic effect on individual cells. We used this model of conditioned medium inhibition as a functional assay to isolate and identify natural inhibitors of glioma invasion using protein purification. Mass spectrometry analysis revealed inter alpha trypsin inhibitor heavy chain 2 (ITI H2) as the most abundant protein in our purified fractions and validation studies confirmed its role as a strong inhibitor of glioma cell invasion and proliferation and a promoter of cell-cell adhesion. Lower levels of ITI H2 in high-grade primary human CNS tumors suggest that ITI H2 may play a role in brain tumor progression. In the final chapter, we demonstrated a role for the guidance cue, Slit2, in medulloblastoma invasion. Similar to ITI H2, Slit2 had an inhibitory effect on the velocity of individual cells; however, there was no concomitant effect on proliferation or adhesion. In contrast to ITI H2, Slit2 did not affect glioma cell invasion in three-dimensions, and RT PCR analysis did not reveal a correlation with malignancy. This study introduced sodium alginate bead “bioreactor” encapsulation as a method to exogenously supply Slit2 or other negative guidance cues.

Mixed beads containing cells overexpressing Slit2 and dominant negative RoboN demonstrated that this method can be used to attenuate the continuous inhibition of Slit2, and may potentially be utilized to introduce molecules targeting multiple biological processes including invasion, proliferation, and apoptosis. Therefore, Slit2 and ITI H2 may play potential therapeutic roles in the treatment of malignant brain tumor invasion, and require further functional characterization.

Résumé

Les tumeurs cérébrales malignes, tels les glioblastomes multiformes (GBM) et les médulloblastomes, sont parmi les cancers les plus dévastateurs et leur infiltration importante dans le tissu cérébral sain cause leur récurrence et un mauvais pronostic pour le patient. Cette thèse se concentre sur les signaux antagonistes à la migration des cellules de tumeur cérébrales dans une matrice de collagène en trois dimensions. Nous avons observé un effet chimiorépulsif dans des co-cultures de sphéroïdes, où les cellules de glioblastomes C6 et U251 sont repoussées par une molécule chimiotropique sécrétée par la sphère adjacente. De plus, l'effet inhibiteur du milieu de culture conditionné par des cellules de gliome sur les sphère de C6 ou de U251 implantées dans le collagène suggère que cet effet chimiorépulsif peut être accompagné d'un effet inhibant la cinétique des cellules individuelles. Nous avons utilisé ce modèle d'inhibition par le milieu de culture conditionné comme essai fonctionnel pour isoler et identifier la ou les molécule(s) impliquée(s), par des techniques successives de purification de protéines. Une analyse de spectroscopie de masse a révélé que la protéine la plus abondante dans la fraction inhibitrice purifiée était inter alpha trypsin inhibitor heavy chain 2 (ITI H2), et des études subséquentes ont confirmé l'effet inhibiteur de cette protéine sur l'invasion et la prolifération des cellules, ainsi qu'un effet renforçant l'adhésion entre les cellules. De plus, les niveaux plus faibles d'expression de ITI H2 dans les gliomes de haut grade suggèrent que ITI H2 peut être impliqué dans la progression de ces tumeurs. Dans le dernier chapitre, nous démontrons le rôle joué par le signal inducteur Slit2 dans l'invasion des médulloblastomes. Comme ITI H2, Slit2 démontre un effet inhibiteur sur la vitesse d'invasion des cellules individuelles; par contre, nous n'avons observé aucun

effet sur la prolifération ou l'adhésion de ces cellules. Contrairement à ITI H2, Slit2 n'influence pas l'invasion des cellules de gliome dans la matrice de collagène, et des analyses par RT-PCR n'ont révélé aucune corrélation d'expression avec le grade du gliome. Lors de cette étude, nous avons utilisé une méthode d'encapsulation de cellules dans des perles d'alginate de sodium pour former des 'bioréacteurs' sécrétant Slit2 ou d'autres facteurs chimiorépulsifs. Des perles contenant un mélange de cellules sécrétant Slit2 et un dominant-négatif RoboN ont pu démontrer que cette méthode peut aussi servir à atténuer l'inhibition continue par Slit2, et pourrait potentiellement être utilisée pour introduire près de la tumeur différents facteurs actifs dans des événements tels que l'invasion, la prolifération et l'apoptose des cellules tumorales. Ainsi, Slit2 et ITI H2 représentent des cibles thérapeutiques potentielles dans le traitement de l'invasion des gliomes malins, tout en nécessitant des études plus approfondies.

Acknowledgements

First of all, I would like to thank my parents Sandra and Bill Werbowetski, my husband to-be, Darren Ogilvie, and my sister Megan Werbowetski for providing me with the strength and courage to persevere and finish my PhD during the good times and the bad. Starting a new life without family in Montreal was extremely difficult, and I would like to thank-you for always being there for me. Without you and the family pets, Arnold, Philly, and Gizmo, I would not be here today.

I would like to thank my friends and colleagues Roberta, Nathalie, Monica, Alexandre, Carmen, Sarah, Mohamad, A.J, Carlos, Debbie and Kevin for providing both the emotional and scientific support needed to always move forward and never look back. It has been a pleasure working with everyone in the lab and I wish you nothing but the best in all future endeavors. I am also very grateful to Pamela Del Maestro for providing me food and shelter during the last few months and always being a pillar of strength.

I would like to thank the Natural Sciences and Engineering Research Council of Canada (NSERC) and the Canadian Institutes of Health Research (CIHR) for providing the funding during my studies, and the members of my committee, Dr. David Kaplan and Dr. Jack Antel, for always providing valuable advice and encouragement.

Finally, I would like to express my gratitude to my supervisor Dr. Rolando Del Maestro, who has always trusted my vision over the years, and has been a shining

example of “why we do what we do”. Thank-you for all your support and encouragement.

Table of contents

Title page	1
Abstract	2
Résumé	4
Acknowledgements	6
Table of contents	8
Lists of figures	11
Preface	15
Introduction: Rational and Objectives	17
Chapter 1: The Problem of malignant brain tumors: from the etiology to molecular mechanisms of malignant brain tumor growth and invasion	20
1.1 Etiology of malignant brain tumors: genetic mutations and amplifications in GBM and medulloblastoma	21
1.2 The invasive cascade	27
1.3 Models of brain tumor cell motility: from Boyden chambers to animal models	38
1.4 Positive and negative regulators of brain tumor invasion: old favorites and new perspectives	47
1.5 Conclusions	59

Chapter 2: Evidence for a secreted chemorepellent that directs glioma cell invasion	73
2.1 Abstract	74
2.2 Introduction	75
2.3 Methods	78
2.4 Results	85
2.5 Discussion	93
2.6 Preface Chapter 3	120
Chapter 3: Isolation of an inhibitor of human malignant glial cell invasion and proliferation: inter alpha trypsin inhibitor heavy chain 2	122
3.1 Abstract	123
3.2 Introduction	124
3.3 Methods	126
3.4 Results	133
3.5 Discussion	140
3.6 Conclusions to Chapter 3 and Preface Chapter 4	163
Chapter 4: Inhibition of medulloblastoma cell invasion by Slit	168
4.1 Abstract	169
4.2 Introduction	170
4.3 Methods	172
4.4 Results	182
4.5 Discussion	191
4.6 Conclusions to Chapter 4	218

4.7 Conclusions and Future Perspectives	222
References	226
Appendix	258

Lists of Figures and Tables

Chapter 1

Table 1.1: A summary of the characteristics of GBM and medulloblastoma. ...	60
Figure 1.1: Genetic aberrations and histological characterization associated with malignant glioma progression.	61
Figure 1.2: The Sonic Hedgehog signaling cascade.	63
Figure 1.3: The Wnt signaling pathway.	65
Figure 1.4: Hematoxylin and Eosin staining of C6 astrocytoma spheroids implanted into three-dimensional type I collagen gels over 22 days.	67
Figure 1.5: Schematic depicting the structure of prototypical Slit and Robo proteins.	69
Figure 1.6: The Ras and Akt/PKB signaling pathways.	71

Chapter 2

Figure 2.1: Single C6 astrocytoma spheroid implanted into three-dimensional type I collagen gel.	102
Figure 2.2: Quantification of glioma cell invasion after 24 hr in culture by counting the number of cells invading certain invasion distances from the initial edge of the spheroid in each quadrant.	104
Figure 2.3: Quantification of glioma cell number after 24 in culture. The number of cells in each quadrant was counted for single spheroids and two-spheroid cultures at various implantation distances.	106

Figure 2.4: Quantification of glioma cell number and invasion distance after 48 hr in culture.	108
Figure 2.5: Two C6 spheroids and spheroid-bead cultures in a type I collagen gel.	110
Figure 2.6: Co-cultures of a C6 astrocytoma spheroid with an aggregate of astrocytes derived from newborn rat brain.	112
Figure 2.7: Confocal scanning laser microscopy images of C6 astrocytoma, C6- astrocyte and human biopsy spheroid co-cultures fluorescently labeled with Cell Trackers™ after 24 -72 hours.	114
Figure 2.8: The effect of C6, U251 and fetal astrocyte conditioned medium on the invasion of C6 and U251 glioma spheroids.	116
Table 2.1: Transwell chamber analysis of C6 and U251 cell migration in response to medium conditioned by C6 astrocytoma spinner culture spheroids.	118

Chapter 3

Figure 3.1: Purified fractions from Resource Q and HiTrap Heparin HP columns contain enriched proteins involved in invasion.	145
Figure 3.2: Western Blot analysis confirms presence of ITI H2 in inhibitory fractions and ITI H2 localizes to perinuclear regions, membrane ruffles and lamellipodia in U251 cells overexpressing ITI H2.	147
Figure 3.3: Overexpression of ITI H2 inhibits U251 cell invasion in type I collagen gels.	149
Figure 3.4: Overexpression of ITI H2 in U251 cells inhibits proliferation without	

causing cell death.	151
Figure 3.5: Cell attachment assay for pLPCX and ITI H2 cells in monolayer culture.	153
Figure 3.6: Time-lapse videomicroscopy confirms ITI H2 as an inhibitor of individual cell velocity and promoter of cell-cell adhesion.	155
Figure 3.7: Expression of ITI H2 is downregulated in high-grade brain tumors.	157
Table 3.1: Mass spectrometry results of proteins present in pooled purified fractions from HiTrap Heparin HP column.	159
Table 3.2: Primers used for all RT PCR reactions.	161
Figure 3.8: Schematic depicting the transesterification reaction that releases covalently bound bikunin and couples ITI heavy chains to hyaluronic acid results in extracellular matrix stabilization.	166
 Chapter 4	
Figure 4.1: Quantification of the effect of Slit on invading medulloblastoma and glioma cells.	199
Figure 4.2: Quantification of time-delayed co-culture and conditioned medium assays.	201
Figure 4.3: Time-lapse videomicroscopy analysis of individual cells in UW3-HEK and UW3-Slit2 co-cultures.	203
Figure 4.4: Expression of Robo1 and Slit2 in brain tumor cell lines, human fetal astrocytes, mouse cerebellum, primary human tumors, and normal brain.	205

Figure 4.5: Sodium alginate bead microencapsulation and the effect of Slit2. ..	207
Figure 4.6: The effect of RoboN and R5 on Slit2 inhibition of UW3 medulloblastoma spheroids.	209
Figure 4.7: Confocal microscope images of UW3 spheroids confronted with human fetal astrocyte aggregates in the presence of HEK sodium alginate beads or Slit2 sodium alginate Beads after 5 days.	211
Figure 4.8: Cell surface biotinylation of U251 cell lines.	213
Figure 4.9: Slit2 decreases activated Cdc42 and Rac1 in medulloblastoma cells.	215
Table 4.1: Primer details for all RT PCR reactions.	217

Preface

The work in this thesis is entirely my own, except for Figure 3.2 panel c which was obtained with the assistance of Dr. Nathalie Agar, and Figure 4.8 and 4.9 which were obtained with the assistance of Mohamad Seyed Sadr. Contributions were made as part of manuscripts under submission.

The third Chapter has been accepted for publication in *Cancer Research*, and Dr. Nathalie Agar is a co-first author on this paper. She was responsible for the initial training on the AKTA FPLC and assistance in the design of the purification strategy, as well as production of Figure 3.2 panel c, and contribution to the written manuscript. Dr. Jack Antel provided the human fetal astrocytes used in this study, and Dr. Nada Jabado and Damien Faury provided some of the RNA samples from primary human brain tumors. Roberta Waldkircher de Oliveira conducted RNA extraction on other primary human brain tumor samples.

The fourth Chapter has been submitted for publication in *Oncogene*, and Mohamad Seyed Sadr is a second author on this paper. He was responsible for the biotinylation studies and the initial work on RhoGTPase involvement in Slit-mediated inhibitory effects on medulloblastoma invasion. Dr. Jack Antel provided the human fetal astrocytes used in this study, and Dr. Nada Jabado and Damien Faury provided some of the RNA samples from primary human brain tumors. Dr. Alexandre Angers-Loustau and Dr. Nathalie Agar provided extensive technical assistance and manuscript advice. Dr.

Jane Wu and Dr. Rolf Bjerkvig provided important reagents for the project, and Dr. Yi Rao was involved in initiating the project.

Introduction: Rationale and Objectives

Malignant brain tumors

Glioblastoma multiforme (GBM) is the most common primary central nervous system tumor in adults and is thought to arise from astrocytes or astrocytic precursors (Chicoine and Silbergeld, 1997; Lopez et al., 1995). Categorized as World Health Organization (WHO) grade IV, GBMs are characterized by endothelial cell proliferation, nuclear pleomorphism, extensive necrosis and a high mitotic index (Kleihues et al., 2000). GBMs can be divided into two subtypes: secondary or progressive, which arises from lower-grade tumors, and primary or *de novo*, which is the major glial malignancy more common in older patients (Wechsler-Reya and Scott, 2001). Current therapeutic strategies include surgery, radiation and chemotherapy; however GBMs rapidly infiltrate the normal brain architecture making complete resection virtually impossible (Kleihues et al., 2000). Consequently, tumors typically recur, and prognosis is poor with a mean survival of approximately 18 months.

Medulloblastoma is the most common malignant brain tumor in children and is believed to originate from granular precursor cells of the cerebellum (Wechsler-Reya and Scott, 2001; Raffel, 2004). Common treatment strategies for this neuronal tumor include surgery followed by radiation and/or chemotherapy. These approaches are often successful at decreasing the size of the primary tumor; however, recurrence and metastasis occur, and consequently, only 60-70% of patients survive 5 years after diagnosis (Wechsler-Reya and Scott, 2001; Louis et al., 2002).

The highly infiltrative nature of malignant central nervous system tumors makes the invasive cascade an important therapeutic target. Both GBM and medulloblastoma share the ability to infiltrate the normal brain tissue; however, other motility properties distinguish the two. GBMs primarily invade along white matter tracts and blood vessels, but rarely metastasize outside the CNS (Kleihues et al., 2000). In contrast, medulloblastoma cells can detach from the major tumor mass and spread within the cerebral spinal fluid (CSF). This results in tumor growth along the cranial and spinal nerves and leptomeningeal surfaces of the brain and spinal cord (Gianaspero et al., 2000). Characteristically, medulloblastoma cells can adhere to and spread over the surface of the brain and other CNS tissues as a monolayer; however this growth pattern is much less commonly seen in GBMs (Gianaspero et al., 2000). In addition, medulloblastomas can metastasize outside the nervous system in about 5-10% of patients (Paulino, 2003).

The different motility characteristics, cells of origin, population distributions and clinical outcomes that characterize GBM and medulloblastoma make these tumor subtypes attractive targets to study and further characterize the motile properties of different brain tumors (Table 1.1).

In vitro and *in vivo* models of malignant brain tumor cell motility including Boyden chambers, co-culture confrontation assays and xenograft mouse models have all been used to examine the molecular biology of brain tumor progression. There are many positive regulators of malignant brain tumor growth and motility; however, little is known about negative modulators of malignant brain tumor cell invasion (Chicoine and

Silbergeld, 1997; Mueller et al., 2003; Wechsler-Reya and Scott, 2001; Werbowetski et al., 2004).

The work presented here examines negative regulators of malignant brain tumor cell invasion and their effect on cell velocity, direction, proliferation, and adhesion. This thesis characterizes the role of two proteins: Inter alpha trypsin inhibitor heavy chain 2 and Slit2 in glioma and medulloblastoma cell invasion in three-dimensions. Chapter 1 outlines a breakdown of the biology of malignant brain tumors. The topics covered include the mutations and amplifications associated with brain tumor progression, the facets of the invasive cascade, the variety of models used to recapitulate malignant brain tumor growth and invasion, and the cellular and molecular targets, both positive and negative, responsible for the highly motile and proliferative phenotype of GBM and medulloblastoma.

Chapter 1: The problem of malignant brain tumors: from the
etiology to molecular mechanisms of malignant brain tumor
growth and invasion

1.1 Etiology of malignant brain tumors: genetic mutations and amplifications in GBM and Medulloblastoma

Malignant brain tumor progression is linked with a variety of genetic aberrations. Both GBM and medulloblastoma are associated with several mutations, many of which are closely linked with neurodevelopment (Wechsler-Reya and Scott, 2001; Behin et al., 2003; Ichimura et al., 2004; Pietsch et al., 2004). Over the past 20 years, the knowledge of the molecular pathogenesis of malignant brain tumors has provided evidence and justification for new therapeutic targets. However, we are still far from understanding the details of brain tumor molecular biology in a way that can be effectively translated in the clinic. It is imperative to combine molecular data with histological diagnosis to provide the best treatment strategy and accurate patient prognosis (Ichimura et al., 2004).

Genetic aberrations in GBM

The mutations associated with GBM are well characterized in the literature. Accompanying oncogenesis and malignant glioma progression from low-grade to high-grade astrocytoma is the accumulation of genetic aberrations that lead to mutations in growth factor-receptor complexes and tumor suppressor genes. Malignant astrocytomas evolving in this manner are termed secondary glioblastoma. Those developing *de novo* are called primary glioblastomas and account for a majority of high-grade gliomas (Wechsler-Reya and Scott, 2001; Behin et al., 2003). Differences in amplification and deletion mutations distinguish the two subtypes (Fig. 1.1).

One of the major genetic abnormalities detected in 40-50% of *de novo* glioblastomas is epidermal growth factor receptor (EGFR) amplification (Liebermann et al., 1985a, 1985b). The EGF receptor is also frequently rearranged, encoding a truncated form, lacking part of the extracellular domain (Ekstrand et al., 1992; Sugawa et al., 1990; Wong et al., 1992). Consequently, the receptor, called EGFRvIII, can no longer bind ligand but is constitutively activated thereby enhancing cell growth both *in vitro* and *in vivo* (Wechsler-Reya and Scott, 2001; Behin et al., 2003; Ichimura et al., 2004). Along with increased cell proliferation, studies have also demonstrated enhanced invasion of glioma spheroids into fetal rat brain aggregates using cell lines and primary gliomas that exhibited high EGFR expression levels or enhanced response to exogenously applied EGF (Lund-Johansen et al., 1990; Engebraaten et al., 1993). Weekly intravenous RNAi gene therapy directed against human EGFR has also been shown to suppress EGFR function and increase survival time in SCID mice implanted with U87 glioma cells (Zhang et al., 2004). Therefore, EGFR modulation is an important therapeutic goal to decrease glioblastoma cell proliferation and invasion.

Another mutation associated with 80-90% of both primary and secondary glioblastomas is frequent deletion of regions of chromosome 10q (Li et al., 1997; Li et al., 1997; Steck et al., 1997). The gene most identified with this region is phosphatase and tensin homology or mutated in multiple advanced cancer (PTEN/MMAC). PTEN is mutated in 20-30% of primary and secondary high grade astrocytomas such as glioblastoma and is typically associated with the Akt pathway (Wechsler-Reya and Scott, 2001). Catalyzing conversion of phosphatidylinositol (3,4,5)-triphosphate (PIP3) to

phosphatidylinositol (4,5)-bisphosphate (PIP₂), PTEN normally suppresses Akt activation, thereby promoting cell cycle arrest and apoptosis (Wechsler-Reya and Scott, 2001). Cells lacking PTEN are resistant to apoptosis and are more tumorigenic. The importance of Akt signaling is evident in mouse models combining Akt and Ras activation in neural progenitor cells to induce glioblastoma (Holland et al., 2000). Specific inhibitors of PI3K/Akt signaling such as LY294002 and Wortmannin, have also been used to pharmacologically decrease invasion and gelatinase activity of C6 cells *in vitro* (Kubiatowski et al., 2001).

Mutations more commonly associated with secondary glioblastoma include deletions in the TP53 and P16/CDKN2A genes and amplification of the platelet-derived growth factor (PDGF) ligand and receptor. Common aberrations in p53 pathway cell cycle dysregulation include inactivation of the TP53 gene itself and amplification of the chromosome 12 locus encoding the gene for the p53 degradation protein Mdm2 (Ichimura et al., 2004; Behin et al., 2003; Wechsler-Reya and Scott, 2001). Studies using transfected cells lines and adenoviruses to restore wild-type p53 expression have demonstrated suppressed cellular growth and tumorigenicity (Asai et al., 1994; Cirielli et al., 1999). Homozygous deletions of the P16/CDKN2A gene are also associated with glioma tumor progression and occur in up to 30-40% of glioblastoma (Wechsler-Reya et al., 2001; Behin et al., 2003). The protein ARF, which is generated by alternative splicing of the p16/CDKN2A transcript, is no longer able to inhibit Mdm2-mediated p53 degradation. Chintala et al. (1997) demonstrated reduced invasion and MMP2 activity

using SNB19 p16-overexpressing glioma cells in Matrigel and spheroid-rat brain confrontation co-culture assays.

High expression levels of platelet derived growth factor receptor (PDGFR) and the PDGF ligand are also associated with secondary glioblastoma suggesting the presence of autocrine/paracrine loops (Hermanson et al., 1992; Lokker et al., 2002). PDGFR signaling has been linked with all facets of glioblastoma biology including proliferation, survival and migration (Lund-Johansen et al., 1992; Guha et al., 1997). Intracranial injections of recombinant PDGFR retrovirus also induce glioblastoma in mice (Uhrbom et al., 1998).

Genetic aberrations in medulloblastoma

The etiology of medulloblastoma progression is closely linked with neurodevelopment and a variety of hereditary disorders. There are two major variants of medulloblastoma. The desmoplastic subtype is believed to be derived from external granular layer cells of the cerebellum; whereas, the cell of origin of the classic variant is still under discussion (Pietsch et al., 2004).

New insights into the developmental biology of medulloblastoma have come from studies of the Sonic-Hedgehog (Shh)-Patched (Ptc1) signaling pathway, which is known for its role in controlling proliferation of external granule cells of the cerebellum (Fig. 1.2) (Wechsler-Reya and Scott, 1999). Sonic Hedgehog is a secreted protein that binds to its receptor Patched 1. Binding inactivates the Patched receptor thereby relieving

inhibition of another transmembrane protein, Smoothed (Fig. 1.2). Smoothed transduces downstream signals that activate the Gli family of transcription factors leading to target gene induction and enhanced cell proliferation (Fig. 1.2). The first evidence of Shh signaling involvement in medulloblastoma came from studies of mutations in nevoid basal cell carcinoma (NBCCS) or Gorlin syndrome, a disorder characterized by developmental abnormalities and increased incidence of medulloblastoma (Taylor et al., 2000). Approximately 10-20% of medulloblastomas contain mutations at the PTCH locus, and these tumors are generally of the desmoplastic subtype (Pietsch et al., 1997; Raffel et al., 1997; Xie et al., 1997). Mouse heterozygote knockout models of PTCH1 develop tumors within 4-6 months and are morphologically similar to medulloblastoma (Goodrich et al., 1997; Wetmore et al., 2000). Investigations of other Shh signaling family members such as Smoothed, Patched 2 and Human Suppressor of Fused (SuFu) have revealed further mutations, and medulloblastoma elimination in *Ptc +/- p53-/-* mice using a small molecular inhibitor of Smoothed has further implicated the importance of this pathway to medulloblastoma progression (Reifenberger et al., 1998; Smyth et al., 1999; Romer et al., 2004).

Studies of medulloblastoma mRNA expression profiles have been able to distinguish the desmoplastic variant based on genetic signature to correctly classify 33 of 34 tumors (Pomeroy et al., 2002). Genes that were most highly correlated with desmoplastic histology include PTCH, GLI, and N-MYC, another downstream Shh target. The transcriptional profiling provided further evidence that like tumors associated

with Gorlin's syndrome, sporadic cases of desmoplastic medulloblastoma are also linked with Shh pathway activation (Pomeroy et al., 2002).

Just as studies of Gorlin's syndrome have implicated Shh signaling in medulloblastoma progression, so too have studies of another hereditary disorder, Turcot's syndrome, suggested a role for the Wnt signaling pathway in medulloblastoma pathogenesis (Fig. 1.3). Patients with Turcot's syndrome have mutations in the adenomatous polyposis coli (APC) gene leading to overactivity of the Wnt signaling cascade (Hamilton et al., 1995). This renders β -catenin resistant to degradation and increases transcription of genes associated with cell cycle progression such as c-myc and cyclin D1 (Fig. 1.3). Although these patients are typically at increased risk for medulloblastoma, somatic mutations of APC are rare in sporadic medulloblastoma and some suggest that they have no functional significance (Huang et al., 2000; Raffel, 2004). Other studies have shown that mutations in other components of the Wnt pathway such as β -catenin and Axin1/Axin2 are associated with sporadic medulloblastoma (Zurawel et al., 1998; Dahmen et al., 2001).

Loss or mutation of a portion of chromosome 17 is also a common genetic aberration associated with 30-50% of medulloblastomas and is usually linked with the classic variant (Bigner et al., 1997; Burnett et al., 1997; Cogen and McDonald, 1996). The most common mutation is the loss of chromosome 17p that is concomitant with the formation of isochromosome 17q (Bayani et al., 2000). However, the medulloblastoma

tumor suppressor gene(s) on chromosome 17 is distinct from p53 and has yet to be identified.

Finally, a gene associated with a favorable outcome is TRKC, a receptor for the neurotrophin NT-3 ligand (Pomeroy et al., 2002; Segal et al., 1994; Kim et al., 1999). Along with its role as a positive prognostic marker, TrkC also inhibits intracerebral medulloblastoma tumor growth in nude mice by the promotion of apoptosis (Kim et al., 1999).

1.2 The invasive cascade

Genetic abnormalities are linked with brain tumor progression; however, the infiltration and destruction of normal brain tissue architecture presents a major obstacle for effective treatment of CNS malignancies such as GBM and medulloblastoma. Although the terms migration and invasion are often used interchangeably, they are distinct concepts. Migration refers to active cell locomotion on a surface or through a three-dimensional matrix without modification of the matrix or normal brain. Examples include migration of neuronal and glial cell precursors during neurodevelopment, stem cell migration in a variety of tissues, lymphocyte migration, and migration of medulloblastoma cells as monolayers over the surface of the brain.

Invasion implies local remodeling and destruction of the matrix or normal tissue architecture followed by cell movement and is a property of many malignant brain tumors (Bolteus et al., 2001). Degraded collagen fragments surrounding individual C6

astrocytoma cells in a collagen type I matrix using scanning electron microscopy have provided evidence for this invasion paradigm (Del Maestro et al., 2001). Invasion of malignant brain tumors encompasses a variety of processes including: i) loss of cell-cell adhesion at the edge of the main tumor mass, ii) establishment of a polarized morphology to initiate cell movement, iii) extracellular matrix degradation and remodeling controlled by multiple proteases and their inhibitors, iv) regulation of cytoskeletal dynamics to provide the protrusive and contractile forces necessary to facilitate cell migration and v) detachment of the cell. Therefore, cell migration is a component of the invasive cascade.

The distinction between migration and invasion is based on the local destruction and remodeling of the ECM that occurs during the invasive cascade. Therefore, any description of medulloblastoma and glioblastoma motility in three-dimensional collagen matrices will be referred to as invasion in the forthcoming chapters. The motility of non-invasive cells such as neurons, leukocytes and stem cell precursors will be referred to as migration.

Loss of cell-cell adhesion

The first stage of the invasion process involves loss of cell-cell adhesion at the edge of the tumor mass in order to generate new interactions with the extracellular matrix (ECM) and host tissue. Cadherins are a family of calcium dependent cell adhesion molecules that facilitate homotypic cell-cell interactions. They can be classified as tumor suppressors and are associated with differentiation and contact inhibition of growth and motility (Demuth and Berens, 2004). The E- and N-cadherins are linked with the actin

cytoskeleton through β -catenin that binds directly to the cadherin cytoplasmic domain, and α -catenin, that binds to β -catenin and is directly linked to actin and the actin-binding protein, α -actinin (Juliano, 2002). A recent study demonstrated that N-cadherin overexpression in C6 glioma cells significantly decreased invasion both *in vitro* and *in vivo* (Asano et al., 2004). In addition, overexpression of other cell adhesion molecules such as neural cell adhesion molecule (NCAM) also decreases glioma cell motility *in vitro* (Prag et al., 2002). Typically, the expression of neural cell adhesion molecule (NCAM) is inversely correlated with glioma malignancy (Maidment et al., 1997; Gratsa et al., 1997)

Establishment of cell polarity

Loss of homotypic cell-cell adhesion is followed by the established of a polarized morphology to initiate cell migration. The Rho-like GTPases, Rho, Rac and Cdc 42, regulate specific morphological changes in the cytoskeleton and play a pivotal role in controlling polarity, migration and invasion (Schmitz et al., 2000). These molecular switches are active when GTP is bound and inactive when GDP is bound. Facilitating the exchange of GTP and GDP are two classes of proteins: guanine nucleotide exchange factors (GEFs) switch GTPases “on” through GTP binding, and GTPase activating proteins (GAPs) increase endogenous Rho-GTPase activity to turn off the molecular switch (Luo, 2000). In addition, guanine nucleotide dissociation inhibitors (GDIs) interfere with both the hydrolysis of GTP and the exchange of GDP for GTP.

The RhoGTPases are involved with directed cell migration through microtubule reorientation to establish cell polarity. In particular, studies have shown that Cdc42 is responsible for microtubule organizing centre (MTOC) reorientation towards the leading edge (Etienne-Manneville and Hall, 2001; Palazzo et al., 2001). This mechanism has been established for migrating astrocytes and involves recruitment of a cytoplasmic mPAR6/protein kinase C zeta (PKC ζ) complex to the leading edge in conjunction with the motor protein dynein to establish polarity (Etienne-Manneville and Hall, 2001). In addition, Etienne-Manneville and Hall (2003) have shown that the Cdc42-PAR6/PKC ζ complex interacts directly with and phosphorylates glycogen synthase kinase 3 β (GSK 3 β). Inactivation of GSK 3 β leads to β -catenin stabilization and localization to the leading edge along with interaction of adenomatous polyposis coli (APC) with the plus end of microtubules (Etienne-Manneville et al., 2003). Interestingly, these components of the Wnt signaling pathway are typically associated with medulloblastoma progression; however, their role in medulloblastoma cell polarity has not been established. (see Fig. 1.3). Involvement of dynein and dynactin in regulating MTOC reorientation has also been shown for 3T3 fibroblasts (Palazzo et al., 2001). Recent evidence, however, has suggested that nuclear repositioning, and not active MTOC movement, is the initial polarizing event in migrating cells, and is dependent on a regulatory pathway that includes Cdc42, MRCK, myosin and actin (Gomes et al., 2005). This pathway is independent of the Par6-PKC ζ regulation of MTOC reorientation, and these authors suggest that this signaling cascade is only involved in MTOC cell-centroid maintenance and not nuclear movement (Gomes et al., 2005). Clearly, the mechanisms associated with cell polarization have yet to be fully understood.

Local tissue remodeling and ECM degradation

The invasive paradigm that defines the motility of malignant brain tumor cells and distinguishes their movement from the migration seen in their non-neoplastic cell counterparts involves proteolytic mechanisms that culminate in ECM degradation and tissue destruction. Two broad classes of proteases typically associated with brain tumor invasion are the zinc-dependent matrix metalloproteinases (MMPs) and serine proteases. The matrix metalloproteinases play an important role in brain tumor cell invasion (Nakagawa et al., 1994; Yoshida et al., 2003; Matsumura et al., 2000). Of all the MMP family members, the 72 kDa gelatinase A and 92 kDa gelatinase B (MMP-2 and MMP-9 respectively) promote invasion in high grade glioma although MMP-1 and 3 have also been detected in human glioblastoma *in vivo* (Uhm et al., 1997; Nakagawa et al., 1994). Furthermore, MMP-9 and membrane-type 1 and 2 MMPs (MT1- and MT2-MMP) were expressed in over 75% of classic and desmoplastic medulloblastoma human tumors (Ozen et al., 2004). Tissue inhibitors of matrix metalloproteinases (TIMPs), including TIMP 1-4, control ECM proteolysis by serving as both inhibitors of MMP activity and activators of some pro-MMP molecules (Strongin et al., 1995). TIMP-3 was most often associated with classic medulloblastoma; whereas, TIMP-2 expression was seen mostly in desmoplastic tumors suggesting a correlation with histological subtype (Ozen et al., 2004).

Treatment of glioma spheroids with anti-MMP agents such as SI-27 and 1,10-phenanthroline significantly reduced invasion into normal brain slices (Yoshida et al.,

2003; Matsumura et al., 2000). In addition, the major green tea polyphenol, epigallocatechin-3-gallate (EGCG) inhibited MT1-MMP dependent activation of pro-MMP2 (Annabi et al., 2002). Taken together, these results suggest that the MMPs play an important role in malignant brain tumor invasion; however, clinical trials using MMP inhibitors such as Marimastat and Prinomastat have not significantly improved survival rates (Tremont-Lukats and Gilbert, 2003). The extensive cross-talk between signaling cascades limits the efficacy of a single drug and suggests that new combination therapies targeting a variety of molecules and pathways are needed.

The serine protease system, consisting of the urokinase plasminogen activator-plasminogen-plasmin cascade, is responsible for the proteolytic activity of most MMPs and the degradation of other ECM components (Uhm et al., 1997). Studies have provided contradictory results concerning the role of this system in brain tumor invasion. For example, serine protease inhibitors did not influence C6 astrocytoma invasion in collagen type I gels; however, both a metalloprotease inhibitor and TIMP-2 significantly inhibited invasion in this model (Tamaki et al., 1997). Mohanam et al. (2001) obtained quite different results using an antisense uPA transcript to transfect SNB19 cells. Invasion into fetal rat brain aggregate co-cultures was significantly inhibited, suggesting that the serine protease system plays an important role in confrontation-co-culture invasion. Differences may be attributed to the variety of model systems and techniques employed to manipulate the invasive cascade.

Cell invasion and actin dynamics

Cell migration combines a series of multiple complex events involving regulation of cytoskeletal dynamics. In particular, the process is initiated by a polarized morphology, and a redistribution of filamentous actin. Accompanying this process is the extension of lamellipodia and filopodia along the cell membrane front gradually leading to directional turning. These processes are coupled with development of new adhesions to the extracellular matrix and occur in conjunction with actin polymerization, providing the protrusive force to extend both the lamellipodia and filopodia at the leading edge (reviewed by Schmitz et al., 2000). The contractile force necessary to drive a cell forward involves myosin motors, and the microtubule network regulates rear retraction thereby facilitating cell migration (reviewed by Schmitz et al., 2000). Many molecules are involved in these highly regulated processes, and here, members of the Rho-like GTPase family will be highlighted.

In addition to their role in establishing cell polarity, the RhoGTPases also play an important role in regulating actin dynamics. Neurite outgrowth studies have demonstrated antagonistic effects of the RhoGTPases where Rho activation typically leads to retraction and Rac/Cdc42 activation culminate in outgrowth or extension (Luo et al., 1994; Jalink et al., 1994). Classic studies using Swiss 3T3 fibroblasts demonstrated that Rac activation leads to lamellipodia formation and membrane ruffling, and Cdc42 and Rho induce filopodia and stress fiber formation respectively (reviewed by Luo, 2000). The coordinated events accompanying actin cytoskeleton rearrangement and RhoGTPase activation control movement and polarization for a variety of cell types.

The implication of the RhoGTPases in fibroblast motility and axon guidance have been well-established; however, extensive crosstalk between RhoGTPases signaling cascades, as well as variation in cell type and model systems employed have often resulted in contradictory effects. For example, Banyard et al. (2000) obtained variable results by showing that both dominant negative and constitutively active forms of Rac, Rho, and Cdc42 inhibited PDGF-BB stimulated Rat1 fibroblast invasion in three-dimensional matrices. Rac activation by both a constitutively active V12Rac1 and Rac-specific activator, Tiam1, induced T-lymphoma cell invasion (Habets et al., 1994; Michiels et al., 1995). Tiam1-mediated Rac activation of TIMP1 and 2 in renal carcinoma cells has also provided a link between the RhoGTPases and ECM proteolysis (Engers et al., 2001). In contrast, Tiam1/Rac signaling has also been shown to inhibit migration of 3T3 fibroblasts through fibronectin-coated filters, an effect that is ECM dependent (Sander et al., 1998; Sander et al., 1999). Rac activation also promotes E-cadherin mediated cell-cell adhesion, and therefore inhibits epithelial cell migration (Braga et al., 1997; Hordijk et al., 1997; Kuroda et al., 1997; Takaishi et al., 1997).

Studies have examined the role of the RhoGTPases in malignant brain tumors as well. For example, Senger et al. (2002) have shown that suppression of Rac leads to apoptosis in a variety of glioma cell lines and short term cultures of primary human glioblastoma and oligodendroglioma. Depletion of Rac1 has also been shown to inhibit U87 glioma invasion through both Matrigel and rat brain slice cultures, and these authors demonstrated that reduction of either synaptojanin 2 or Rac1 inhibited formation of

invadopodia and lamellipodia (Chuang et al., 2004) This study did not address the possible concomitant effect of Rac1 depletion on other cellular processes such glioma cell proliferation or survival. Another study has shown that attachment of malignant astrocytoma cells to an osteopontin substrate induced a rapid Rho and slow, prolonged Rac activation suggesting that the RhoGTPases are involved in glioma cell adhesion in addition to survival and migration/invasion (Ding et al., 2002). Our laboratory has also demonstrated a role for Rho in glioma cell invasion in three-dimensional collagen type I matrices using pharmacological inhibitors (unpublished results).

The formation of new adhesions to the ECM occurs in conjunction with actin polymerization and helps facilitate forward movement. Integrins are transmembrane glycoproteins that consist of two subunits (α and β), and are responsible for facilitating cell adhesion to various ECM substrates. The cytoplasmic domain of the β -subunit directly interacts with cytoskeletal proteins leading to changes in cell shape required to initiate motility. Integrin expression is upregulated in glioma cells in comparison with normal brain/astrocytes, and $\alpha 3 \beta 1$, $\alpha v \beta 1$, $\alpha v \beta 3$, and $\alpha v \beta 5$ have all been shown to play a role in astrocytoma migration (Lefranc et al., 2005; Paulus and Tonn, 1994; Rooprai et al., 1999). For example, overexpression of the $\beta 1$ subunit increases C6 glioma cell invasion in nude mice (Paulus et al., 1996). In addition, an αv subunit antagonist induced apoptosis in U87 glioma cells by preventing adhesion to vitronectin and tenascin, further demonstrating the motility-promoting properties of the integrin family (Taga et al., 2002). Interestingly, Pilorget et al. (2003) have shown that the major green tea polyphenol, epigallocatechin-3-gallate (EGCG) decreases the migration of the

medulloblastoma cell line DAOY, by increasing gene and protein expression of the $\beta 1$ subunit suggesting that migration is controlled by a regulated equilibrium of adhesion, de-adhesion, and integrin expression.

Detachment of the cell

Cell adhesion to the ECM is required to facilitate movement at the leading edge. However, when a cell moves forward, the trailing edge remains attached to the substratum greatly extending its length under the resulting tension (reviewed by Kassis et al., 2001). To complete the movement cycle, the trailing edge must shed adhesive contact with the ECM. This is accomplished by the collapse and backward movement of ruffled extensions on the dorsal cell surface, followed by rupture and retraction of the major tail into the cell body (reviewed by Kassis et al., 2001). A small portion of the tail is left behind and remains attached to the ECM. Studies have shown that fibroblasts and melanoma cells shed their integrins to facilitate detachment (Friedl et al., 1997; Regen and Horwitz, 1992; Palecek et al., 1996). In addition, growth factor receptor signaling and calcium influx have been shown to induce M-calpain and μ -calpain respectively mediating cleavage of the integrin β subunit and targeting other molecules such as talin and focal adhesion kinase (FAK) (reviewed by Kassis et al., 2001). Overall, an intermediate adhesiveness is required for optimal cell movement. Low adhesion interferes with cell-ECM attachments at the leading edge; whereas, high adhesion prevents rear retraction and leaves cells extended.

The dynamics of the invasive cascade are not a simple order of events. The multitude of growth factors, integrins, proteases, cadherins, and cytoskeletal machinery are intertwined in an intricate web more complicated than the sum of individual component parts. Consequently, therapeutic intervention successfully targeting multiple facets of the invasive cascade remains difficult.

The “Grow or Go” Hypothesis

A controversy associated with brain tumor cell invasion is the “grow or go hypothesis.” This hypothesis states that cells defer proliferation in order to invade and supports the idea that the two processes are mutually exclusive. Many studies support this concept. For example, in co-cultures of biopsy spheroids with fetal rat brain aggregates, there was no correlation between invasion measurements and Ki67 labeling suggesting that the two processes are unrelated (Khoshyomn et al., 1999). Giese et al. (1996) demonstrated that on permissive substrates such as merosin, the most peripheral rapidly migrating glioma cells had the lower proliferation index. Similarly, NG2+ cells in biopsy spheroids were more proliferative and less invasive than their NG2- counterparts (Chekenya et al., 1999). In addition, Roth et al. (2000) have shown that secreted frizzled-related proteins (sFRPs) inhibit motility and promote growth of human malignant glioma cells *in vitro* and *in vivo* respectively. Although a lot of evidence has accumulated supporting the “grow or go” hypothesis in glioblastoma multiforme, experiments comparing migration/invasion and proliferation in medulloblastoma cells do not support this concept. Corcoran et al. (2003) showed that medulloblastoma cell lines do not defer proliferation while migrating on uncoated surfaces and invading type I collagen gels.

Furthermore, recent data from our laboratory suggests that ITI H2, a negative regulator of glioma invasion concomitantly inhibits proliferation providing further evidence refuting the “grow or go” hypothesis (see Chapter 3). Taken together, these results suggest that therapeutic strategies targeting the invasive cascade should be approached with caution; as inhibiting cell motility may or may not initiate proliferation. This emphasizes the need for, tumor specific, combination therapies that target multiple biological processes.

1.3 Models of brain tumor cell motility: from Boyden chambers to animal models

To study the complexity of the invasive paradigm, many *in vitro* and *in vivo* models of glioblastoma and medulloblastoma have been developed. Each model has its own unique benefits and disadvantages when studying malignant brain tumor cell invasion and, and these points are addressed below.

The Boyden chamber is a common two-dimensional assay that examines cellular movement from one chamber to another through a porous membrane of known ECM molecules (Chicoine and Silbergeld, 1997). In this model, the treatment substance or factor of interest is added to culture medium and placed in either the lower, or upper chamber or both. Glioblastoma or medulloblastoma cells plated into the upper chamber, migrate through the pores and the number of cells counted in the lower chamber is compared with controls to assess potential kinetic and chemotropic responses. Although this model assesses cell motility, it does not permit translation of data into the three-dimensional cell invasion represented in the brain. Thus, a more accurate depiction of

brain tumor cell invasion can be demonstrated using spheroid or three-dimensional hanging-drop aggregate models.

Spheroids are generated by culturing cells in agar-coated multi-well dishes, or by taking confluent monolayer cultures and seeding them into spinner culture flasks containing medium. Spheroids grown in spinner culture are spun at 180 rotations per minute for 2-6 weeks, depending on the desired size, and a homogeneous spheroid population of specific diameter can be harvested for implantation (Farrell et al., 1987). Glioma cell lines such as C6 rat astrocytoma and U251 glioblastoma are amenable to the spinner culture flask model; however, other glioma and medulloblastoma cell lines do not form spheroids in this manner. To alleviate this problem, we use the hanging drop model to resuspend fixed cell solutions from Petri dishes lids for 2-3 days followed by transfer to agar-coated plates (Del Duca et al., 2004; Corcoran et al., 2004).

Spheroids made by either spinner culture or hanging drop methods are eventually implanted into type I collagen gels. Using this model, it is possible to investigate morphological changes in cell shape, invasive rate, and proliferative index in a three-dimensional environment that can be monitored daily (Tamaki et al., 1997). Individual cell invasive paradigms can also be examined and imaged using time-lapse videomicroscopy over extended periods of time (Del Maestro et al., 2001; Werbowetski et al., 2004; Del Duca et al., 2004; Corcoran and Del Maestro, 2003; Angers-Loustau et al., 2004). Spheroids implanted in collagen type I gels more closely recapitulate the tumor microenvironments *in vivo*. For example, after 10-20 days in culture, an extensive

central necrotic region surrounding a rim of actively proliferating cells is evident in Haematoxylin and Eosin (H&E) stains of paraffin embedded C6 spheroids implanted in collagen gels (Fig. 1.4). Presumably, these morphological changes are linked with the molecular framework of the spheroid environment, and as a consequence, the invasive paradigm is manipulated. Although this model is excellent for studying the dynamics of spheroid invasion in a simple three-dimensional system, there is one limitation: collagen type I is scarce in the brain, and this model does not reconstitute the molecular complexity of the ECM *in vivo*. Other molecules such as laminin, hyaluronic acid, fibronectin can be added to the collagen gels to increase matrix complexity to more closely recapitulate the ECM *in vivo* (Tamaki et al., 1997). Nevertheless, this model has also been used to examine the dynamics of cell-cell and cell matrix interactions, as well as the effects of radiation on malignant brain tumor invasion (Tamaki et al., 1997; Bauman et al., 1999a; Bauman et al., 1999b).

To study malignant brain tumor invasion in a more biologically relevant environment, spheroids from both glioma and medulloblastoma cell lines or human biopsy cultures can be co-cultured with fetal rat brain/fetal human astrocyte aggregates to assess invasion into non-neoplastic tissue in three-dimensions (Bjerkvig et al., 1986; Werbowetski et al., 2004; Werbowetski-Ogilvie et al., submitted). Evaluation of numerous rat glioma cell lines has revealed that confrontation co-cultures mimic the growth and invasion demonstrated by these cells after intracranial implantation in rats, and thus closely approximates invasion *in vivo* (Bjerkvig et al., 1986). Despite the advantages of this model, confrontation co-cultures can only be assessed using end-point

values obtained from confocal microscopy. This makes the study of individual cell dynamics difficult.

The limitations associated with *in vitro* models of malignant brain tumor invasion are evident. Therefore, a variety of glioblastoma and medulloblastoma murine models have been developed based on genetic mutations and aberrant signaling cascades. Transgenic mice are based on the “gain of function” approach where expression of an oncogene is driven by a tissue-specific promoter; whereas, knockout mice are based on targeted deletion of tumor suppressor genes known to be involved in malignant brain tumor progression.

Glioblastomas are thought to arise from astrocytes or astrocytic precursors; however, the morphological heterogeneity of these glial tumors makes it often difficult to draw conclusions about their cell of origin (Lopez et al., 1995). Consequently, the histopathological diagnosis of mouse tumor models of GBM can be complicated (Hesselager and Holland, 2003). Introduction of activated Ras and Akt into nestin progenitor cells, but not differentiated GFP-expressing astrocytes, leads to production of primary GBM (Holland et al., 2000). This model produced GBM tumors only when both pathways were activated. Another murine model of GBM combined breeding of mice having p53 deletions with those having deletions in the neurofibromatosis gene, NF1 (Reilly et al., 2000). The protein product of the NF1 gene, Neurofibromin is known to inhibit Ras signaling, and therefore, deletion of this gene results in Ras overactivity.

In other murine model systems, expression of H-ras or v-src in GFAP astrocytes induced astrocytoma formation (Ding et al., 2001; Weissenberger et al., 1997). These tumors exhibit features of high-grade GBM; however, they also fit the histological criteria of WHO Grade II-III astrocytoma. Most murine models of high-grade glioma target two main intracellular signaling cascades: the mitogenic Ras/MEK/MAPK pathway and the anti-apoptotic PI3K/Akt pathway. Both targets are downstream of various growth factor receptors and are typically activated in human GBMs.

Medulloblastoma murine models have taken advantage of the relationship between tumorigenesis and neurodevelopment. A well known murine medulloblastoma model is the Ptc +/- heterozygote (Goodrich et al., 1997; Hahn et al., 1998). Approximately 30% of these mice develop cerebellar tumors that histologically resemble medulloblastoma and display features of Gorlin syndrome. Patched mutations lead to constitutive activation of the Shh pathway and consequent transcription of GLI followed by extensive cell proliferation. In addition, a combination of Ptc +/- heterozygotes in a p53 null background leads to medulloblastoma in greater than 95% of mice, and tumors develop by 12 weeks (Wetmore et al., 2001). These models have been used to study the effects of a small Shh pathway pharmacological inhibitor as well as the visualization of tumor progression using magnetic resonance imaging (MRI) (Romer et al., 2004; Nelson et al., 2003). Typically, Ptc +/- and Ptc +/- p53 -/- medulloblastoma murine models are representative of the desmoplastic variant, and do not recapitulate the classic subtype.

Weiner et al. (2002) have also used retroviral infection to introduce the Shh gene into early cerebellar precursors of embryonic day 13 mice under ultrasound guidance. Medulloblastoma-like lesions developed in over 75% of mice, and examination at P14 and P21 showed persistent EGL proliferation suggesting that these cells are indeed the medulloblastoma cell of origin. Furthermore, other studies have shown that combined activation of Shh and insulin-like growth factor (IGF) enhances medulloblastoma formation in mice (Rao et al., 2004).

Interestingly, some murine models have been accidentally developed in an attempt to generate astrocytic tumors. For example, Marino et al. (2000) used the Cre/LoxP system to conditionally knockout the retinoblastoma gene (RB) in a p53 null background. Under the GFAP promoter, it was expected that only astrocytes would form tumors; however, surprisingly, within months, cerebellar tumors resembling medulloblastoma developed.

The developmental origin of CNS malignancies can be studied using murine models; however, these methods do not always recapitulate the human condition. For example, mutations such as p53 and pRB are rarely found in human medulloblastoma. Alternative *in vivo* systems include xenograft models of both glioblastoma and medulloblastoma in nude mice and/or rats and the C6 intracerebral implantation model.

Xenograft models of medulloblastoma and GBM have been used to examine a variety of potential therapeutic targets and strategies. For example, Vachon et al. (2004)

have recently shown that basic fibroblast growth factor (bFGF) inhibits medulloblastoma development in nude mice. Tumor volume was reduced approximately 75% in bFGF-treated mice, and this was accompanied by a histological examination suggesting bFGF-induced necrosis and differentiation. Other studies have demonstrated significant reduction in spinal and leptomeningeal medulloblastoma metastasis as well as prolonged survival after repeated injections of reovirus, a replication-competent virus that targets the Ras pathway (Yang et al., 2003). Although studies using medulloblastoma xenografts have illustrated the potential of a variety of therapeutic strategies, many are limited by the cell lines utilized. For example, the Daoy cell line, although highly invasive and proliferative *in vitro*, has mutations in p53 and the CDKN2 gene (Raffel et al., 1993; Raffel et al., 1995; Corcoran and Del Maestro, 2003). These mutations are rare in medulloblastoma and the Daoy cell line is actually more characteristic of other tumor types such as high-grade glioma.

Another problem encountered with xenograft models of medulloblastoma in nude mice has also made it difficult to study the characteristics of this tumor *in vivo*. In particular, cell lines that invade or migrate on various substrates *in vitro* do not always demonstrate the same motile properties in xenograft models despite extensive growth over time (unpublished results). In fact, studies have shown that the addition of Matrigel enhanced subcutaneous engraftment of primary medulloblastoma/primitive neuroectodermal tumors in a xenograft model where implantation of cell suspensions alone yielded no results (White et al., 2001). This has made the study of *in vivo* medulloblastoma invasion difficult. Recent studies demonstrating that only a small

percentage of CD133+ positive cancer stem cells are responsible for brain tumor progression will facilitate the development of better *in vivo* models of this neuronal tumor in the future (Singh et al., 2003; Singh et al., 2004). Their exclusive ability to drive malignant tumor formation and dissemination make these cells an obvious target for all therapeutic strategies.

Along with medulloblastoma xenograft models, GBM xenograft models are also extensively used to complement *in vitro* data and validate potential therapeutic strategies. The number of studies using xenograft GBM models is too vast to discuss in detail here; however, a few will be highlighted.

Neural stem cell gene therapy has also been examined in xenograft models of GBM. A study by Aboody et al. (2000) demonstrated that neural stem cells exhibited chemotropism towards glioblastoma tumor cells, and could therefore be used as a vector to deliver anti-tumoral genes (ie. cytosine deaminase) to the tumor site. In addition, the C6 rat astrocytoma implantation model has also been utilized to examine the potential of stem cell gene therapy (Ehtesham et al., 2002; Benedetti et al., 2000). Interleukin-producing neural stem cells have been used to target intracranial glioblastoma, and studies have shown that this strategy prolongs survival in mice (Ehtesham et al., 2002; Benedetti et al., 2000).

Alginate bead microencapsulation

Alginate encapsulation is a well established technique for immobilization of living cells and has been utilized for hormone treatment of diabetes, and for diseases of the parathyroid and liver (Darquay and Sun, 1987; Lim and Sun, 1980; Miura et al. 1986; Soon-Shiong et al., 1992). For example, dogs treated with alginate encapsulated Islets of Langerhans have demonstrated a high reversal of spontaneous diabetes (Soon-Shiong et al., 1999). Alginate is derived from brown seaweed extract and is composed of two types of monosaccharides: L-guluronic (G) and D-mannuronic (M) acid. The content of L-guluronic (G) acid in alginate determines the porosity and stability of the beads, as well as the mechanical strength and volume, where alginate with higher L-guluronic acid (G) has larger pore sizes (Thu, 1996). In the presence of divalent cations such as calcium, the alginate forms an extended gel network that immunoisolates cells when implanted *in vitro* or *in vivo* and provides an environment for continuous delivery of the molecule of interest over time as opposed to single injections. The pores allow for simultaneous free diffusion of the recombinant protein of interest out and other macromolecules in while immobilizing cells within the alginate.

Alginate microencapsulation bioreactor technology has been used to assess the efficacy of anti-angiogenic compounds such as endostatin on the growth of gliomas both *in vitro* and *in vivo* (Joki et al., 2001; Read et al., 2001a; 2001b). In xenograft models of glioblastoma, injection of endostatin-secreting alginate poly-L-lysine beads led to a 72% reduction in U87 glioma tumor weight over 3 weeks (Joki et al., 2001). Other studies have shown a concomitant inhibition of glioblastoma tumor growth and invasion in nude mice (Read et al., 2001a). Furthermore, rats that received transplants of BT4C glioma

cells, together with endostatin secreting sodium alginate microencapsulates survived 84% longer than controls (Read et al., 2001b). Alginate bead microencapsulation therapy can therefore be effectively used to target malignant brain tumor progression, and sodium alginate encapsulation is an important component of this thesis (see Chapter 4).

Recent studies in our laboratory have also utilized the C6 intracerebral implantation model to examine the effect of novel molecular probes on brain tumor growth and invasion using magnetic resonance imaging. The combination of *in vivo* malignant brain tumor models with molecular imaging will enable scientists to more accurately test the efficacy of novel therapeutic strategies targeting a variety of cellular processes including angiogenesis, proliferation and invasion.

1.4 Positive and negative regulators of brain tumor invasion: old favorites and new perspectives

Growth factors serving as both mitogens and motogens are perhaps the most frequently studied molecules in malignant brain tumors. Their effects on proliferation, migration and invasion, angiogenesis, survival and differentiation make growth factors and their receptors attractive therapeutic targets in both GBM and medulloblastoma.

Since the early 1990s, many studies have examined the role of growth factors in malignant brain tumor proliferation and motility. Lund-Johansen et al. (1992) tested a variety of growth factors including epidermal growth factor (EGF), fibroblast growth factor (FGF) and isoforms of platelet-derived growth factor (PDGF AA or BB) on the

glioma cell line GaMG. Both EGF and FGF increased cell growth and invasion into fetal rat brain aggregates; however, PDGF did not affect tumor cells despite stimulating proliferation of oligodendrocyte-like cells in the brain aggregates. Other studies have demonstrated quite different results. For example, Chicoine et al. (1995) examined the effects of growth factors on glioma cells in a modified radial dish assay. Although EGF had a persistent chemoattractive effect, PDGF bb, bFGF, and nerve growth factor (NGF) maintained a chemorepulsion over the entire 6-10 days. Tumor necrosis factor alpha (TNF α) initially had a chemorepulsive effect over the first 24-48 hours followed by a strong chemoattractive response (Chicoine et al., 1995). Furthermore, NGF did not influence invasion in confrontation co-cultures, and only enhanced spheroid migration in 1 of 5 glioblastoma cell lines (Engebraaten et al., 1993). The discrepancies in the literature with regards to growth factor effects can be attributed to the variety of models and cell lines employed. While confrontation co-cultures directly assess invasion, the radial dish assay only examines cell migration, a facet of the invasive cascade.

In addition to the growth factors described above, transforming growth factor beta (TGF β) also affects malignant brain tumor invasion. Merzak et al. (1994) showed that TGF β exerted a growth inhibitory effect on three glioma cell lines derived from primary tumors while increasing both glioma cell migration and invasion. These results support the “grow or go” hypothesis, and suggest that glioma cell proliferation and migration/invasion are indeed mutually exclusive events.

Other growth factors known for their roles in malignant brain tumor biology include vascular endothelial growth factor (VEGF) and hepatocyte growth factor/scatter factor (HGF/SF). VEGF is known for its role as a potent stimulator of angiogenesis, and is highly expressed by perinecrotic palisading cells in high-grade gliomas (Hamel and Westphal et al., 2000; Mueller et al., 2003). C6 rat astrocytoma cells transfected with an antisense VEGF expression vector exhibited decreased growth *in vivo*, and monoclonal anti-VEGF antibodies also reduced both *in vivo* tumor cell growth and vascular permeability (Saleh et al., 1996; Borgstrom et al., 1996; Pham et al., 1998; Yuan et al., 1996). Interestingly, overexpression of membrane-type 1 MMP increased VEGF production and resulted in stimulation of glioma xenograft angiogenesis and growth (Deryugina et al., 2002).

In contrast to VEGF, HGF/SF is primarily known for its role in glioma cell motility. Both HGF/SF and its tyrosine kinase receptor MET are expressed by gliomas *in vivo*, and increased expression is associated with transition from low to high-grade gliomas (Hamel and Westphal, 2000; Mueller et al., 2003). Koochekpour et al. (1997) have shown that HGF/SF induces glioma cell proliferation, migration and invasion *in vitro*. Moreover, HGF/SF induce glioma cell invasion by autocrine induction of MMP-2 expression and activation (Hamazuna et al., 1999).

In addition to the growth factors described above, the protein kinase Src has been shown to play a role in malignant brain tumor biology. A study from our laboratory has demonstrated that the Src family kinase inhibitor, PP2, caused the disappearance of

membrane ruffles on monolayer cultures of U251 glioblastoma cells (Angers-Loustau et al., 2004). In three-dimensional collagen gels, PP2 induced loss of actin bursting at the tip of the invadopodium, suggesting that Src plays an important role in cytoskeletal dynamics for both glioblastoma cell migration and invasion *in vitro* (Angers-Loustau et al., 2004). The pharmacological Src kinase inhibitors PP2 and SU6656 also decreased cell proliferation without a concomitant effect on cell viability, providing further evidence refuting the “grow or go” hypothesis (Angers-Loustau et al., 2004).

There are many positive regulators of malignant brain tumor cell invasion; however, little is known about natural inhibitors of invasion both *in vitro* and *in vivo*. Hemopexin (PEX) is a non-catalytic fragment of matrix metalloproteinase-2 (MMP-2) known to disrupt tumor growth and angiogenesis (Brooks et al., 1998). Bello et al. (2001) examined the effect of PEX on glioblastoma cell biology, and demonstrated inhibition of both glioma and endothelial cell proliferation and migration in Boyden chamber assays. Furthermore, tumor growth was suppressed by 99% in both subcutaneous and intracranial *in vivo* glioma models without any concomitant toxicity. Although these methods successfully decreased the growth of glioma tumors *in vivo*, PEX is rapidly cleared from the blood, and prolonged administration of the protein is essential to limit the quantities needed to sustain significant biological effects. To address this issue, polymeric microspheres composed of poly (lactic-co-glycolic acid) (PLGA) were loaded with low amounts of PEX, and were shown to inhibit endothelial cell and tumor cell proliferation *in vitro* and *in vivo* (Benny et al., 2005). Furthermore, these findings demonstrated that polymeric microspheres serve as a potential therapeutic strategy that can be utilized to

locally, and continuously deliver endogenous inhibitors of brain tumor growth (Benny et al., 2005). The effect of PEX PLGA microspheres on *in vivo* glioma cell invasion has yet to be examined; however, a similar “bioreactor” approach will be introduced in Chapter 4, as a method to deliver anti-invasive compounds to malignant brain tumors.

Secreted proteins that guide neuronal and glial cell precursors in the developing central nervous system have also been linked with tumorigenesis. Long-range chemotropic factors including netrins, semaphorins, ephrins and the slit family of proteins are known for their roles in neuronal and glial cell migration (Tessier-Lavigne and Goodman, 1996; Dickson, 2002). These molecules play an important role in neurodevelopment and it is reasonable to assume that they will also influence glioblastoma and/or medulloblastoma progression.

The netrins are a family of secreted proteins that are known for their role as tropic cues in axon guidance. Netrin1 is a bifunctional cue that acts as both an attractant and repellent depending on the cell type. The dual role of netrin-1 is mediated by two receptor classes: the deleted in colorectal cancer (DCC) family is required for the attractive response; however, this family is also involved in repulsion (Dickson, 2002). In contrast, the UNC-5 receptor family appears to function exclusively in netrin-mediated chemorepulsion (Dickson, 2002). Studies have demonstrated that DCC mRNA and protein expression levels are reduced in higher grade gliomas, suggesting that the netrin-1 receptor is a tumor suppressor gene (Nakatani et al., 1998; Hara et al., 2001). However, the functional significance of DCC downregulation to malignant brain tumor cell biology

has yet to be determined. It is unclear whether netrin-1/DCC or netrin-1/Unc5 signaling is important for glioma and/or medulloblastoma cell proliferation, survival or invasion *in vitro* and *in vivo*. DCC expression promoted netrin-1 mediated filopodia formation and cell spreading by Cdc42 and Rac1 activation in neuroblastoma cells, and these results suggested that this family of guidance cues and receptors may influence tumor cell motility by modulating cytoskeletal organization (Shekarabi and Kennedy, 2002).

Semaphorins are another family of secreted and cell surface guidance cues linked with malignant brain tumor progression. Although they serve as mainly chemorepellents and short-range inhibitors in axon guidance, chemoattractive properties have also been demonstrated (Raper, 2000; Cheng et al., 2001; Wong et al., 1999; Spassky et al., 2002). There are 8 classes of semaphorins; however, class 3 has been associated with brain tumors. Class 3 semaphorins bind to the neuropilin/plexin co-receptor complex, where neuropilins provide binding sites and specificity, and plexins transduce signals intracellularly (Raper, 2000).

Rieger et al. (2003) recently demonstrated neuropilin, plexin and semaphorin 3A and 3C mRNA and protein expression in various human malignant glioma cell lines. However, co-cultures of Sema3A-HEK 293T cells and U87 glioma cells did not induce a chemorepulsive effect in collagen gels. Moreover, conditioned medium from Sema3A cells did not affect U87 cell morphology providing further evidence that class 3 semaphorins do not influence malignant glioma cell direction or kinetics *in vitro* (Rieger et al., 2003). In light of this issue, Broholm and Laursen (2004) proposed that neuropilin-

1 is a receptor for VEGF-induced angiogenesis, based on the high expression levels in endothelial cells and neoplastic astrocytes. Furthermore, Sema3B appears to be a target of p53 in U373 glioblastoma cells, and ectopic expression decreased the number of colonies formed suggesting a role for semaphorins in cell cycle arrest or apoptosis (Ochi et al., 2002). These studies suggest that class 3 semaphorins may be more important in malignant brain tumor cell growth and angiogenesis than in migration and invasion *in vitro*.

In addition to the netrins and semaphorins, the membrane bound ephrins and their Eph tyrosine kinase receptors are also linked to brain tumorigenesis. Ephrins and their Eph receptors are divided into two main categories: ephrinAs which are membrane anchored by a glycosylphosphatidylinositol (GPI) linkage and are bound to EphA receptors, and ephrinBs that are bound to EphB receptors and exhibit a transmembrane domain (Wilkinson, 2001).

Recent studies have shown ephrin/Eph upregulation in glioblastoma (Nakada et al., 2004; Hoelzinger et al., 2005). Gene expression profiling revealed increased expression of ephrinB3 in white matter invading GBM cells compared with patient tumor core cells (Hoelzinger et al., 2005). In addition, expression of EphB2 in U251 cells stimulated cell migration and invasion *in vitro* and in a rat brain slice model (Nakada et al., 2004). The higher expression of EphB2 in glioblastoma compared with low-grade astrocytomas and normal brain suggests that the ephrin/Eph family plays a role in malignant glioma invasion (Nakada et al., 2004). The expression profile and biological

significance of this axon guidance family in other malignant brain tumors such as medulloblastoma have yet to be determined.

The Slit family of secreted proteins has been shown to function in axon guidance and neuronal migration (Wong et al., 2002). There are three Slit proteins in mammals, and while Slit1 expression is mostly restricted to the nervous system, Slit2 and 3 are also expressed in other organs (Wong et al., 2002). A typical Slit protein contains an N-terminal signal peptide, four leucine-rich repeats (LRRs), seven (in *Drosophila*) or nine (in vertebrates) EGF repeats, a laminin G domain, and a C-terminal cysteine knot (Fig. 1.5) (Wong et al., 2002). The receptor for Slit is the transmembrane protein Robo (Roundabout), and four *ROBO* genes have been identified (Park et al., 2003; Sabatier et al., 2004). Typically, Robo proteins, including Robo1, consist of five extracellular immunoglobulin (Ig) domains, three fibronectin repeats, and a conserved intracellular region of four cytoplasmic motifs (Fig. 1.5).

Expression of Robo proteins has traditionally been associated with migrating axons in the developing nervous system. Examples include expression in commissural axon growth cones after ventral midline crossing and expression in olfactory bulb axons on route from the olfactory epithelium to the primary olfactory cortex (reviewed by Wong et al., 2002). In the *Drosophila* spinal cord, Slit functions as a short-range cue to prevent ipsilateral projecting commissural fibres from crossing the midline, and contralateral projecting commissural fibres from re-crossing the midline. A combinatorial code of Robo receptors on medial, intermediate and lateral axons helps control lateral

positioning in response to a Slit gradient in the CNS (Simpson et al., 2000; Rajagopalan et al., 2000). These results suggested that in *Drosophila*, Slit also functions as a long-range cue that controls the longitudinal tract positioning on each side of the midline (Simpson et al., 2000; Rajagopalan et al., 2000). Other studies have shown that Slit proteins act as chemorepellents in axon guidance in the mouse visual system as well as in neuronal migration and axon guidance in the mammalian forebrain both *in vitro* and using knockout mice deficient in Slit1 and/or Slit2 *in vivo* (Plump et al., 2002; Bagri et al., 2002; Shu and Richards, 2001; Hu, 1999).

Although the function of Slit in axon guidance and neuronal migration is well characterized, other developmental roles have been demonstrated. For example, homozygous knockout mice for the first Ig domain of the Robo1 gene frequently die at birth due to respiratory failure and inadequate lung maturation (Xian et al., 2001). Survivors demonstrated severe lung hyperplasia and bronchial abnormalities suggestive of early lung cancer (Xian et al., 2001). Human patients with horizontal gaze palsy with progressive scoliosis (HGPPS) were reported to have mutations in Rig1/Robo3, and functional studies have shown defects in commissural hindbrain projections and pontine nuclei (Jen et al., 2004). Furthermore, Slit2 and 3 and Robo1 and 2 expression have been detected in non-neuronal cells including pulmonary mesenchyme and airway epithelium, kidney, heart, spleen, thymus and lymph nodes (Wu et al., 2001; Anselmo et al., 2003; Greenberg et al., 2004). Wang et al. (2003) have recently demonstrated a role for Slit-Robo in tumor angiogenesis and implicated PI3K signaling in this process. Other studies have identified Slit2 as a potential tumor suppressor gene in gliomas, lung, breast and

colorectal cancer, as well as in neuroblastoma (Dallol et al., 2002; 2003a; 2003b; Astuti et al., 2004). Dallol et al. (2003a) used a colony forming assay as a measure of tumor cell growth in response to Slit2 overexpression; however, these results do not indicate whether Slit and Robo influence brain tumor cell migration or invasion. The role of Slit2-Robo1 in malignant brain tumor invasion will be discussed in detail in Chapter 4 of this thesis.

The vast array of molecules that modulate malignant brain tumor proliferation, angiogenesis and invasion converge on multiple downstream signaling cascades. Intracellular pathways typically associated with glioblastoma and medulloblastoma tumor progression include the Ras/MEK/MAPK and the phosphatidylinositol-3' kinase PI3K/Akt cascades (Fig. 1.6).

Ras is a member of the small GTP-binding protein family, and similar to the RhoGTPases, Ras is active when GTP is bound and inactive in a GDP-bound state. Regulating the molecular switch are the GDP-exchange factors (GEFs) and the GTPase activating proteins (GAPs). Once Ras is activated, Raf is recruited to the membrane followed by phosphorylation of MEK and the MAPK proteins respectively (Fig. 1.6). The extensive crosstalk between multiple signaling cascades is evident as additional frequent Ras targets include the JNK pathway, the RhoGTPases, and PI3K. Overall, the Ras pathway is associated with cell proliferation, cell cycle progression and apoptosis. In astrocytomas/glioblastoma, oncogenic Ras mutations are not prevalent; however, activated GTP-bound Ras is elevated in high-grade astrocytomas compared to normal

brain samples (Feldkamp et al., 1999; Guha et al., 1997). Stimulation of the receptor tyrosine kinases EGFR and PDGFR increases Ras pathway activation (Guha et al., 1997). This effect could be abrogated by a dominant-negative Ras, which decreased EGF induced MAPK activation in U373 glioblastoma cells. Furthermore, the oncolytic reovirus, that targets activated Ras, leads to U87 tumor regression in immunodeficient mice (Coffey et al., 1998). Pharmacological inhibitors of the Ras pathway are also of therapeutic importance to malignant brain tumors. Currently, Ras inhibitors in clinical trials include SCH66336 and R115777. These compounds inhibit the enzyme farnesyl transferase that controls farnesylation, a post-translational lipid modification involved in anchoring Ras to the membrane (Tremont-Lukats and Gilbert, 2003). *In vitro* studies using glioma cell lines result in decreased cell viability and growth in addition to increased radiosensitivity (Glass et al., 2000; Delmas et al., 2002).

The PI3K/Akt pathway plays an integral role in tumor cell growth and survival. Typically, growth factors stimulate PI3K activation followed by an increase in cellular phosphatidylinositol (3,4,5)-triphosphate (PIP3) levels and Akt activation. The protein PTEN negatively regulates PI3K/Akt signal transduction by converting PIP3 to PIP2 making cells more likely to undergo apoptosis. Mutations in PTEN are common in 20-30% glioblastomas leading to overactivity of the PI3K/Akt pathway, increased cell survival and enhanced proliferation (Fig. 1.6) (Wechsler-Reya and Scott, 2001).

The PI3K signaling cascade is not only involved with malignant brain tumor cell proliferation and survival, but also migration/invasion and attachment. Pharmacological

inhibitors of PI3K signaling including LY294002 and Wortmannin, significantly inhibited glioblastoma invasion through a Matrigel barrier (Kubiatowski et al., 2001). These compounds significantly reduced MMP-2 and MMP-9 activity suggesting a link between matrix metalloproteinase activity and PI3K signaling. In addition, the serine protease urokinase-type plasminogen activator (uPA) also inhibited glioblastoma cell migration through PI3K/Akt signaling (Chandrasekar et al., 2003). Ling et al. (1999) demonstrated decreased U251 glioblastoma cell attachment to vitronectin, fibronectin, laminin and collagen after addition of PI3K inhibitors, suggesting a role for PI3K/Akt signaling in facilitating cell-matrix adhesion, an important facet of the invasive cascade.

Similar to Ras, PI3K/Akt signaling inhibitors are also being tested in clinical trials. For example, the rapamycin analog CCI-779 targets mTOR, an enzyme downstream of Akt, induced cell cycle arrest in G1 (Tremont-Lukats and Gilbert, 2003). Growth of Daoy medulloblastoma xenografts was significantly reduced with CI-779 treatment, and interestingly xenografts derived from U251, a rapamycin resistant glioblastoma cell line, were also growth inhibited (Geoerger et al., 2001). In addition, combination therapy of the EGFR/VEGFR inhibitor AEE788 and RAD-001, another mTOR inhibitor increased cell cycle arrest and apoptosis *in vitro* and induced growth inhibition in glioma tumor xenografts *in vivo* (Goudar et al., 2005). These results confirm PI3K/Akt signaling as a valid therapeutic target for both glioblastoma and medulloblastoma tumors. The extensive crosstalk between intracellular signaling cascades confirms the need for combination therapies targeting common downstream effectors. Pharmacological compounds that inhibit multiple biological processes such as

proliferation, angiogenesis, and invasion are more likely to have a significant clinical impact and improve patient survival.

1.5 Conclusions

Medulloblastoma and glioblastoma are among the most devastating of malignant brain tumors. Although surgery, chemotherapy and radiation are common therapeutic strategies, the highly infiltrative invasive subpopulation usually remains and tumors recur. It is clear that the mechanisms underlying malignant brain tumor invasion are not yet fully understood.

This thesis focuses on negative regulators of malignant brain tumor invasion in three-dimensions. Chapter 2 presents evidence for a chemorepellent that directs glioma cell invasion. The inhibitory effect of C6 and U251 conditioned medium on glioblastoma spheroids in collagen type I matrices is the basis for a functional assay outlined in Chapter 3. Using this model, inter alpha trypsin inhibitor heavy chain 2 (ITI H2) was isolated and identified from purified fractions having the most inhibitory effect on spheroid invasion in three-dimensions. ITI H2 has a concomitant effect on other cell biological processes such as proliferation and adhesion, and the inverse correlation with malignancy in a variety of CNS tumors points to ITI H2 as an important therapeutic target. Finally, Chapter 4 examines the role of Slit2/Robo1 in medulloblastoma and glioma cell invasion. Sodium alginate bead microencapsulation is highlighted as a potential strategy for future introduction of Slit2 and other negative guidance cues *in vivo*.

Table 1.1: A summary of the characteristics of GBM and medulloblastoma.

	Glioblastoma Multiforme (GBM)	Medulloblastoma
Cell of origin	Astrocyte or astrocytic precursors	Neuronal external granular layer precursors of cerebellum
Population distribution	Adult (predominantly)	Children (predominantly)
Invasion/Migration	Invasion along white matter tracts and blood vessels	Invasion Migration as monolayers over the surface of the brain
Metastasis and CSF spread	rare	yes
Mitotic Index	high	high
Survival	12-18 months (5 year survival – very rare)	5 year survival rate: 60-70%
Treatment	Surgery, Radiation and Chemotherapy	Surgery, Radiation and/or Chemotherapy

Figure 1.1: Genetic aberrations and histological criteria associated with malignant glioma progression. Note the differences between primary “*de novo*” and secondary GBM. For example, p53 is a common mutation characteristic of secondary GBM but not usually associated with primary GBM. Accompanying progression from a low-grade to high-grade astrocytoma is the accumulation of a series of histopathological features including endothelial cell proliferation, necrosis, nuclear atypia, and a high mitotic index.

Primary "de novo"
glioblastoma



EGFR mutation, EGFR
amplification, PTEN loss, RB
mutation, INK4a/ARF loss

Glioblastoma multiforme

Secondary glioblastoma

PDGF/R overexpression, p53
mutation

Low-grade astrocytoma



CDK4 amplification, 19q loss,
11p loss, PTEN loss, RB
mutation, INK4a/ARF loss

Anaplastic astrocytoma



EGFR mutation, EGFR
amplification, PTEN loss, RB
mutation, INK4a/ARF loss

Glioblastoma multiforme

WHO
histological
criteria

1-2 of: endothelial cell
proliferation, nuclear
atypia, mitosis and
necrosis

3 of: endothelial cell
proliferation, nuclear
atypia, mitosis and
necrosis

all: endothelial cell
proliferation, nuclear
atypia, mitosis and
necrosis

Figure 1.2: The Sonic Hedgehog signaling cascade. Secreted Sonic Hedgehog binds to and inactivates the Patched receptor thereby relieving inhibition of another transmembrane protein, Smoothened. Smoothened transduces downstream signals that activate the Gli family of transcription factors leading to target gene induction and enhanced cell proliferation.

The Sonic Hedgehog Pathway

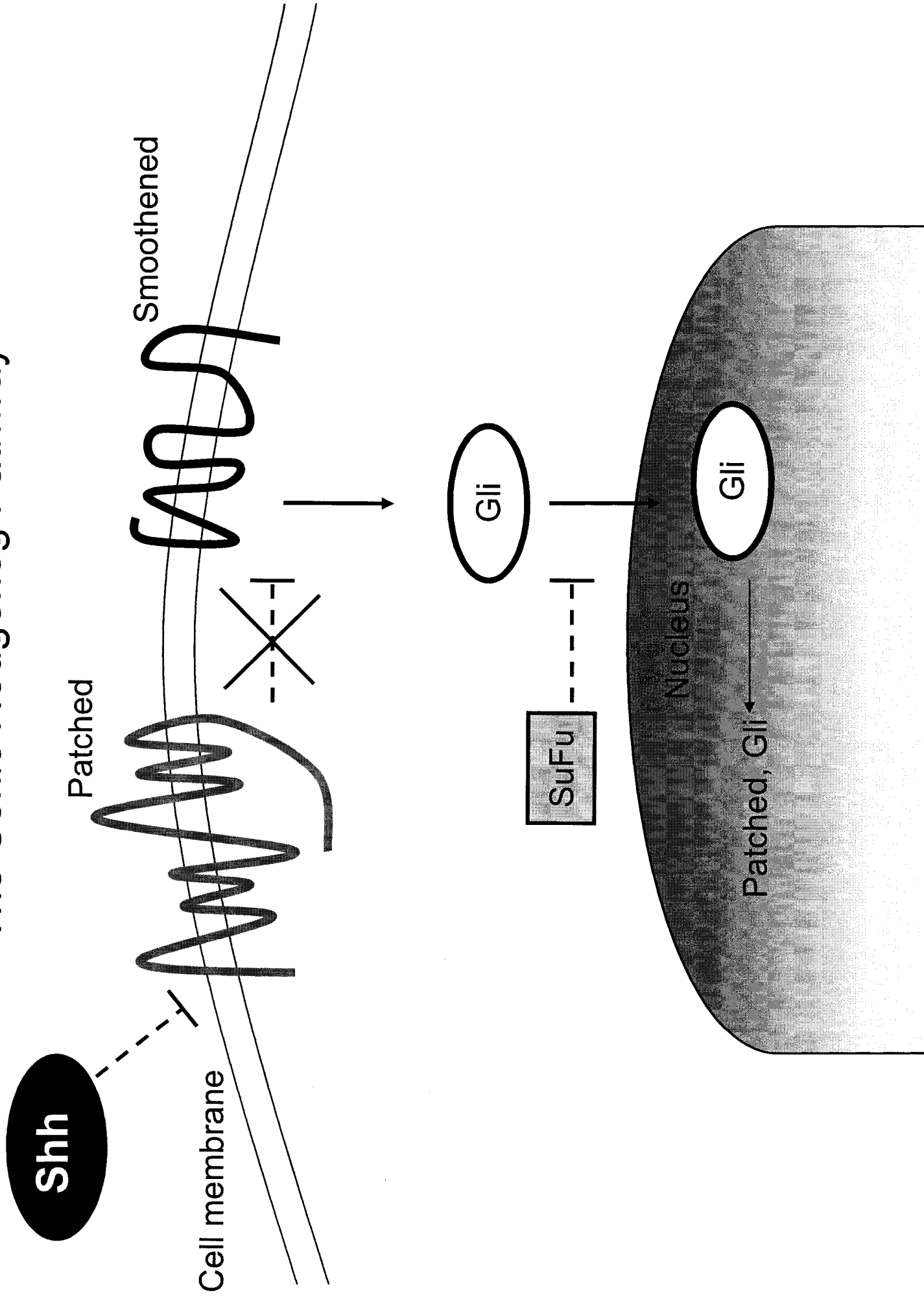


Figure 1.3: The Wnt signaling pathway. Secreted Wnt family proteins bind to the Frizzled receptors and inactivate GSK3 β , reducing phosphorylation and degradation of β -catenin. Accumulation of intracellular β -catenin leads to its nuclear translocation, where it binds to members of the Lef/Tcf family and converts them into transcriptional activators. Complexes of β -catenin and the Lef/Tcf family induce expression of cyclin D1 and c-myc promoting cell cycle progression. In the absence of Wnt, β -catenin is phosphorylation and targeted for degradation by the “destruction complex” composed of GSK3 β , Axin, and the tumor suppressor, adenomatous polyposis coli (APC).

The Wnt Pathway

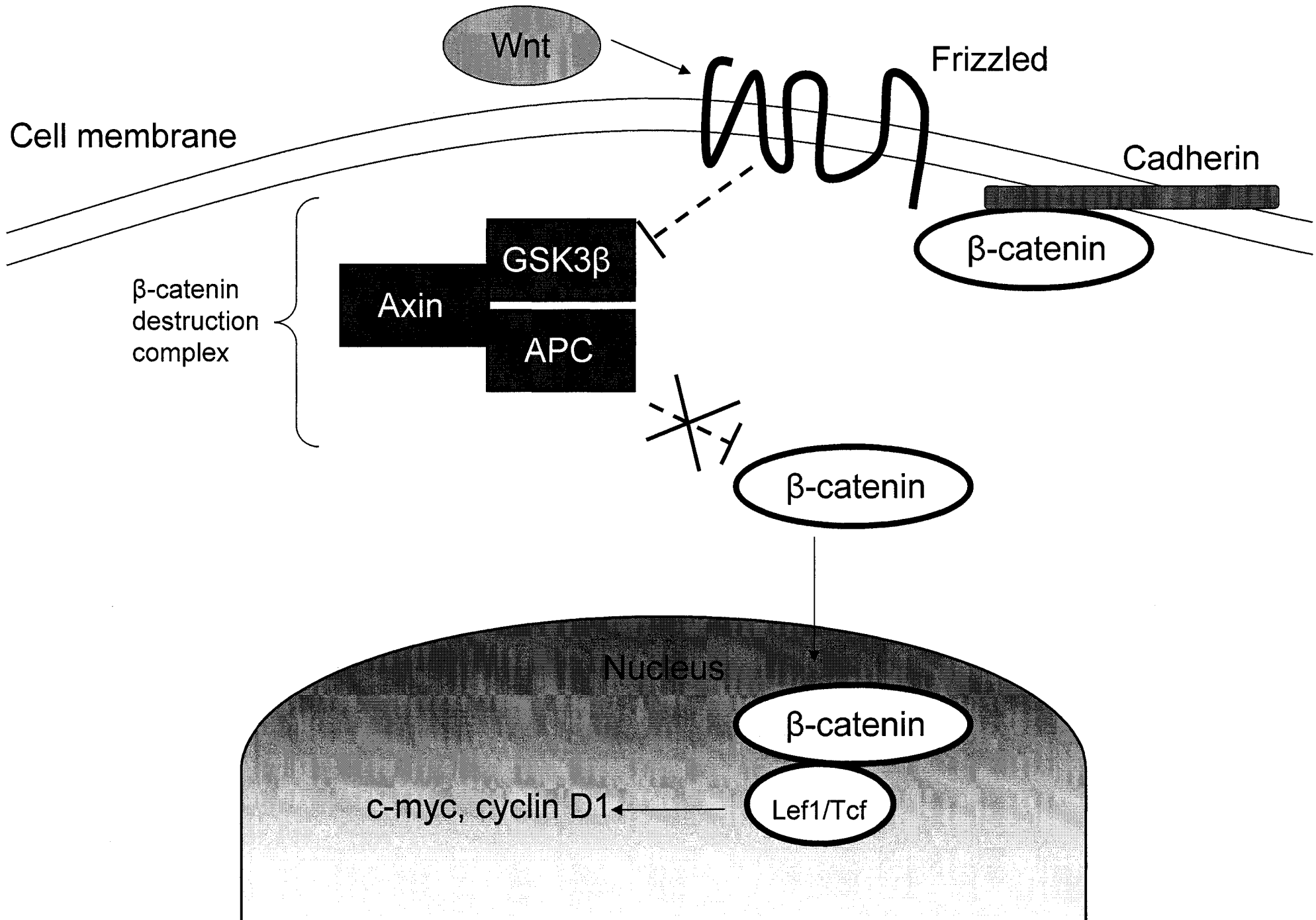


Figure 1.4: Hematoxylin and Eosin staining of C6 astrocytoma spheroids implanted into three-dimensional type I collagen gels over 22 days. During the first 3 days, the invasion rate is high, and cells reach an average of 800-1000 μm from the spheroid. After 6 days in culture, a necrotic center begins to develop and is accompanied by the appearance of nuclear pleomorphism. After 22 days in culture, the outer proliferating rim surrounds an extensive necrotic region, and invasion into the collagen type I gel is minimal. Scale Bar: 200 μm .

Histology of C6 astrocytoma spheroids in three-dimensional collagen type I gels

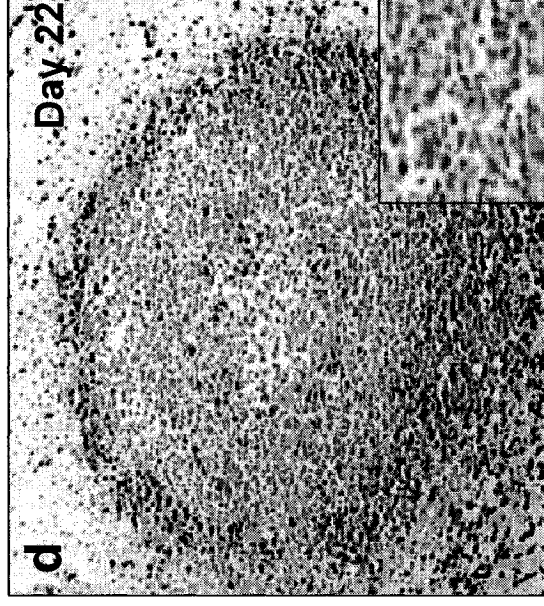
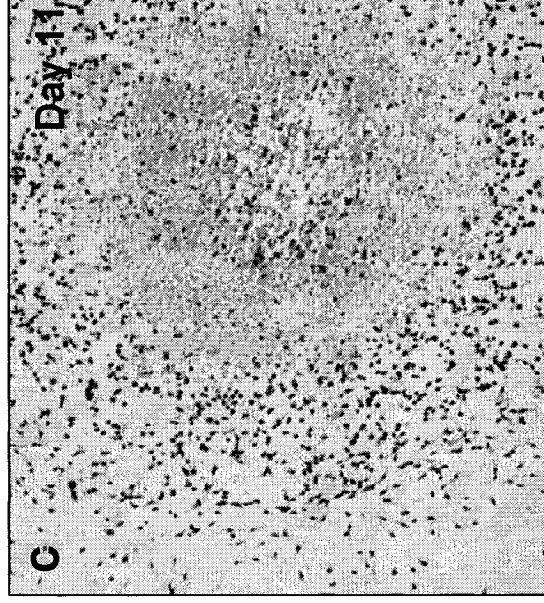
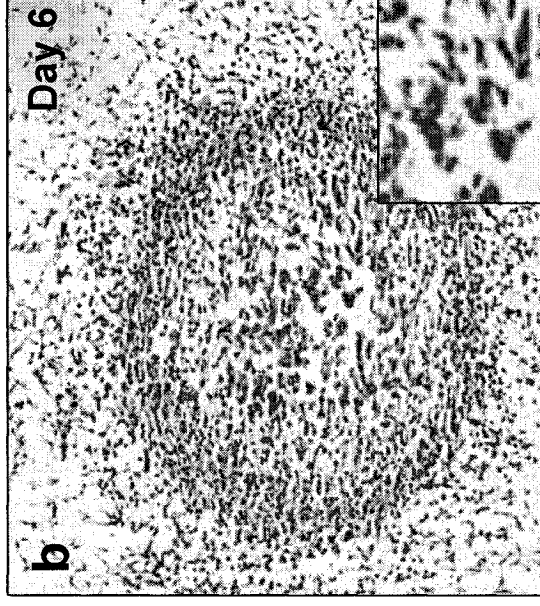
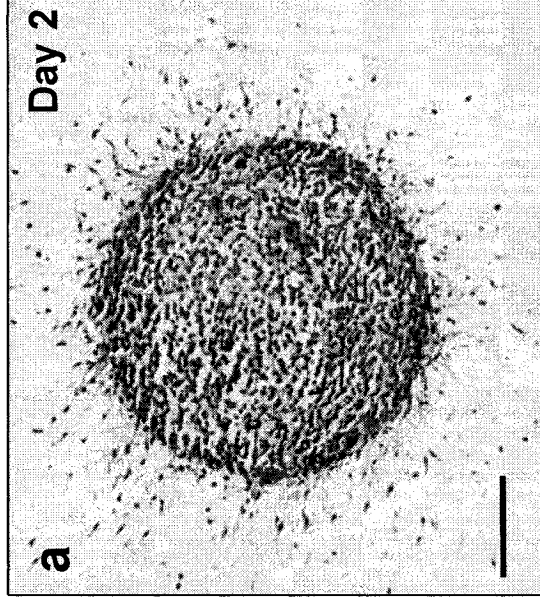
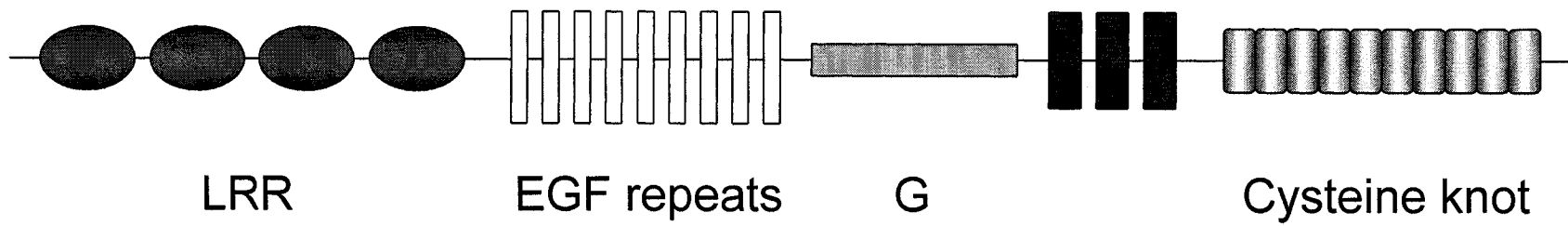


Figure 1.5: Schematic depicting the structure of prototypical Slit and Robo proteins. The mammalian Slit protein contains an N-terminal signal peptide, four leucine-rich repeats (LRRs), nine (in vertebrates) EGF repeats, and a C-terminal cysteine knot. A typical Robo1 receptor consists of five extracellular immunoglobulin (Ig) domains, three fibronectin repeats, and a conserved intracellular region of four cytoplasmic motifs. Robo3 (also known as Rig1) is missing one of the cytoplasmic motifs and Robo4 encodes only two Ig domains, two fibronectin repeats and two cytoplasmic motifs.

Slit Protein



Robo Protein

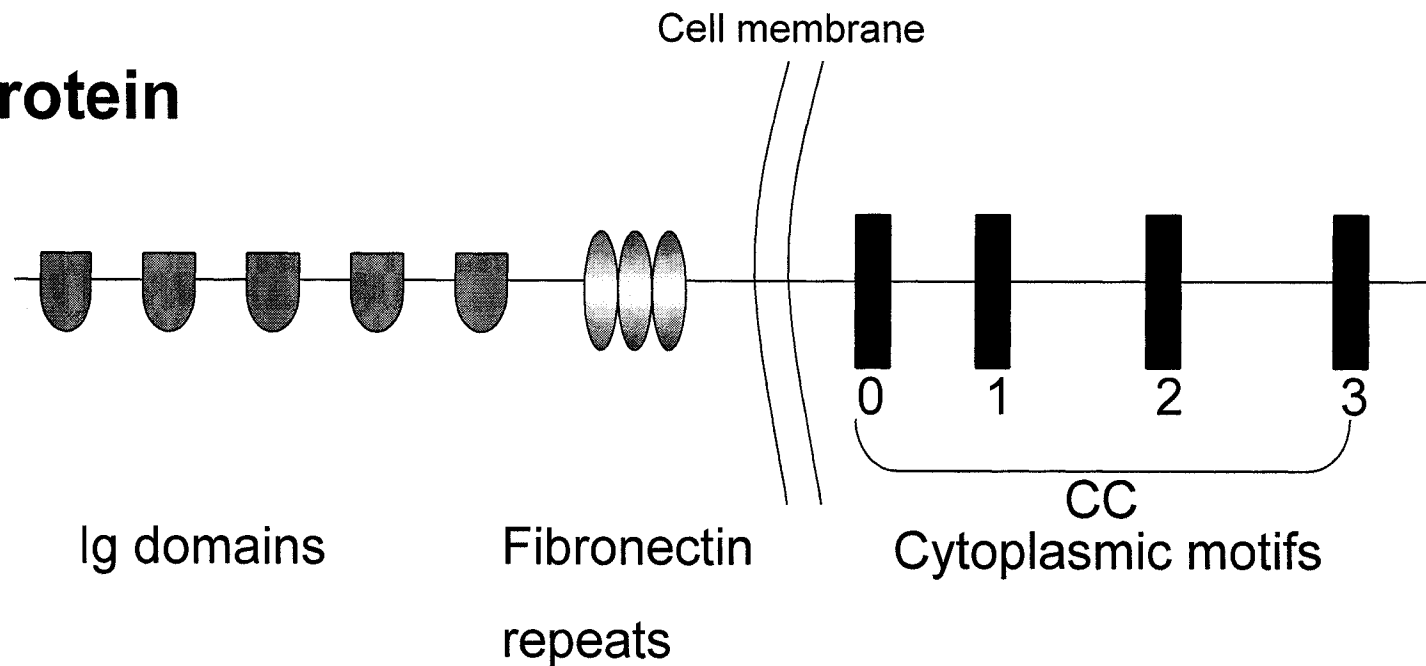
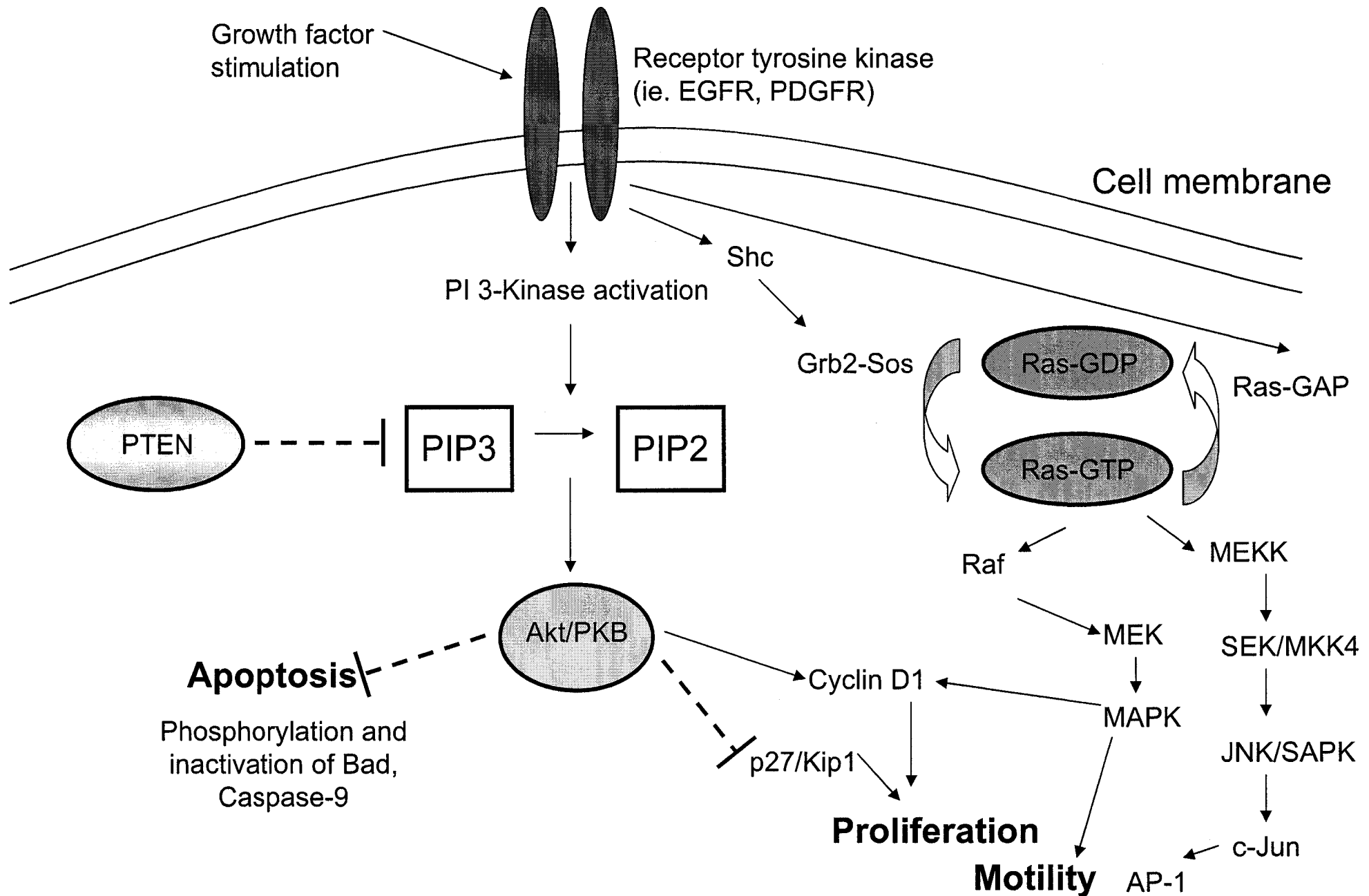


Figure 1.6: The Ras and Akt/PKB signaling pathways. Activation of receptor tyrosine kinases by growth factor stimulation leads to upregulation of PI3K and increased cellular levels of PIP3. PIP3 attracts Akt to the plasma membrane, which then becomes activated, and phosphorylates and inactivates proteins associated with apoptosis leading to increased cell survival. PTEN negatively regulates this pathway by catalyzing PIP3 to PIP2 and reducing Akt activation. In this scheme, cells are more likely to undergo apoptosis. In the absence of PTEN, cell survival and proliferation increase, thereby promoting tumorigenesis and the likelihood of forming a GBM. Growth factor stimulation also leads to Ras activation that is accompanied by Raf recruitment to the membrane followed by phosphorylation of MEK and the MAPK proteins respectively.

Ras and Akt signaling pathways



Chapter 2: Evidence for a secreted chemorepellent that directs glioma cell invasion

2.1 ABSTRACT

Secreted chemotropic cues guide the migration of neuronal and glial cell precursors during neural development. It is not known if chemotropism contributes to directing the invasion of brain tissue by glioma cells. A model system has been developed that allows quantification of invasive behavior using glioma spheroids embedded in collagen gels. Here we provide evidence that glioma spheroids secrete a chemorepellent factor(s) that directs cells away from the spheroid and into the collagen matrix. The relationship between total invasion, cell number, and implantation distance suggests that glioma cells respond to a gradient of the chemorepellent cue(s) that is well established at 48 hours. C6 astrocytoma cells normally invade the collagen at an angle perpendicular to the spheroid edge. In contrast, an adjacent spheroid causes cells to turn away from their normal trajectory and slow their rate of invasion. Astrocytoma cells are repelled by an adjacent glioma spheroid but rapidly infiltrate astrocyte aggregates, indicating that astrocytes do not express the repellent cue. Uniform concentrations of repellent factor(s) in spheroid conditioned medium overwhelm endogenous gradients and render glioma cells less able to exhibit this chemotropic response. Concentration gradients of spheroid conditioned medium in cell migration assays also demonstrate the chemorepellent cue(s) tropic effect. Our findings indicate that glioma spheroids produce a secreted diffusible cue(s) that promotes glioma cell invasion. Identification of this factor(s) may advance current therapies that aim to limit tumor cell invasion.

2.2 INTRODUCTION

Cell migration occurs during development, wound healing and also during tumor invasion and metastasis. Secreted proteins have been shown to function as chemotropic cues that guide neuronal and glial precursors in the developing central nervous system (Tessier-Lavigne and Goodman, 1996; Dickson, 2002). Long-range secreted chemotropic guidance cues such as the netrins, semaphorins and hepatocyte growth factor/scatter factor guide neuronal and glial cell migration (Ebens et al., 1996; Kennedy et al., 1994; Sugimoto et al., 2001; Yee et al., 1999). The slit family of extracellular proteins not only plays a role in axon guidance (Wang et al., 1999; Brose et al., 1999; Kidd et al., 1999; Li et al., 1999) and neuronal migration (Wu et al., 1999), but also leukocyte chemotaxis (Wu et al., 2001) and tumor angiogenesis (Wang et al., 2003). Other studies have used neural stem cells to track astrocytic tumors *in vivo* providing evidence for positive chemotropism in experimental intracranial glioma models (Aboody et al., 2000). These investigations have prompted further analysis of potential mechanisms for glioma chemotropism in both two- and three- dimensional *in vitro* systems.

Malignant astrocytomas are the most common primary supratentorial cerebral neoplasms in adults (Chicoine and Silbergeld, 1997). Thought to arise from astrocytes or astrocytic precursors, their morphological heterogeneity often makes conclusions about their origin difficult (Lopes et al., 1995). The hallmark of malignant astrocytic tumors lies in their ability to rapidly invade the brain and disrupt the normal tissue architecture (Uhm et al., 1997). Despite surgical removal and other available treatment modalities, diffuse infiltrative growth of the remaining invasive cells leads to recurrence and death within 1-2 years of diagnosis (Berens et al., 1990). Studies are presently focused on identification

of the diffusible molecules and cell signaling cascades that result in glial tumor cell migration and invasion.

Researchers have developed several methods of producing tumor cell aggregates or “spheroids” to study tumor invasion in three-dimensions. Sutherland et al. (1971) were the first to produce spheroids from a rotating cell suspension of Chinese hamster V79 lung cells in spinner culture. We have adapted this system for glioma cells and utilized this model for quantification of invasive behavior using glioma spheroids as well as human tumor explants in collagen gels (Tamaki et al., 1997; Bauman et al., 1999a; Bauman et al., 1999b). This three-dimensional spheroid implantation model has been used to elucidate the dynamics of the invasive paradigm in collagen type I gels (Vitrogen 100) (Corcoran and Del Maestro, 2003; Corcoran et al., 2003; Del Maestro et al., 2001). Using this system, it is possible to evaluate both long-range and contact-mediated tropic mechanisms using co-cultures of glioma spheroids and/or normal brain aggregates in a three-dimensional environment.

Studies have suggested that glioma spheroids release a factor(s) that directs cells away from the spheroid and into the three-dimensional matrix (Tamaki et al., 1997; Del Maestro et al., 1997). A direct correlation exists between the development of larger spheroids exhibiting hypoxic and necrotic centers and invasive rate (Tamaki et al., 1997). These findings led to the hypothesis that a repellent factor(s) is secreted by glioma spheroids and that a gradient of this repellent cue(s) directs cell invasion away from the spheroid. Here, we test this hypothesis using two-spheroid co-cultures, time-lapse videomicroscopy and cell migration assays. Our findings provide evidence for an

autocrine chemorepellent cue produced by glioma cells that promotes tumor cell invasion.

2.3 METHODS

Spheroid culture and the three-dimensional collagen type I implantation model

C6 (murine astrocytoma) and U251 (human glioblastoma) cells were cultured in Dulbecco's modified eagle medium (DMEM) supplemented with 10% fetal bovine serum (FBS), 125 U/ml penicillin G, 125 µg/ml streptomycin sulfate, and 2.2 µg/ml amphotericin B (Fungizone). Cultures were maintained at 37 °C in a humidified atmosphere of 5% CO₂. Upon reaching confluency, cells were trypsinized using 0.05% trypsin, 0.53 mM EDTA, and 3 X 10⁶ cells/100ml DMEM were seeded into spinner culture flasks and spun at 180 rotations per minute for 3-8 weeks depending on the desired spheroid size (Tamaki et al., 1997). All culture reagents were obtained from Gibco BRL (Invitrogen, Burlington, ON) unless otherwise stated. Both C6 and U251 cell lines were purchased from American Type Culture Collection (ATCC) (Rockville, MD).

A collagen solution was prepared consisting of 3.2 mg/ml collagen type I in 0.012 M HCl (Vitrogen 100) (COHESION, Palo Alto, CA) and 10-fold concentrated DMEM. The pH of the solution was adjusted by the addition of 0.1 M NaOH. From this solution, 500 µl aliquots were added to 24-well culture dishes and spheroids of defined size were implanted into each well using a Pasteur pipette. After gelling at 37 °C in a humidified atmosphere of 5% CO₂ for 30-60 minutes, the gel was overlaid with 500 µl DMEM + 10% FBS or 250 µl DMEM + 250 µl of medium conditioned by C6 spheroids, U251 spheroids, or fetal human astrocytes. Cell invasion was assessed daily using an inverted phase contrast light microscope. Total invasion distance was calculated at the same time each day from the centre of the spheroid to the population of invasive cells most distant from the spheroid. The original radius was subtracted from these values, and

measurements were taken after 24 hours (time-lapse videomicroscopy) and 9 days (conditioned medium experiments).

Newborn rat astrocytes and U251 aggregate culture

Astrocytes were obtained from the cortex of newborn Sprague Dawley rat cortex and maintained as a mixed glial culture for 2-3 weeks in DMEM supplemented with 10% FBS. Enriched populations of astrocytes were obtained as described (Armstrong, 1998) and hanging-drop aggregates were prepared as described (Corcoran and Del Maestro, 2003; Corcoran et al., 2003; Kennedy et al., 1994). Briefly, confluent cultures of newborn astrocytes and U251 cells were washed in phosphate buffered saline (PBS), trypsinized (0.05% trypsin/0.53 mM EDTA) and resuspended in a small volume of media. Twenty microliter drops containing an equal amount of cells (25,000 cell/drop for U251 cells and 45,000 cells/drop for astrocytes) were suspended from the lids of 100 mm Petri dishes for 2-3 days. Cell aggregates were harvested using a sterilized spatula, and placed on 2% agar/PBS base-coated 100 mm Petri dishes for 2-3 days and then individually implanted into three-dimensional type I collagen gels adjacent to C6 astrocytoma (newborn astrocytes) or U251 glioblastoma spinner culture spheroids (U251 drop aggregates).

Human biopsy spheroids and human fetal astrocytes

The Haukeland Hospital ethics board in Bergen, Norway approved collection of human tumor tissue. Glioblastoma tumor fragments 1 cm or smaller in size were obtained at surgery. The specimens were collected from macroscopically viable tumor regions corresponding to areas of contrast enhancement on computerized tomography (CT) and magnetic resonance (MRI) scans. The specimens were immediately transferred to test tubes containing complete growth medium consisting of DMEM, supplemented with

10% heat-inactivated newborn calf serum, 2% L-glutamine, 100 IU/ml penicillin and 100 IU/ml streptomycin.

Human biopsy spheroids were prepared as described (Bjerkvig et al., 1990). Briefly, glioblastoma tumor tissue was cut into 300-500 μm pieces and incubated in 80- cm^2 tissue culture flasks base-coated with 10 ml 0.75% agar (Difco, Detroit, MI) in complete growth medium. The biopsy spheroids were maintained at 37 °C in a humidified atmosphere of 5% CO_2 , and medium was changed once a week. After 3-4 weeks in culture, spheroids with diameters between 200-400 μm were selected for implantation as described above. Confocal scanning laser microscopy using Cell Tracker dyes was carried out using a BioRad MRC 1000 (BioRad, Hertfordshire) microscope.

Human fetal astrocytes were prepared from fetal CNS tissue as previously described (Ladiwala et al., 1998). Briefly, human fetal CNS tissue was obtained at 12-16 weeks gestation following Canadian Institutes of Health Research (CIHR) guidelines. The tissue was mechanically dissociated using a scalpel and then treated with 0.25% trypsin and 50 $\mu\text{g}/\text{ml}$ DNase for 45 min at 37 °C. Dissociated tissue was passed through a 130 μm mesh, washed twice with PBS and plated onto tissue culture flasks in MEM supplemented with 5% FCS. Populations of proliferating fetal astrocytes were obtained after three to four passages and used to prepare hanging drop aggregates for collagen implantation as described above.

Cell Tracker Dye Labeling and spheroid co-culture quantification

Stock solutions of 10 mM CellTracker Green CMFDA (5-chloromethylfluorescein diacetate) and Cell Tracker Orange CMTMR (5-(and 6)-(((4-chloromethyl) benzoyl)amino) tetramethylrhodamine) (Molecular Probes, Eugene, OR)

were prepared in DMSO, diluted to 25 μM in DMEM + 10% FBS and used for cell labeling. Spheroids were collected from spinner culture and allowed to settle. Conditioned media was removed and replaced with 1 ml 25 μM Cell Tracker Green or Cell Tracker Orange solution. The spheroids were placed on a rocker in a 5% CO_2 incubator for 20 minutes and then washed twice with DMEM + 10% serum. Fluorescently labeled spheroids were implanted both alone and adjacent to unlabeled C6 and U251 spheroids (400-600 μm) at various distances, and photographed 24 and 48 hours post-implantation. Co-cultures were imaged using a Retiga 1300 CCD digital camera (Q Imaging, Burnaby, BC) mounted on an Axiovert 200M microscope (Carl Zeiss, Toronto, ON) and Northern Eclipse 6.0 time-lapse software (Empix Imaging Inc., Mississauga, ON). Fluorescently labeled spheroids were divided into four quadrants with respect to the position of the adjacent spheroid (quadrant A). The total cell number and invasive distance per cell in each quadrant were calculated for both single spheroids and two-spheroid co-cultures.

Time-lapse videomicroscopy

Spheroids were cultured as described, and individual astrocytoma spheroid implants between 450 and 600 μm were prepared for time-lapse videomicroscopy. For two-spheroid co-cultures, C6 astrocytoma spheroids were implanted approximately 300 μm apart. Cultures were maintained at 37°C and 5% CO_2 using a heating microscope stage including a 37-2 digital temperature control unit (Carl Zeiss, Toronto, ON). Invading cells were imaged for 24 hours using a Retiga 1300 CCD digital camera mounted on an Axiovert 25 microscope and Northern Eclipse 6.0 time-lapse software. One still image was taken every four minutes compressing 20-24 hours into

approximately 30 seconds of video (Corcoran and Del Maestro, 2003). For each video, invasion rate and deviation from the expected invasive path (angle change from perpendicular) were calculated for individual C6 cells. Randomly selected cells were followed for single spheroid controls and compared with cell measurements obtained from spheroid co-cultures.

Spheroid/ glass bead controls

Individual C6 spheroids approximately 450-600 μm in size were prepared and implanted as stated in three-dimensional type I collagen gels. Glass beads (Sigma-Aldrich Co. Canada Ltd., Oakville, ON) 425-600 μm in size were washed in 95% ethanol followed by DMEM + 10% FBS before implanting them adjacent to C6 spheroids. Six 24 hour videos were recorded, and the angle of deviation measured.

Confocal scanning laser microscopy

C6-C6, C6-astrocyte and U251-human fetal astrocyte co-cultures were labeled with Cell Tracker Green CMFDA and Cell Tracker Orange CMTMR, implanted into collagen and analyzed using a LSM 510 confocal scanning laser microscope (Carl Zeiss, Toronto, ON) and a 10X objective. Cell Trackers were detected with argon 2 (488 nm) and helium-neon (543 nm) lasers for the green and orange fluorescent probes respectively. Samples were optically sectioned from the surface to the spheroid centre with 12 μm between each slice, and images 1024 X 1024 pixels were collected. Human biopsy spheroids were similarly labeled and analyzed using a BioRad MRC 1000 confocal scanning laser microscope (BioRad, Hertfordshire, UK). Co-cultures were optically sectioned from the surface to the spheroid centers with 16 μm between each slice.

Conditioned medium experiments

Conditioned medium was collected from C6 and U251 spinner cultures at various time points to assess the effect of spheroid size on the quantity of the hypothesized chemorepellent cue secreted. Conditioned medium was also collected from confluent monolayer cultures of human fetal astrocytes. C6 and U251 spheroids were implanted into collagen type I gels as described above and overlaid with 500 μ l DMEM + 10% FBS or 250 μ l conditioned medium 250 μ l DMEM +10% FBS. Medium was changed every three days, and measurements were taken daily for 9 days.

Transwell migration assays

Migration assays were performed using 24-well transwell units with 8 μ m polycarbonated filters (Corning Costar, Cambridge, MA). The lower chamber was filled with 500 μ l DMEM + 10% FBS or 500 μ l conditioned medium from C6 spinner culture spheroids. C6 and U251 glioblastoma cells were harvested, fluorescently labeled using 25 μ M Cell Tracker Green as described above, and 2.0×10^4 cells in 100 μ l DMEM + 10% FBS or C6 spheroid conditioned medium were placed in the upper chamber. Cells were left for 20 hours at 37°C, and unmigrated cells on the upper side were removed with a cotton tip applicator. Cells remaining in the lower chamber were counted using an Axiovert 200M microscope at 10X magnification. Each value represents the average of 4 individual wells.

Statistical Analysis

All tests were performed using SPSS Graduate Pack 9.0 statistical software (SPSS Inc., Chicago IL). Descriptive statistics including mean and standard error of the mean along with one-way ANOVA's, independent sample t-tests and Tukey's test for multiple comparisons were utilized to determine significant differences between pairs for all experiments. P values less than 0.05 were considered significant.

2.4 RESULTS

Glioma cells invade away from spheroids grown in 3-dimensional collagen gels

When a glioma spheroid is cultured in a 3-dimensional collagen gel, cells leave the spheroid and invade at an angle nearly perpendicular to the spheroid surface where the cell detaches (Fig. 2.1). Although this behavior has been well described (Tamaki et al., 1997; Del Maestro et al., 2001), the factors regulating movement of these cells as they invade the surrounding matrix are not well understood. Here, we provide evidence that a spheroid derived repellent cue directs the invasion of these cells away from the glioma cell mass.

Inhibition of glioma cell invasion by the spheroid-derived cue is distance and time dependent

We first tested the hypothesis that a spheroid derived repellent cue might direct the invasion of glioma cells in a distance and time-dependent manner. Spheroids were co-cultured and the distance and time over which this activity affects glioma cell invasion were monitored. Co-cultures were labeled using different cell tracker fluorescent dyes before implanting them into the collagen gel. This labeling allows for identification of individual cells from each spheroid during glioma cell invasion. Previous studies with fluorescent labels or cell markers have demonstrated an adverse effect on glioma cell migration in two-dimensions (Goldbrunner et al., 1997; Vince et al., 1997). Data obtained in our laboratory show that the cell trackers used in this study do not influence invasion distances in the three-dimensional implantation model (data not shown). C6 spheroids were dyed with Cell Tracker Green CMFDA and implanted at various distances apart from unlabeled spheroids C6 or U251 spheroids. After 24 and 48 hours, cultures were

photographed, and cell number and invasion distance quantified for each labeled spheroid quadrant (Fig. 2.2a). Figure 2.2 presents the analysis of the distance traveled by individual cells in each quadrant after 24 hours. There was no significant difference in the total invasion distance for all four quadrants in single spheroid controls (N=8) (Fig. 2.2b). When the co-cultures were implanted a short distance apart (1-100 μm), the invasion into quadrant A was significantly less than values obtained for the remaining quadrants (N=5) (Fig. 2.2c). With distances greater than 100 μm , cell invasion into quadrant A, although lower, was not significantly different from the other quadrants for C6-C6 co-cultures (Fig. 2.2d). A similar pattern was observed when C6 spheroids were co-cultured with U251 glioblastoma spheroids although the effect was significant over greater distances of 100-400 μm (Fig. 2.2 e,f). These findings provide direct evidence for a distance dependent effect of a cue secreted by the glioma spheroid.

If the repellent cue only affected invasion but not detachment, equivalent numbers of cells would be seen in each quadrant despite decreases in total invasion. To test this hypothesis, total cell number in each quadrant was analyzed for various implantation distances. For single spheroid controls, there was no significant difference in cell number between the four quadrants (N=8) (Fig. 2.3b). Addition of the second C6 or U251 spheroid resulted in a decrease in the number of cells in the quadrant facing the adjacent spheroid (Fig. 2.3c-f). Lower cell numbers were found in quadrant A when the C6 spheroids were co-cultured 1-100 μm apart (N=5) and 100-200 μm apart (N=7) (Fig. 2.3-d). A significant decrease in the cell number in quadrant A was also seen for C6-U251 co-cultures implanted 1-400 μm apart. In C6 co-cultures implanted 100-200 μm apart, there was a non-significant increase in the number of cells in quadrant B and D; however,

this was not the case for all remaining co-cultures (Fig 2.3. c,e,f). The general failure of cells to egress into the both adjacent B and D quadrants combined with the decrease in the cell number in quadrant A suggest that a chemorepellent(s) may also decrease cell detachment from the glioma spheroid.

To demonstrate that the effects described above are attributed to a secreted and not a contact-mediated chemorepellent cue(s), single C6 spheroids and C6-C6 co-cultures were implanted further apart and analyzed at 48 hours. For single C6 spheroids, there was no significant difference between total cell number and individual cell invasion distances in each quadrant (Fig. 2.4 a,d). The repulsive effect could be seen for C6-C6 co-cultures at increased implantation distances with an average 59% decline in cell number compared to the remaining quadrants at 250-400 μm and 40% at 400-600 μm (Fig. 2.4 b,c). There was no significant difference between the number of cells in quadrant B-D (Fig. 2.4b,c). Cell invasion into quadrant A was significantly less than invasion into the remaining quadrants at 48 hours (Fig. 2.4 e,f). These findings demonstrate that a secreted cue(s) and not a contacted-mediated factor directs glioma cells away from the repellent source.

Glioma cells turn away in response to a second spheroid

The effect on glioma cell invasion could be produced by a kinetic effect of a cue that slows cell invasion, or through a tropic effect of a cue that directs cell invasion, or by a cue that exerts both kinetic and tropic effects on the invading cells. To investigate the mechanism of action of the secreted repellent cue on individual cells, glioma spheroids were implanted into collagen type I gels and imaged using time-lapse videomicroscopy. For single spheroid controls, C6 astrocytoma cells leave the spheroid at angle nearly perpendicular to the spheroid surface where the cell detaches (N=46, Fig. 2.1). In

contrast, when two spheroids were co-cultured adjacent to each other in the collagen gel, they changed their expected trajectory and turned away from the second spheroid when the cells reached the mid-point between the two spheroids (N=45) (Fig. 2.5 a-c). In addition to this evasive turning response, a subset of C6 astrocytoma cells appeared to stall and remained stationary between the two spheroids. These cells maintained a ruffled appearance throughout the time period of observation and did not extend invadopodia (Figure 2.5 b-c). Quantification of the turning angle observed for individual cells invading toward an adjacent spheroid indicated a deviation from perpendicular invasion ($63.7 \pm 4.5^\circ$), that was significantly different from invading cells from single spheroids (Fig. 2.5g).

To determine if migratory turning is caused by a physical modification in the matrix rather than a chemical factor, we repeated the above experiments replacing one of the spheroids with a glass bead. Invading C6 cells from the spheroid followed a perpendicular trajectory as did cells from single spheroid controls (N=25) (Fig. 2.5 d-f). The mean angle of deviation from the perpendicular was $14.9 \pm 2.6^\circ$, not significantly different from data obtained for single spheroid controls ($16.7 \pm 0.8^\circ$) (Fig. 2.5g). Cells continued along this path until they contacted the glass bead. In some cases following contact, the cells appeared to repeatedly bounce off the bead surface (data not shown). After 48 hours, the invading cells proceeded around the bead's surface (data not shown). At no point did the glioma cells change directions and migrate back toward the spheroid. To determine if the spheroid derived cue exerts an influence on the rate of glioma cell invasion, cell invasion rate was measured in cultures containing either a single spheroid or two spheroid co-cultures. Invading cells from two spheroid co-cultures infiltrated the

gel at rates significantly lower ($12.6 \pm 0.9 \mu\text{m/hr}$) than cells derived from single spheroid controls ($16.7 \pm 0.8 \mu\text{m/hr}$) ($P < 0.01$) (Fig. 2.5h).

These results provide evidence for the presence of a repellent cue secreted by glioma spheroids that directs invading glioma cells away from the spheroid mass. They indicate that the repellent cue secreted by the spheroid exerts a tropic effect by causing glioma cells to turn. The decrease in glioma cell invasion rate may be attributed to the presence of a more shallow gradient with increasing distances from the spheroids. These findings do not differentiate between the actions of one or more cues.

The chemorepellent cue is not expressed by astrocyte aggregates

To investigate the specificity of expression of the glioma spheroid derived repellent cue, we replaced one of the spheroids with an aggregate of primary newborn rat astrocytes. C6 spheroids implanted adjacent to newborn rat astrocyte aggregates invade in the direction of the astrocyte aggregates within the first 24-72 hours (Fig. 2.6). The absence of an inhibitory effect on invasion was found for both co-cultures in direct contact or implanted 100-200 μm apart ($N=12$ and $N=5$ respectively). Newborn astrocytes also appeared to invade into C6 spheroids within the first 72 hours (Fig. 2.6). Extensive invasion is seen on the side proximal to the C6 spheroid; however, relatively little invasion is observed into the type I collagen gel around the rest of the astrocyte aggregates ($N=12$). These findings provide evidence that astrocytes neither produce the repellent factor nor respond to it. To test the possibility that differences in the cell culture method might account for the differences observed, the hanging drop method that was used to produce the newborn rat astrocyte aggregates was also used to produce aggregates of U251 cells. U251 aggregates repelled invasion of U251 cells and C6

similar to the findings described above for U251 spheroids (data not shown). These findings provide evidence that the spheroid derived repellent cue is not ubiquitously expressed by all glial cell types, but might be a characteristic acquired by the glioma cells during their transformation process.

To determine the extent that a glioma derived repellent cue might inhibit the infiltrative capacity of astrocytes and glioma cells, C6-C6 astrocytoma, human glioblastoma biopsy spheroids, C6-astrocyte and U251-astrocyte aggregate co-cultures were examined using scanning laser confocal microscopy to visualize the co-culture centers. When two C6 spheroids were implanted 1-200 μm apart, despite spheroid growth, overlap was predominantly restricted to the fusion site with very few cells infiltrating the adjacent spheroid or invading around it after 72 hours (Fig. 2.7 a-c). Similar results were obtained using C6-U251 and U251-U251 glioblastoma co-cultures (data not shown). C6 spheroids implanted adjacent to fetal human astrocyte aggregates or aggregates of newborn rat astrocytes, invaded the aggregates 24-72 hours after implantation (Fig. 2.7 d-i). Similar results were obtained for U251 drop aggregate - human fetal astrocyte aggregate co-cultures after 48 hours (Fig. 2.7j). Confocal analysis indicated that individual astrocytes did not invade the spheroid after 72 hours (Fig. 2.7 d-j). However, astrocytes invaded both over and around the adjacent spheroid (data not shown). Spheroids derived from different human biopsy cultures exhibited long invadopodia that extended throughout the collagen and around the adjacent spheroid (Fig. 2.7 k-l). Individual human tumor cells did not infiltrate the adjacent spheroid 48 hours after implantation. These results provide further evidence for a glioma derived repellent cue, as inhibition was restricted to glioma spheroid co-cultures and was not found in

glioma spheroid-astrocyte aggregate co-cultures implanted together or a short distance apart.

Conditioned medium from C6 and U251 spheroid culture significantly inhibits glioma invasion

If indeed glioma cells secrete and respond to a repellent factor that exerts a detachment or inhibitory effect as well as a tropic influence, then addition of this factor throughout the matrix should have a net inhibitory effect on invasion from the spheroid. We then determined if medium conditioned by C6 or U251 astrocytoma cells could influence glioma cell invasion. Medium was collected from C6 astrocytoma and U251 glioblastoma spinner culture containing different sized spheroids and applied to spheroids implanted in three-dimensional collagen gels (Fig. 2.8). For C6 astrocytoma spheroids, both U251 and C6 conditioned media had a significant inhibitory effect on invasion (N=4) (Fig. 2.8a). C6 day 33 media had the most significant effect, inhibiting invasion by 44% compared with DMEM + 10% FBS controls (Fig. 2.8a). Similar results were obtained for U251 spheroids, as both U251 and C6 conditioned media had a significant inhibitory effect on invasion (Fig. 2.8b). U251 day 27 and C6 day 30 conditioned media had the most significant effect on invasion at 63% and 44% inhibition respectively (N=4) (Fig. 2.8b). For both U251 and C6 spheroids, conditioned medium collected from larger spheroids, as indicated by higher day number generally had a more significant effect on invasion suggesting that the quantity of the chemorepellent cue(s) secreted is related to the size of the spheroid (Fig. 2.8 a,b). Medium collected from confluent monolayer fetal astrocyte cultures had no significant effect on C6 and U251 spheroid invasion (Fig. 2.8 c-d). These results provide further evidence that glioma spheroids and not astrocytes

secrete a repellent cue(s) that affects glioma cell invasion possibly by inhibiting cell motility in addition to directing cells away from a gradient of the repellent cue(s).

Glioma cells are chemotactically repelled by a gradient of C6 spheroid conditioned medium in cell migration assays

A chemorepellent cue(s) and migration inhibitor are two different phenomena. To determine the chemotactic and chemokinetic properties, transwell migration assays were performed on U251 and C6 cells using medium conditioned by C6 spinner culture spheroids. Because the transwell migration assay does not involve cell detachment from a spheroid in a three-dimensional model, the repellent cue(s)'s ability to directly affect glioma cell migration can be assessed. The number of C6 and U251 cells was higher when C6 conditioned medium was placed in the upper chamber and lower when the medium was placed in the lower chamber (Table 2.1a-b). Interestingly, the number of C6 and U251 cells was even lower when conditioned medium was placed in both chambers to eliminate the gradient (Table 2.1a-b). These results suggest that C6 and U251 astrocytoma cells are chemotactically repelled by a secreted factor(s) from spheroid conditioned medium. However, the observation that a uniform concentration of the repellent cue(s) decreases migration indicates that it also exerts a kinetic effect on glioma cell motility.

2.5 DISCUSSION

This study provides evidence for a tumor-derived chemorepellent cue(s) that directs glioma cell invasion. Previous investigations have focused on chemotropism in glial cell and neuronal precursors (Armstrong et al., 1990; Sugimoto et al., 2001; Kennedy et al., 1994; Jarjour et al., 2003). For example, the directional migration of glial precursors along the optic nerve is guided by the chemorepellent factors netrin1 and semaphorin 3a (Sugimoto et al., 2001). These molecules, known for their directional role in neuronal and axonal migration, originate near the optic chiasm and guide glial precursors along the optic nerve (Sugimoto et al., 2001). Even polypeptide growth factors such as PDGF and extracellular matrix molecules have been shown to elicit a chemoattractive response in glial precursors and type 1 astrocytes respectively (Armstrong et al., 1990).

Glioma chemotropism and growth factors

Studies have examined growth and motility factors such as EGF, bFGF, autocrine motility factor and PDGFbb that act predominantly via chemoattractant mechanisms (Chicoine et al., 1995; Liotta et al., 1986; Engebraaten et al., 1993; Lund-Johansen et al., 1990). Two-dimensional models such as the Boyden chamber chemotaxis and modified radial dish assays have often been used to evaluate tropic effects in glioma cells (Chicoine et al., 1995; Liotta et al., 1986; von Bulow et al., 2001). Checkerboard migration assays have demonstrated potent induction of both melanoma and glioblastoma cell migration towards endothelial cells (von Bulow et al., 2001). However, endothelium-derived chemotactic molecules have yet to be identified (von Bulow et al., 2001).

Although there is some discrepancy in the literature with regards to the effect of

growth factors on glioma cell motility, the differences may be attributed to the variety of model systems employed in different studies (Chicoine and Silbergeld, 1997). In contrast to previous investigations, this study provides evidence for glioma-derived chemorepellent cue in a three-dimensional collagen type I co-culture model. Although the results with the chemotaxis migration assay are also indicative of a secreted repellent(s) in conditioned medium, our spheroid model allows quantification of cell-cell and cell-matrix interactions in a three-dimensional collagen type I environment where cells undergo alterations in morphology and degradative enzyme release (Tamaki et al., 1997; Unemori and Werb, 1986). The use of time-lapse videomicroscopy and still photographs to quantify cell number and total invasion in all quadrants as well as direction changes allow for evaluation of chemotropic mechanisms at various implantation distances and examination of the effect over time.

Evidence for a glioma chemorepellent cue

Using the C6 rat astrocytoma spheroid implantation model, our laboratory first proposed the glioma repellent factor gradient hypothesis based on two observations (Tamaki et al., 1997). Larger spheroids, having well-established areas of hypoxia and necrosis, had higher invasive rates 1-5 days post-implantation, and after 10-13 days, invasion plateaus when cells reach approximately 2000-2500 μm from the spheroid source. We suggested that physically stressful conditions, such as decreased tissue pH, oxygen and metabolic substrate(s) concentrations may lead to generation of a chemotropic repellent factor(s) concentration gradient that results in increased cell invasion from the spheroid and cell invasion arrest when the gradient is no longer present. Larger spheroids, exhibiting extensive stressful microregions, may secrete more

of the factor(s), and consequently further accelerate invasion. A number of scatter growth promoting factors and guidance cues have been tested for their role in the spheroid implantation model; however, none appear to exhibit the proposed repellent factor(s) properties (unpublished data). Platelet derived growth factor (PDGF) AA, BB, basic fibroblast growth factor (bFGF) at concentrations between 10 and 200 ng/ml, as well as conditioned medium from 293T overexpressing secreted slit2 and netrin1 have been added to medium and applied to spheroids implanted in collagen gels. Analysis of glioma spheroids co-cultured with 293T cell aggregates overexpressing slit2 and netrin1 has also been conducted. All experiments have resulted in either an increase in glioma invasion or no effect. Although the data presented in this study support the chemorepellent cue(s) hypothesis, the relationship of the secretion of the factor(s) to the presence of stressful microregions is unclear. Co-cultures consisting of U251 or human biopsy spheroids both exhibit invasion inhibition similar to C6 astrocytoma co-cultures, and these spheroids do not have established areas of necrosis and hypoxia (Corcoran et al., 2003). The apparent higher concentrations of chemorepellent cue(s) from larger spheroids may be related to total cell number.

In this study, a two-spheroid co-culture system was employed using the three-dimensional spheroid implantation model. Based on the repellent factor hypothesis, invading glioma cells should be repelled by an endogenous gradient of a secreted repellent cue derived from the adjacent spheroid. Monitoring cell number and invasion in glioma co-cultures confirmed this hypothesis. Fluorescently labeled glioma cells facing the adjacent spheroid invade the gel and infiltrate the other spheroid less when implantation distances are below 200-400 μm . At implantation distances exceeding 400

μm , the chemorepellent cue(s) does not have a statistically significant effect on cell number and invasion at 24 hours. The effect over this distance is consistent with studies of chemotropic molecules in other systems. Localized sources of floor plate derived chemoattractant re-oriented dorsal spinal cord axons over a mean distance of 243 μm after 40 hours in culture (Placzek et al., 1990). When the co-cultures are examined at 48 hours, there is a significant effect between 250 and 600 μm . These results suggest that the gradient is well established at 48 hours and the chemorepellent cue(s) is secreted. There is a direct correlation between tumor cell number/invasion and implantation distance on the side facing an opposing spheroid. The effect on cell number may reflect a chemorepellent cue(s)' negative influence on proliferation or the ability to detach from the spheroid and invade the gel. Videomicroscopy studies showed cell division between glioma co-cultures, and therefore confirmed that the chemorepellent cue(s) does not influence cell proliferation (data not shown). Data obtained from quadrant cell number analysis suggests a detachment problem. Invading glioma cells in quadrant A did not move into the adjacent B and D quadrants, as cell numbers here were not significantly different from those in the distal C quadrant. The transwell migration assay does not directly assess cell detachment, and can be used to differentiate between chemorepellent cue(s) and glioma cell migration inhibitors. Because both a gradient and a uniform concentration of the repellent cue(s) significantly inhibited glioma cell migration, it seems that the factor exerts both a tropic and a kinetic influence. The inhibitory effects seen with a uniform concentration of glioma conditioned medium on C6 and U251 spheroids also supports a role for the repellent cue(s) in inhibiting glioma cell migration.

Lumsden and Davies (1983;1986) conducted similar quadrant experiments to demonstrate that secreted chemoattractants guide earliest sensory nerve fibers to their peripheral targets. Co-cultures of trigeminal ganglion and peripheral maxillary epithelial target tissue explants were used to demonstrate the presence of a chemotactic molecule(s) guiding trigeminal sensory neurons to their targets (Lumsden and Davies, 1983; 1986). Secreted chemotropic cues such as the netrin and semaphorin families were later identified and shown to play a major role in the neuronal guidance mechanisms seen in previous studies (Tessier-Lavigne and Goodman, 1996).

To further investigate the specific mechanism of action of the chemorepellent cue(s), we imaged C6 rat astrocytoma co-cultures using time-lapse videomicroscopy. Our results are consistent with the concept of a secreted repellent factor since glioma cells changed their expected invasive path in the presence of an adjacent spheroid. A significant deviation from the expected perpendicular angle was found, and this was not related to the presence of a physical object in the glioma cells' path. The decrease in cell velocity seen in co-culture experiments may be related to a change in cell trajectory that renders cells less able to commit their metabolic and cytoskeletal machinery to invade the matrix at rates similar to controls. This effect may be secondary to an alteration in the concentration of the chemorepellent gradient in the microenvironment between the two spheroids. Highly concentrated chemorepellent gradients may also explain why some cells do not invade following detachment when they are in the immediate microenvironment between two adjacent spheroids. Conditioned medium placed in both chambers of the transwell migration assay prevented glioma cell migration in a similar manner.

Astrocyte invasion and migration

The direct relationship between cell number/invasion and implantation distance does not hold true for spheroid-astrocyte aggregate co-cultures. The results obtained using fetal human and newborn rat astrocytes aggregates are consistent with data obtained for confrontation cultures of spheroid/fetal rat brain aggregates on agar (Bjerkvig et al., 1986). Invading glioma cells are not hindered by the presence of the newborn rat astrocyte aggregates and are able to infiltrate the normal fetal rat brain as demonstrated by scanning and confocal laser microscopy (Bjerkvig et al., 1986; Steinsvag, 1985; Nygaard et al., 1995; Engebraaten et al., 1990).

In the light microscopy images, newborn rat astrocytes appear to invade adjacent C6 spheroids. This was clearly seen in both touching co-cultures, and cultures implanted 100-200 μm apart. Confocal microscopy studies revealed that astrocytes are moving over the tumor surface and around the spheroid. These results suggest either the presence of a glioma spheroid secreted or contact-mediated chemoattractant molecule or perhaps a more permissive substrate provided by the spheroid surface. Similar studies using fetal astrocytes demonstrate variable results depending on the substrate employed. Bernstein et al. (1991) showed that C6 glioma cells, but not fetal astrocytes rapidly invade artificial basement membrane substrates. However, when experiments were conducted with hydrated collagen I wafers, both cell types migrated through the entire thickness of the substrate (Goldberg et al., 1992). The invasion displayed in our co-culture assays may reflect not only the substrate difference but also the three-dimensional nature of the model. The use of confocal microscopy is important to distinguish between cells invading a glioma tumor spheroid and cells migrating along its surface.

Although confrontation cultures are commonly used to study glioma invasion, most models utilize aggregates on plastic or agar, and thus do not reconstruct the brain's more complex three-dimensional architecture. A drawback to standard confrontation co-cultures is the use of fetal/newborn rat brain instead of adult brain aggregates.

Glioblastomas are primarily adult supratentorial cerebral neoplasms, and so adult brain aggregates would most accurately represent brain tumor invasion in three-dimensional models (Chicoine and Silbergeld, 1997). Studies with human glioma explant co-cultures and multiple patient white matter tissue samples may further substantiate the chemotropic responses demonstrated here.

A glioma derived chemorepellent cue(s)

The inhibition of glioma invasion by C6 and U251 conditioned medium supports the chemorepellent factor(s) hypothesis. A uniform concentration of factor(s) may have less discernible effect on tumor invasion if the glioma cells respond to an established chemorepellent cue concentration gradient. The data obtained for both quadrant quantification and angle deviation suggest that the glioma cells are responsive to localized higher concentrations of the factor(s). However, a uniform concentration may overwhelm existing endogenous gradients, thus eliminating signaling mechanisms that deter cells away from the spheroid mass. Less able to exhibit a chemotropic response, the glioma cells decrease their overall invasive rate while others may arrest cell movement or exhibit decreased cell detachment. Previous studies using conditioned medium containing secreted chemoattractant molecules also provide evidence for uniform concentration effects (Placzek et al., 1990). When conditioned medium was collected from E13 floor plate and applied to E11 dorsal spinal cord explants, there was extensive axon outgrowth

from the explant edges. This floor-plate derived chemoattractant, later identified as netrin1, appeared to exhibit both directional and possibly outgrowth-promoting properties, as commissural axons respond to both uniform concentrations and gradients of the floor plate factor (Placzek et al., 1990; Kennedy et al., 1994).

Identification of chemotropic secretion products using the spheroid implantation model may shed light on the issue of glial cell movement in the central nervous system. The highly infiltrative nature of some human gliomas such as glioblastoma multiforme and gliomatosis cerebri may be attributed to yet unidentified chemorepellent cues that are secreted by the main tumor mass. These chemorepellent cues may help tumor cells detach and guide them from their source into normal brain architecture (DeAngelis et al., 2002). Similar chemorepellent cues may also play a role in normal brain growth. Knowledge of chemorepellent factors may enable introduction of novel therapies that force cells to change their invasive path, stop or even return to the original resection site thus diminishing the risk of recurrence. Alternatively, chemoattractants may stimulate cells to invade towards and potentially infiltrate gliomas thereby creating the potential to treat brain tumors from the inside out using specific drug biodelivery approaches. Although one must proceed with caution when extrapolating *in vitro* results to the clinical situation, a thorough understanding of chemotropic cues and their influence on glioma invasion is essential, as more advanced therapies may target a combination of chemotropic factors and their downstream effectors.

Conclusions

Our study supports the chemorepellent cue(s) hypothesis. We have provided evidence for a secreted repellent factor that not only exerts a tropic influence by directing glioma cell invasion in the direction of less inhibition but also a kinetic influence by decreasing glioma cell motility. The combined effects on tumor cell invasion make the chemorepellent cue(s) an attractive target for future studies.

Figure 2.1: Single C6 astrocytoma spheroid implanted into three-dimensional type I collagen gel. (a-c) Images extracted from time-lapse videomicroscopy over 24 hours. Objective: 20X. Scale bar = 100 μm .

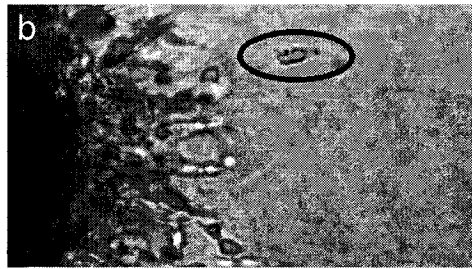
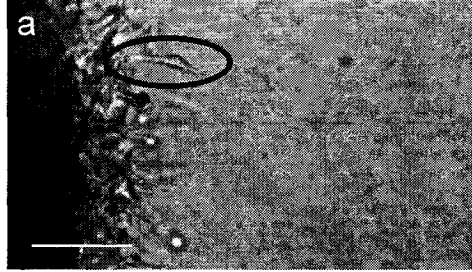


Figure 2.2: Quantification of glioma cell invasion after 24 hr in culture by counting the number of cells invading certain invasion distances from the initial edge of the spheroid in each quadrant. Individual cells were counted 0-75, 75-150, 150-225, 225-300, 300-375, 375-450 and 450+ μm from the spheroid edge. (a) Spheroid quadrant quantification model. Dashed circle represents unlabeled spheroid. (b) Single C6 astrocytoma spheroids (N=5). (c) C6 co-cultures 1-100 μm apart (N=5). (d) C6-co-cultures 100-200 μm apart (N=6). (e) C6-U251 co-cultures 100-200 μm apart (N=5). (f) C6-U251 co-cultures 200-400 μm apart (N=4). Asterisks indicate significant difference at $P < 0.05^*$, $P < 0.01^{**}$ and $P < 0.001^{***}$ when comparing quadrant A to other quadrants.

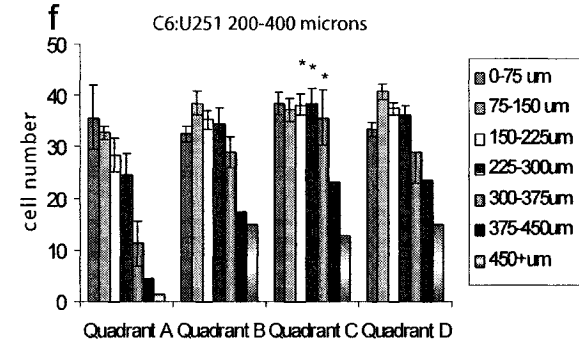
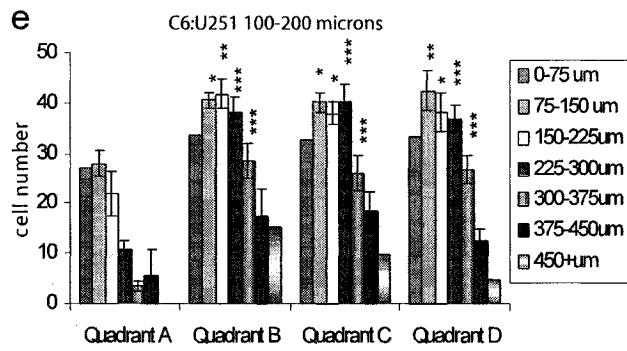
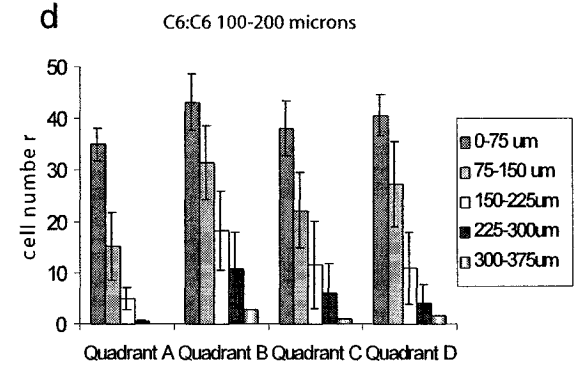
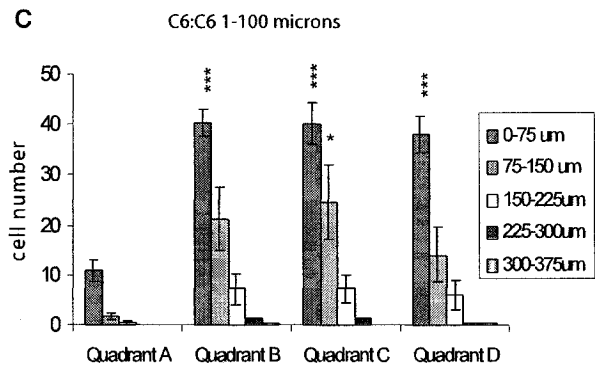
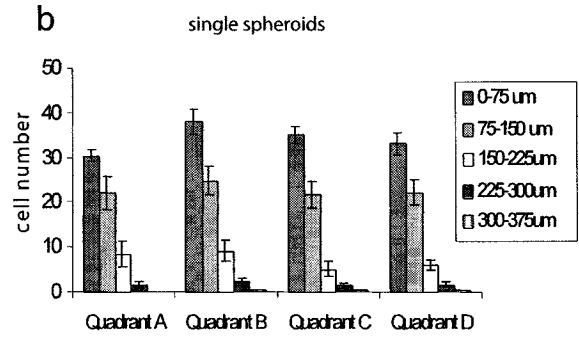
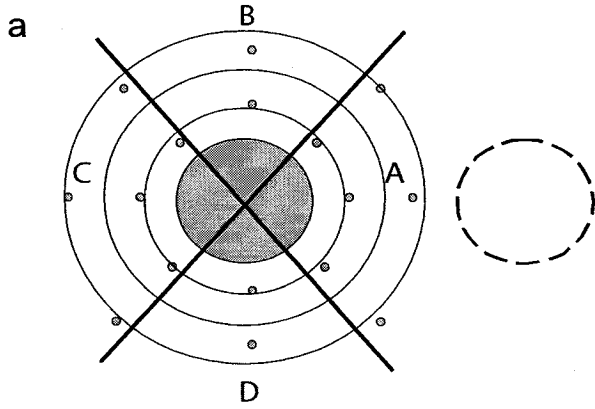


Figure 2.3: Quantification of glioma cell number after 24 in culture. The number of cells in each quadrant was counted for single spheroids and two-spheroid cultures at various implantation distances. (a) Spheroid quadrant quantification model. (b) Single C6 astrocytoma spheroids (N=5). (c) C6 co-cultures 1-100 μm apart (N=5). (d) C6-co-cultures 100-200 μm apart (N=7). (e) C6-U251 co-cultures 100-200 μm apart (N=5). (f) C6-U251 co-cultures 200-400 μm apart (N=4). Asterisks indicate significant difference at $P < 0.05^*$, $P < 0.01^{**}$ and $P < 0.001^{***}$ when comparing quadrant A to the other quadrants.

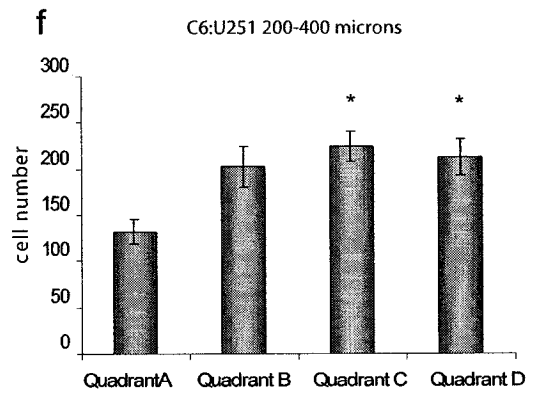
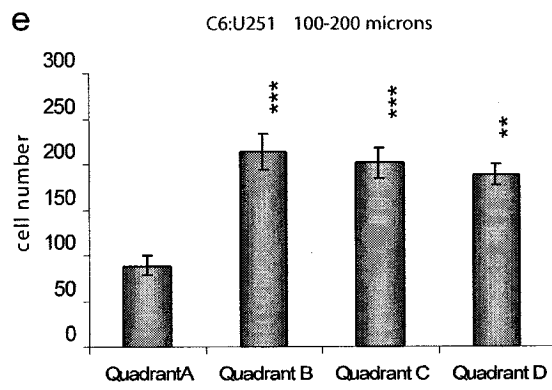
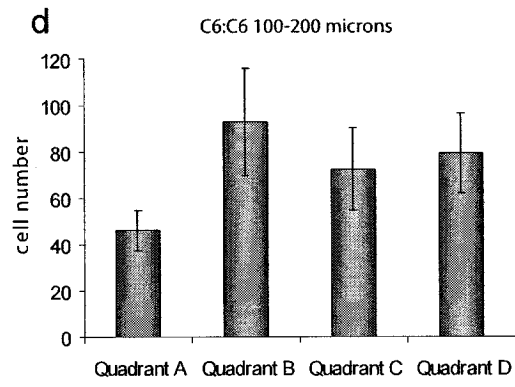
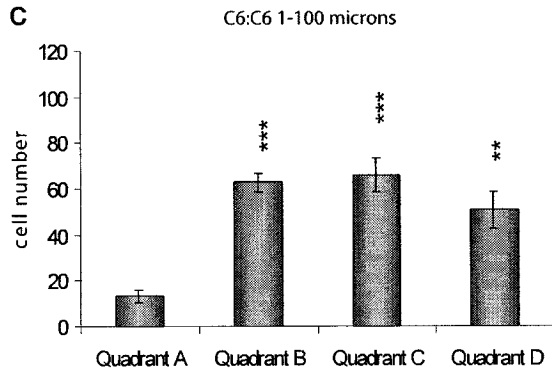
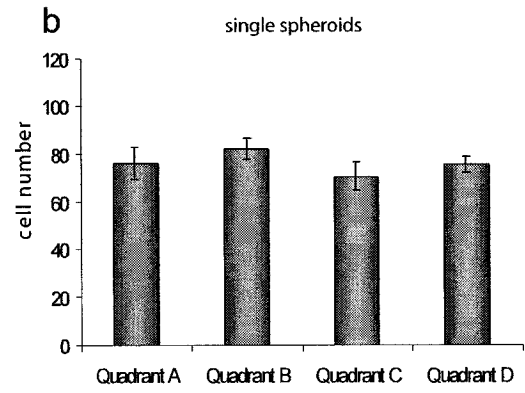
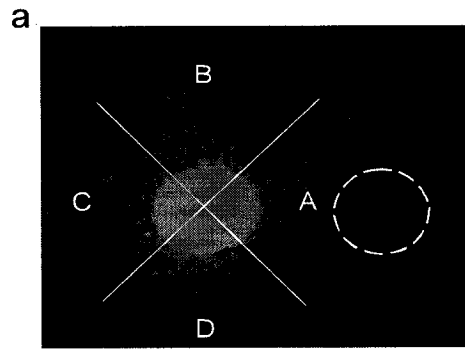


Figure 2.4: Quantification of glioma cell number and invasion distance after 48 hr in culture. (a) Quadrant cell number for single C6 astrocytoma spheroids. (b) Cell number for C6 co-cultures 250-400 μm apart (N=6). (c) C6 co-cultures 400-600 μm apart (N=4). (d) Individual cell invasion distances for single C6 spheroids. (e) Invasion distances for C6 co-cultures 250-400 μm apart (N=6) f) Invasion distances for C6 co-cultures 400-600 μm apart (N=4). Asterisks indicate significant difference at $P < 0.05^*$, $P < 0.01^{**}$ and $P < 0.001^{***}$ when comparing quadrant A to the other quadrants.

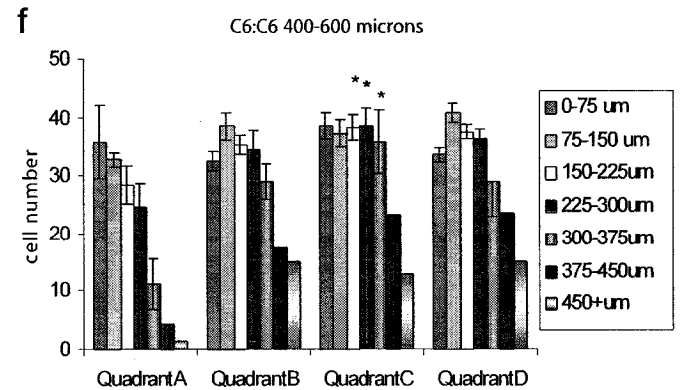
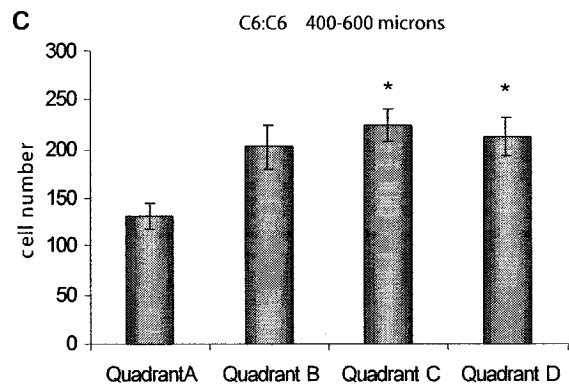
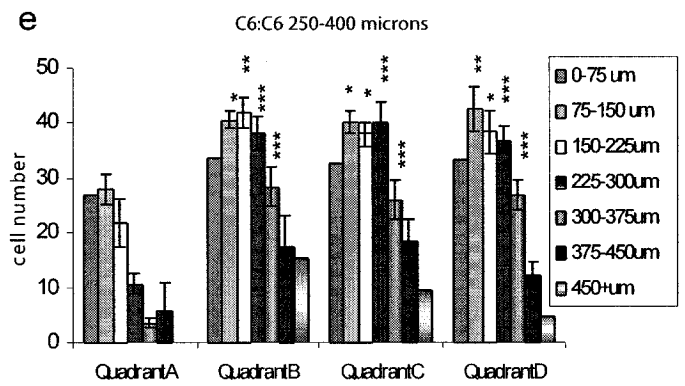
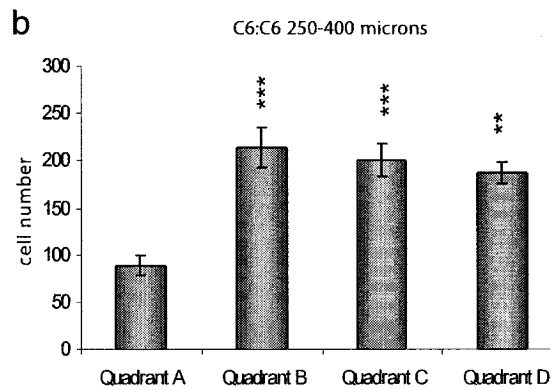
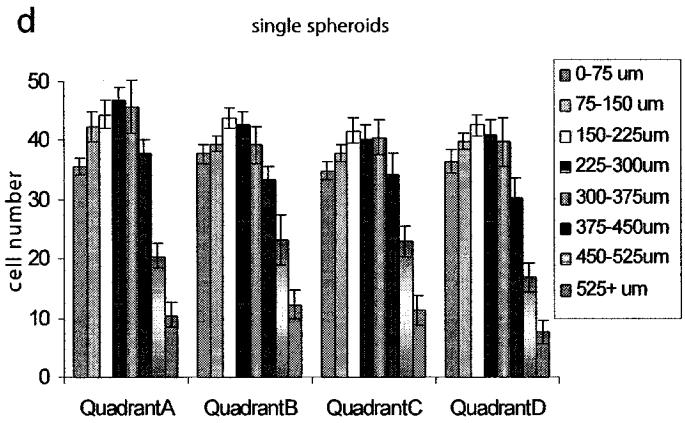
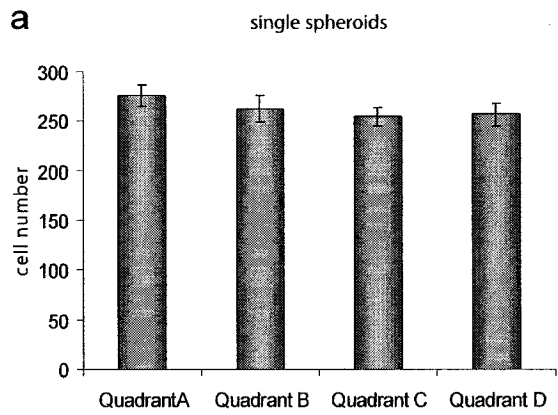


Figure 2.5: Two C6 spheroids and spheroid-bead cultures in a type I collagen gel. (a-c) Images extracted from time-lapse videomicroscopy over 24 hours. Circles follow the path of an individual cell. When challenged with a second spheroid, cells deviate from their perpendicular trajectory. Arrows denote stationary ruffling cells in the microenvironment between spheroids. Objective: 20X. Scale bar = 100 μm . (d-f) Single C6 spheroid adjacent to a glass bead. Images extracted over 24 hours. In both cases, invading cells move perpendicularly away from the spheroid. Objective: 10X. Scale bar = 150 μm . (g) Mean single cell angle deviation from a trajectory perpendicular to the spheroid surface for individual spheroids (N=45), spheroid-glass bead cultures (N=25) and two-spheroid co-cultures (N=46). Error bars: Standard error of the mean (SEM). Asterisks indicate a significant difference at $P < 0.001^{***}$. (h) Mean invasion rates for individual C6 cells when cultured alone (N=45) and with another C6 astrocytoma spheroid (N=46). Error bars: Standard error of the mean (SEM). Asterisk indicates significant difference at $P < 0.05^*$.

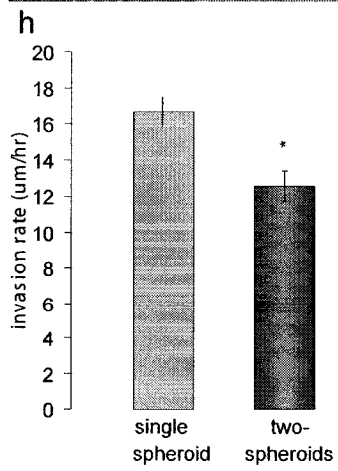
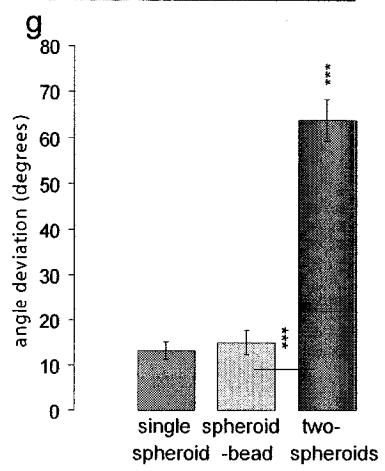
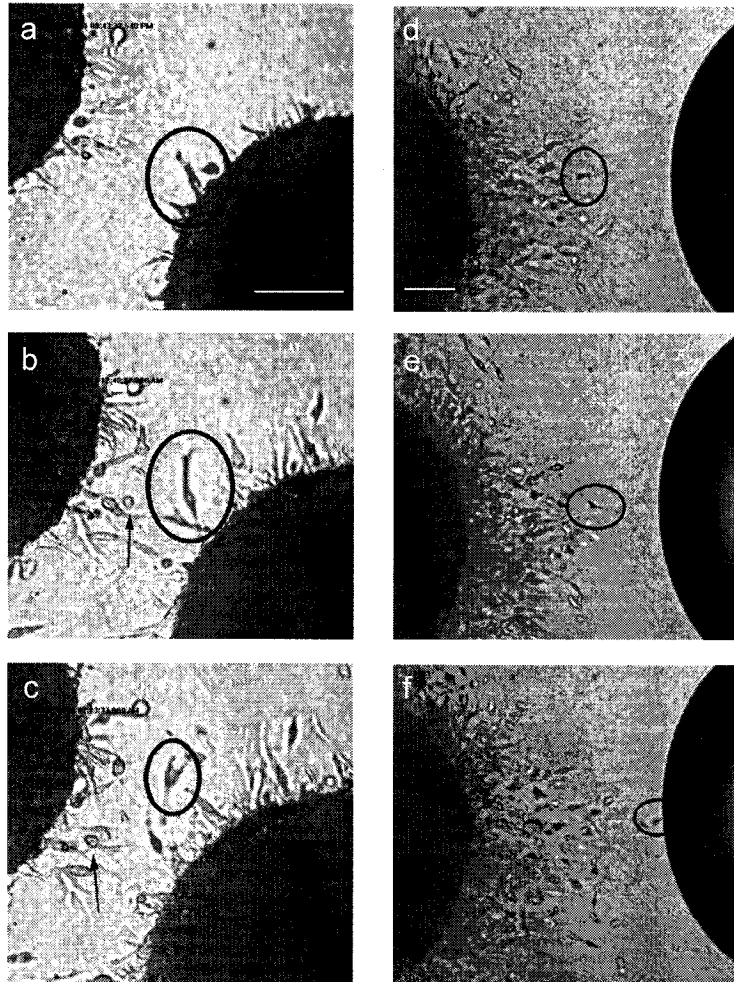


Figure 2.6: Co-cultures of a C6 astrocytoma spheroid with an aggregate of astrocytes derived from newborn rat brain. Cells were labeled with Cell Tracker™ dyes. (a-b) Co-cultures placed in contact with one another after 24 and 72 hours respectively. (c-d) Co-cultures implanted 150 μm apart after 24 and 72 hours respectively. Objective: 10X.

Scale bar = 250 μm .

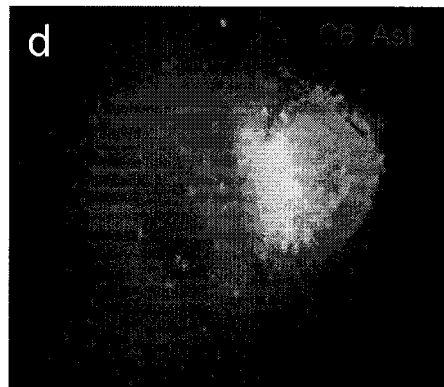
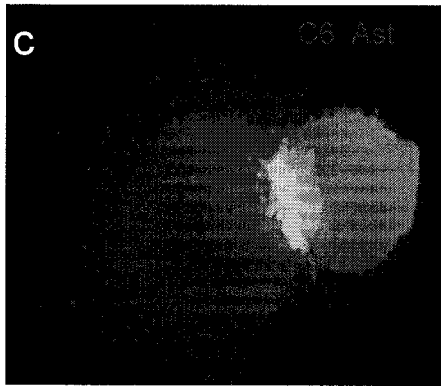
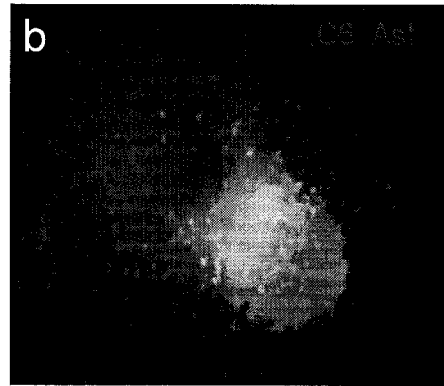
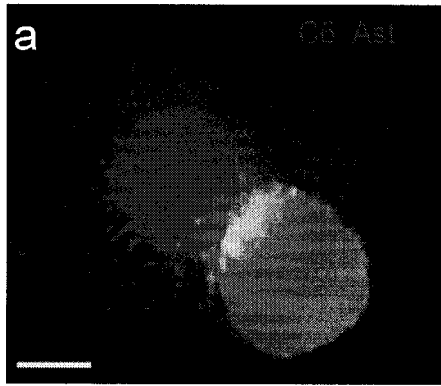


Figure 2.7: Confocal scanning laser microscopy images of C6 astrocytoma, C6-astrocyte, U251-astrocyte and human biopsy spheroid co-cultures fluorescently labeled with Cell Trackers™ after 24 -72 hours. (a-c) Split images (a-b) and overlay (c) through the centre of two C6 spheroids demonstrating the lack of invasion into and migration around the adjacent spheroid after 72 hours. (d-i) C6 astrocytoma spheroid co-cultured with fetal human (d-f) and newborn rat (g-i) astrocyte aggregates at 24, 48, and 72 hours respectively. After 48-72 hours, extensive invasion of C6 glioma cells into the fetal human and newborn rat astrocyte aggregate is observed. (g-i) Co-culture of C6 astrocytoma spheroid and newborn rat astrocyte aggregate after 24, 48 and 72 hours respectively. (j) Co-culture of U251 glioblastoma drop aggregate spheroid with fetal human astrocyte aggregate at 48 hours. Invasion into the astrocyte aggregate is similar to results obtained using C6 rat astrocytoma spheroids. (k-l) Two human biopsy spheroids implanted in contact with one another and 150 μm apart at 24 and 48 hours respectively demonstrating no invasion into adjacent spheroids but migration of some cells around the spheroid mass. Objective: 10X. Scale bar=250 μm .

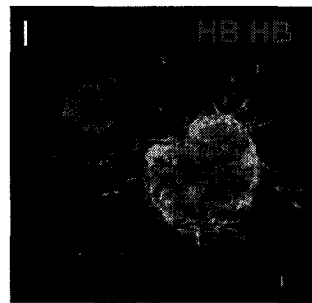
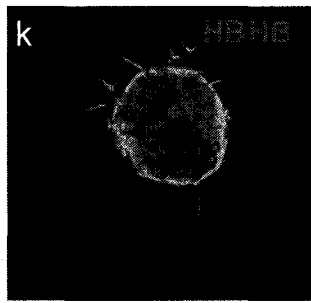
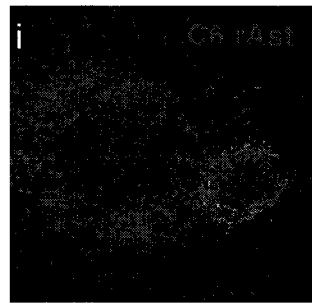
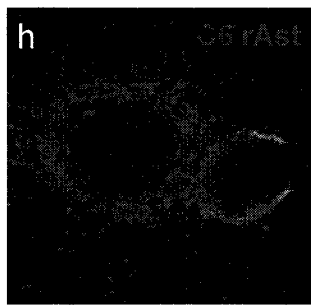
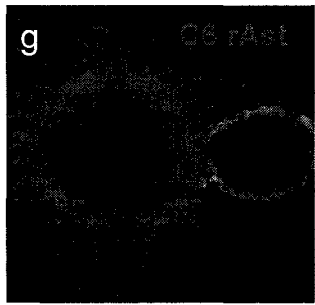
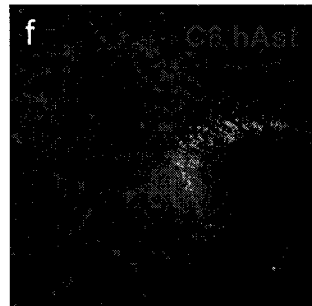
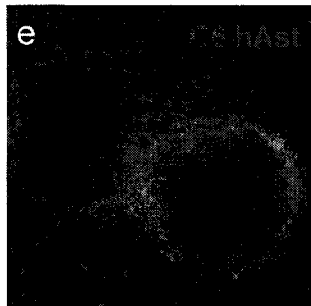
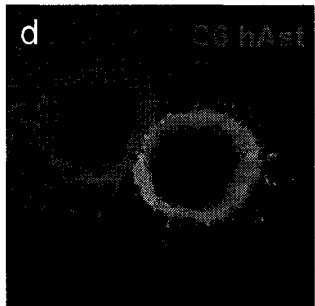
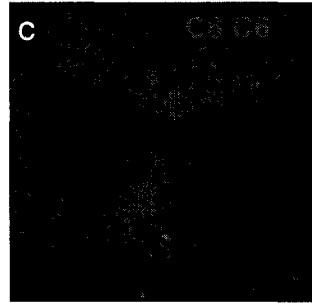
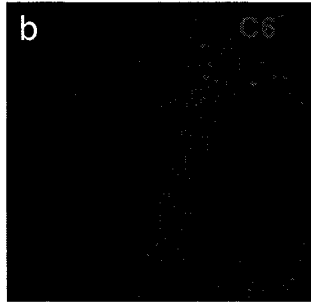
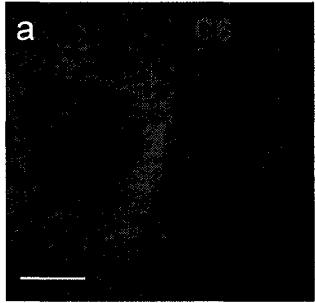


Figure 2.8: The effect of C6, U251 and fetal astrocyte conditioned medium on the invasion of C6 and U251 glioma spheroids. (a) C6 spheroid invasion after 9 days application of C6 and U251 conditioned medium from various-sized spheroids (N=4). (b) U251 spheroid invasion after days application of C6 and U251 conditioned medium from various-sized spheroids (N=4). (c) C6 spheroid invasion after 9 days application of conditioned medium from confluent monolayer fetal astrocyte cultures (N=5 for DMEM control and N=7 for astrocyte medium). (d) U251 spheroid invasion after 9 days application of conditioned medium from confluent monolayer fetal astrocyte cultures (N=8). Error Bars: Standard error of the mean. Asterisks indicate a significant difference at $P < 0.05^*$, $P < 0.01^{**}$ and $P < 0.001^{***}$.

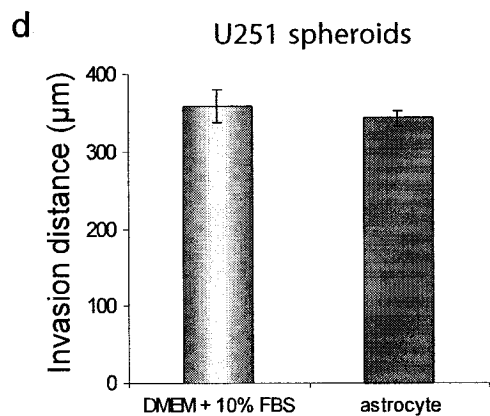
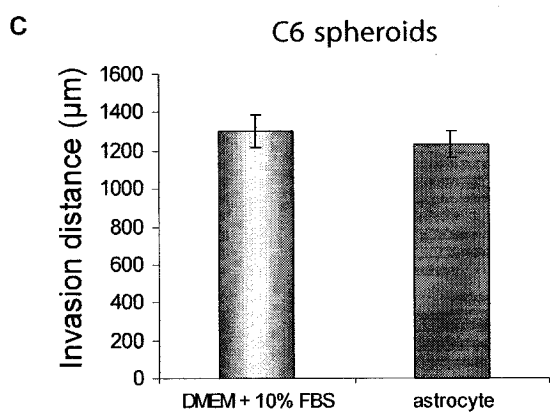
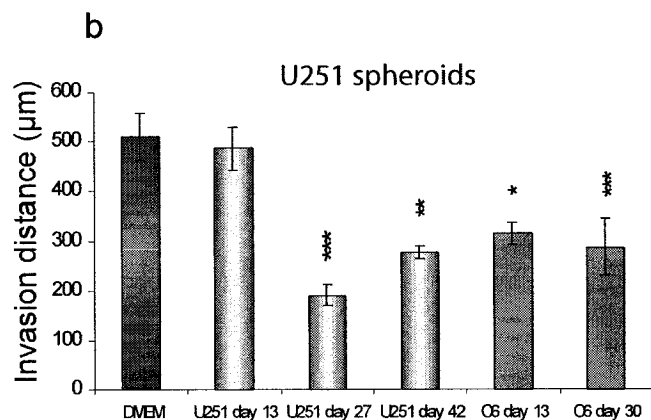
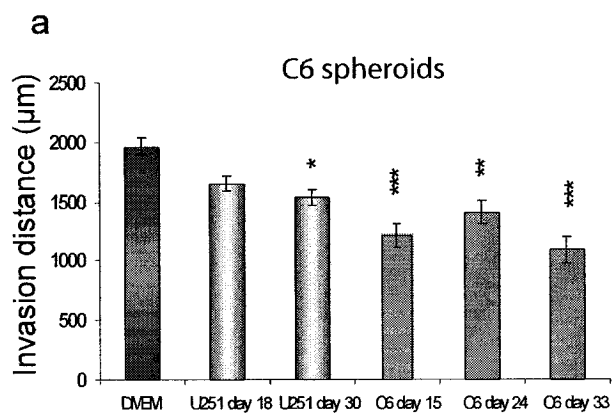


Table 2.1: Transwell chamber analysis of C6 (a) and U251 (b) cell migration in response to medium conditioned by C6 astrocytoma spinner culture spheroids. Conditioned medium was added to either the upper or lower chamber or both. Note that migration is maximal when C6 conditioned medium is added to the upper chamber and is reduced when medium is added to the lower chamber or both, indicating that C6 and U251 cells are inhibited by a secreted cue from the conditioned medium in a chemotropic and chemokinetic manner. The data represents the mean of four replicates $P < 0.05$ * $P < 0.001$

***.

a

Upper Chamber		
Lower Chamber	<i>0%</i>	<i>100%</i>
<i>0%</i>	182	187
<i>100%</i>	89 ***	0 ***

b

Upper Chamber		
Lower Chamber	<i>0%</i>	<i>100%</i>
<i>0%</i>	75	106
<i>100%</i>	3 *	1 *

2.6 Preface Chapter 3

We have provided evidence for a chemorepellent that directs glioma cell invasion while having an inhibitory effect on invasion as well. This does not rule out the possibility that multiple proteins are involved in this process or that different proteins are responsible for the directional and kinetic effects. Hence, there is a need to design an efficient and reproducible strategy to identify these factors and validate their function. The genes and proteins associated with malignant brain tumor progression have been extensively examined using techniques such as microarray and proteomic analysis. For example, a study has compared the gene expression profiles of medulloblastoma subtypes and has provided further evidence for SHH signaling dysregulation in sporadic medulloblastoma in addition to medulloblastoma linked with Gorlin's syndrome (Pomeroy et al., 2002). Nevertheless, these methods involve rationally selecting a key player for further investigation, and do not guarantee a true association with cell proliferation, angiogenesis or invasion. In particular, gene expression profiling using microarray analysis does not necessarily correlate with protein expression and the functional importance to the malignant phenotype is poorly understood.

To isolate genes involved in specific cellular processes, large scale analysis of gene expression using microarrays of cDNA sequences has been particularly important in examining the phenotype of highly motile subpopulations in malignant brain tumors *in vitro* and *in vivo* (Mariani et al., 2001; Tatenhorst et al., 2005). Recently, Tatenhorst et al. (2005) have compared the expression profiles of genes associated with hypermotility

using an *in vitro* monolayer migration assay and an *in vivo* C6 implantation model in nude mice. As expected, there were many differences in motility-associated genes between *in vivo* and *in vitro* models, suggesting that caution should be taken when considering the therapeutic potential of genes obtained from *in vitro* analysis.

Furthermore, proteomic analysis of fetal human astrocytes (FHA), U87 malignant glioma cells, and U87 cells expressing EGFR receptor mutations identified differentially expressed proteins falling into a variety of categories (Zhang et al., 2003). Although this study compares the protein expression profiles of highly malignant cell lines to normal cells, it did not utilize functional assays to investigate the significance of different proteins to malignant brain tumor motility or invasion.

We have utilized our three-dimensional collagen type I invasion model as a functional assay to isolate and identify a natural inhibitor of glioma cell invasion from C6 spheroid conditioned medium. Our biochemical approach utilizes traditional protein purification technology, and is based on the premise that we only select fractions that have the most inhibitory effect on C6 spheroid invasion for further analysis. In this way, we aim to isolate and identify factors having the most potent inhibitory effect, and follow this analysis with validation using molecular biology approaches. This method allows for isolation of both potential inhibitors and repellents, and the precise role in glioma invasion can be pursued after identification. The following chapter examines the identification and validation of inter alpha trypsin inhibitor heavy chain II as a natural and potent inhibitor of glioma invasion and proliferation in a three-dimensional collagen matrix.

**Chapter 3: Isolation of a natural inhibitor of human malignant
glial cell invasion: Inter Alpha Trypsin Inhibitor
Heavy Chain 2**

3.1 ABSTRACT

Malignant central nervous system tumors such as glioblastoma multiforme invade the brain and disrupt normal tissue architecture making complete surgical removal virtually impossible. Here, we have developed and optimized a purification strategy to isolate and identify natural inhibitors of glioma cell invasion in a three-dimensional collagen type I matrix. Inter alpha trypsin inhibitor heavy chain-2 (ITI-H2) was identified from the most inhibitory fractions, and its presence confirmed as both a single protein and a bikunin-bound form. Stable overexpression in U251 glioma cells validated ITI H2's strong inhibition of human glioma cell invasion together with significant inhibition of cell proliferation, and promotion of cell-cell adhesion. Analysis of primary human brain tumors showed significantly higher levels of ITI H2 in normal brain and low-grade tumors compared to high-grade gliomas, indicating an inverse correlation with malignancy. These findings suggest that reduction of ITI H2 expression correlates with brain tumor progression, and that targeting factors responsible for its loss or restoring the ITI supply exogenously may serve as potential therapeutic strategies for a variety of CNS tumors.

3.2 INTRODUCTION

Glioblastoma multiforme (GBM) is the most common malignant central nervous system (CNS) tumor in adults (Chicoine and Silbergeld, 1997). It is characterized by extensive necrosis, a high mitotic index, endothelial cell proliferation and nuclear pleomorphism. Invading glioblastoma cells rapidly infiltrate and disrupt normal tissue architecture making complete surgical removal virtually impossible (Kleihues et al., 2000; Giangaspero et al., 2000). This diffuse infiltrative growth leads to early recurrence and poor patient prognosis. Consequently, the invasive cascade is an important therapeutic target for GBM.

There are many known positive regulators of malignant brain tumor cell proliferation and invasion; however, little is known about negative modulators of malignant glial cell invasion (Chicoine and Silbergeld, 1997; Mueller et al., 2003; Wechsler-Reya and Scott, 2001; Werbowetski et al., 2004). Our laboratory has provided evidence for a secreted chemorepellent that directs glioma cell invasion (Werbowetski et al., 2004). Conditioned medium from both U251 and C6 spheroids significantly inhibited invasion of both spheroid types when implanted into three-dimensional collagen type I gels providing evidence for a potential inhibitory or kinetic effect as well (Werbowetski et al., 2004). Since this model can be used as a functional assay to identify endogenous and/or serum-derived inhibitors/repellents of glioma invasion, a purification strategy was designed and optimized to isolate these inhibitors/repellents from the conditioned medium of glioma spheroids.

This study presents the isolation and identification of inter alpha trypsin inhibitor heavy chain 2 (ITI H2) as a strong natural inhibitor of brain tumor invasion. Overexpression of ITI H2 in the U251 glioma cell line confirmed its inhibitory role in malignant glioma invasion and revealed an inhibitory effect on proliferation with a concomitant increase in cell adhesion. Moreover, expression levels of ITI H2 in primary human tumors and cultured human glioma cell lines were inversely correlated with malignancy, indicating a possible role for the ITI family members in CNS tumor progression. Our results present ITI H2 as both a potential indicator of tumor malignancy and a novel target for therapeutic intervention that merits further functional characterization.

3.3 METHODS

Cell culture and activity assay

C6 (murine astrocytoma) cells were cultured in Dulbecco's modified eagle medium (DMEM) supplemented with 10% fetal bovine serum (FBS), 125 U/ml penicillin G, 125 µg/ml streptomycin sulfate, and 2.2 µg/ml amphotericin B (Fungizone) and seeded into spinner culture flasks as described (Werbowetski et al., 2004; Tamaki et al., 1997).

Tumor spheroids were implanted into 48-well culture dishes containing 500 µl aliquots of a collagen type I solution (Vitrogen 100) (COHESION, Palo Alto, CA) and cell invasion was assessed daily as previously described (Werbowetski et al., 2004; Tamaki et al., 1997). All culture reagents were obtained from Gibco BRL (Invitrogen, Burlington, ON) unless otherwise stated. Cell lines were purchased from the American Type Culture Collection (ATCC) (Rockville, MD).

Protein Purification

Conditioned medium was collected from C6 spheroids in spinner culture between 2 and 5 weeks, and cell debris was removed by ultracentrifugation for 60 min at 45 000 rpm.

Conditioned medium was then concentrated 30X by ultrafiltration using a stirred cell equipped with a YM-10 membrane (Millipore, Etobicoke, ON). A wash buffer containing 20 mM MOPS pH 7.2, and an elution buffer containing 20 mM MOPS pH 7.2 and 1.5 M NaCl were prepared. The concentrated C6 conditioned medium was reconstituted in 100 ml 2 mM MOPS wash buffer, passed through a 0.2 µm filter, and loaded onto a Resource Q anion-exchange column (Amersham Biosciences, Baie d'Urfe, QC) equilibrated with 20 mM MOPS wash buffer. Chromatography was performed on an AKTA FPLC (Amersham Biosciences). The column was operated at a flow-rate of 2.5 ml/minute.

Bound proteins were eluted with a linear gradient of NaCl from 0-1.5M over 30 column volumes, re-equilibrated in DMEM without serum and applied over C6 spheroids in triplicate. Fractions having an inhibitory effect on invasion were pooled, collected and reconstituted in 10 mM sodium phosphate buffer pH 7 and loaded onto a 5 ml HiTrap Heparin HP column (Amersham Biosciences) equilibrated with the same buffer.

Fractions were eluted with a linear gradient of 10 mM sodium phosphate + 2M NaCl pH 7 over 45 column volumes, and then re-equilibrated in DMEM without serum.

Chromatographs for each column were obtained. Fractions were then applied over C6 spheroids in triplicate and those that had an inhibitory effect on invasion were collected, pooled, and stored at -80°C until further analysis. Inhibitory fractions from both Resource Q and HiTrap Heparin HP columns were resolved using SDS polyacrylamide gel electrophoresis on a 10% gel. Gels were silver stained according to established procedures (Amersham Biosciences). Protein concentrations were determined using the BioRad Protein assay dye reagent concentrate (BioRad, Mississauga, ON).

Mass spectrometry analysis of purified fractions

Tryptic digest and MS-MS analysis were conducted on pooled fractions with the most inhibitory activity from the HiTrap Heparin HP column (McGill University and Genome Quebec Innovation Centre, Montreal, QC). Mascot scores were obtained, and significance was determined as the minimum threshold required to be considered a non-random assignment (Perkins et al., 1999).

Cloning and stable cell line production

pCMV Sport6 vectors containing the ITI H2 and bikunin full-length cDNAs were obtained from ATCC. The BglIII and EcoRI restriction sites were used to subclone the ITI

H2 and bikunin full length constructs into the pLPCX retroviral expression vector (Clontech, Palo Alto, CA). The new constructs were introduced into the U251 human glioblastoma cell line following manufacturer guidelines (Retroviral Gene Transfer and Expression User Manual, BD Biosciences, Palo Alto, CA). Cells were cultured in selection medium containing 1 µg/ml Puromycin (Sigma-Aldrich Co. Canada Ltd., Oakville, ON) for 3 weeks. Confirmation of stable ITI H2 and bikunin overexpression was assessed using RT PCR (see below). See Table 3.2 (1-3) for primer details.

Hanging-drop aggregates and time-lapse videomicroscopy

Confluent cultures of wild-type U251 cells, U251 pLPCX cells, and U251 cells stably overexpressing ITI H2 and bikunin were trypsinized (0.05% trypsin/0.53 mM EDTA) and hanging-drop aggregates were prepared (Werbowetski et al., 2004; Corcoran and Del Maestro, 2003; Corcoran et al., 2003; Del Duca et al., 2004). Aggregates were implanted into collagen type I gels and invasion was assessed (Werbowetski et al., 2004; Tamaki et al., 1997). Implanted aggregates were imaged for 20 hours using time-lapse equipment and software as previously described (Angers-Loustau et al., 2004; Del Maestro et al., 2001). For each video, individual cell invasion rate, the number of cells detached from the spheroid after 8 hours and the number of individual cell divisions were calculated.

Proliferation Assay and Live-Dead Cytotoxicity Assay

To evaluate the effect of ITI H2 and bikunin overexpression on U251 glioma cell proliferation, monolayers of U251 wild-type, U251 pLPCX, U251 ITI H2, and U251 bikunin cells were plated on 6-well culture dishes (40,000 cells/well and three replicates for each time point). Cells were counted on days 2 and 4 using a Coulter Z™ Series counter (Beckman-Coulter Inc., Miami FA) and doubling time for each cell line was

calculated. Cell viability was determined using the Live/Dead Viability/Cytotoxicity kit (Molecular Probes, Invitrogen Detection Technologies, Eugene, OR). Briefly, 2 μ l of a 50 μ M calcein AM (detects live cells) working solution and 4 μ l of a 2 mM ethidium homodimer-1 stock (detects dead cells) were added to 1 ml U251 pLPCX and ITI H2 cell suspension in PBS. As a control for possible induction of cell death, both infected cell lines were also pre-treated with 0.1% saponin for 10 minutes. Samples were mixed, and incubated at room temperature for 20 minutes in the dark. Cells were rinsed 2X for 5 min in PBS and then visualized using the imaging equipment and software previously described (Angers-Loustau et al., 2004; Del Maestro et al., 2001).

Cell Attachment Assay

U251 pLPCX and ITI H2 overexpressing cells were seeded at 40 000 cells/well in 6-well dishes in triplicate. After 1,2,3 and 4 hours at 37°C, the wells were imaged and the number of attached cells was calculated for both empty vector and ITI H2 cells using the time-lapse videomicroscopy imaging system and software described.

Antibody production and Western Blot analysis

An anti-ITI H2 polyclonal antibody was generated against the C-terminal region of the protein by injecting rabbits with the synthetic peptide PGKDPEKPEASMEVK coupled to KLH (Sheldon Biotechnology Centre, McGill University, Montreal, Canada). To verify that ITI-H2 was enriched in purified fractions, 1 μ g protein from each fraction was subjected to SDS-PAGE on a 10% polyacrylamide gel. The ITI H2 specific polyclonal antibody was used at a concentration of 1:500. The anti-rabbit bikunin antibody (1:2000) has been generously donated by Dr. Bo Akerstrom (Lund University, Lund, Sweden) and a commercial antibody against all inter alpha trypsin inhibitor heavy and the light chain

(1:2000) was also used to validate ITI H2 enrichment (Dako Cytomation Inc., Mississauga, ON). The HRP-conjugated goat anti-rabbit IgG secondary antibody (1:5000) was used and visualized by enhanced chemiluminescence (Perkin-Elmer Life Sciences Inc., Markham, ON).

Immunocytochemistry

To examine intracellular localization of ITI H2 in the U251 ITI H2 stable cell line, immunocytochemistry was performed. Briefly, U251 ITI H2 cells were plated on collagen-coated coverslips for 48 hours (BIOCOAT, BD Biosciences, Discovery Labware, Mississauga ON). The ITI H2 specific polyclonal antibody was used at a concentration of 1:50 in 0.5% BSA 0.02% TritonX-100/PBS. Pre-immune serum and staining without primary antibody were used as negative controls. Donkey anti-rabbit Alexa 555 secondary antibody in 0.5% BSA 0.02% TritonX-100/PBS was used. Cells were co-labeled for actin by adding Phalloidin Alexa Fluor 488 (1:400) (Molecular Probes, Eugene, OR) to the secondary antibody mixture. Coverslips were mounted and imaged using a LSM 510 confocal scanning laser microscope at 63X magnification using the helium-neon (543 nm) and argon (488 nm) lasers (Carl Zeiss, Toronto, ON)

Human brain tumor samples

Twenty-seven human brain tumor samples were obtained from the Department of Molecular Pathology and Neurology, University of Lodz tissue bank, Simmelweiss University tissue bank in Hungary, Centre de Neuro-pathologie, Clermont-Ferrand tissue bank in France, the Brain Tumor Tissue Bank London Health Sciences Centre in London, Ontario and the Brain Tumour Research Centre Tissue Bank at the Montreal Neurological Institute in Montreal, Quebec. Among the samples were 5 pilocytic

astrocytoma, 11 glioblastoma multiforme (GBM), 5 meningioma, 4 low grade oligodendroglioma and 2 anaplastic oligodendroglioma. Samples of human fetal astrocytes obtained at 12-16 weeks gestation following Canadian Institutes of Health Research (CIHR) guidelines were acquired from the Albert Einstein College of Medicine Human Fetal Tissue Repository. A sample of normal brain was also analyzed, and all relevant clinical information for the tumors was available.

RT PCR of malignant glioma cell lines and primary human brain tumors

The endogenous expression of ITI H2 and β -actin mRNA in U251, U87, U343 and U373 glioma cells lines and primary human brain tumors was examined by RT-PCR. Total RNA was extracted from malignant glioma cell lines using RNeasy kit (QIAGEN) according to manufacturer's guidelines. For primary human brain tumors, total RNA was extracted from frozen samples using the TRIzol Reagent (Gibco BRL) according to manufacturers' guidelines. First strand cDNA was synthesized using the First-Strand cDNA Synthesis Kit (Amersham Biosciences). See Table 3.2 (1,4) for primer details. For all RT-PCR reactions, PCR using a template generated without reverse transcriptase or PCR in the absence of templates was used as a negative control. β -actin was used as an internal control. The following PCR conditions were used: 95 °C for 2 min, 80 °C for 2-4 min (during which Taq is added), and 30 cycles of 95 °C for 60s, 55°C (60°C for β -actin) for 30 s, and 72°C for 60s followed by 10 min at 72°C. PCR products were separated by agarose gel electrophoresis.

Immunohistochemistry

Normal brain and brain tumor samples embedded in paraffin were sectioned in 7 μ m intervals, deparaffinized in xylene, and processed through a graded series of alcohol

concentrations. Samples were subjected to antigen retrieval and placed in a Dako Autostainer (Dako Diagnostics Canada Inc., Mississauga, ON) using standard protocols. The ITI H2 antibody and pre-immune serum (1:100 dilution) were used for immunohistochemical staining. Samples were counterstained in Hematoxylin for 1 minute, mounted using a water soluble mountant and imaged using a standard light microscope at 40X magnification.

Statistical Analysis

All tests were performed using SPSS Graduate Pack 9.0 statistical software (SPSS Inc., Chicago IL). Descriptive statistics including mean and standard error of the mean along with one-way ANOVA's, independent sample two-tailed t-tests, and Tukey's test for multiple comparisons were utilized to determine significant differences. P values less than 0.05 were considered significant.

3.4 RESULTS

Inhibitory fractions contain enriched protein bands involved in invasion

To isolate potential inhibitors of glioma cell invasion, we concentrated C6 conditioned medium and applied it to a Resource Q anion exchange column. Fractions were collected, and applied to C6 astrocytoma spheroids implanted in collagen gels to assay for inhibition of cell invasion. Under control conditions, the average invasive rate was 10.2 $\mu\text{m}/\text{hour}$ (Fig. 3.1a). Fractions 16-21 had an inhibitory effect on invasion (Fig. 3.1a). Fractions 18-19 yielded the highest inhibitory effect on cell invasion, and induced a significant decrease of the average invasive rate for C6 spheroids from 10.2 to 6.2 $\mu\text{m}/\text{hour}$ (Tukey's test, $p < 0.001$) (Fig. 3.1a). Fractions 16-21 were pooled and applied to a HiTrap Heparin HP column. Fractions were then collected, and applied to C6 spheroids implanted in collagen gels. Fractions 1-8, and 17-22 displayed the highest inhibitory effect on invasion with an average invasive rate of 6.85 $\mu\text{m}/\text{hour}$ (Fig. 3.1b). Silver staining of inhibitory fractions revealed the presence of two enriched bands at approximately 90 and 140 kDa (Fig. 3.1c). Mass spectrometry identified ITI H2 as the most abundant protein in the pooled purified fractions from the HiTrap Heparin column (Table 3.1). Mascot scores over 38 were considered significant at $p < 0.05$.

Western Blot analysis confirms the presence of ITI H2 and ITI H2-bikunin complexes in purified fractions

To confirm the presence of ITI H2 in the purified fractions, we designed an antibody against ITI H2 and used Western blot analysis to compare bands obtained with those using a commercial antibody against all ITI chains and a bikunin-specific antibody. Western blot analysis confirmed the presence of an ITI H2 band around 90 kDa, and an

ITI H2-bikunin band around 140 kDa (Fig. 3.2a). Another band running at approximately 260 kDa suggested a combination of multiple heavy chains and bikunin (Fig. 3.2a). This is consistent with previous reports showing that the ITI heavy chain (ITI) family members are characterized by a unique covalent bond between the heavy chains and the chondroitin sulfate chain of bikunin (Zhuo et al., 2004). Therefore, ITI heavy chain-bikunin complexes will be present on reducing PAGE gels. Taken together, these results confirm that the enriched proteins in our purified inhibitory fractions were ITI H2 and combinations of ITI H2 and/or other heavy chains and bikunin. These results do not indicate whether ITI H2 alone is inhibiting C6 cell invasion or whether the serine protease inhibitory activity of bikunin is having a concomitant effect on the cells.

Stable overexpression of ITI H2 in U251 cells is localized to perinuclear regions and lamellipodia

After confirming the presence of ITI H2 and ITI H2-bikunin in our purified fractions, we wanted to validate the role of ITI H2 as an inhibitor of glioma cell motility by stably overexpressing both ITI H2 and the light chain bikunin in U251 cells. Infection of U251 cells with individual ITI H2 and bikunin chains should allow for the distinction between the effect of ITI H2 alone and/or the serine protease inhibitory activity of bikunin. RT PCR analysis of stable cell lines showed that U251 ITI H2 and bikunin cell lines expressed only the respective ITI H2 and bikunin mRNAs; whereas U251 cells infected with the control empty vector pLPCX did not have any ITI mRNA expression (Fig. 3.2b). Further characterization of U251 ITI H2 was performed using immunocytochemistry to examine intracellular localization (Fig. 3.2c). U251 cells expressing ITI H2 cells showed increased ITI H2 localization in the perinuclear regions

as well as in thin, extensive lamellipodia and membrane ruffles (Fig. 3.2c left panel). Membrane ruffle and lamellipodia ITI H2 expression appeared to co-localize with actin (Fig. 3.2c right panel).

ITI H2 inhibits U251 invasion in three-dimensional collagen gels

Since ITI H2 was originally identified from our functional screen for inhibitors of glioma cell invasion *in vitro*, it is important to confirm its role as an invasion inhibitor in our stable U251 ITI H2 cell line. To demonstrate this, we implanted spheroids from U251 cells infected with the empty vector pLPCX, ITI H2 and bikunin in collagen type I gels, and monitored invasion for 3 days. Within the first 24 hours, cell invasion of U251 ITI H2 spheroids was inhibited by approximately 55% compared with pLPCX control spheroids and bikunin spheroids (Fig. 3.3a,c). The inhibitory effect was maintained after three days in culture (Fig. 3.3b,d). These results suggest that ITI H2 inhibits cell invasion in three-dimensions. However, they do not differentiate between an effect of ITI H2 on individual cell invasive rate, adhesion or proliferation.

ITI H2 inhibits U251 cell proliferation without causing cell death

To examine the effect of ITI H2 and bikunin overexpression on cell proliferation in our U251 glioma model, we cultured U251 wild-type, and U251 cells infected with control pLPCX, ITI H2 and bikunin in 6-well dishes for 4 days. Cell number and doubling time were calculated at day 2 and day 4. There was no significant difference between U251 wild-type, pLPCX and bikunin cell lines; however, the number of U251 ITI H2 cells was significantly lower after 4 days in culture (Fig. 3.4a). The calculated *in vitro* doubling time for ITI H2 cells was 32.8 hours, and this was significantly different

from the 25.3 and 26.7 hours doubling times for U251 wild-type and pLPCX respectively (Tukey's test, $p < 0.05$) (Fig. 3.4b).

To validate the role of ITI H2 as an inhibitor of glioma cell proliferation and not a promoter of cell cytotoxicity or death, a live-dead assay was performed on control U251 cells infected with pLPCX and ITI H2 cells in monolayer culture over 4 days. As a control for possible induction of cell death, both infected cell lines were pre-treated with 0.1% saponin for 10 minutes. U251 pLPCX and U251 ITI H2 cells that received no detergent treatment showed no evidence of cell death or cytotoxicity after 4 days in monolayer culture (upper panels) (Fig. 3.4c). All cells pre-treated with 0.1% saponin died (lower panels) (Fig. 3.4c). Taken together, these results suggest that in addition to its role in glioma cell invasion, ITI H2 significantly inhibits glioma cell proliferation without increasing cell death or cytotoxicity.

ITI H2 increases cell attachment in monolayers

In order to test the hypothesis that the inhibitory effect on cell proliferation may be accompanied by an increase in cell attachment, we cultured U251 pLPCX and ITI H2 cells on monolayer culture and counted the number of attached cells as a percentage of the total number of cells at 1, 2, 4 and 6 hours. After 4-6 hours, ITI H2 cells maintained a slightly more "spread out" appearance on the plate and exhibited a small increase in the number of fan-like lamellipodia (Fig. 3.5a). One and 2 hours after plating, there was a small increase in the number of attached cells for ITI H2 cultures; however, the effect was only significant at 4 hours (68% and 80% attached for U251 pLPCX and U251 ITI H2 cells respectively) and 6 hours (83% and 88% attached for U251 pLPCX and U251 ITI H2 cells respectively) (t-test, $p < 0.01$ at 4 hours and $p < 0.05$ at 6 hours) (Fig. 3.5b).

These results suggest that the inhibitory effect on cell proliferation may be accompanied by an increase in cell attachment.

ITI H2 inhibits individual glioma cell velocity while increasing cell-cell adhesion

Previous results using U251 ITI H2 spheroids only examined average invasion of the entire cell population. To directly characterize the effect of ITI H2 on individual cell velocity and spheroid detachment, U251 pLPCX and U251 ITI H2 spheroids were implanted into collagen gels, allowed to invade for 6 hours and then imaged using time-lapse videomicroscopy for the following 20 hours. This time period was chosen based on previous results obtained for doubling time. Since the doubling time for the pLPCX and ITI H2 cells is approximately 26.7 and 32.8 hours respectively, significant differences in cell proliferation are not expected during the 20 hour video. The average invasion of U251 ITI H2 spheroids compared with U251 pLPCX spheroids over 20 hours is shown in Figure 3.6a. Quantification of individual cell invasive rates demonstrated an average cell velocity of 15.5 $\mu\text{m}/\text{hour}$ and 8.8 $\mu\text{m}/\text{hour}$ for pLPCX and ITI H2 cells respectively (N=30 cells for each cell line tested) (Fig. 3.6b). The inhibitory effect on cell velocity was also seen for detached U251 ITI H2 cells imaged 24-44 hours post-implantation (data not shown). In addition to the effect on individual cell velocity, 60% of U251 pLPCX cells had detached from the spheroids within 8 hours; however, only 17% of ITI H2 cells had detached suggesting a role for ITI H2 in cell-cell adhesion (N=30 cells for each cell line) (Fig. 3.6c). There was a small inhibitory effect on ITI H2 cell proliferation, but the effect was not statistically significant (Fig. 3.6c). These results further validate ITI H2 as an inhibitor of glioma cell invasion and demonstrate an additional potential role for ITI H2 in cell-cell adhesion.

ITI H2 expression is downregulated in high-grade brain tumors

To explore the significance of our findings to primary brain tumors, we assessed the expression of ITI H2 in pilocytic astrocytoma, GBM, low and high-grade oligodendroglioma, meningioma, normal brain and human fetal astrocyte cultures using RT-PCR. Representative samples are shown in Figure 3.7. ITI H2 mRNA was detected for both cultures of primary human fetal astrocytes and normal adult brain (Fig. 3.7a). ITI H2 was present in 4 of 5 (80%) pilocytic astrocytoma but in only 2 of 11 (22%) GBM samples (Fig. 3.7a). A similar trend was observed for oligodendroglioma tumors with 3 of 4 (75%) low grade oligodendroglioma expressing ITI H2 mRNA and only 1 of 2 anaplastic oligodendroglioma exhibiting faint bands (Fig. 3.7a). Similarly, 4 of 5 (80%) non-metastatic, low grade meningioma expressed ITI H2. RT PCR analysis was also conducted for glioma cell lines, and faint levels of ITI H2 were detected for both U251 and U87 (Fig. 3.7b). No expression was detected in U373 (Fig. 3.7b). ITI H2 mRNA levels were higher in U343 (Fig. 3.7b). Interestingly, invasion rates of U343 spheroids in collagen type I gels are lower than those for U87, U251 and U373 spheroids (unpublished results).

To examine ITI H2 protein expression patterns in primary human brain tumors and normal brain, we performed immunohistochemical analysis. Normal brain samples stained with the ITI H2 antibody showed a strong perinuclear/cytoplasmic signal and a homogenous staining of the extracellular matrix (Fig. 3.7c, upper panels). In contrast, highly cellular GBM samples showed practically no cellular localization and the observed ITI H2 signal was typically a weak and sporadic staining of the extracellular matrix (Fig. 3.7c, lower panels). In two GBM samples, we observed isolated clonal cell

populations expressing ITI H2, but this pattern was very distinct from the homogeneous staining seen in normal brain and other lower grade tumor samples (data not shown).

Taken together, these results suggest that ITI H2 is expressed in normal brain and in low grade CNS tumors including pilocytic astrocytoma and meningioma. This expression seems to be lost in higher grade tumors including GBM suggesting that its loss is associated with an increased malignant potential.

3.5 DISCUSSION

Over the last 20 years, there have been very few new developments in therapeutic strategies targeting malignant brain tumors. In this era of time-efficient production of cumulative lists of protein and gene players associated with a disease or cellular process of interest, one is still confronted with having to rationally choose a key player for further investigation. To avoid this dilemma, we opted to design and optimize a purification strategy to isolate natural inhibitors of glioma cell invasion from conditioned medium of C6 spheroids. In the present study, we have purified, identified, and validated ITI H2, as a natural inhibitor of glioma cell velocity and proliferation with a concomitant positive effect on cell-cell adhesion to produce an overall strong inhibition of human glioma cell invasion *in vitro*. The quantity and purity of our sample enabled us to identify ITI H2 by mass spectrometry analysis of tryptic digest products as the most abundant protein in our purified fractions from conditioned medium. The inter alpha trypsin inhibitor (ITI) proteoglycan family is an example of a protein-glycosaminoglycan-protein (PGP) complex derived from alternative combinations of multiple heavy chains (ITI H1-H4) and one common light chain, bikunin encoded by 4 genes on 3 different chromosomes (Zhuo et al., 2004). Interestingly, the ITI H2 gene resides on the human chromosome 10p15, and deletions of portions of chromosome 10 are typically associated with malignant glioma progression (Wechsler-Reya and Scott, 2001; Diarra-Mehrpour et al., 1989). Recently, a fifth heavy chain, ITI H5 has been identified, and structural analysis has revealed early divergence from a common ITI ancestor (Himmelfarb et al., 2004).

The ITI heavy chain (ITI) family members are characterized by a unique covalent bond between the heavy chains and the chondroitin sulfate chain of bikunin (Zhuo et al.,

2004). In our study, silver staining of purified fractions revealed the presence of two enriched protein bands at 140 kDa and 90 kDa. These bands correspond with those obtained from Western blot analysis using our antibody raised against the heavy chain 2, a bikunin antibody and a commercial antibody that recognizes the various ITI chains, and confirm the presence of individual ITI H2 and a bikunin-bound form in the conditioned medium. Although ITI is principally produced by the liver and secreted into serum, individual heavy chain and bikunin expression have been detected in other tissues and are produced as components of ITI-related proteins in these tissues (Mizushima et al., 1998; Chan et al., 1995). In particular, high levels of individual ITI H2 mRNA have also been detected in brain, adrenal gland, kidney and lung (Mizushima et al., 1998; Chan et al., 1995).

ITI H2 was identified in our functional selection for inhibitors of glioma cell invasion in type I collagen gels; however, this does not rule out the possibility that other heavy chain family members (H1, H3, H4 and H5) may also play a role in glioma cell motility and proliferation. For example, overexpression of ITI H1 and H3 induced a significant decrease in lung tumor metastasis number; whereas, ITI H2 had no effect (Paris et al., 2002). Recently, a cleavage fragment of ITI H4 has been identified as a marker for early stage ovarian cancer and plasma bikunin levels are indicative of a favorable prognosis for ovarian cancer (Zhang et al., 2004; Matsuzaki et al., 2005). In addition, ITI H5 is downregulated in breast cancer, thus further implicating the ITI heavy chains as tumor suppressor genes (Himmelfarb et al., 2004).

Using immunocytochemistry analysis of stable U251 ITI H2 cells, we demonstrated that ITI H2 localizes to perinuclear regions as well as to thin extensive

lamellipodia and membrane ruffles. This intracellular expression does not rule out the possibility that ITI H2 is secreted or is secreted in a modified form. We have not detected ITI H2 in the serum-free medium from our U251 stable cell line (unpublished data). It has been shown that proteolytic processing of ITI heavy chains during biosynthesis varies greatly with cell type, suggesting that cleavage is not autocatalytic and further reiterating the structural complexity of the ITI family (Thogersen et al., 1995). Co-localization of ITI H2 with actin in U251 membrane ruffles and lamellipodia suggests a relationship with cytoskeletal dynamics and a role in the control of invasion.

Our results show that overexpression of the individual ITI H2 chain decreases invasion of U251 glioma cells in collagen type I matrices, while stable bikunin overexpression does not affect U251 cell proliferation or invasion. This indicates an exclusive role for ITI H2 in the control of cell invasion that is independent from bikunin. In addition to the invasion assays utilized here, bikunin has also been previously examined in glioma cell migration models where transient overexpression of placental bikunin alone did not significantly affect migration, despite an inverse correlation of primary tumor mRNA levels with malignancy (Hamasuna et al., 2001). Therefore, it is reasonable to assume that ITI H2 isolated and identified in our purified fractions is individually responsible for the inhibitory effects on glioma cell invasion, rather than covalently bound bikunin. However, these results do not completely rule out the possibility that bikunin levels may contribute to the invasion process *in vivo*.

An interesting finding in the presented study was the concomitant effect of ITI H2 on glioma cell proliferation and cell adhesion both in three-dimensional collagen gels and on monolayer cultures. Previous studies assessing the role of other molecules in glioma

proliferation and motility have also demonstrated an increase in cell attachment on a variety of brain ECMs with a delay in tumor cell growth corresponding to the log phase of the growth curve (Rempel et al., 2001). Overexpression of molecules that promote cell-cell adhesion (i.e. neural cell adhesion molecule (NCAM)) decreases glioma cell motility *in vitro* (Prag et al., 2002). Cadherins, as another example, can be classified as tumor suppressors and are associated with differentiation and contact inhibition of growth and motility (Demuth and Berens, 2004). In our study, glioma cells overexpressing ITI H2 were less able to detach from the spheroid, and consequently, invasion was inhibited within the first 24 hours post-implantation. However, even individual cells that had already detached from the spheroid exhibited slower invasive rates. The additional inhibitory effect of ITI H2 on U251 cell doubling time suggests that ITI H2 targets multiple biological processes making it an interesting therapeutic target.

An important finding in our study was the higher ITI mRNA and protein levels in lower grade tumors and normal brain. Studies have also implicated other ITI chains such as bikunin and an ITI H4 cleavage fragment as biomarkers for early stage ovarian cancer and are thus positive prognostic factors for this disease (Zhang et al., 2004; Matsuzaki et al., 2005). Our results demonstrate higher ITI H2 levels not only in normal brain and low-grade gliomas such as pilocytic astrocytoma and oligodendroglioma, but also in other CNS tumors such as meningioma. Meningiomas are slow-growing, typically benign tumors that usually present themselves as World Health Organization (WHO) grade I (Perry et al., 2004). Interestingly, ITI H2 mRNA levels also seemed higher in cultures of human fetal astrocytes compared with samples of adult normal brain suggesting a potential role for ITI H2 in neural development. The relationship of ITI H2 levels with

tumor progression combined with the effects on proliferation, invasion and adhesion *in vitro* suggest that ITI H2 may potentially serve as a biomarker for a variety of low-grade CNS tumors.

The results presented here are the first to demonstrate an inhibitory role for ITI H2 in glioma cell invasion and proliferation while increasing cell attachment and adhesion. The positive correlation of invasion with proliferation indicates that in our model, the two events are not mutually exclusive, and that ITI H2 can be used to clinically target both processes. The higher ITI H2 levels in normal brain, fetal astrocytes, low-grade gliomas and meningiomas suggest that ITI H2 may function as a tumor suppressor and potential biomarker for low-grade tumors. In our opinion, the classical biochemical approach presented here to identify a key player in the development of CNS tumor malignancy is quintessential to the significance of the study's outcome. Targeting factors responsible for ITI H2 loss or restoring the supply exogenously may serve as potential therapeutic strategies for a variety of high grade invasive CNS tumors.

Figure 3.1: Purified fractions from Resource Q and HiTrap Heparin HP columns contain enriched proteins involved in invasion. (a) Quantification of inhibitory effect of fractions obtained from a Resource Q anion exchange column. Note the maximum inhibition of C6 spheroid invasion rate with fractions 16-17, 18-19 and 20-21. Error bars represent SEM. Asterisks indicate significance at $P < 0.01^{**}$ and $P < 0.001^{***}$. (b) Quantification of inhibitory effect of fractions obtained from a HiTrap Heparin HP column. Note the maximum inhibition of C6 spheroid invasion rate with fractions 1-8, 17-19 and 20-22. Error bars represent SEM. Asterisks indicate significance at $P < 0.05^{*}$, $P < 0.01^{**}$, $P < 0.001^{***}$. (c) Silver stained PAGE gel of C6 conditioned medium, DMEM + 10% FBS, and inhibitory fractions from the Resource Q anionic exchange and HiTrap Heparin HP column. Note enrichment of two bands running at approximately 140 kDa and 90 kDa.

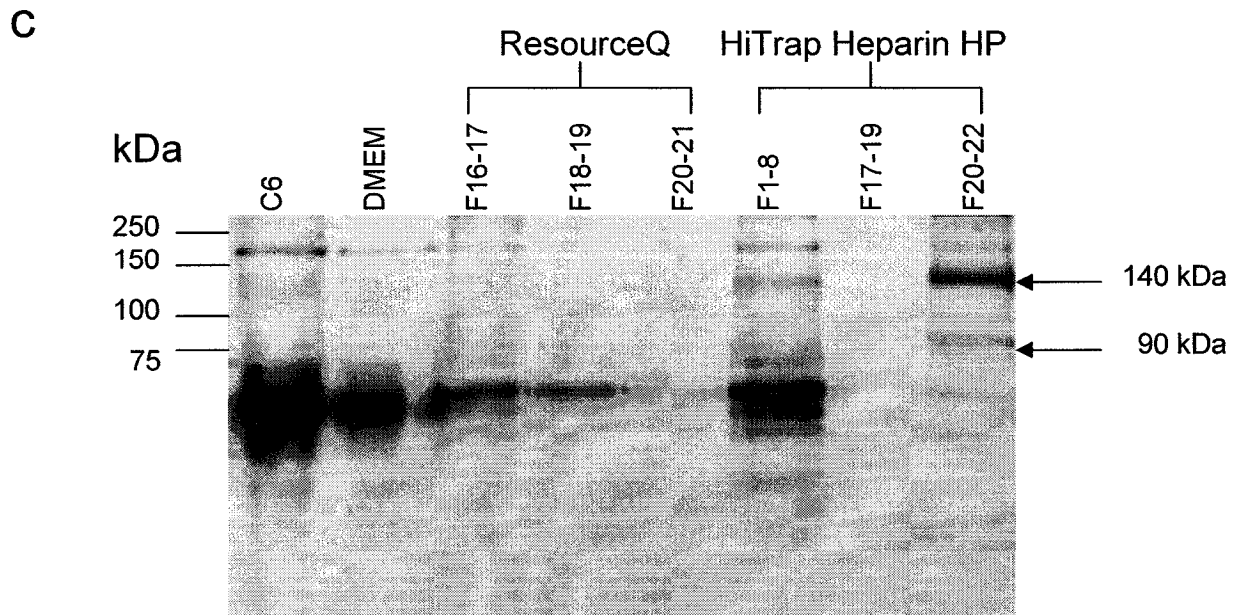
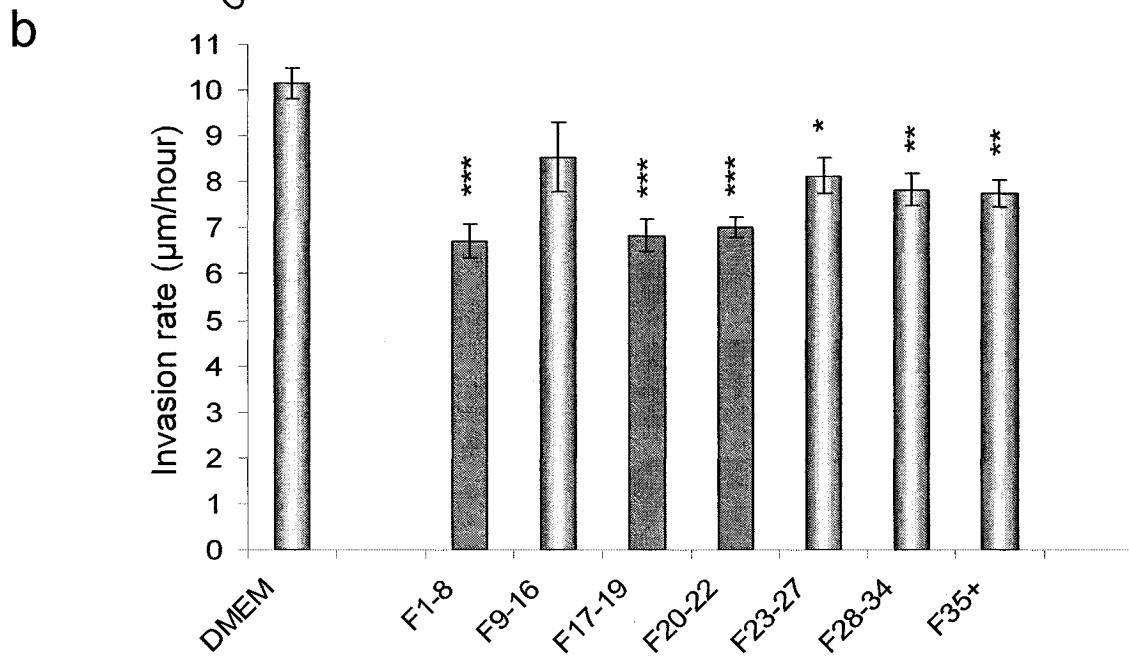
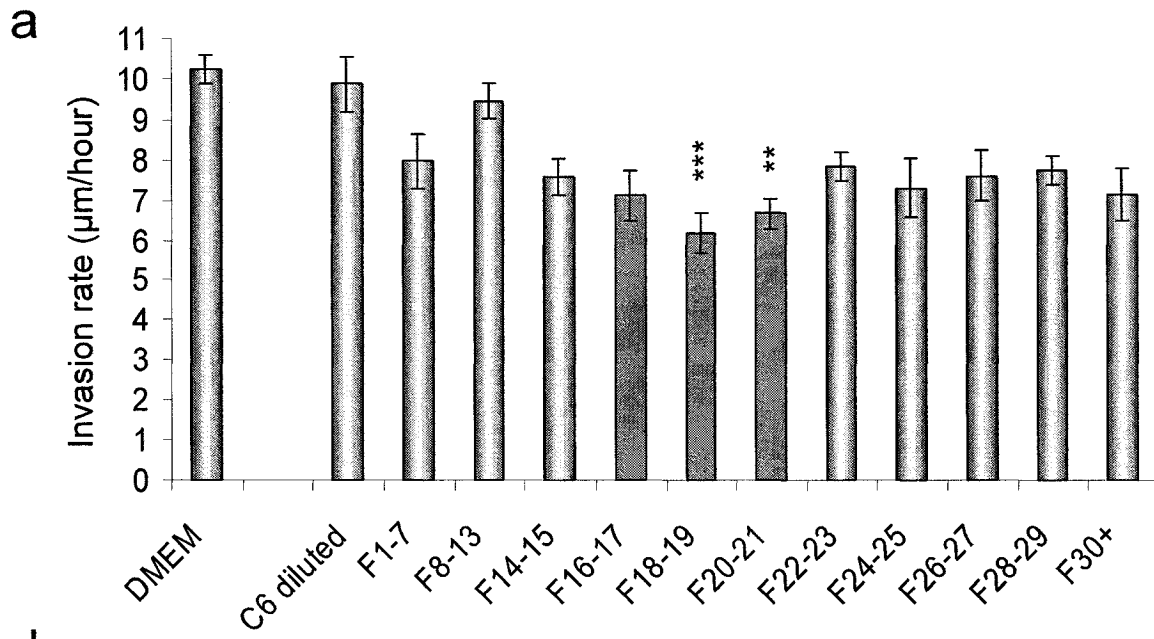
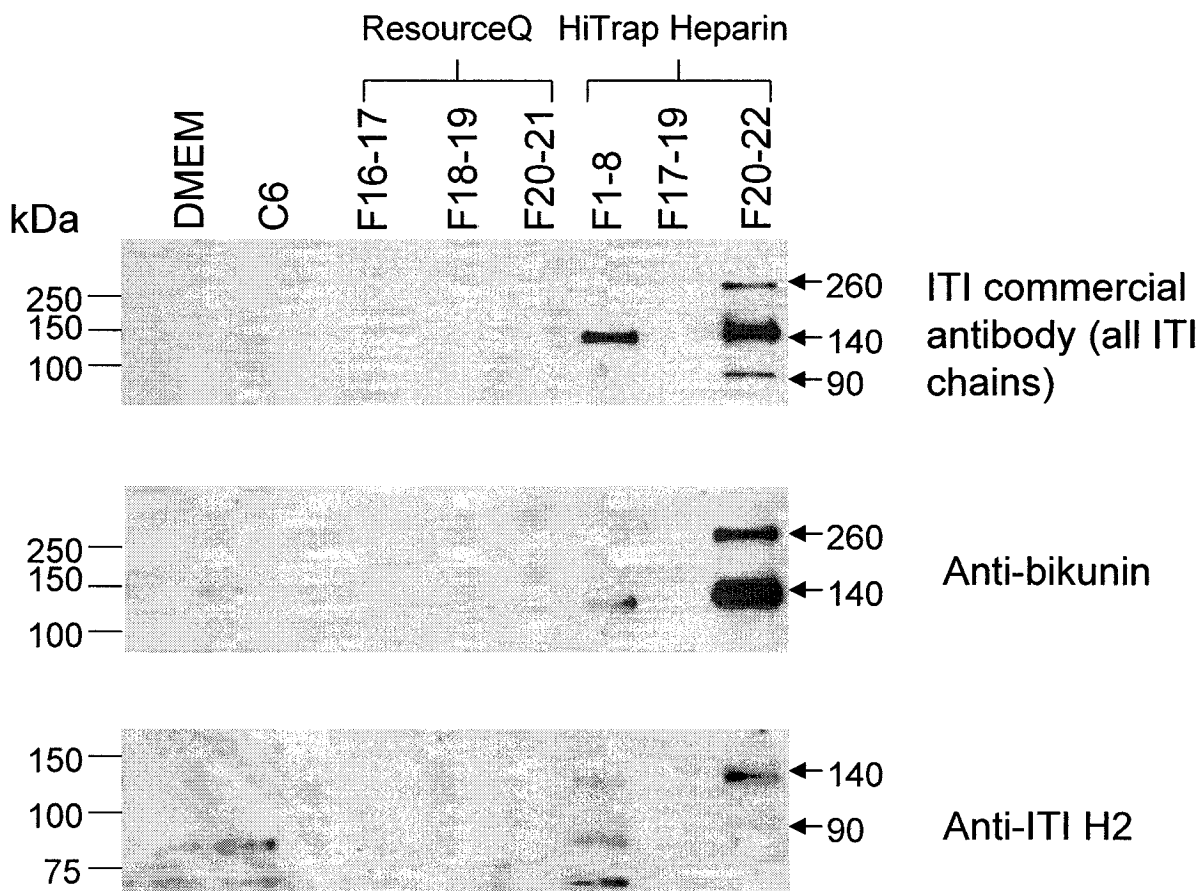
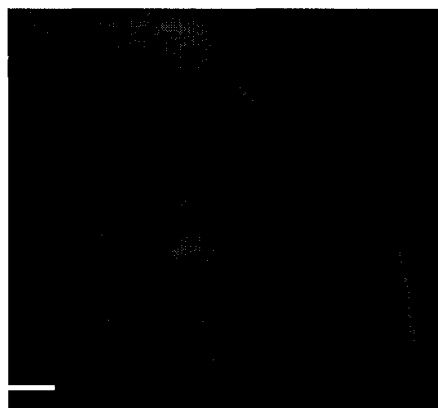
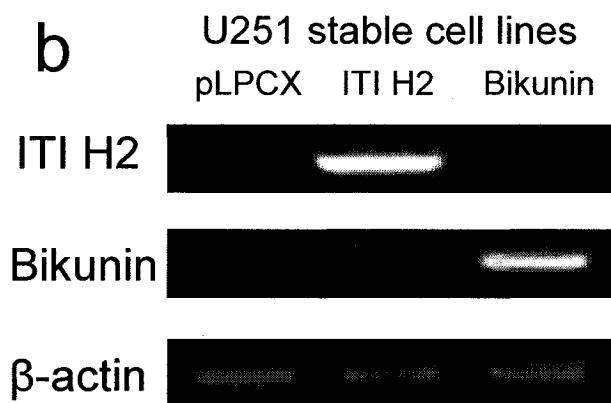


Figure 3.2: Western Blot analysis confirms presence of ITI H2 in inhibitory fractions and ITI H2 localizes to perinuclear regions, membrane ruffles and lamellipodia in U251 cells overexpressing ITI H2. (a) Western blot analysis of purified inhibitory fractions from Resource Q and HiTrap Heparin columns. For the commercial ITI antibody, enriched bands at 260, 140 and 90 kDa were detected. The bikunin antibody detected a 260 and a 140 kDa band, and the ITI H2 anti-serum detected a 140 and 90 kDa band. Note that all bands correspond to the same molecular weights using all three antibodies and represent various combinations of ITI heavy chains and bikunin. (b) RT PCR analysis of ITI H2, bikunin, and β -actin expression in U251 stable cell lines. (c) Immunocytochemistry of U251 ITI H2 cells labeled with ITI H2 antibody (left panel), phalloidin Alexa-488 for actin (middle panel) and image overlay (right panel). Note the localization of ITI H2 in perinuclear regions, membrane ruffles and thin, extensive lamellipodia. Actin co-localizes with ITI H2 in membrane ruffles and lamellipodia. Scale Bar: 10 μ m.

a



b



ITI H2



actin (Phalloidin Alexa-488)



Figure 3.3: Overexpression of ITI H2 inhibits U251 cell invasion in type I collagen gels. (a) Still photographs of U251 pLPCX, ITI H2 and bikunin spheroids 24 hours after implantation in collagen type I gels. Scale Bar: 250 μm . (b) Still photographs of U251 pLPCX, ITI H2 and bikunin spheroids 72 hours after implantation. Scale Bar: 250 μm . (c-d) Quantification of invasion distances for pLPCX, ITI H2 and bikunin spheroids after 24 hours (c) and 72 hours (d) in collagen type I gels. Note that invasion distances for ITI H2 spheroids are significantly lower than both pLPCX and bikunin spheroids. N=21, N=20 and N=19 for U251 pLPCX, ITI H2 and bikunin spheroids respectively at both 24 and 72 hours. Error bars represent SEM. Asterisks indicate significance at $P < 0.001^{***}$.

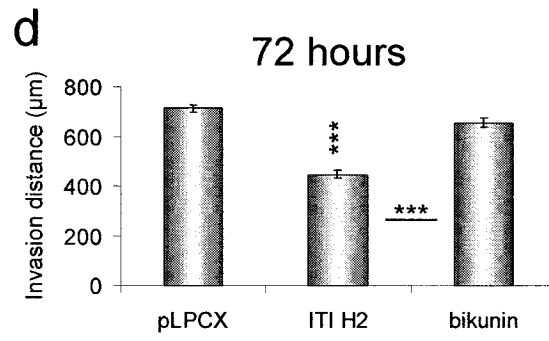
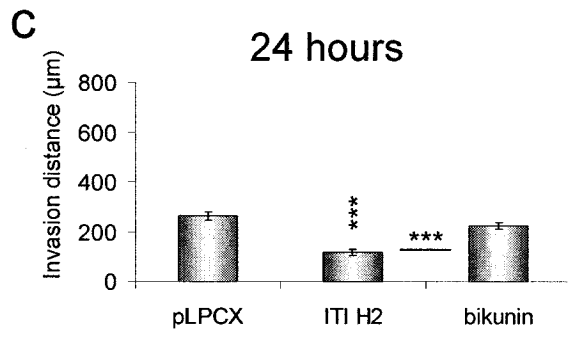
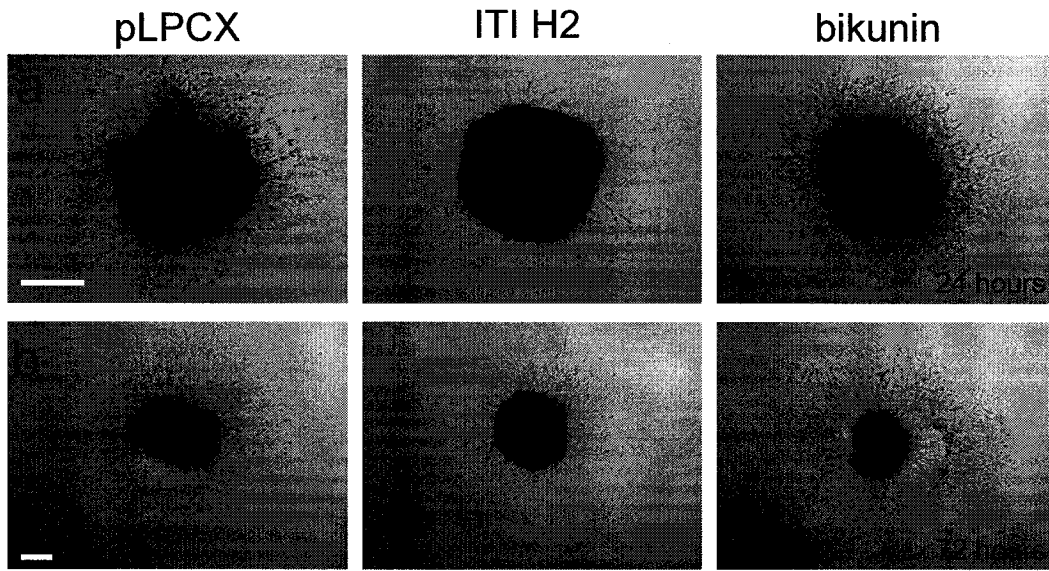


Figure 3.4: Overexpression of ITI H2 in U251 cells inhibits proliferation without causing cell death. (a) Total cell number calculated for U251 wild-type, pLPCX, ITI H2 and bikunin stable cell lines after 2 and 4 days in monolayer culture. (b) Quantification of doubling time for U251 wild-type, pLPCX, ITI H2 and bikunin stable cell lines after 4 days in monolayer culture. Data represents 4 independent trials. Error bars represent SEM. Asterisks indicate significance at $P < 0.05^*$. (c) Live-dead cell death/cytotoxicity assay for U251 pLPCX and ITI H2 cells in monolayer culture for 4 days. Upper 2 panels represent pLPCX and ITI H2 cells under normal culture conditions. Lower 2 panels represent pLPCX and ITI H2 cells pre-treated with 0.1% saponin as a control for cell death/cytotoxicity. Scale Bar: 200 μm .

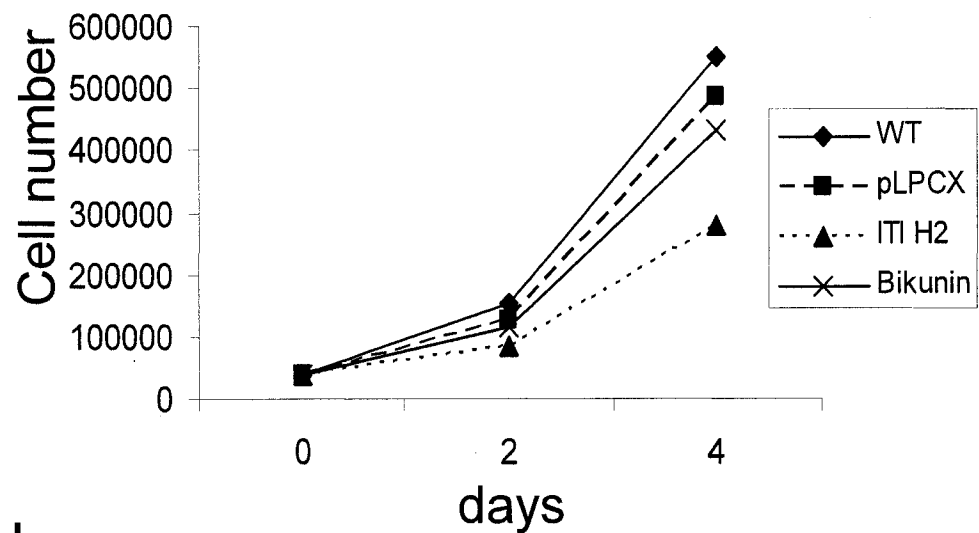
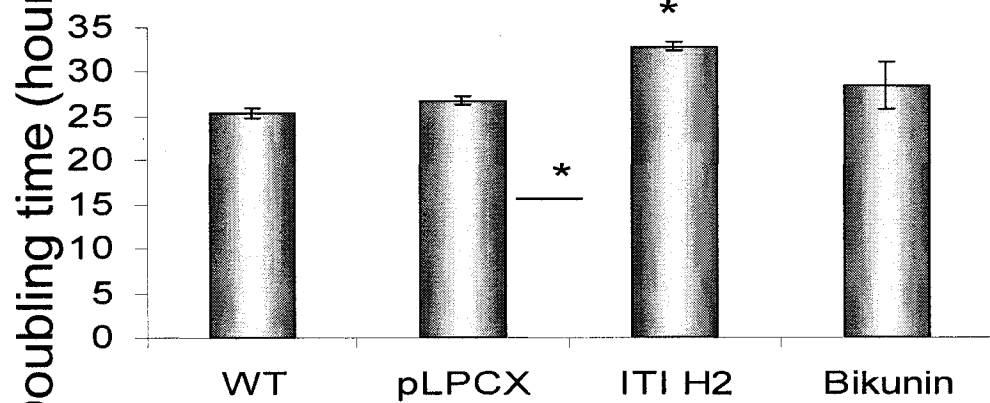
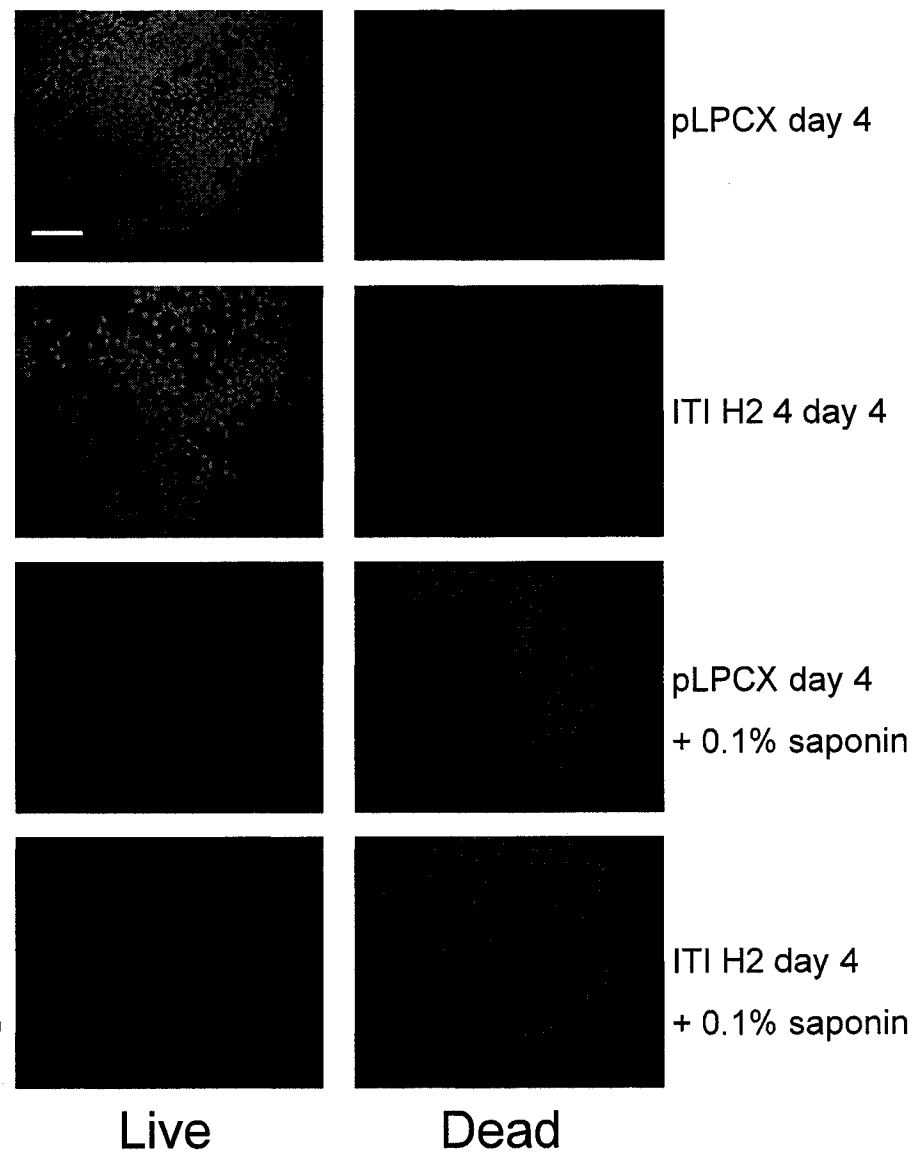
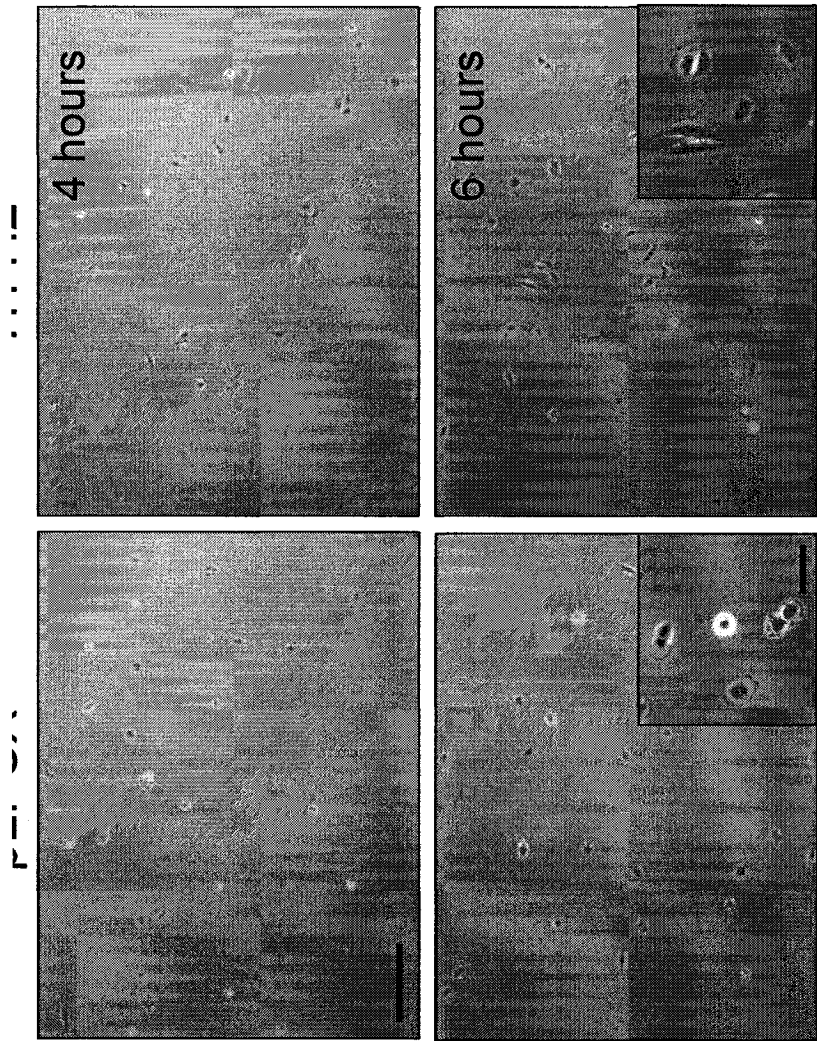
a**b****c**

Figure 3.5: Cell attachment assay for pLPCX and ITI H2 cells in monolayer culture. (a) Still photographs of attached pLPCX and ITI H2 cells in monolayer culture after 4 hours (upper panels) and 6 hours (lower panels). Note the similar morphology between both cell types with a slight increase in the number of attached ITI H2 cells with more extensive fan-like lamellipodia. Scale Bar: 200 μm . Insets: higher magnification of pLPCX and ITI H2 cells after 6 hours in monolayer culture. Scale Bar: 50 μm . (c) Quantification of the number of attached cells as a percentage of total cell number for U251 pLPCX and ITI H2 cells. There is a significant increase in the number of attached cells at both 4 and 6 hours for ITI H2 cells. Error bars represent SEM. Asterisks indicate significance at $P < 0.05^*$ and $P < 0.01^{**}$.



b

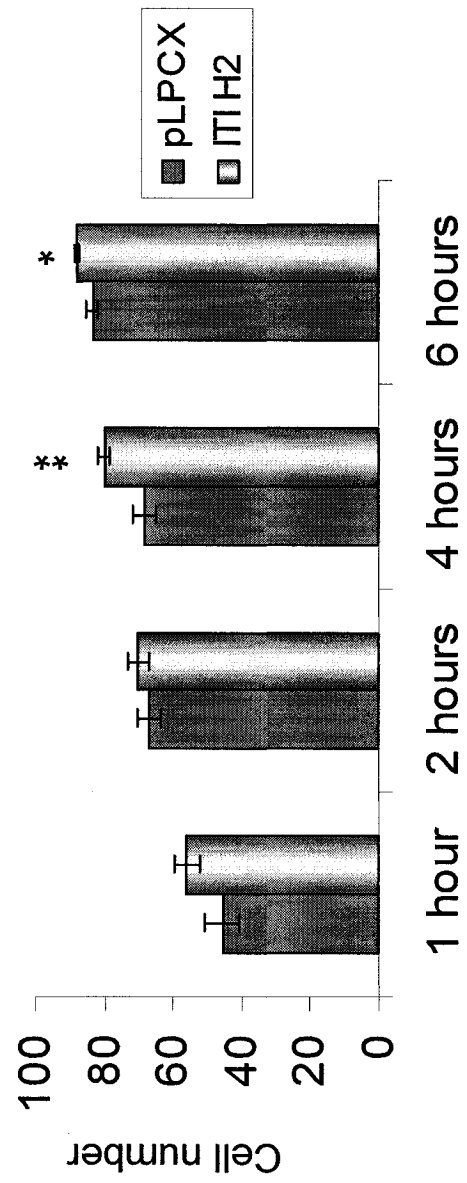
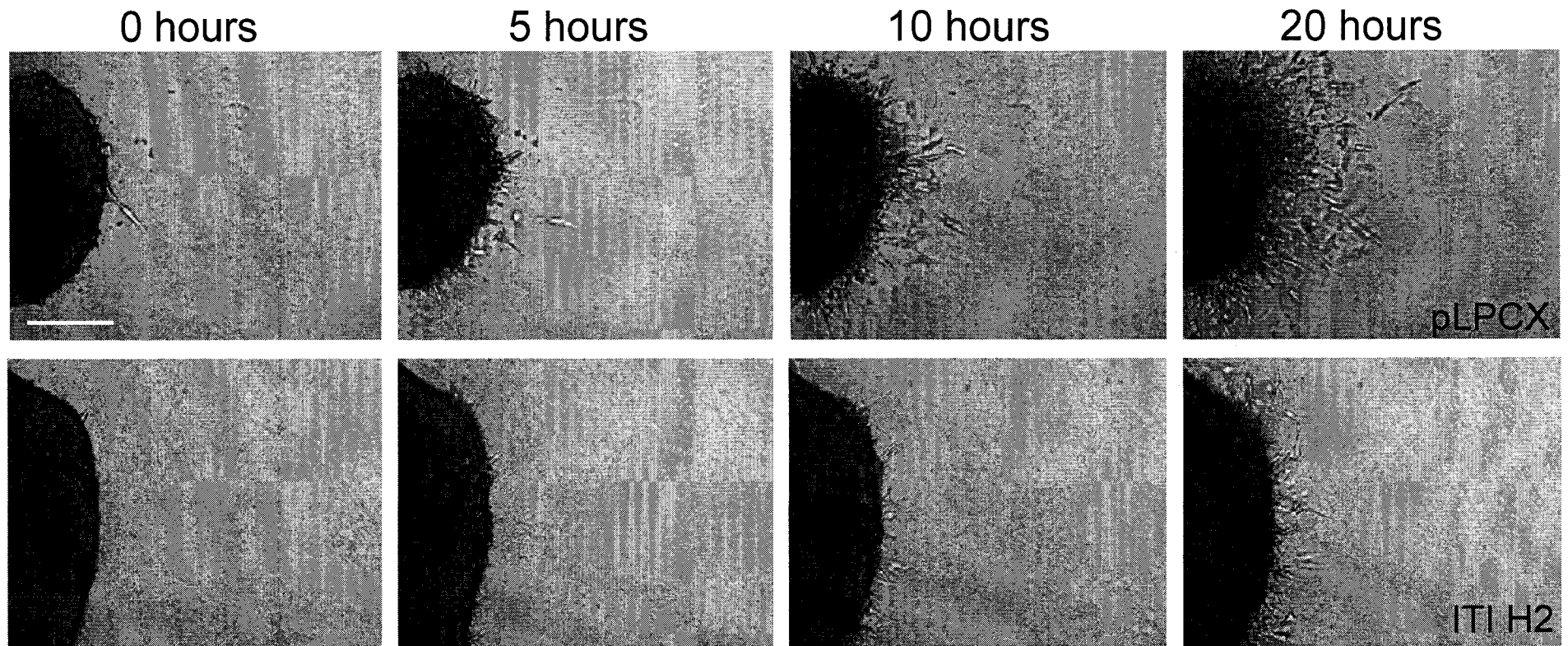
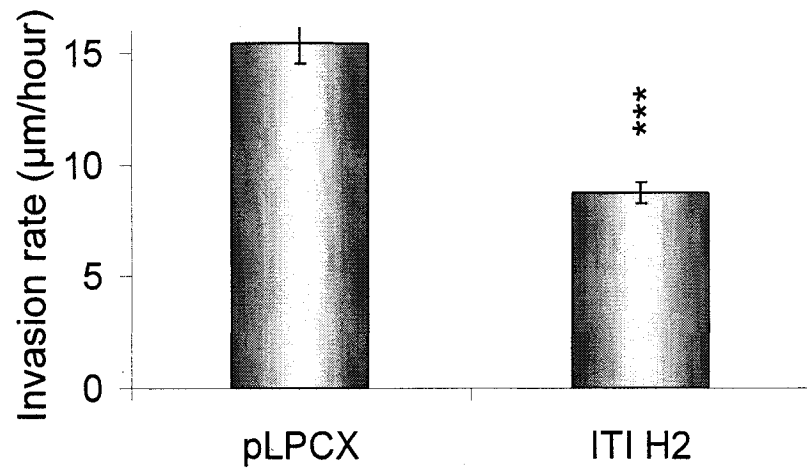


Figure 3.6: Time-lapse videomicroscopy confirms ITI H2 as an inhibitor of individual cell velocity and promoter of cell-cell adhesion. (a) Still photographs depicting cell invasion for U251 pLPCX (upper panels) and U251 ITI H2 (lower panels) over 20 hours. Note that the representative U251 pLPCX spheroid (upper panels) invades approximately twice the distance of the representative U251 ITI H2 spheroid (lower panels). Scale Bar: 250 μm . (b) Quantification of individual cell invasive rates for U251 pLPCX and U251 ITI H2 after 20 hours. N=30 cells for each cell line. Error bars represent SEM. Asterisks indicate significance at $P < 0.001^{***}$. (c) Quantification of the number of individual cell divisions and the percentage of cells detached from the spheroid after 8 hours for pLPCX and ITI H2 cells. N=30 cells for each cell line. Asterisks indicate significance at $P < 0.001^{***}$.

a



b



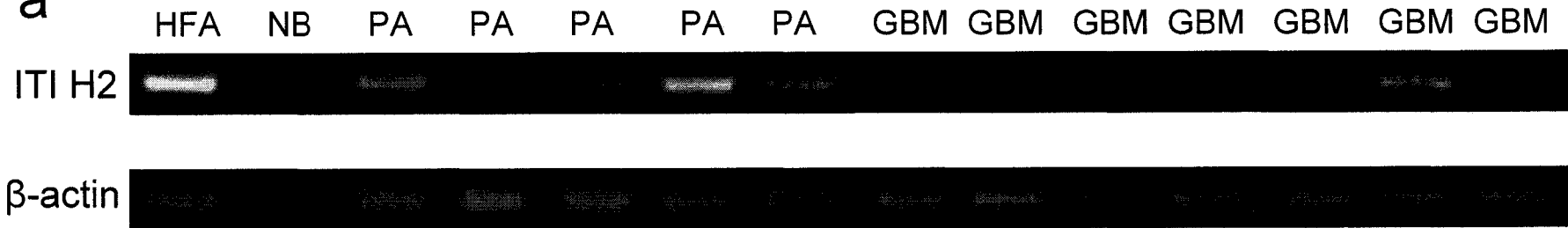
c

cell type	% of cells dividing	% of cells detaching from the spheroid in 8 hours
pLPCX	24	60
ITI H2	10	17 ^{***}

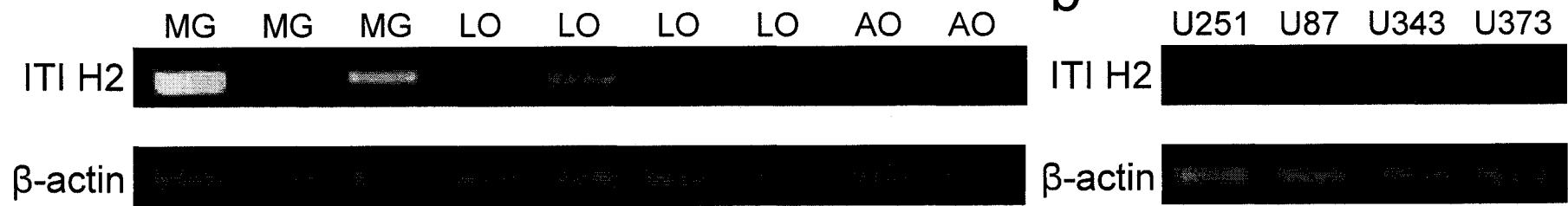
N=30 cells for each cell line tested

Figure 3.7: Expression of ITI H2 is downregulated in high-grade brain tumors. (a) RT PCR analysis of ITI H2 and β -actin mRNA levels in human fetal astrocyte cultures (HFA), normal brain (NB), pilocytic astrocytoma (PA), glioblastoma multiforme (GBM), meningioma (MG), low-grade oligodendroglioma (LO), and anaplastic oligodendroglioma (AO). (b) RT PCR analysis of ITI H2 and β -actin mRNA levels in U251, U87, U343 and U373 glioma cell lines. Note the higher ITI H2 mRNA levels in low-grade tumors and normal brain samples. (c) Immunohistochemical analysis of ITI H2 protein expression in normal brain (upper panels) and GBM (lower panels) representative paraffin sections. Samples were stained with anti-ITI H2 antibody and pre-immune serum as a negative control.

a



b



C

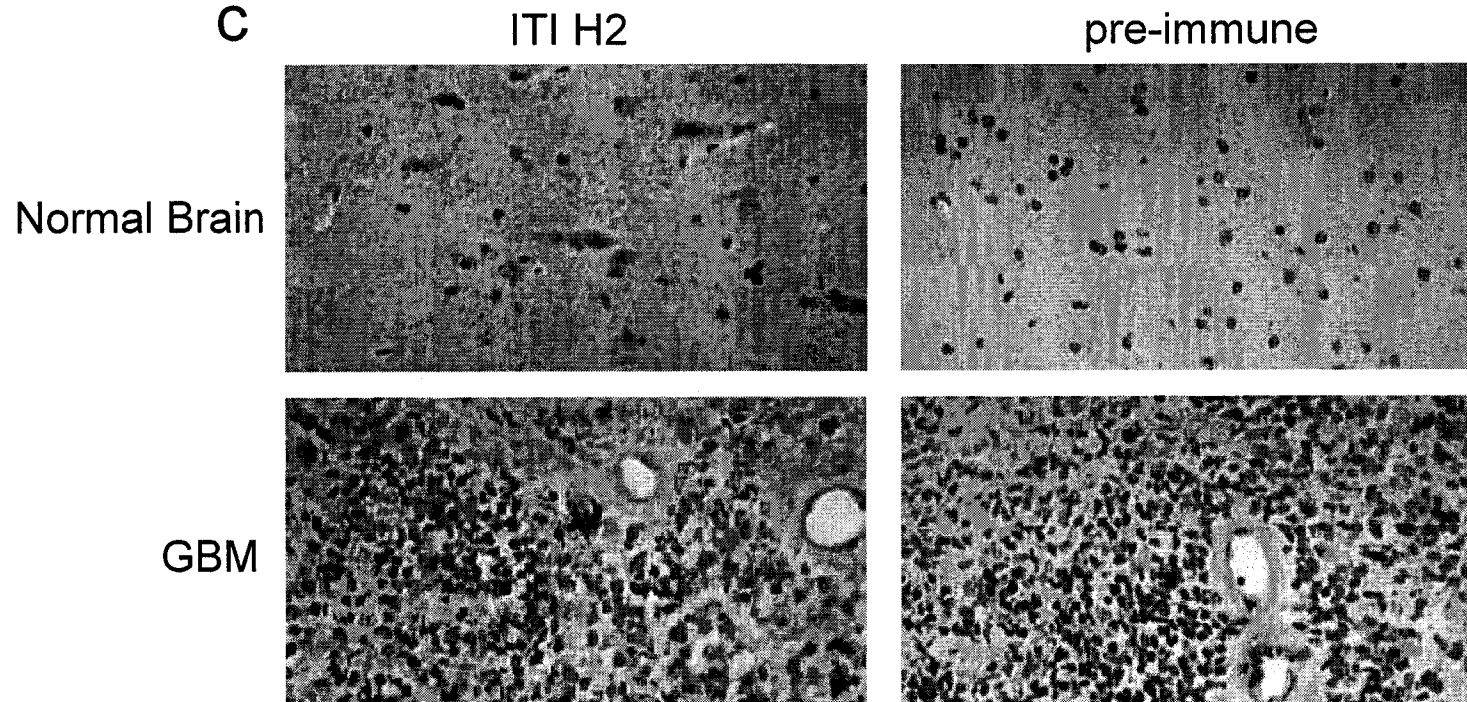


Table 3.1: Mass spectrometry results of proteins present in pooled purified fractions from HiTrap Heparin HP column. Note that Mascot scores above 38 were considered significant at $P < 0.05^*$.

Table 3.1: Mass spectrometry results of proteins present in pooled purified fractions from HiTrap Heparin HP column

Name of Protein Hit	Score
Inter alpha trypsin inhibitor heavy chain 2	66
Vasodilator-stimulated phosphoprotein (VASP)	9
Nuclear autoantigen	8
Similar to expressed sequence AU041783	7
Unnamed protein product	6
Ribonucleotide reductase M2 polypeptide	6
RIKEN cDNA 0710001B24	5
KIAA1914 protein	5
Unnamed protein product	5

Table 3.2: Primers used for all RT PCR reactions. Note that primers 1-3 were used for RT PCR analysis of U251 stable cell lines, and primers 1 and 4 were used for RT PCR analysis of primary human tumors, normal brain, human fetal astrocytes, and glioma cell lines.

Table 3.2: Primer details for all RT PCR reactions

Primer name	Sense	Antisense	Expected product size (bp)
1. β -actin	5'-TCC CCC AAC TTG AGA TGT ATG AAG-3'	5'-AAC TGG TCT CAA GTC AGT GTA CAG G-3'	67
2. ITI H2	5'-GAC TGT CCT GGT CCG ACA CAG-3'	5'-TCC GGA ATT CTT AAG GCC GCT TG-3'	473
3. bikunin	5'-CAA GAG AGG TAT TAC TAC AAC GGC G-3'	5'-CCC GGA ATT CTC AAC TGC GTA TTA G-3'	323
4. ITI H2	5'-CGA ATC AGA GGG TGC AGA TCT C-3'	5'-GGC CGT TTG AGA AAG CTG TAG-3'	437

3.6 Conclusions to Chapter 3 and Preface Chapter 4

We have demonstrated that ITI H2 inhibits glioma cell invasion and proliferation while increasing cell adhesion; however, the intracellular mechanisms remain to be established. Early ITI studies focused on the serine protease inhibitory activity of the light chain bikunin (Zhuo et al., 2004; Bost et al., 1998). Since the early 1990s, it has also been known that ITI heavy chains interact with hyaluronic acid to generate the serum-derived-hyaluronan-associated protein (SHAP)-HA complex (Zhuo et al., 2004; Bost et al., 1998). The transesterification reaction that releases covalently bound bikunin and couples ITI heavy chains to hyaluronic acid results in extracellular matrix stabilization (Fig. 3.8) (Zhuo et al., 2004; Bost et al., 1998). The mechanism is dependent on a currently unidentified esterase produced by cells, and therefore, requires conditioned medium for the reaction to take place. In addition, it has also been shown that TSG-6, the protein product of the Tumor Necrosis Factor stimulated gene-6 is a cofactor and catalyst in the production of HC-HA complexes (Rugg et al., 2005). TSG-6-HC complexes serve as intermediates in the formation of HC-HA (Rugg et al., 2005). The HA coupling activity has been detected in follicular fluid and in conditioned medium from follicular granulosa cells (Chen et al., 1996; ODum et al., 2002). It remains to be determined whether the combined effect of ITI H2 on proliferation, invasion and adhesion in our study can be attributed or partially attributed to HA coupling. The role played by the modulation of both extracellular ITI H2 and levels of intracellular ITI H2 in brain tumor invasion is presently unclear.

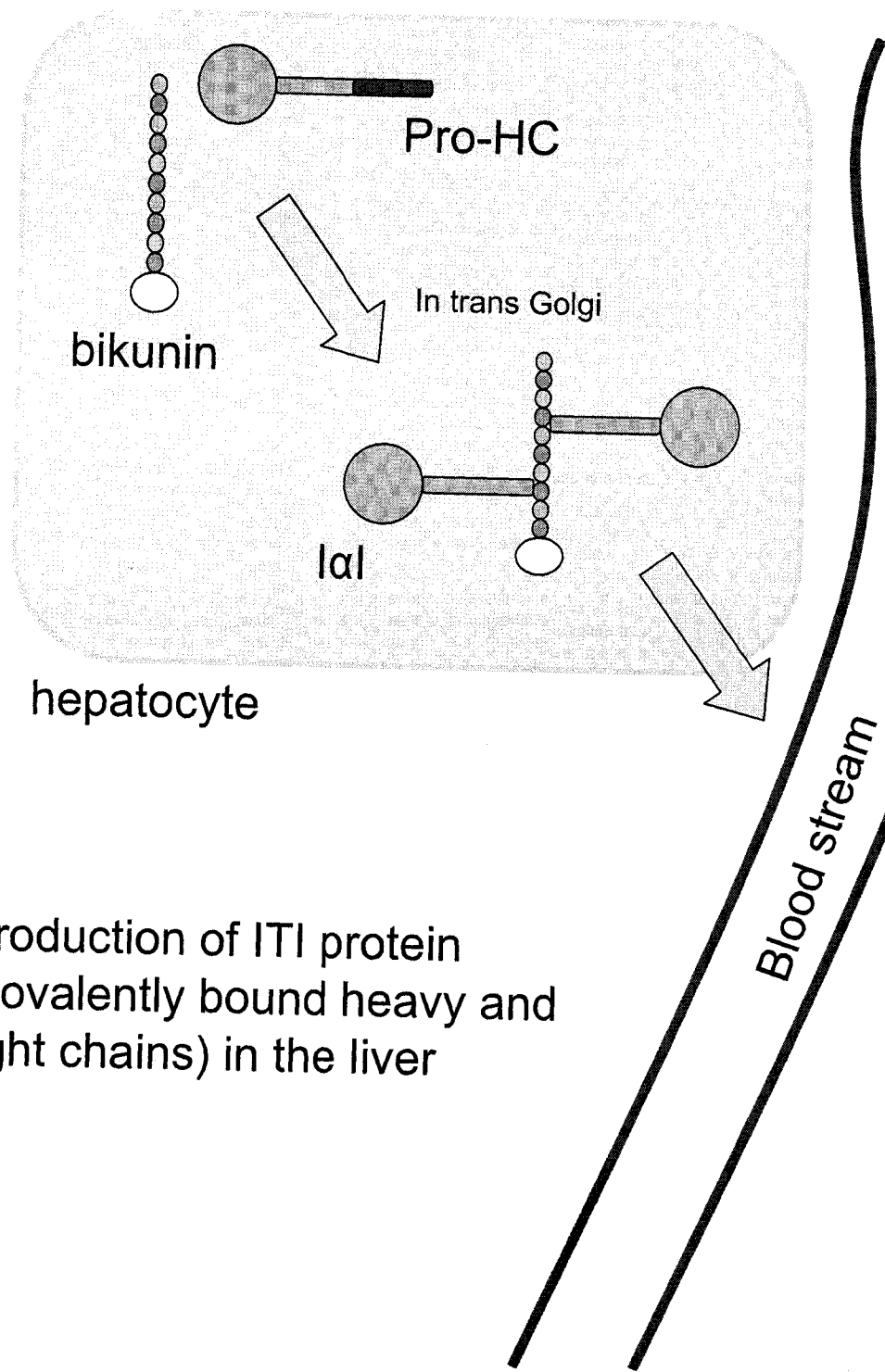
We identified ITI H2 in purified fractions from C6 conditioned medium; however, the mechanism of action for ITI H2 inhibition of invasion and proliferation in our stable overexpressing cell lines may not be the same. Martin-Vandeleet et al. (1999) demonstrated that in COS-7 cells, only co-transfection of ITI H2 with bikunin, and not ITI H2 alone, lead to the processing of ITI H2 into the mature, proteolytically cleaved ITI HC2. Processing of ITI H1 did not require the presence of bikunin (Martin-Vandeleet et al., 1999). Thus, it is clear that the mechanism(s) responsible for the effects of the ITI family are poorly understood.

There are many families of molecules involved in malignant brain tumor invasion. Integrins, cadherins, matrix metalloproteinases, serine proteases, and growth factors all play important roles in multiple facets of the invasive cascade. Other clues about the malignant brain tumor phenotype have come from molecules associated axon guidance and neuronal precursor cell migration. We have focused on negative regulators of malignant brain tumor invasion, and in neurodevelopment, the Slit family of axon guidance cues are known to have both a chemorepellent and inhibitory role (Wong et al., 2002). We have provided evidence for a chemorepellent that directs glioma cell invasion; however, the identity of this molecule(s) is currently unknown (Werbowski et al., 2004). Inter alpha trypsin inhibitor has been shown to have an inhibitory effect on individual glioma cell velocity, but did not influence direction (data not shown), and is therefore, not responsible for the chemorepellent effect seen in glioma co-cultures. We did not find a prospective chemorepellent in our purified fractions, and our mass spectrometry analysis demonstrated only one significant protein in the most inhibitory

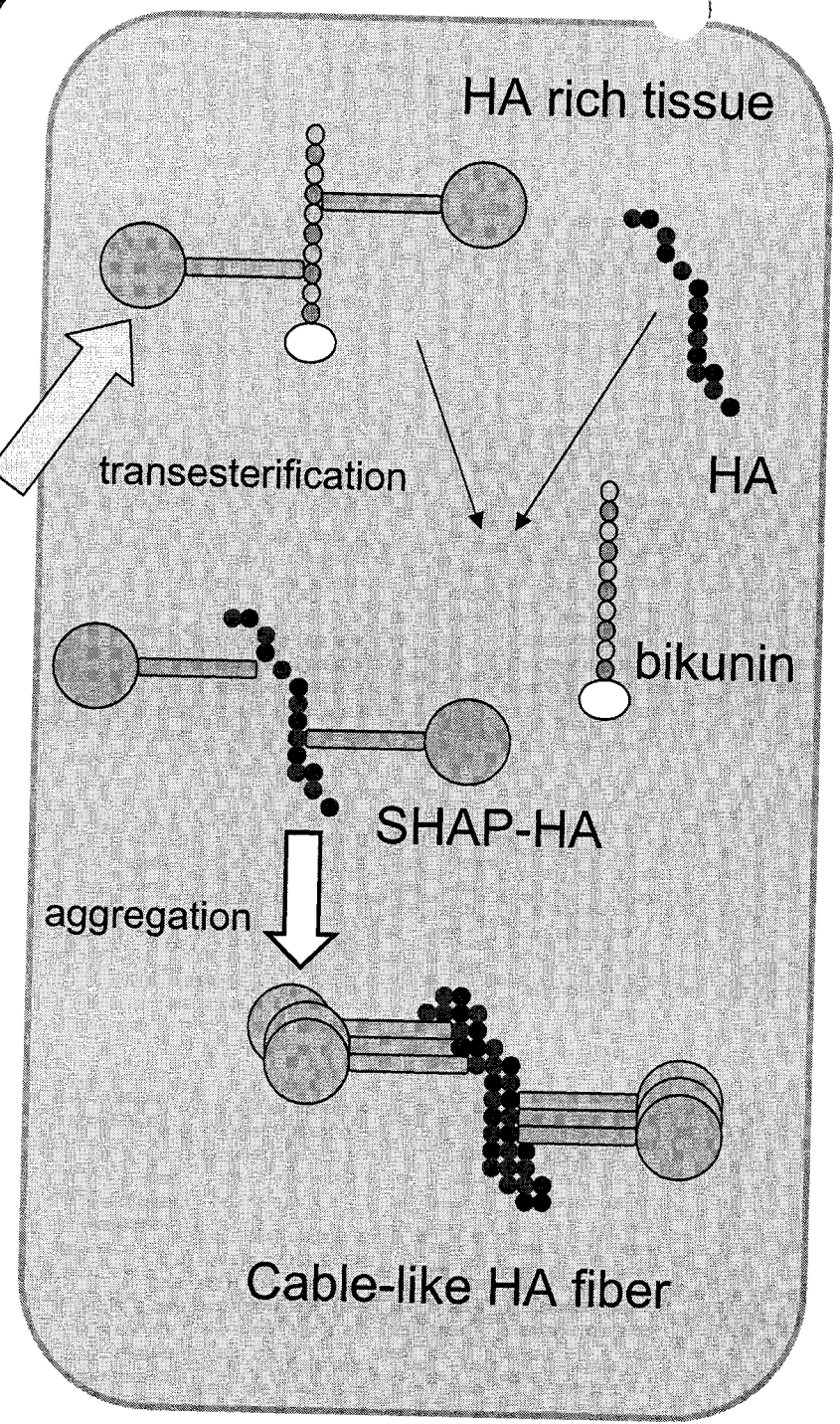
fractions from the HiTrap Heparin HP column. Increasing the quantity of starting material should increase the number of significantly abundant proteins in our fractions, one or more which may be the chemorepellent(s) of interest.

We have used our three-dimensional collagen gel spheroid implantation model to examine the role of Slit2, a known chemorepellent, in malignant brain tumor invasion. The following chapter focuses on the effect of Slit2 on both medulloblastoma and glioma cell invasion with an emphasis on the use of sodium alginate bead microencapsulation therapy as a potential strategy to introduce negative regulators of malignant brain tumor invasion in a clinical setting.

Figure 3.8: Schematic depicting the transesterification reaction that releases covalently bound bikunin and couples ITI heavy chains to hyaluronic acid resulting in extracellular matrix stabilization. ITI heavy chains are typically coupled to the bikunin light chain in the trans-Golgi network of the hepatocytes, and are secreted into the bloodstream. ITI proteins enter hyaluronic acid (HA)-rich tissue, where the transesterification reaction takes place, and free-bikunin is released.



Production of ITI protein
(covalently bound heavy and
light chains) in the liver



Chapter 4: Inhibition of medulloblastoma cell invasion by Slit

4.1 ABSTRACT

Invasion of brain tumor cells has made primary malignant brain neoplasms among the most recalcitrant to currently available therapeutic strategies. Here, we have tested whether the secreted protein Slit2, previously known to be important for guiding the projection of normal axons and developing neurons, can control brain tumor cell invasion. We found that Slit2 inhibited the invasion of medulloblastoma cells *in vitro* and the invasion of these cells into human fetal astrocyte aggregates. The effect of Slit2 was inhibited by either an anti-Robo1 antibody or the Robo ectodomain. Time-lapse videomicroscopy indicated that Slit2 reduced the invasive velocity of medulloblastoma cells without affecting direction or proliferation. Both medulloblastoma and glioma tumors express Robo1 and Slit2, but only medulloblastoma invasion is inhibited by recombinant Slit2 protein. Our findings reinforce the concept that selective neurodevelopmental cues may provide significant insights into tumor invasion and suggest a new therapeutic approach using bioreactor technology for controlling brain tumor invasion by applying Slit2 and other negative guidance cues.

4.2 INTRODUCTION

Medulloblastoma is the most common malignant brain tumor in children, and is believed to originate from granule precursor cells of the cerebellum (Wechsler-Reya and Scott, 2001). Glioblastoma multiforme (GBM) is the most common malignant central nervous system tumor in adults, and is thought to arise from astrocytes or astrocytic precursors (Chicoine and Silbergeld, 1997; Lopez et al., 1995). Both tumors rapidly invade the brain and disrupt normal tissue architecture often leading to early recurrence and poor patient prognosis (Kleihues et al., 2000; Giangaspero et al., 2000). Recent studies placing brain tumors in the context of neurodevelopment have led to the recognition of new tumor suppressors and oncogenes involved in brain tumor progression (Pomeroy et al., 2002; Oliver et al., 2003).

The Slit family of secreted proteins is known to be important for guiding the projection of normal axons and developing neurons (Wang et al., 1999; Brose et al., 1999; Kidd et al., 1999; Li et al., 1999; Wu et al., 1999). There are three Slit proteins in mammals, and all are expressed at the ventral midline of the neural tube. While Slit1 expression is mostly restricted to the nervous system, Slit2 and 3 are also expressed in other organs (Wong et al., 2002). The receptor for Slit is the transmembrane protein Robo (Roundabout), and four ROBO genes have been identified to date (Wong et al., 2002; Park et al., 2003; Sabatier et al., 2004). Typically Robo proteins consist of five extracellular immunoglobulin (Ig) domains, three fibronectin repeats, and a conserved intracellular region of four cytoplasmic motifs (Wong et al., 2002). Robo3 (also known as Rig1) is missing one of the cytoplasmic motifs and Robo4 encodes only two Ig domains,

two fibronectin repeats and two cytoplasmic motifs (Wong et al., 2002; Park et al., 2003; Sabatier et al., 2004).

Recent studies have demonstrated a role for Slit-Robo signaling in leukocyte chemotaxis and tumor angiogenesis (Wu et al., 2001; Wang et al., 2003). Findings of SLIT gene inactivation suggest SLIT2 as a potential tumor suppressor gene in gliomas, lung, breast and colorectal cancer, as well as in neuroblastoma (Dallol et al., 2003a; 2003b; Dallol et al., 2002; Astuti et al., 2004). Our study focuses on the expression and functional significance of Slit2 and Robo1 in medulloblastoma and glioblastoma cell invasion. Our results demonstrate a role for Slit2 as an inhibitor of medulloblastoma but not glioma invasion and suggest a novel approach for treating brain tumor invasion by applying Slit2 and other negative guidance cues.

4.3 METHODS

Spheroid/hanging drop preparation and three-dimensional collagen gels

C6 (murine astrocytoma) cells were cultured in Dulbecco's modified eagle medium (DMEM) supplemented with 10% fetal bovine serum (FBS), 125 U/ml penicillin G, 125 µg/ml streptomycin sulfate, and 2.2 µg/ml amphotericin B (Fungizone) and seeded into spinner culture flasks as described (Werbowetski et al., 2004).

Confluent cultures of U251 (human glioblastoma) UW228-3 (UW3), and DAOY (human medulloblastoma), HEK 293 and HEK 293 cells stably overexpressing full-length human Slit2 with a c-Myc tag at the carboxy terminus were trypsinized (0.05% trypsin/0.53 mM EDTA) and hanging drops were prepared (Werbowetski et al., 2004; Corcoran et al., 2003; Kennedy et al., 1994; Del Duca et al., 2004). Aggregates consisting of 25,000 cells/drop (U251) and 40,000 cells/drop (UW3, DAOY, HEK 293, and Slit2) were utilized.

Spheroids and hanging drop aggregates were implanted into 24-well culture dishes containing 500 µl aliquots of a collagen type I solution (Vitrogen 100) (COHESION, Palo Alto, CA) and cell invasion was assessed daily as previously described (Werbowetski et al., 2004). All culture reagents were obtained from Gibco BRL (Invitrogen, Burlington, ON) unless otherwise stated. All cell lines were purchased from the American Type Culture Collection (ATCC) (Rockville, MD) except the UW3 cell line which was a gift from Dr. John R. Silber (University of Washington, Seattle, WA).

Cell Tracker Dye Labeling and spheroid co-culture quantification

Spheroids and hanging drop aggregates were collected and placed in a 1 ml 25 μ M Cell Tracker Green solution prepared as described previously (Werbowski et al., 2004). Fluorescently labeled spheroids were co-cultured with HEK 293 or Slit2 drop aggregates at various distances, and photographed 24 and 72 hours post-implantation. Co-cultures were imaged using the time-lapse imaging system and Northern Eclipse 6.0 software (Werbowski et al., 2004). Fluorescently labeled spheroids were divided into four quadrants with respect to the position of the adjacent spheroid. The total cell number in the proximal and distal quadrants was calculated for both wild type HEK 293 control and Slit2 co-cultures.

Time-delayed co-culture and conditioned medium assays

UW3 medulloblastoma spheroids were prepared and implanted into collagen type I gels. After 48 hours, medium was removed from the collagen gel, and an aggregate of Slit2 secreting cells or HEK control cells was placed next to the tumor spheroid. Additional collagen was added to the top of the co-culture and allowed to harden, followed by the application of 250 μ l DMEM + 10% FBS. Co-cultures were photographed immediately before and both 24 and 72 hours after implantation of HEK or Slit2 secreting aggregates as described above. Images were divided into 6 regions according to the position of the implanted aggregate, and the number of cells in each area counted for both HEK control and Slit2 co-cultures.

Conditioned medium was collected from HEK and Slit2 confluent monolayer cultures to assess the effect of a uniform concentration of Slit2 on UW3 spheroids implanted in collagen type I gels. Five-hundred microliters of DMEM + 10% FBS, HEK

or Slit2 conditioned medium was placed on top of the collagen gel, and measurements of total invasion were obtained over 5 days with a medium change on day 3.

Time-lapse video microscopy

UW3 medulloblastoma spheroids and HEK or Slit2 hanging drop aggregates were co-cultured as described, and after 24 hours incubation, the cultures were imaged for 20 hours using the imaging system and Northern Eclipse 6.0 software described (Werbowski et al., 2004). For each video, invasion rate, deviation from the expected invasive path (angle change from perpendicular) and number of divisions were calculated for individual UW3 cells in regions proximal to the Slit2 or HEK aggregate source. Only cells that had detached from the spheroid and could be followed during the entire 20 hours were analyzed.

Patients and samples

A total of 15 human brain tumor samples were obtained from the Department of Molecular Pathology and Neurology, University of Lodz tissue bank, Simmelweiss University tissue bank in Hungary, Centre de Neuro-pathologie, Clermont-Ferrand tissue bank in France and the Brain Tumor Tissue Bank London Health Sciences Centre (London, ON). Among the samples, 7 were classified as medulloblastoma, 2 were pilocytic astrocytoma (low grade glioma), 4 were childhood glioblastoma multiforme (GBM) and 2 were meningioma. A sample of normal brain was also analyzed, and all relevant clinical information for the tumors and normal brain was available.

RT PCR in tumor cell lines and primary human brain tumors

Total RNA was extracted using RNeasy kit (Qiagen) according to manufacturer's guidelines. First strand cDNA was synthesized using the First-Strand cDNA Synthesis

Kit (Amersham Biosciences, Baie D'Urfe, QC). For all RT-PCR reactions, PCR using a template generated without reverse transcriptase was used as a negative control. The following PCR conditions were used: 40 cycles at 95 °C for 60 s, 55°C for 30 s, and 72°C for 60s. See Table 4.1 (1-4) for primer details. PCR products were separated by agarose gel electrophoresis.

For primary human brain tumors, total RNA was extracted from frozen samples using the TRIzol Reagent (Gibco BRL) according to manufacturers' guidelines. RNA from the medulloblastoma, pilocytic astrocytoma and meningioma tumors was used directly for RT PCR. See Table 1 (5-7) for primer details. Glioblastoma multiforme (GBM) and normal brain samples were obtained after preparation for microarray analysis in other laboratories and were therefore processed separately. The RiboAmp™ RNA Amplification Kit (Arcturus, MountainView, CA) was used for linear amplification of mRNA from total RNA by two rounds of amplification. The aRNA obtained was used for further RT PCR analysis. First strand cDNA was synthesized using the First-Strand cDNA Synthesis Kit (Amersham Biosciences) for both total RNA and aRNA according to manufacturers' guidelines. The GAPDH was used as an internal control for RT PCR on total RNA samples (medulloblastoma, pilocytic astrocytoma, and meningioma). RT PCR of aRNA requires primers designed within 200-300 bp of the polyA tail for each gene, and therefore, new Slit2 and Robo primers were designed for this analysis and also used for RT PCR on total RNA. See Table 4.1 (4,6,7) for primer details. β -actin was used as an internal control, and standard primer sequences were obtained from Arcturus. For all RT-PCR reactions, PCR in the absence of templates and PCR using templates generated without reverse transcriptase were used as negative controls. The following

PCR conditions were used: 95°C for 2 minutes, 80°C for 3 minutes 30 seconds (during which Taq is added), 40 cycles at 95 °C for 60 s, 55°C (60°C for β -actin) for 30 s, and 72°C for 60s. PCR products were separated by agarose gel electrophoresis.

Encapsulation of 293T cells in sodium alginate

Sodium alginate bead cell encapsulation for treatment of brain tumors has been described (Read et al., 1999; Read et al., 2001). Briefly, a stock solution of 0.137 M NaCl, 5.5 mM D-glucose, 5.45 mM HEPES was prepared at a final pH of 7.3. Confluent cultures of HEK 293 cells and cells overexpressing Slit2 and Netrin1 were trypsinized and resuspended in alginate solution at a cell density of 1.6×10^6 cells/ml. From these solutions, droplets of cells dispersed in 1.5% sodium alginate were released into a 0.1 M CaCl_2 solution prepared from the stock. After polymerization, the alginate beads were washed two times in PBS and once in DMEM + 10% FBS. The encapsulated cells were cultured in 10 cm Petri dishes containing 20 ml medium that was replaced every three days.

C6, U251, UW3 and Daoy spheroids were prepared and implanted into type I collagen gels. Four empty beads, control HEK beads, or beads encapsulating Slit2 and Netrin1 overexpressing cells were implanted 1 cm from the tumor spheroids at all four corners of the wells. Total invasion was measured for 6 days, and the medium was replaced on day 3. For functional blocking antibody or dominant negative experiments, R5 (an IgG_{2b} monoclonal antibody to the first immunoglobulin domain of Robo1) and RoboN (an extracellular fragment of Robo1 that is a known inhibitor of Slit2-Robo1 interaction) (Wong et al., 2002; Wu et al., 2001; Wang et al., 2003); were used to block the effect of secreted Slit2 from microencapsulated cells. R5 was added to the medium at

a concentration of 15 µg/ml. RoboN-293 cells with an HA tag at the carboxy terminus were cultured, conditioned medium was collected upon reaching confluency and diluted 1:10 before application. For mixed bead cultures, Slit2 and RoboN or Slit2 and HEK cells were encapsulated in sodium alginate at a cell density of 1.2×10^6 cells/ml. Mixed beads and HEK beads were implanted along with UW3 spheroids into collagen gels, and total invasion was measured for 5 days with a medium change on day 3.

Western-Blot analysis

To verify that Slit2 and RoboN were secreted from the beads, conditioned medium from encapsulated HEK Slit2-c-myc cells, encapsulated mixed Slit2 and HEK cells or Slit2 and RoboN-HA cells was collected, concentrated 10X and 20µg protein was subjected to SDS-PAGE on a 7.5% polyacrylamide gel. Myc expression was detected using an anti-Myc antibody (1:1000) that recognizes a C-terminal myc epitope tag on Slit2 and HA expression was detected using an anti-HA antibody (1:500) (COVANCE, Berkeley, CA). The HRP-conjugated goat anti-mouse and anti-rabbit IgG secondary antibodies (1:5000) were used and visualized by enhanced chemiluminescence (Perkin-Elmer Life Sciences Inc., Markham, ON). Conditioned medium was also collected from HEK encapsulated cells and from Slit2 and RoboN monolayer cultures.

Proliferation Assay

Monolayers of UW3, Daoy, U251 and C6 cells were plated on 6-well culture dishes (40,000 cells/well for UW3, Daoy and U251; 20,000 cells/well for C6, two replicates for each time point). Cells were allowed to adhere before being exposed to either HEK or Slit2 encapsulated beads. UW3 and Daoy medulloblastoma and U251 glioma cells were counted on days 2, 4 and 6 using a Coulter ZTM Series counter

(Beckman-Coulter Inc., Miami FA). C6 were counted on days 2 and 4 only because of the high proliferation rate of this cell line.

Confocal Microscopy and Human Fetal Astrocyte Aggregate Infiltration

Human fetal astrocytes were obtained from the Albert Einstein College of Medicine Human Fetal Tissue Repository and prepared from fetal CNS tissue as previously described (Ladiwala et al., 1998). Briefly, human fetal CNS tissue was obtained at 12-16 weeks gestation following Canadian Institutes of Health Research (CIHR) guidelines. The tissue was mechanically dissociated and treated with 0.25% trypsin and 50 µg/ml DNase for 45 min at 37 °C. Dissociated tissue was passed through a 130 µm mesh, washed twice with PBS and plated onto tissue culture flasks in MEM supplemented with 5% FCS. Populations of proliferating fetal astrocytes were obtained after three to four passages and used to prepare hanging drop aggregates at a concentration of 45,000 cells/drop as previously described (Werbowski et al., 2004).

UW3-human fetal astrocyte co-cultures were labeled with DiI and DiO respectively (Molecular Probes, Eugene OR). DiI (2.5 mg) was dissolved in 1ml 100% ethanol, and DiO (2.5 mg) was dissolved in 1ml 10% DMSO in 100% ethanol. Both were diluted in DMEM to give a final concentration of 0.075 mg/ml. Co-cultures were implanted in collagen gels with either four sodium alginate beads encapsulating HEK or Slit2 secreting cells placed around them. Cultures were analyzed using a LSM 510 confocal scanning laser microscope (Carl Zeiss, Toronto, ON) and a 10X objective 5 days after implantation. DiI and DiO were detected with helium-neon (543 nm) and argon 2 (488 nm) lasers respectively. Samples were optically sectioned from the surface to the spheroid centre with 12 µm between each slice, and 10-12 serial images of 512X512

pixels were collected for each sample. Slices were then combined into one image of approximately 100 μm through the centre of the co-cultures. The number of cells infiltrating the astrocyte aggregates, and the total invasion distances for each were calculated using Northern Eclipse 6.0 time-lapse video software. Results are representative of three independent trials.

Robo1 transfection and Biotinylation

A pCEP4 (Invitrogen) plasmid expressing full-length rat Robo1 tagged with HA was constructed as described (Li et al., 1999). To obtain stable transfections of U251 cells overexpressing Robo1, Robo1-HA vectors were transfected into U251 cells. Antibiotics were added 48 hours after transfection, and selection was carried out for 5 weeks with a medium change every 3 days. Hygromycin B (Sigma) was used to select for stable U251-Robo1-HA cell lines at a concentration of 500 $\mu\text{g}/\text{ml}$. Stable cell lines were obtained after isolating clones and testing for protein expression by Western Blot analysis using an anti-HA antibody.

Subconfluent U251 wild-type and U251-Robo-HA cells were washed 3X in ice cold PBS, and a fresh 0.5 mg/ml EZ-Link Sulfo-NHS-LC-Biotin solution (Pierce, MJS BioLynx, Brockville, ON) was placed on monolayer cultures for 30 min at 4°C to prevent endocytosis. Excess biotin was quenched 3X with ice-cold quenching solution followed by 3X washing with ice-cold PBS. Cells were lysed with 1 ml RIPA buffer and scraped. One hundred microliters of ImmunoPure Immobilized Streptavidin (Pierce) was added to total cell lysates, and then rocked overnight at 4°C. Streptavidin beads were pelleted by centrifugation at 13 000 rpm (4°C), supernatant was discarded, and pelleted beads were washed with 1ml RIPA buffer. This step was repeated three times. After the third wash in

RIPA buffer, the supernatant was removed and sample buffer was added to dissociate biotin-streptavidin interactions. Samples were then prepared for SDS PAGE and Western Blot analysis as described above. Anti-HA antibody was used to detect recombinant Robo1 and anti p42/44 was used as a cell surface biotinylation control.

Cdc42 and Rac1 GTPase Activity Assays

Rac1 and Cdc42 assays were performed using nonradioactive Activity Assay kits according to manufacturers' instructions (Upstate Biotechnology, Lake Placid, NY). Briefly, monolayer cultures of UW3 and C6 cells were treated with concentrated conditioned medium diluted in serum-free DMEM either from Slit2 expressing HEK cells or control HEK cells for 24 hours, and lysed. Cell lysates were affinity-precipitated with a GST fusion-protein corresponding to the p21-binding domain of human PAK1 bound to glutathione-agarose and run on 15% SDS-PAGE. Western Blot analysis was used to probe blots for activated Rac1 and Cdc42-GTP proteins pulled down by glutathione-agarose beads. Cdc42 and Rac1 levels were determined by Western Blot analysis and used as loading controls. Cdc42 and Rac1 antibodies were obtained from Santa Cruz Biotechnology Inc. (Santa Cruz, CA) and BD Transduction Laboratories (BD Biosciences, Pharmingen, Mississauga, ON) respectively. Results are representative of three independent experiments.

Statistical Analysis

All tests were performed using SPSS Graduate Pack 9.0 statistical software (SPSS Inc., Chicago IL). Descriptive statistics including mean and standard error of the mean along with

one-way ANOVA's, independent sample two-tailed t-tests, paired t-tests and Tukey's test for multiple comparisons were utilized to determine significant differences. P values less than 0.05 were considered significant.

4.4 RESULTS

Medulloblastoma spheroids respond to a local concentration of Slit2

To test the hypothesis that malignant brain tumor cells are affected by Slit2, medulloblastoma and glioma spheroids were co-cultured with HEK 293T or HEK aggregates overexpressing Slit2 in collagen type I matrices (Fig. 4.1a). After 48 and 72 hours, cultures were photographed, and the total cell number in the proximal and distal quadrants was calculated (Fig. 4.1b). When wild type HEK aggregates were co-cultured with both glioma (C6 and U251) and medulloblastoma (UW3 and Daoy) spheroids, there was no significant difference in the number of cells in the proximal versus distal quadrant for UW3, Daoy and C6 (Fig. 4.1c,e, g). There was a significant increase in the number of cells in the proximal quadrant for U251 co-cultures (t-test: $p < 0.05$; $n = 5$ co-cultures) (Fig. 4.1i). In the presence of Slit2 aggregates, fewer UW3 and Daoy medulloblastoma cells were found in the quadrant proximal to the Slit2 source (t-test: $p < 0.01$; $n = 5$ co-cultures for UW3; $p < 0.05$; $n = 7$ co-cultures for Daoy) (Fig. 4.1d,f). There was no significant difference between quadrant cell numbers for C6 glioma but the number of cells in the proximal quadrant of U251 co-cultures was significantly higher (t-test: $p < 0.05$; $n = 5$ co-cultures) (Fig. 4.1h,j respectively). These results suggest that medulloblastoma cells respond to the guidance cue Slit2, but glioma cells do not. They do not differentiate between a repulsive or inhibitory action of Slit2.

Slit2 inhibits medulloblastoma cell invasion

To investigate whether Slit2 functions as a repellent or inhibitor of medulloblastoma cell invasion, we used a time-delayed co-culture assay previously described (Fig. 4.2a) (Ward et al., 2003). After placement of control HEK 293

aggregates, the number of medulloblastoma cells should increase uniformly around the spheroid circumference. If Slit2 acts solely as an inhibitor, the number of medulloblastoma cells on the proximal side of the Slit aggregate should remain the same or increase. Any increase should be less than the increase seen on the distal side of the explant. A chemorepellent effect of Slit2 should result in a decrease in the number of cells on the proximal side, as the cells move away from the Slit2 source and back toward the medulloblastoma spheroid.

Twenty-four hours after the placement of control aggregates, a statistically significant increase in the number of medulloblastoma cells was observed for all sampling areas (paired t-test: $p < 0.01$ for Areas I, V, and VI; $p < 0.001$ for Areas II, III and IV; $n = 8$ co-cultures) (Fig. 4.2b). When a Slit2 aggregate was placed adjacent to the spheroid and its invading cells, there was no significant change in the number of cells 24 hours after placement in the proximal areas I and II (Fig. 4.2b). There was a significant increase in the number of medulloblastoma cells for all other sampling areas counted (paired t-test: $p < 0.01$ for Areas III, V and VI, $p < 0.001$ for Area IV; $n = 8$ co-cultures) (Fig. 4.2b). At 72 hours, there was a significant increase in the number of cells in regions I and II; however, this increase is less than that seen in the other regions more distal to the Slit2 source as well as corresponding areas in HEK control co-cultures (paired t-test: $p < 0.01$ for Areas I, III and V in HEK control co-cultures, $p < 0.001$ for all Areas in Slit-2 co-cultures and Areas II, IV and VI in HEK control co-cultures; $n = 14$ Slit-2 co-cultures, and $n = 6$ for HEK control co-cultures) (Fig. 4.2c). These results are consistent with the idea that Slit2 functions as an inhibitor, and not a chemorepellent, of medulloblastoma cells.

To further support Slit2 as an inhibitor of medulloblastoma cell invasion, conditioned medium from confluent monolayer cultures of HEK or Slit2 cells was applied over single UW3 spheroids in collagen. Uniform concentrations of Slit2 conditioned medium significantly inhibited invasion of UW3 cells compared with DMEM and HEK controls (Fig. 4.2d).

Slit2 does not affect medulloblastoma cell proliferation or turning

To further characterize the response of invading medulloblastoma cells to Slit2, we performed time-lapse videomicroscopy on individual UW3 spheroids from 24-44 hours after implantation adjacent to either an HEK or Slit2 aggregate (Fig. 4.3). During the 20 hour observation period, there was a significant inhibition of medulloblastoma cell velocity (54%) for Slit2 co-cultures compared with HEK co-cultures (t-test; $p < 0.001$) (Fig. 4.3a-c). In addition to the kinetic effect, a subset of cells (7 of 32 or 22%) in Slit2 co-cultures appeared to stall and remained stationary (Fig. 4.3b). They maintained a “ruffled” appearance and failed to invade the gel during the observation period. There was no significant difference in cell direction for Slit2 and HEK co-cultures (data not shown). Proliferation was not significantly different between the two co-cultures with 14% of the cells dividing in HEK cultures and 16% of cells dividing for Slit2 cultures. Taken together, these results suggest that Slit2 inhibits invading medulloblastoma cell velocity without affecting direction or proliferation, and further support the role for Slit2 as an inhibitor, and not a repellent, of medulloblastoma cells.

Medulloblastoma and glioma cell lines as well as primary human brain tumors express Robo1 and Slit2

Using RT-PCR, we found that all medulloblastoma cell lines tested (UW3, Daoy and UW1) and all glioma cell lines (C6, U251, U87 and U373) expressed Robo1 and Slit2 mRNA; however, U87 glioma cells expressed negligible levels of Slit2 (Fig. 4.4a). Human fetal astrocytes and mouse cerebellum from P4 and P8 were also both positive for both Slit2 and Robo1 (Fig. 4.4a). Slit1 was not detected in any medulloblastoma or glioma cell lines (data not shown). Taken together, these results demonstrate mRNA expression of Slit2 and Robo1 by both medulloblastoma and glioma cell lines and suggest that the lack of glioma cell responsiveness to exogenous Slit2 may be regulated by other mechanisms.

To explore the significance of our findings to primary human brain tumors, we used RT-PCR to assess Robo1 and Slit2 expression. Representative samples are shown in Fig 4.4b,c. In total, 57% (4 of 7) and 86% (6 of 7) of medulloblastomas express Robo1 and Slit2 respectively; 100% (2 of 2) of meningiomas and pilocytic astrocytomas express both Robo1 and Slit2; 100% (4 of 4) GBM's express Robo1 and 75% (3 of 4) express Slit2, and the normal brain sample expresses both Robo1 and Slit2. Human fetal astrocytes cultures were also positive for Robo1 expression (data not shown). These results demonstrate that the expression of Robo1 and Slit2 in tumor cell lines is also applicable to primary human tumor samples and are consistent with recent reports of expression in other types of human cancers (Dallol et al., 2003a; 2003b; Dallol et al., 2002; Astuti et al., 2004; Latil et al., 2003).

Slit2 secreted from sodium alginate bead microcapsules inhibits medulloblastoma cell invasion in collagen gels

The sodium alginate secreting bioreactor approach provides prolonged sustained delivery of recombinant proteins from producer cells and high levels of the secreted molecule that can be maintained for weeks to months (Read et al., 1999; Read et al., 2001; Joki et al., 2001). To assess the effect of continuous Slit2 release from cells without the concomitant invasion of producer cells, four beads encapsulating Slit2 cells were placed around individual spheroids, and invasion was monitored over 6 days (Fig. 4.5a). Empty beads were used to assess the effect of sodium alginate incorporation in the matrix on implanted spheroids, and wild-type HEK beads were used as a negative control. Beads encapsulating HEK cells overexpressing Netrin1 were also used to assess the influence of another overexpressed guidance cue on spheroids in collagen.

Western blot analysis was used to confirm the presence of Slit2 in the conditioned medium of encapsulated Slit2 cells (Fig. 4.5b). Conditioned medium from Slit2 monolayer cultures was used as a positive control, and conditioned medium from HEK monolayer cultures was used as a negative control (upper panel lanes 1 and 2; lower panel lane 1) (Fig. 4.5b). Western blots of conditioned medium from encapsulated Slit2 cells showed a band around ~200 kD corresponding to Slit2 protein for the six days of *in vitro* experiments in collagen I (upper panel), and this band was still present after 18 days in culture (lower panel).

Compared to empty and HEK 293 control sodium alginate beads, encapsulated Slit2 secreting cells had a significant inhibitory effect on UW3 medulloblastoma cell invasion (Fig. 4.5c-f). A small 15% inhibition was seen for Daoy medulloblastoma cell invasion (Fig. 4.5g). Microencapsulated Slit2 secreting cells had no effect on C6 and U251 glioma cell invasion (Fig. 4.5h,i). Slit2 secreting bioreactors implanted around

UW3 and Daoy spheroids also had a significant inhibitory effect on invasion compared to Netrin1 secreting microencapsulated cells (Fig. 4.5f-g). The effect of Netrin1 beads on medulloblastoma invasion was not different from that seen for empty and HEK 293 controls (Fig. 4.5f-i). These results demonstrate that medulloblastoma cells are also inhibited by continuous, sustained exogenous levels of the guidance cue Slit2.

To confirm the specificity of the effect to Slit2-Robo1 signaling, R5 (an IgG_{2b} monoclonal antibody to the first immunoglobulin domain of Robo1) and RoboN (an extracellular fragment of Robo1 that is a known inhibitor of Slit2-Robo1 interaction) were used to block the effect of secreted Slit2 from microencapsulated cells (Wu et al., 1999; Wang et al., 2003). At the concentrations tested, both R5 and RoboN rescued the inhibitory effect of Slit2 on UW3 medulloblastoma invasion by 50%. The values obtained using R5 and RoboN were not significantly different from UW3 invasion distances using empty and HEK bead controls (Fig. 4.6a).

The addition of R5 and RoboN conditioned medium just on day 0 and day 3 may not be able to completely block the continuous sustained delivery of Slit2 into the collagen matrix over 5 days. To address this issue, mixed sodium alginate beads containing Slit2 and RoboN secreting cells were implanted with UW3 spheroids into the collagen matrix and compared with the effect of mixed beads containing Slit2 and HEK 293 cells or HEK 293 beads alone. Western blot analysis was used to confirm the presence of Slit2 and RoboN in the conditioned medium of microencapsulated Slit2-RoboN cells (Fig. 4.6b). After 5 days in culture, mixed Slit2-HEK beads had a significant inhibitory effect on invasion; however, mixed Slit2-RoboN beads had the same effect as HEK 293 beads alone (Fig. 4.6c). The invasion inhibition for Slit2-HEK beads was 28%

compared with Slit2-RoboN mixed beads and 26% compared with HEK beads. Taken together, these results demonstrate that the inhibitory effect of continuous, sustained delivery of Slit2 can be partially blocked by the functional blocking R5 antibody and RoboN conditioned medium but is completely blocked by encapsulating RoboN cells with Slit2 secreting cells.

Slit2 inhibits UW3 medulloblastoma cell invasion into aggregates of fetal human astrocytes

To demonstrate an inhibitory effect on invasion in a more biologically relevant model, UW3 spheroids and human fetal astrocyte aggregates were labeled with DiI and DiO respectively, and co-cultured in collagen gels. Four sodium alginate beads encapsulating either HEK or Slit2 cells were implanted around the UW3-astrocyte co-culture. Invasion was monitored over 5 days, and confocal images were obtained through the center of the co-culture to determine medulloblastoma cell infiltration into the astrocyte aggregate (Fig. 4.7a-b). Compared with HEK sodium alginate beads, beads encapsulating Slit2 secreting cells significantly inhibited both the number of cells infiltrating the astrocyte aggregates as well as the total invasion distance for individual cells (Fig. 4.7c-d respectively). These findings demonstrate that Slit2 inhibits medulloblastoma invasion on multiple substrates, and that confrontation co-cultures using human fetal astrocytes can also be used to assess the effect of a secreted molecule on medulloblastoma invasion.

Slit2 does not affect medulloblastoma and glioma cell proliferation

To confirm that the effects in our previous *in vitro* microencapsulation studies are attributed to tumor cell invasion and not proliferation or cytotoxic effects, monolayer

cultures of medulloblastoma and glioma cells were exposed to sodium alginate encapsulated HEK cells or cells overexpressing Slit2 for 6 days (4 days for C6). In all cell lines tested, conditioned medium from Slit2 encapsulated sodium alginate beads did not significantly affect tumor cell proliferation or doubling time compared to controls (data not shown).

Slit2 downregulates activated Cdc42 in medulloblastoma cells

In our study, medulloblastoma cells respond to exogenous Slit2 but glioma cells do not. To understand the mechanism responsible for this difference, we biotinylated cell surface proteins to examine expression levels of Robo1 at the surface of U251 cells stably transfected with Robo1-HA. Similar to wild-type glioma, U251 cells overexpressing Robo1-HA did not respond to Slit2 using both co-culture and sodium alginate bead assays (data not shown). Biotinylation showed that Robo1 protein was highly expressed at the cell surface of both stably transfected HEK and U251 cells (Fig. 4.8). These findings demonstrate that the lack of glioma responsiveness to Slit2 cannot be explained by aberrant receptor shuttling or expression and suggest that differences are intracellular.

Studies have shown that Cdc42 and Rac1 play a role in Slit-mediated repulsive effects (Wong et al., 2001; Fan et al., 2003; Lundstrom et al., 2004). To assess Cdc42 and Rac1 activation by Slit2 in medulloblastoma and glioma cells, we cultured both UW3 medulloblastoma and C6 glioma cells in monolayer cultures with medium conditioned by HEK cells or HEK cells overexpressing Slit2. Pull-down assays of activated Cdc42 and Rac1 demonstrated a decrease in Cdc42-GTP and a slight decrease in Rac1-GTP activities, for UW3 cells cultured with Slit2 conditioned medium (Fig. 4.9). In contrast, C6 cells did not display any differences in Rac1- or Cdc42-GTP activity when cultured in

Slit2 conditioned medium (Fig. 4.9). Similar results were also obtained for the other glioma cell line U251 (data not shown). These results suggest that Cdc42-GTP levels, and to a lesser extent Rac1-GTP levels, may play a role in the inhibitory effect of Slit2 on medulloblastoma cells. The inability of Slit2 to modulate activated Cdc42 and Rac1 in glioma cells may contribute to the functional differences seen in our invasion assays.

4.5 DISCUSSION

Current treatment strategies for medulloblastoma include surgery, radiation therapy and/or chemotherapy (Wechsler-Reya and Scott, 2001). These approaches, although successful in decreasing tumor volume, do not consistently control invading tumor cells. Local recurrence along with cerebral spinal fluid (CSF) and systemic metastasis develop, and account for the fact that only 60-70% of patients survive 5 years after diagnosis (Louis et al., 2002).

Here we provide evidence for Slit2 inhibition of invading medulloblastoma cells in several experimental models used in this study. There was no similar inhibitory effect of this molecule on the invasion of malignant glioma cells as shown by the lack of response to Slit2. Other Robo homologues were not tested in these models and their influence on brain tumor invasion is not known. Both glial and neuronal tumor cell lines express Slit2 and Robo1; however, medulloblastomas respond to exogenous Slit2 but glioma cells do not. The lack of responsiveness of highly invasive glioma cells to Slit2 may be attributed to a variety of mechanisms. Dallol et al. (2003a) have analyzed SLIT2 expression and the hypermethylation status of the promoter region CpG islands of this gene in gliomas. They found by quantitative real-time RT-PCR that SLIT2 expression was downregulated in gliomas with methylated SLIT2 promoter compared to gliomas and normal brain samples showing no methylation of this promoter. These authors suggested that SLIT2 may function as a tumor suppressor gene but this study did not address the functional significance of Slit2/Robo1 interaction on the invasion of tumor cells (Dallol et al., 2003a; 2003b; Dallol et al., 2002; Astuti et al., 2004). Our results in

primary glioblastoma multiforme (GBM) tumors suggest a decrease in Slit2 expression when we compared levels in GBM samples to the normal brain sample; however, these results were not quantitative.

Keleman et al. (2005) have addressed the role of Commissureless (Comm) in regulating surface levels of Robo in *D. Melanogaster* and have provided evidence for the “sorting” model of Comm control of Robo expression. This model supports the hypothesis that Comm prevents Robo from reaching the cell surface by regulation at the level of the trans-Golgi network (Keleman et al., 2002). In contrast, the “clearance” (or internalization) model proposes that Comm assists in rapidly removing surface Robo by endocytosis (Myat et al., 2002). We have assessed Robo1 surface expression levels by biotinylation of cell surface proteins and our results confirm that differential responses to Slit2 are attributed to mechanisms downstream of the cell membrane. Robo1 surface levels in U251-Robo1-HA were quite high however the Slit2-Robo1 interaction may be insufficient to inhibit the extensive invasion seen in glioblastoma cells lines such as U251 and C6 but effective in modulating the velocity of less invasive medulloblastoma cell lines.

An interesting finding in the U251 glioma cell line was the increase in the number of cells in proximal versus the distal quadrant for both HEK and Slit2 co-cultures. These results suggest the presence of a strong chemoattractant or inducer of motility secreted by HEK cells. Many cells produce growth factors and their receptors in an autocrine or paracrine manner that influences glioma cell motility but very few endogenous secreted factors are known to inhibit or repel glioma cells (Mueller et al., 2003; Werbowetski et al., 2004).

Expression of Robo proteins has traditionally been associated with migrating axons and neurons in the developing nervous system (Wong et al., 2002). Marillat et al. (2004) have recently demonstrated a role for Rig1/Robo3 in controlling midline crossing of hindbrain precerebellar neurons and axons. Human patients with horizontal gaze palsy with progressive scoliosis (HGPPS) were reported to have mutations in Rig1/Robo3, and functional studies have shown defects in commissural hindbrain projections and pontine nuclei (Jen et al., 2004). Astuti et al. (2004) have demonstrated hypermethylation of the SLIT2 promoter in a series of neuroblastoma tumors. Investigation of Slit2-Robo1 interactions in neuroblastoma and other neuronal cell tumors may help clarify their role in invasion.

Although Slit proteins have usually been associated with a chemorepellent role in axon guidance, an inhibitory effect of Slit on neurons and other migratory systems has been described. Studies have shown that cells migrating from neurospheres generated from SVZ of P0-P3 Slit1 $-/-$ mice were found to migrate further than cells from Slit1 $+/-$ neurospheres suggesting that Slit1 plays an inhibitory role in addition to its function as a repellent (Nguyen-Ba-Charvet et al., 2004). Moreover, there was also a difference in the pattern of migration between neurospheres derived from both mice where Slit1 $-/-$ cells displayed a more dispersed pattern of migration as opposed to classic chain migration (Nguyen-Ba-Charvet et al., 2004). Our time-lapse videomicroscopy studies also showed a change in cell morphology, as the presence of Slit2 aggregates increased the number of non-invading ruffling cells in addition to inhibiting medulloblastoma cell velocity. Other studies have suggested that Slit alone inhibits migration from subventricular zone explants; however, when combined with an astrocyte-derived migration inducing activity

(MIA), Slit acts as a repellent (Mason et al., 2001). Furthermore, Slit2 has been shown to inhibit leukocyte chemotaxis induced by chemokines (Wu et al., 2001). These studies are consistent with our finding that Slit2 is an inhibitor of medulloblastoma invasion.

Microencapsulation bioreactor technology has been used previously to assess the efficacy of anti-angiogenic compounds on the growth of gliomas both *in vitro* and *in vivo* (Read et al., 1999; Read et al., 2001; Joki et al., 2001). Our results show that this technology can be expanded to target invasive or metastatic brain tumor cells such as medulloblastoma. Sodium alginate bioreactors provide an isolated and efficient environment for continuous Slit2 delivery over time as opposed to single application in the medium, and we have shown sustained bioreactor Slit2 secretion for several weeks. Using this model, we have confirmed that Slit2 inhibits medulloblastoma cell invasion without affecting doubling time or proliferation *in vitro*. This model also demonstrates that the inhibition of medulloblastoma cell invasion by continuous Slit2 delivery can be partially rescued by both a Robo1 functional blocking antibody and conditioned medium from RoboN cells. Furthermore, the effect can be completely rescued by mixed alginate beads encapsulating both Slit2 and RoboN cells. The effects of alginate bead bioreactors could therefore be regulated and controlled as needed. Bioreactor technology can potentially be used for combination therapy with encapsulated cells overexpressing anti-invasive, anti-proliferative and pro-apoptotic molecules. Bioreactor implantation targeting CSF pathways with anti-adhesive molecules may help control medulloblastoma cells in this environment.

The problems encountered with xenograft models of medulloblastoma in nude mice have made it difficult to study the characteristics of this tumor *in vivo* (Raffel,

2004). In particular, cell lines that invade or migrate on various substrates *in vitro* do not always demonstrate the same motile properties in xenograft models despite extensive growth over time (unpublished results). This has made the study of *in vivo* medulloblastoma invasion difficult. To model the inhibitory effect of Slit2 in a more biologically relevant environment, we used confrontation co-cultures of spheroids and astrocyte aggregates. Using this model, we have assessed the dynamics of medulloblastoma cell invasion into normal brain aggregates that more closely recapitulate the normal tissue architecture and extracellular environment. Although we have shown that Slit2 does not affect medulloblastoma cell proliferation using sodium alginate bead microencapsulation with monolayer cultures and time-lapse videomicroscopy *in vitro*, the effect on medulloblastoma tumor growth in our confrontation co-culture model was not addressed. Recent studies demonstrating that only a small percentage of CD133+ positive cancer stem cells are responsible for brain tumor progression will facilitate the development of better xenograft *in vivo* models of this neuronal tumor in the future (Singh et al., 2003; Singh et al., 2004). Their exclusive ability to drive malignant tumor formation and dissemination make these cells an obvious target for Slit-Robo inhibition. In addition, the recent isolation of postnatal cerebellar stem cells may provide more insight into medulloblastoma development and progression as well as the invasive potential of this tumor *in vivo* (Lee et al., 2005).

Wong et al. (2001) have demonstrated a role for a new family of GAP's (Slit-Robo GAPs or srGAPs) in Slit-Robo signaling. Interaction of srGAP's with the RhoGTPase, Cdc42 is essential for the repulsive activity of this guidance cue (Wong et al., 2001). Other studies support a role for Phosphatidylinositol 3 kinase, Dock and Pak,

and the Abelson (Abl) kinase and Enabled (Ena) proteins further implicating actin and microtubule re-organization in Slit-Robo signaling (Wang et al., 2003; Fan et al., 2003; Bashaw et al., 2000). In our study, we have demonstrated decreased Cdc42 activation for medulloblastoma cells in response to Slit2. This agrees with previous results obtained by Wong et al. (2001) where Slit increased srGAP1-Robo1 interaction with and inactivation of Cdc42. Therefore, there may be a conserved mechanism regulating both the repellent and inhibitory response to Slit2.

In addition, Cdc42 has been shown to play an important role in establishment of cell polarity (Etienne-Manneville and Hall, 2001; Palazzo et al., 2001; Gomes et al., 2005). Etienne-Manneville and Hall (2003) have shown that a Cdc42-PAR6/PKC ζ complex interacts directly with and phosphorylates glycogen synthase kinase 3 β (GSK 3 β) leading to β -catenin stabilization and localization to the leading edge along with interaction of adenomatous polyposis coli (APC) with the plus end of microtubules to establish cell polarity in primary rat astrocytes. Interestingly, these components of the Wnt signaling pathway have been linked with medulloblastoma progression (Raffel, 2004). Although studies have demonstrated that microtubule organizing center (MTOC) reorientation initiates cell polarity, recent evidence has shown that nuclear repositioning is actually the initial polarization event leading to cell migration and is regulated in a Cdc42 dependent manner (Etienne-Manneville and Hall, 2001; Palazzo et al., 2001; Gomes et al., 2005). The inhibitory effect of Slit2 on medulloblastoma may be mediated by a Cdc42-regulated effect on cell polarity.

We have demonstrated a slight decrease in Rac1 activity in response to Slit2. Contradictory results for Rac activation in Slit-mediated repulsion have been observed.

For example, Slit stimulation leads to recruitment of a Dock and Pak complex to the Robo receptor and increases Rac activation (Fan et al., 2003). In contrast, recent evidence suggests that Vilse, a conserved family of RhoGAPs, regulate the repellent response to Slit by binding to the intracellular domain of Robo receptors and promoting Rac inactivation (Lundstrom et al., 2004). These authors reconcile the contradictory evidence by suggesting that these molecules sequentially affect the Robo receptor leading to regulation of cytoskeletal dynamics and a sustained turning response to Slit (Lundstrom et al., 2004). Our results are indicative of an inhibitory, and not a directional, effect of Slit2 on medulloblastoma cells. It is clear that the effect of RhoGTPases on cell migration is variable and dependent on cell type, and our results do not rule out the possibility that other signaling pathways are also involved in Slit2 inhibition of medulloblastoma invasion.

This study suggests a novel strategy to control tumor invasion, and provides a *proof of principle* that this strategy may work for different types of tumors if the appropriate inhibitory cues can be identified. Our results reinforce the concept that selective neurodevelopmental cues may provide significant insights into tumor growth and invasion and outline the need for detailed assessments of how to implement this strategy for other tumor types. A new role for Slit2 as an inhibitor of medulloblastoma invasion has been identified. Although there are many known positive regulators of malignant tumor cell motility further assessment of the role of developmental inhibitors of cell movement is needed to implement this bioreactor strategy. This article suggests the possibility of using sodium alginate bead “bioreactors” as a new therapeutic approach

for controlling brain tumor invasion by continuously applying developmental cues such as Slit2.

Figure 4.1: Quantification of the effect of Slit on invading medulloblastoma and glioma cells. (a) Model of the tumor spheroid co-cultured with HEK or Slit2 aggregate in a three-dimensional collagen gel. Arrow denotes placement of HEK or Slit2 aggregate. (b) Still photograph of UW3 medulloblastoma spheroid labeled with Cell Tracker TMGreen and implanted 550 μm from a Slit2 aggregate after 72 hours. Scale bar = 250 μm . (c,e,g,i) Proximal and distal quadrant distribution of UW3 (c), Daoy (e) medulloblastoma cells and C6 (g), U251 (i) glioma cells co-cultured with aggregates of control HEK cells over (c,e) 72 hours and (g,i) 48 hours. (d,f,h,j) Proximal and distal quadrant distribution of UW3 (d), Daoy (f) medulloblastoma cells and C6 (h), U251 (j) glioma cells co-cultured with cells expressing Slit2 over (d,f) 72 hours and (h,j) 48 hours. Error bars represent SEM. Asterisks denote significance at $p < 0.05$ (*) and $p < 0.01$ (**).

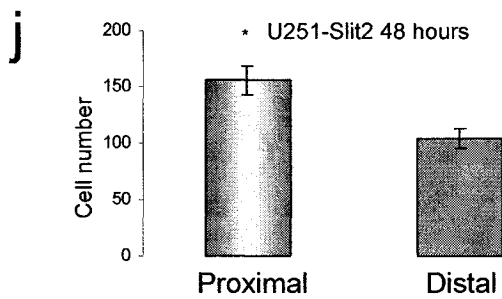
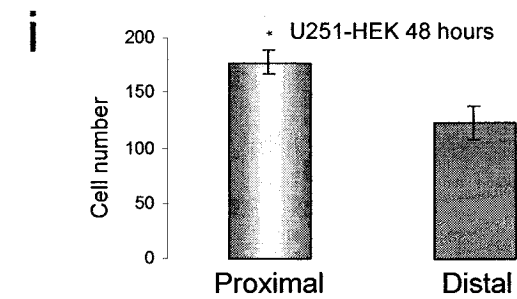
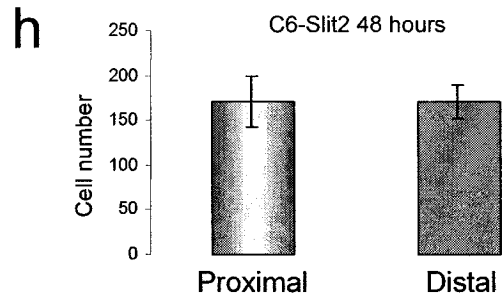
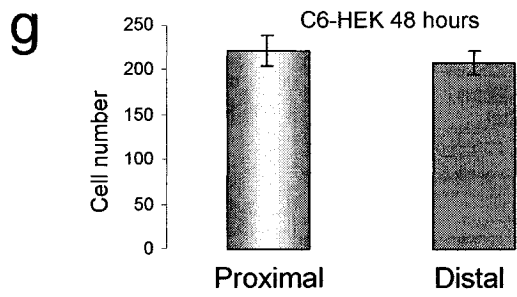
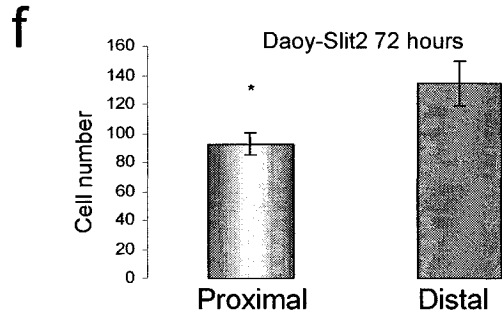
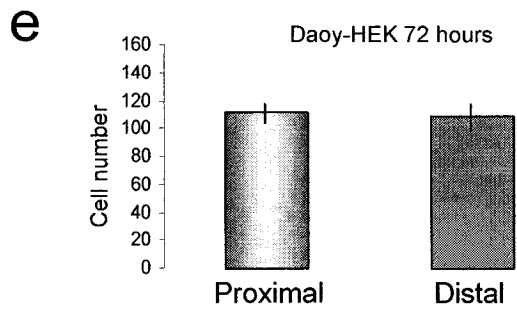
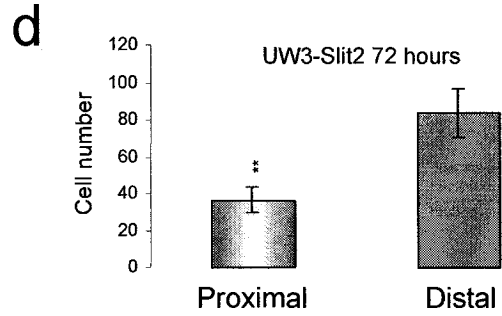
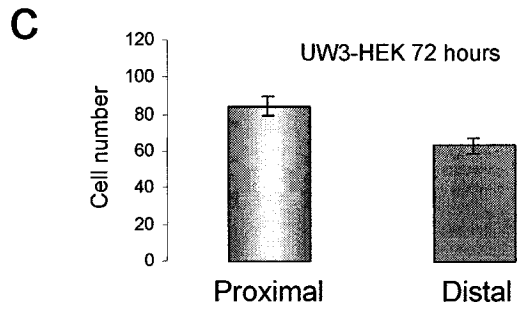
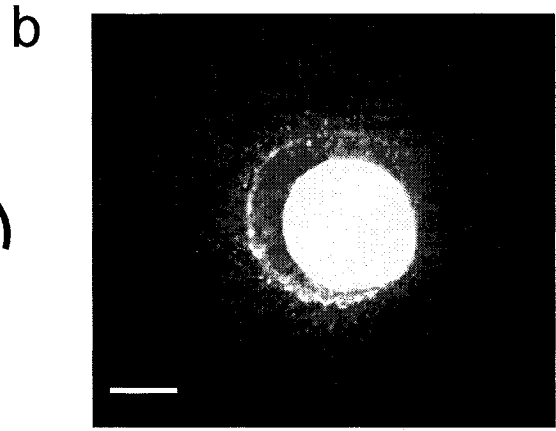
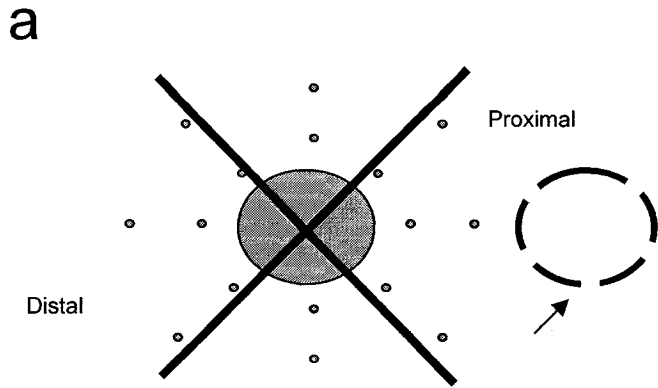
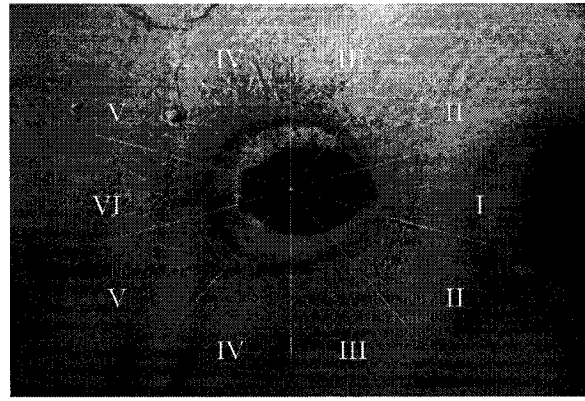
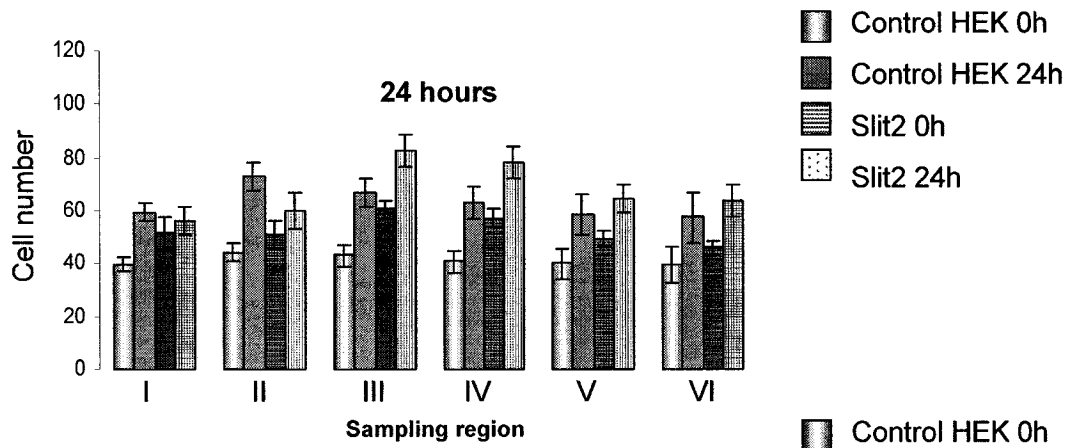


Figure 4.2: Quantification of time-delayed co-culture and conditioned medium assays. (a) Still photograph of time-delayed co-culture assay. UW3 medulloblastoma spheroids were first cultured in the absence of cell aggregates for 48 hours. Control HEK or Slit2 aggregates were placed next to the spheroids, and explants were cultured for an additional 24 and 72 hours. Scale bar = 250 μm . Individual cells were counted at 0h and both 24 (b) and 72h (c) after aggregate implantation and assigned to sampling regions I-VI. Error bars represent SEM. (b) For the 24 hour time-delay group, $n=8$ spheroid co-cultures. Note that there is no statistical difference in the number of UW3 cells in Areas I and II 24 hours after Slit2 aggregate placement, but there is a difference for all other sampling regions counted (paired t-test: $p<0.01$ for areas III, V and VI; $p<0.001$ for Area IV). A significant increase in the number of medulloblastoma cells was observed for all regions in HEK co-cultures (paired t-test: $p<0.01$ for Areas I, V, and VI; $p<0.001$ for Areas II, III and IV). (c) For the 72 hour time-delay group, $n=14$ for Slit2 co-cultures and $n=6$ for HEK 293 control co-cultures (paired t-test: $p<0.01$ for Areas I, III and V in HEK co-cultures; $p<0.001$ for all Areas in Slit-2 co-cultures and Areas II, IV and VI in HEK co-cultures). (d) The effect of HEK and Slit2 conditioned medium on the invasion of UW3 spheroids after 5 days implantation in collagen gels. $N=4$ for DMEM +10% FBS cultures, $n=3$ for Slit2 cultures, and $n=5$ for HEK cultures. Figure is representative of multiple independent trials. Error bars: standard error of the mean. Asterisks indicate a significant difference at $p<0.01$ (**) and $p<0.001$ (***).

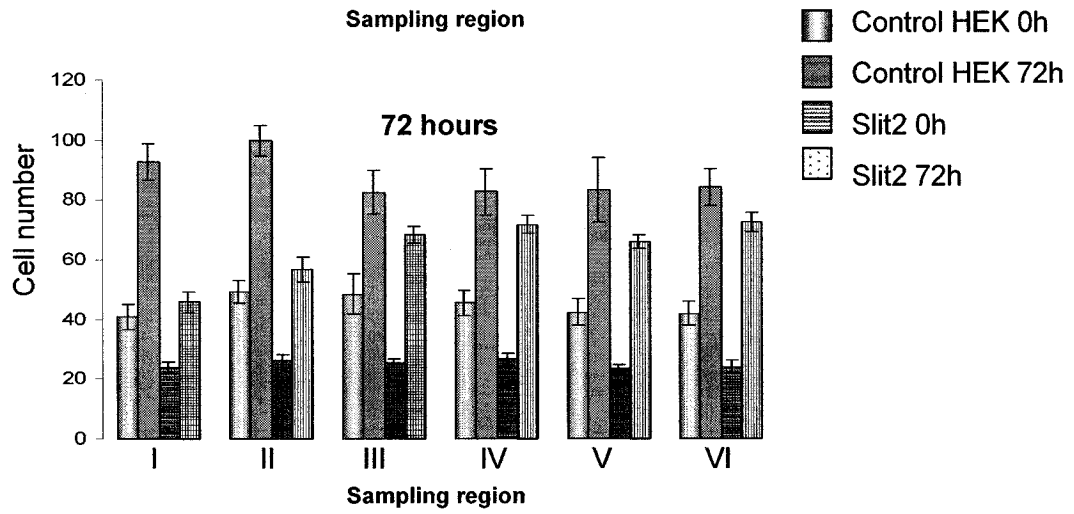
a



b



c



d

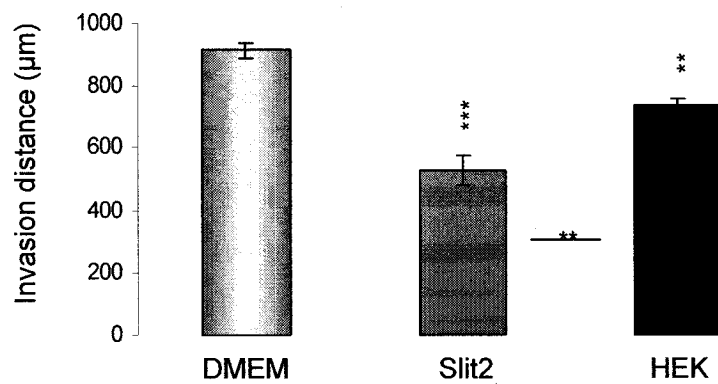


Figure 4.3: Time-lapse videomicroscopy analysis of individual cells in UW3-HEK and UW3-Slit2 co-cultures. (a) Still photographs depicting individual cell invasion when UW3 spheroids were co-cultured with HEK aggregates (upper panels) and Slit2 aggregates (lower panels) over 20 hours. Note that the representative cell in the HEK co-culture (upper panels) invades approximately twice as fast as the representative cell in the Slit2 co-culture (lower panels). Arrows denote individual cell tracking. Scale bar = 50 μm (b) Image of stationary “ruffling” cell that fails to invade in UW3-Slit2 co-cultures over 20 hours. Arrows denote individual cell tracking. Scale bar = 50 μm . (c) Mean invasion velocity of individual UW3 cells in the presence of HEK aggregates (n=35) or Slit2 aggregates (n=32). Note the 54% inhibition of medulloblastoma cell speed in the presence of Slit2 aggregates. Error bars: standard error of the mean. Asterisks indicate a significant difference at $p < 0.001$ (***)

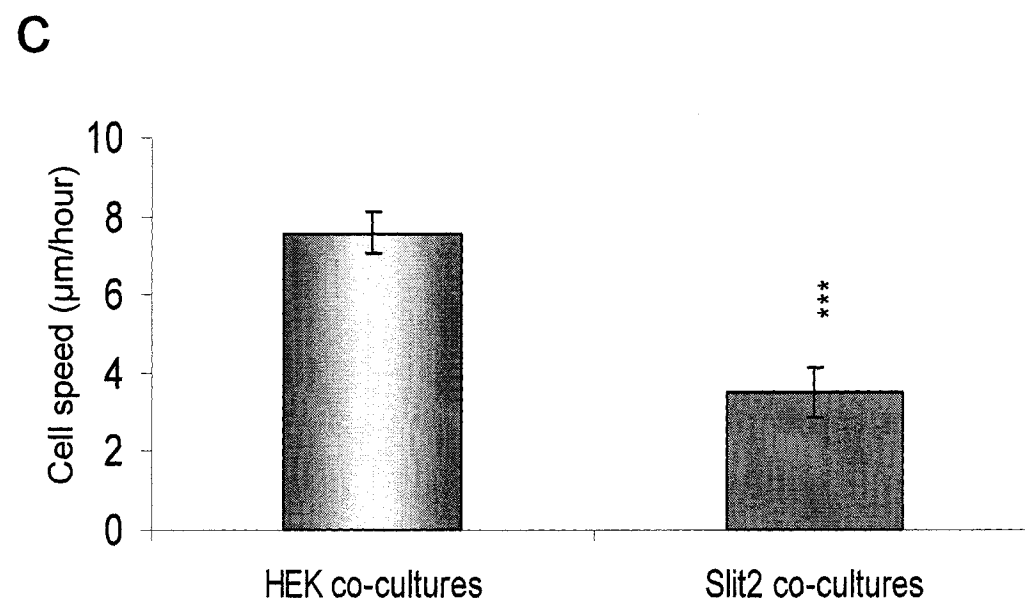
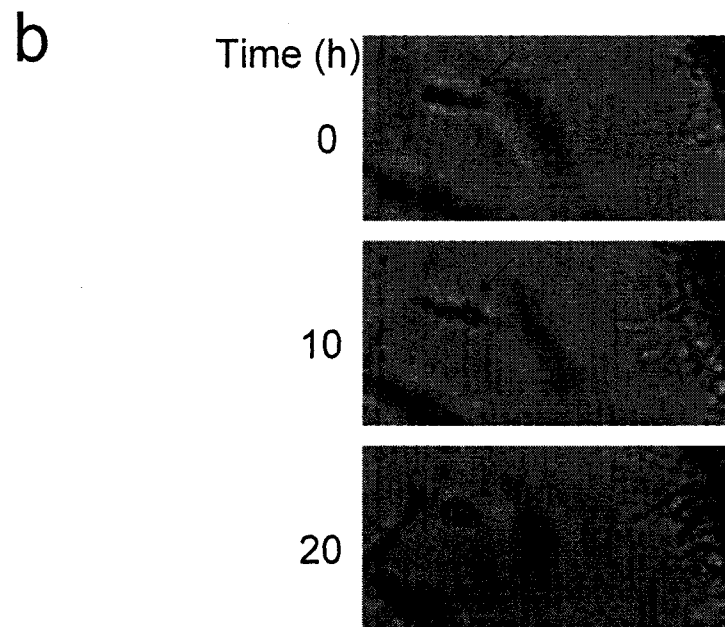
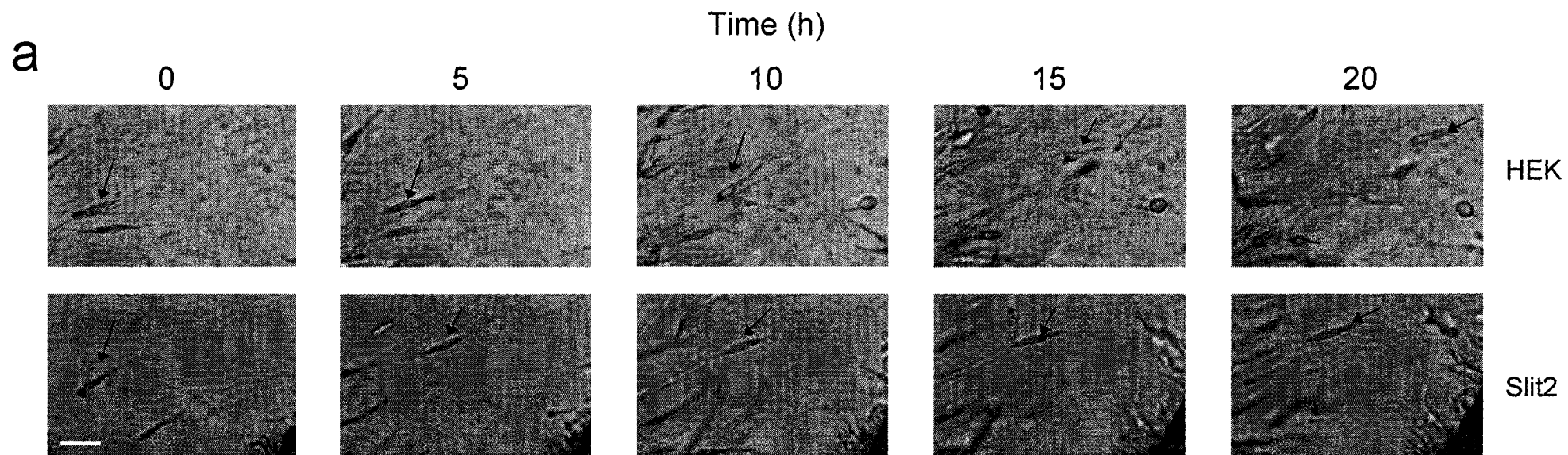
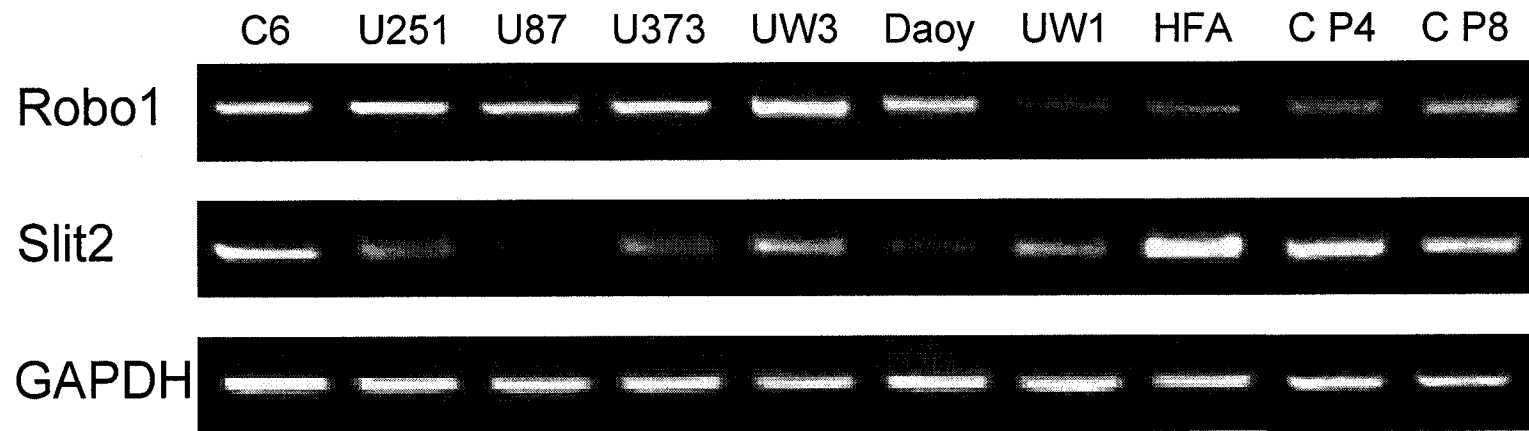


Figure 4.4: Expression of Robo1 and Slit2 in brain tumor cell lines, human fetal astrocytes, mouse cerebellum, primary human tumors, and normal brain. (a) RT-PCR expression of Robo1, Slit2 and GAPDH mRNA in medulloblastoma and glioma cell lines. Human fetal astrocytes (HFA) and mouse neonatal cerebellum (C P4 and C P8) were screened as positive controls. (b) RT-PCR expression of Robo1, Slit2 and GAPDH in medulloblastoma (MD), meningioma (MN) and pilocytic astrocytoma (PA) primary human tumors. (c) RT-PCR expression of Robo1, Slit2 and β -actin in glioblastoma multiforme (GBM) tumors and normal brain (NB).

a



b



c

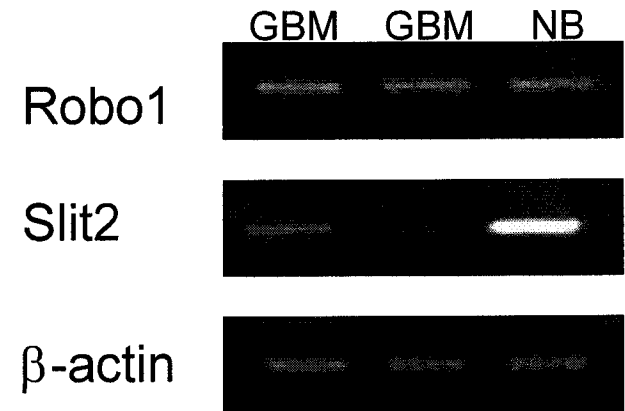


Figure 4.5: Sodium alginate bead microencapsulation and the effect of Slit2. (a) Diagram of the experimental design showing the position of the sodium alginate beads relative to the glioma or medulloblastoma spheroid. Arrow represents placement of sodium alginate bead. (b) Western Blot analysis of Slit2 expression (~200 kD) in conditioned medium of encapsulated cells over 6 days (upper panel) and 18 days (lower panel) respectively. Lanes 1 and 2 in the upper panel represent conditioned medium from HEK and Slit2 monolayer cultures as negative and positive controls respectively. Lanes 3-5 represent conditioned medium from Slit2 beads on days 1,3 and 6 in culture. Lanes 6-7 represent conditioned medium from HEK beads on day 3 and 6. The lower panel demonstrates Slit2 secretion from the encapsulated cells over 18 days in culture. Lane 1 represents conditioned medium from Slit2 monolayer cultures as a positive control. (c-e) Photographs of UW3 medulloblastoma spheroids surrounded by four empty beads (c), four beads encapsulating HEK 293 control cells (d) and four beads encapsulating Slit2 cells (e). Scale bar= 250 μm . (f-i) Quantification of total invasion by UW3 and Daoy spheroids (f-g) and C6 and U251 glioma spheroids (h-i) implanted with empty, HEK 293, Slit2 or Netrin1 beads. Error bars represent SEM. Asterisks indicate significance at $p < 0.05$, $p < 0.01^{**}$ and $p < 0.001^{***}$.

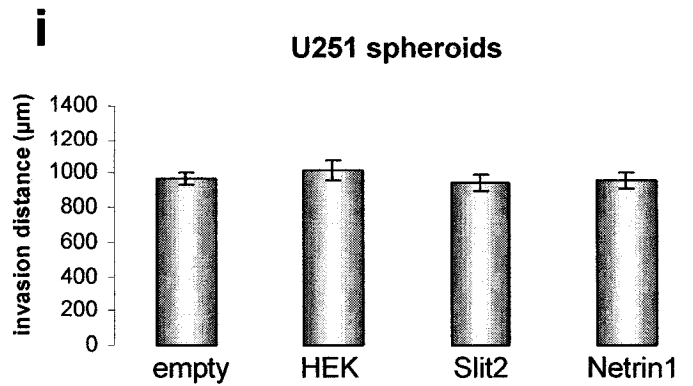
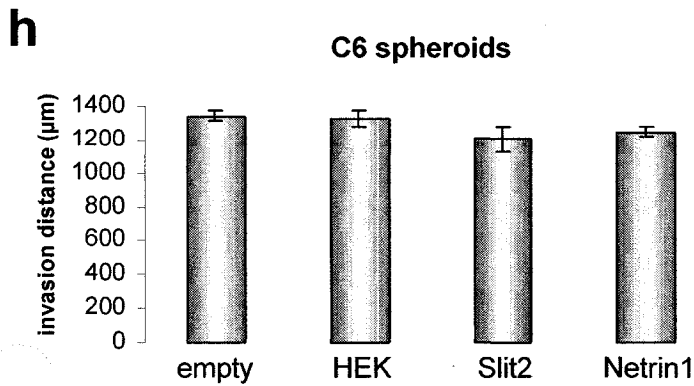
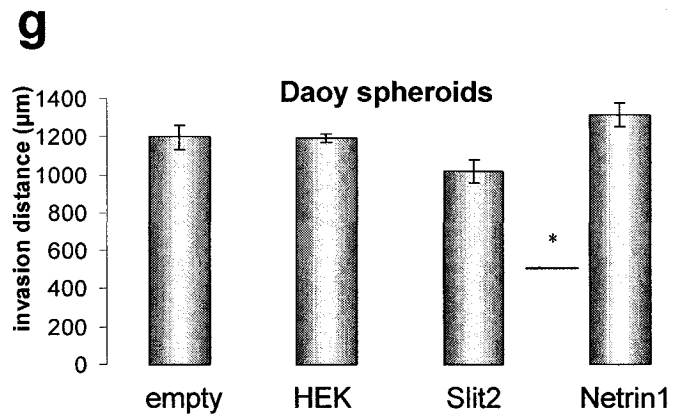
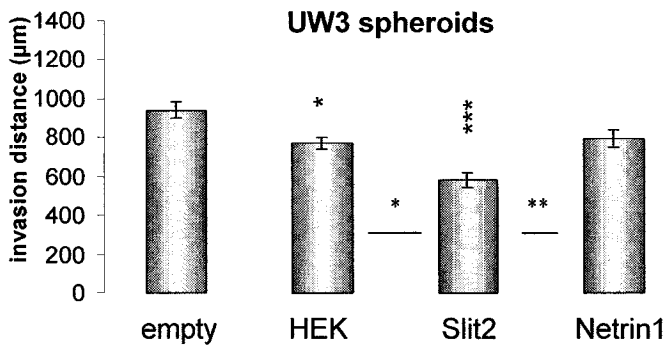
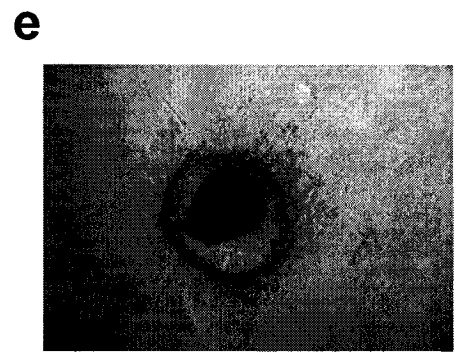
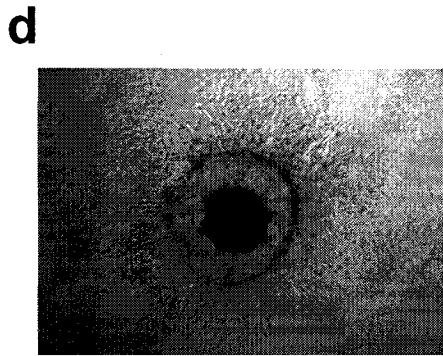
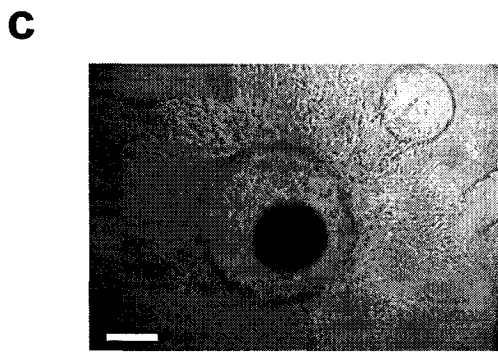
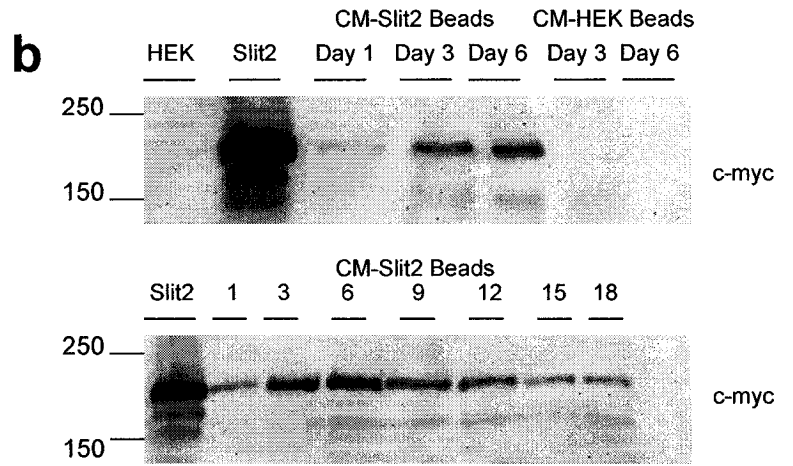
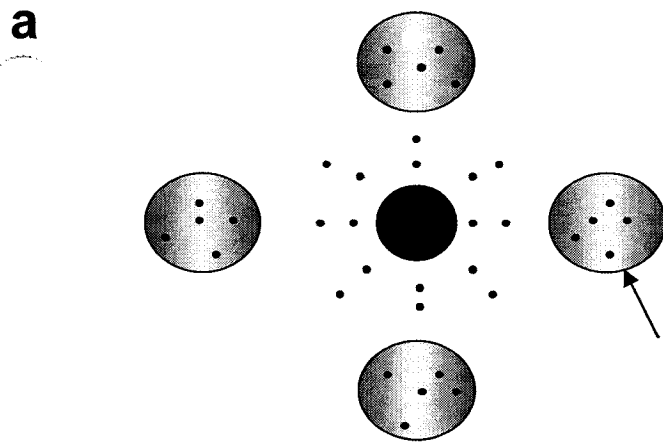


Figure 4.6: The effect of RoboN and R5 on Slit2 inhibition of UW3 medulloblastoma spheroids. (a) Quantification of UW3 total invasion with R5 antibody and RoboN conditioned medium. Note that the inhibitory effect of Slit2 was rescued by about 50%, and invasion distances for UW3 spheroids with the addition of R5 and RoboN are not statistically different from controls. (b) Western Blot analysis of Slit2 and RoboN expression (~200 kDa and ~100 kDa respectively) in conditioned medium of encapsulated mixed Slit2-HEK and Slit2-RoboN cells at days 3 and 6. Conditioned medium from Slit2 (lane 1) and RoboN (lane 2) monolayer cultures were used as positive controls for Slit2 and RoboN respectively. (c) Quantification of UW3 total invasion when co-cultured with HEK, Slit2-HEK or Slit2-RoboN beads. Note that the inhibitory effect of Slit2 is eliminated by encapsulation of RoboN cells together with Slit2 cells. Error bars represent SEM. Asterisks indicate significance at $p < 0.05^*$, and $p < 0.01^{**}$.

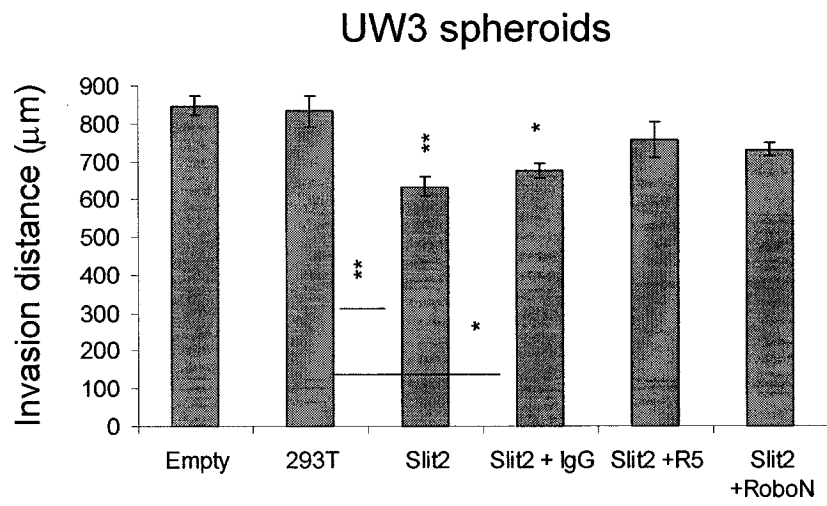
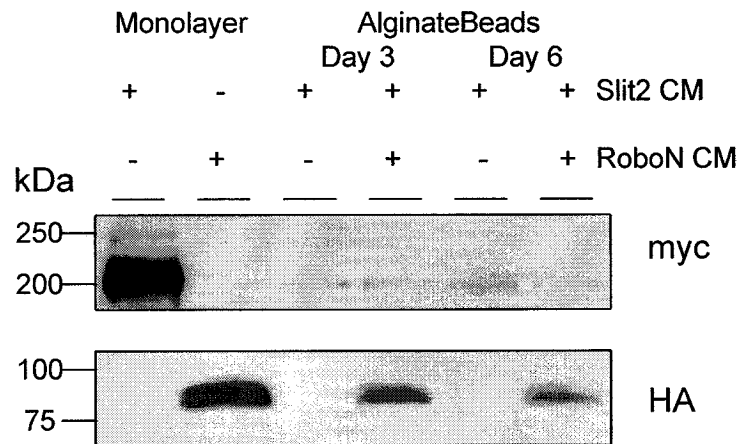
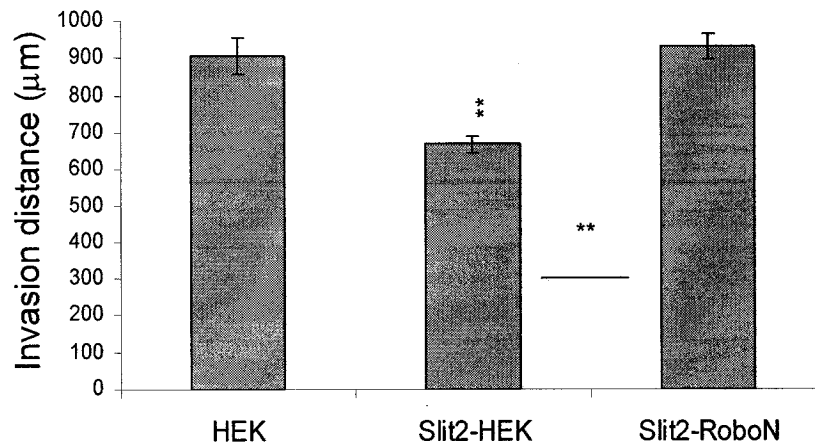
a**b****c**

Figure 4.7: Confocal microscope images of UW3 spheroids (DiI labeled-red) confronted with human fetal astrocyte aggregates (DiO labeled-green) in the presence of (a) HEK sodium alginate beads or (b) Slit2 sodium alginate beads after 5 days. Scale bar 250 μ m. (c) Quantification of the number of medulloblastoma cells infiltrating astrocyte aggregates after 5 days culture. (d) Quantification of the number of UW3 cells infiltrating various distances into the astrocyte aggregates after 5 days. Asterisks indicate significance at $p < 0.05^*$.

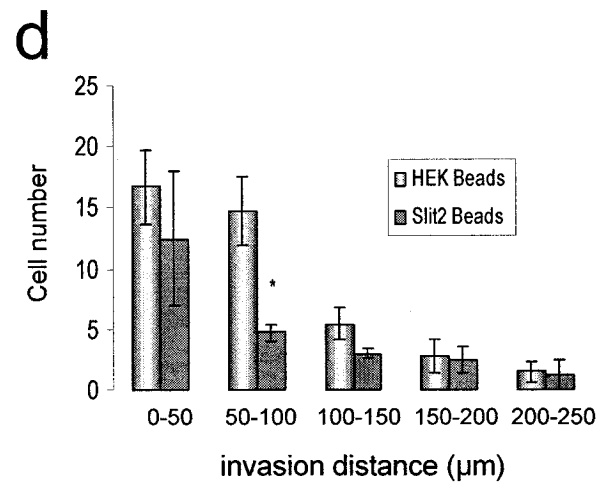
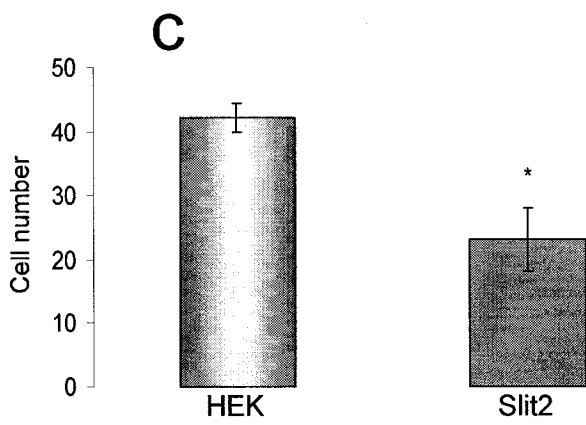
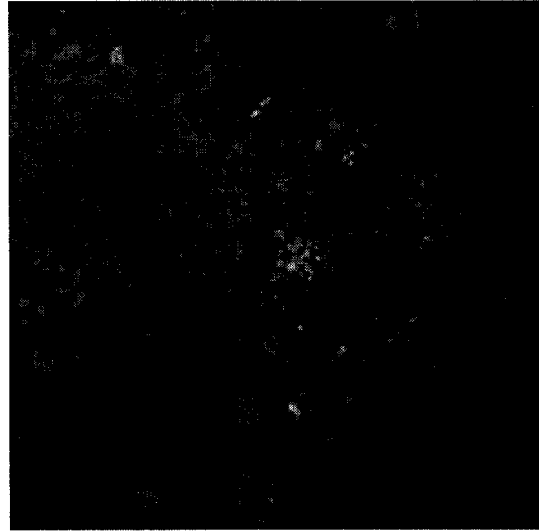
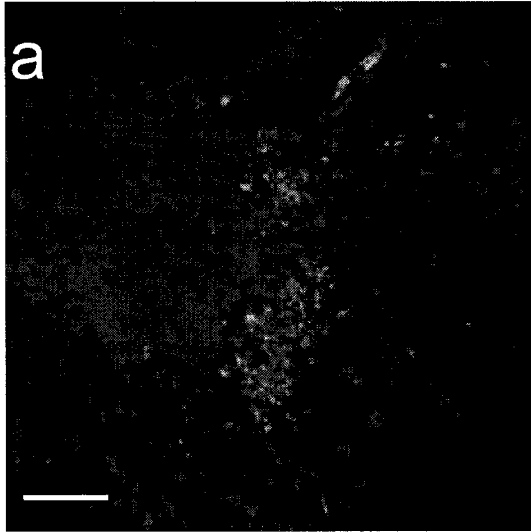


Figure 4.8: Cell surface biotinylation of U251 cell lines. The surface proteins of U251 wild-type and U251-HA Robo1 (overexpressing Robo1) cell lines were biotinylated. Input total cell lysates (I) and enriched cell surface proteins (S) were resolved and subjected to Western Blot analysis. Anti-HA antibody was used (upper panel) to detect recombinant Robo1. Anti p42/44 was used (lower panel) as a cell surface biotinylation control.

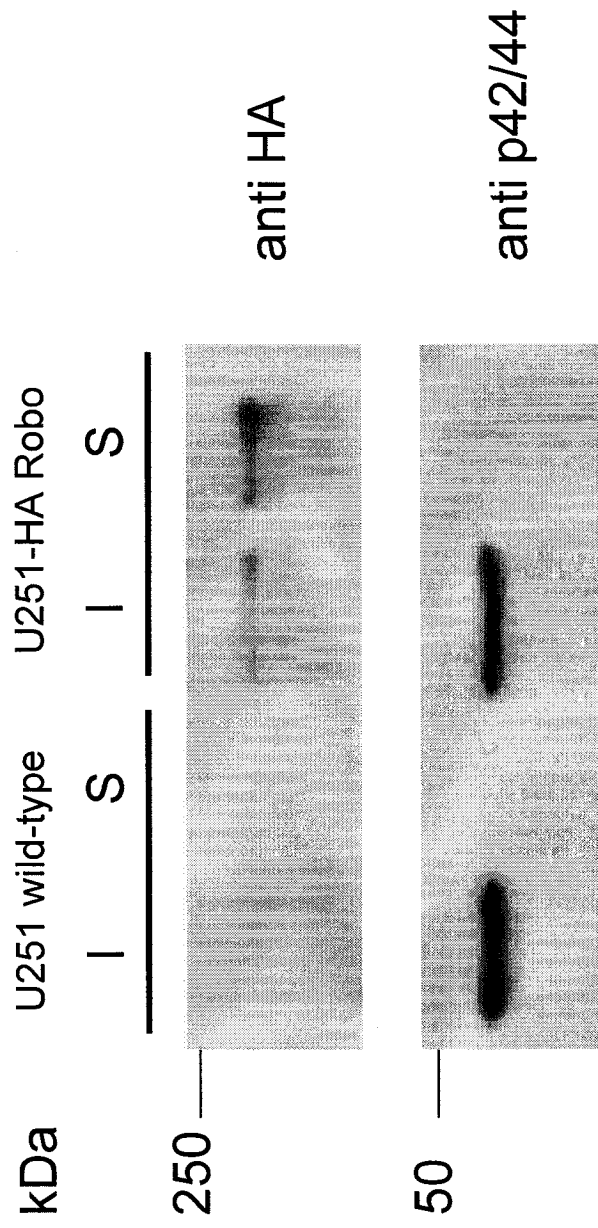
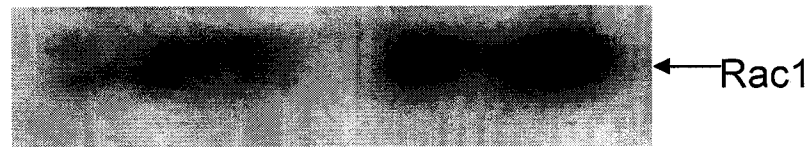


Figure 4.9: Slit2 decreases activated Cdc42-GTP in medulloblastoma cells. Cells were pre-treated with either wild-type HEK or Slit2 conditioned medium for 24 hours and Cdc42/Rac-GTP activity was measured. Cdc42 and Rac loading controls levels were estimated by Western blot analysis. Note that Slit2 conditioned medium decreases Cdc42-GTP activity in UW3 medulloblastoma cells.

UW3

HEK CM

Slit2 CM



C6

HEK CM

Slit2 CM

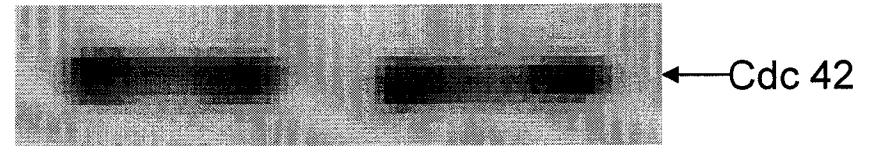


Table 4.1: Primer details for all RT PCR reactions

Primer name	Sense	Antisense	Expected product size (bp)
1. human Robo1	5' -GCA TCG CTG GAA GTA GCC ATA C-3'	5' -GTG TAT GAA CCC ATG TCA CCA GC-3'	514
2. human Slit2	5' -GGT GTC CTC TGT GAT GAA GAG-3'	5' -GTG TTT AGG AGA CAC ACC TCG-3'	387
3. human Slit1	5' -AGG TGC TGA CCC TGA ACA AC-3'	5' -GCA TTC AGG AGC AGG AGC TG-3'	618
4. GAPDH	5' -GCC TCC TGC ACC ACC AAC TG-3'	5' -CCG ACG CCT GCT TCA CCA CCT TCT-3'	545
5. β -actin	5'-TCC CCC AAC TTG AGA TGT ATG AAG-3'	5'-AAC TGG TCT CAA GTC AGT GTA CAG G-3'	67
6. human Robo1	5' -GCC CTC TGA CTA GTA GAT TTC -3'	5' -GTT CCC TTA GTA CTG CAC GCC-3'	245
7. human Slit2	5' -GAA GGT GTC CCG ATT AGA GTG C-3'	5' -CAA AGA CAG AGC TGC CGG GAG TG-3'	191

4.6 Conclusions to Chapter 4

In the present study, we have tested whether the secreted protein Slit2, known to be important for guiding the projection of normal axons and migration of developing neurons, can regulate brain tumor cell movement. As stated previously, Slit has also been shown to play an important role in non-neuronal cells, as an inhibitor of leukocyte chemotaxis and promoter of tumor-induced angiogenesis and endothelial cell attraction (Wu et al., 2001; Wang et al., 2003). We have shown an inhibitory role for Slit2 in medulloblastoma, but not glioma, cell invasion in three dimensions. Initial studies suggest a role for the RhoGTPases in Slit2 inhibition of medulloblastoma invasion, the mechanism responsible for this effect requires further characterization.

The intracellular pathways downstream of Slit-Robo signaling are just beginning to be identified. In order to fully understand Slit-mediated repellent and inhibitory responses, it will be imperative to identify the downstream effectors. Studies examining Slit-Robo signaling can be divided into three basic categories. The first paradigm involves the RhoGTPases and the regulation of the actin cytoskeleton to generate a turning response.

Recent evidence has accumulated suggesting an important role for regulation of the actin cytoskeleton machinery in Slit-mediated repulsion. For example, Wong et al. (2001) have identified a new family of GTPase activating proteins, srGAPs that facilitate hydrolysis of Cdc42 that ultimately leads to actin depolymerization. Furthermore,

addition of a constitutively active Cdc42 virus, and a dominant negative srGAP1 inhibited the repulsive effect of Slit in neurons migrating from subventricular zone (SVZ) explants and promoted cell migration (Wong et al., 2001). These authors suggested a role for Cdc42 in the migration of SVZ neurons, but the roles of both RhoA and Rac 1 were not clear.

Studies have demonstrated opposing roles for Rac in the regulation of axon repulsion in *Drosophila*. Fan et al. (2003) have shown that Slit stimulation leads to recruitment of the SH3-SH2 adaptor protein Dreadlocks (Dock) and the p21-activated serine-threonine kinase (Pak) to the Robo receptor CC2 and CC3 cytoplasmic motifs. Recruitment of this complex increases Rac activity to regulate axon repulsion at the CNS midline (Fan et al., 2003). In contrast, Vilse, a conserved family of RhoGAPs has been shown to promote hydrolysis of RacGTP, and less efficiently, Cdc42GTP to mediate Robo repulsion in *Drosophila* tracheal cells and axons (Lundstrom et al., 2004). These authors suggested that the contradictory models can be explained in terms of a temporal model of Slit effectors where sequential interaction with the Robo receptors leads to a sustained turning response (Lundstrom et al., 2004).

It is clear that the effect of RhoGTPases on cell migration is variable and dependent on cell type. For example, Cdc42 is often associated with filopodia formation and increased cell migration; however, studies have established a role for Cdc42 in suppressing cell motility as well. For example, Yamauchi et al. (2002) demonstrated that endothelin suppresses cell migration by activating Rac and Cdc42 via the JNK signaling

pathway. Cells use the adaptor protein Nck1 to transduce the Cdc42-mediated inhibition of HEK cell migration (Miyamoto et al., 2004). Another study has demonstrated an inhibitory role for Cdc42 in macrophage chemotaxis stimulated by CSF1 (Allen et al., 1998). Therefore, caution must be taken when interpreting mechanistic RhoGTPase data, as the cell type and models employed will often yield variable results.

In addition to the involvement of the RhoGTPases, another study has shown a role for the Abelson kinase (Abl) and its substrate Enabled (Ena) in Slit-mediated repulsion (Bashaw et al., 2000). Abl binds to CC3 and phosphorylates a tyrosine in CC1; whereas, Ena associates with CC2 to regulate the repulsive effect of Slit. Genetic and biochemical evidence suggests that Abl and Ena play opposing roles in Robo mediated repulsion where Abl antagonizes Slit-Robo signaling and Ena promotes the repulsive effect. Furthermore, the authors suggested that other signaling pathways are also involved in Slit-Robo signaling, as Robo-mediated repulsion still functions fairly well in the absence of Ena (Bashaw et al., 2000). Therefore, these components are not exclusive to the Slit-Robo pathway. In addition, Abl has also been linked with a supramolecular complex consisting of Robo and N-cadherin that facilitates inactivation of N-cadherin mediated adhesion in response to Slit (Rhee et al., 2002). This mechanism uncouples the association of N-cadherin with the actin cytoskeleton and is accompanied by a loss of growth cone traction and axon extension (Rhee et al., 2002).

Another mechanism associated with Slit-Robo signaling is the “silencing” of the Netrin receptor DCC (Stein and Tessier-Lavigne, 2001). Activation of the Robo receptor

leads to the silencing of Netrin1's attractive effect through direct binding of Robo's cytoplasmic domain to that of the DCC receptor without a concomitant affect on the stimulation of growth cone extension rate in embryonic *Xenopus* spinal axons (Stein and Tessier-Lavigne, 2001). This hierarchical organization contributes to the finely-tuned controlled mechanisms guiding growth cones to their final targets.

The majority of studies examining the signaling cascades responsible for Slit effects have focused on the repulsive response. In light of the recent evidence demonstrating a role for Slit in leukocyte chemotaxis, angiogenesis, and now, medulloblastoma invasion, it will be necessary to further functionally characterize the intracellular mechanisms mediating non-neuronal Slit effects. Wong et al. (2003) have demonstrated a role for PI3K signaling in Slit2-induced migration and tubulogenesis of endothelial cells. The PI3K inhibitors, LY294002 and Wortmannin, attenuated the Slit2 induced migration of human umbilical cord endothelial cells (HUVECs) and therefore, contributed to the attractant effect of Slit2. The role of PI3K signaling in the repellent effect of Slit on growth cones and neurons, as well as the inhibitory effect on leukocytes and medulloblastoma tumor cells has yet to be determined. The variability in the cell types and models employed will inevitably lead to differences in the intracellular mechanisms responsible for Slit-mediated effects.

4.7 Conclusions and Future Perspectives

Invasion of malignant brain tumor cells into the normal tissue architecture makes GBM and medulloblastoma among the most devastating of cancers and are very difficult to resect. Therefore, the invasive cascade is an important therapeutic target. This thesis has focused on negative regulators of malignant brain tumor invasion in three-dimensional collagen gels. From the review in Chapter 1, it is clear that there are many promoters of malignant brain tumor invasion; however, very few naturally occurring negative regulators of the invasive cascade have been identified. Within the literature, there is a vast array of cell types and models systems employed. This often makes the true biological and clinical relevance of the data difficult to interpret. Consequently, few new therapeutic strategies targeting brain tumor invasion have been developed over the past few decades.

A recent surge of studies examining the developmental origin of cancer and the relationship between tumor cells and stem cells have shed light on this issue. For example, “brain tumor stem cells” comprising a fraction of the entire tumor population are responsible for driving malignant brain tumor formation and dissemination (Singh et al., 2003; Singh et al., 2004). These cells stain positive for the cell surface neural stem cell marker CD133+, and are capable of self-renewal, proliferation and differentiation. In addition, the self renewal capacity was highest in the most aggressive medulloblastoma tumors in comparison with low-grade pilocytic astrocytoma suggesting that these brain tumor stem cells are a novel cellular target for more effective therapeutic strategies less

directed towards the global population of tumor cells (Singh et al., 2003). Further characterization of these “brain tumor stem cells” will hopefully enable the development of better *in vivo* model systems where the true clinical relevance of molecular targets can be tested.

Chapter 2 provided evidence for a secreted chemorepellent that directs glioma cell invasion. This observational study led to the development of a reproducible functional assay that was utilized to isolate natural inhibitors of malignant glioma cell invasion from serum-containing C6 astrocytoma conditioned medium. Further analysis identified ITI H2 as the most abundant protein in our purified fractions, and subsequent validation studies confirmed its role as a potent inhibitor of proliferation and promoter of cell-cell adhesion in addition to its inhibitory effect on invasion. The higher levels in normal brain and lower-grade tumors suggest that ITI H2 may have a potential role in malignant glioma progression. The structural complexity and proteolytic processing of the ITI family members not only make ITI H2 an interesting molecular target for future mechanistic studies, but also the other ITI heavy chain family members that have yet to be investigated. Very few studies have examined the mechanism(s) responsible for the transesterification reaction and extracellular matrix stabilization resulting from HA coupling. In fact, there are no studies linking this mechanism with any of the effects seen on tumor cells. Only the serine protease inhibitory activity of bikunin has been addressed. The intracellular mechanisms mediating the effects of the ITI heavy chains are currently unknown.

The technology utilized in Chapters 2 and 3 can also be used to evaluate the role of other known molecules in malignant brain tumor invasion. We have tested whether Slit2, a known chemorepellent, can control brain tumor invasion using co-culture and conditioned medium assays in collagen type I gels as well as time-lapse videomicroscopy to investigate the dynamics of individual cell movement. Both medulloblastoma and glioma tumors express Robo1 and Slit2, but only medulloblastoma invasion is inhibited by recombinant Slit2 protein. The highly invasive glioma cell lines C6 and U251 did not respond to Slit2. Therefore, the glioma-derived chemorepellent(s) introduced in Chapter 2 have yet to be identified. Chapter 4 also established sodium alginate bead microencapsulation as a method to apply negative guidance cues. In addition, this bioreactor strategy can also be used to continuously supply any inhibitor or repellent of malignant brain tumor invasion. Future experiments will not only target the molecular mechanisms responsible for Slit2 inhibition of medulloblastoma invasion, but also the *in vivo* applicability of our bioreactor strategy. Xenograft models utilizing sodium alginate bead microencapsulation will confirm this technique as a potential therapeutic strategy targeting highly invasive malignant brain tumors cells. Our results suggest that neurodevelopmental cues may play an important role in malignant brain tumor invasion, and that application of negative guidance cues may be potentially used to target a variety of CNS tumor types.

In conclusion, we have used a variety of techniques to identify two molecules with previously unknown functions in malignant brain tumor invasion. ITI H2 and Slit2 inhibit glioblastoma and medulloblastoma cell invasion respectively, and ITI H2 also has

an additional role in glioblastoma cell proliferation and cell-cell adhesion. Therefore, successful treatment strategies in the future will involve implementation of combination therapies that target multiple biological processes such as invasion, proliferation, apoptosis and adhesion. The clinical potential of these molecules is still unclear and needs to be pursued; however, our results are promising and warrant further functional characterization.

References

1. Aboody, K.S., et al. Neural stem cells display extensive tropism for pathology in adult brain: evidence from intracranial gliomas. *Proc. Natl. Acad. Sci. USA.* 97(23), 12846-12851 (2000).
2. Allen, W.E., Zicha, D., Ridley, A.J., Jones, G.E. A role for Cdc42 in macrophage chemotaxis. *J. Cell Biol.* 141(5), 1147-1157 (1998).
3. Angers-Loustau, A., Hering, R., Werbowetski, T.E., Kaplan, D.R., Del Maestro, R.F. Src regulates actin dynamics and invasion of malignant glial cells in three dimensions. *Mol. Cancer Res.* 2(11), 595-605 (2004).
4. Annabi, B., et al. Green tea polyphenol (-)-epigallocatechin-3-gallate inhibits MMP2 secretion and MT1-MMP driven migration in glioblastoma cells. *Biochim. Biophys. Acta.* 1542, 209-220 (2002).
5. Anselmo, M.A., et al. Slit and Robo: expression patterns in lung development. *Gene Expr. Patterns.* 3, 13-19 (2003).
6. Armstrong, R.C. Isolation and characterization of immature oligodendrocyte lineage cells. *Methods* 16, 282-292 (1998).
7. Armstrong, R.C., Harvath, L., Dubois-Dalcq, M.E. Type 1 astrocytes and oligodendrocyte-type 2 astrocyte glial progenitors migrate toward distinct molecules. *J. Neurosci. Res.* 27, 400-407 (1990).
8. Asai, A., et al. Negative effects of wild-type p53 and s-myc on cellular growth and tumorigenicity of glioma cells. *J. Neurooncol.* 19, 259-268 (1994).

9. Asano, K., et al. Correlation of N-cadherin expression in high grade gliomas with tissue invasion. *J. Neurooncol.* 70(1), 3-15 (2004).
10. Astuti, D., et al. SLIT2 promoter methylation analysis in neuroblastoma, Wilms' tumor and renal cell carcinoma. *Br. J. Cancer* 90(2), 515-521 (2004).
11. Bagri A., et al. Slit Proteins prevent midline crossing and determine the dorsoventral position of major axonal pathways in the mammalian forebrain. *Neuron* 33, 233-248 (2002).
12. Banyard, J., Anand-Apte, B., Symons, M., Zetter, B.R. Motility and invasion are differentially modulated by Rho family GTPases. *Oncogene.* 19, 580-591 (2000).
13. Bashaw, G.J., Kidd, T., Murray, D., Pawson, T., Goodman, C.S. Repulsive axon guidance: abelson and enabled play opposing roles downstream of the roundabout receptor. *Cell* 101, 703-715 (2000).
14. Bauman, G.S., et al. Effects of radiation on a three-dimensional model of malignant glioma invasion. *Int. J. Dev. Neurosci.* 17, 643-651 (1999a).
15. Bauman, G.S., et al. Effect of radiation on a model of malignant glioma invasion. *J. Neurooncol.* 44, 223-231 (1999b).
16. Bayani, J., et al. Molecular cytogenetic analysis of medulloblastoma and supratentorial primitive neuroectodermal tumors by using conventional banding, comparative genomic hybridization, and spectral karyotyping. *J. Neurosurg.* 93(3), 437-448 (2000).
17. Behin, A., Hoang-Xuan, K., Carpentier, A.F., Delattre, J-Y. Primary brain tumor in adults. *Lancet.* 361, 323-331 (2003).

18. Bello, L., et al. Simultaneous inhibition of glioma angiogenesis, cell proliferation, and invasion by a naturally occurring fragment of human metalloproteinase-2. *Cancer Res.* 61, 8730-8736 (2001).
19. Benedetti, S., et al. Gene therapy of experimental brain tumors using neural progenitor cells. *Nat. Med.* 6(4), 447-450 (2000).
20. Benny, O., et al. Continuous delivery of endogenous inhibitors from poly (lactic-co-glycolic acid) polymeric microspheres inhibits glioma tumor growth. *Clin. Cancer Res.* 11, 768-776 (2005).
21. Berens, M.E., Rutka, J.T., Rosenblum, M.L. Brain tumor epidemiology, growth and invasion. *Neurosurg. Clin. N. Am.* 1:1-18 (1990).
22. Bernstein, J.J., et al. C6 glioma-astrocytoma cell and fetal astrocyte migration into artificial basement membrane: a permissive substrate for neural tumors not fetal astrocytes. *Neurosurgery* 28, 652-658 (1991).
23. Bigner, S.H., McLendon, R.E., Fuchs, H., McKeever, P.E., Friedman, H.S. Chromosomal characteristics of childhood brain tumors. *Cancer Genet. Cytogenet.* 97, 125-134 (1997).
24. Bjerkvig, R., Laerum, O.D., Mella, O. Glioma cell interactions with fetal rat brain aggregates *in vitro* and with brain tissue *in vivo*. *Cancer Res.* 46, 4071-4079 (1986).
25. Bjerkvig, R., Tonnesen, A., Laerum, O.D., Backlund, E. Multicellular tumor spheroids from human glioma maintained in organ culture. *J. Neurosurg.* 72, 463-475 (1990).
26. Bolteus, A.J., Berens, M.E., Pilkington, G.J. Migration and invasion in brain neoplasms. *Curr. Neurol. Neurosci. Rep.* 1, 225-232 (2001).

27. Borgstrom, P., Hillan, K.J., Sriramarao, P., Ferrara, N. Complete inhibition of angiogenesis and growth of microtumors by anti-vascular endothelial growth factor neutralizing antibody; novel concepts of angiostatic therapy from intravital videomicroscopy. *Cancer Res.* 56, 4032-4039 (1996).
28. Bost, F., Diarra-Mehrpour, M., Martin, J.P. Inter- α -trypsin inhibitor proteoglycan family: A group of proteins binding and stabilizing the extracellular matrix. *Eur. J. Biochem.* 252, 339-346 (1998).
29. Braga, V.M., Machesky, L.M., Hall, A., Hotchin, N.A. The small GTPases Rho and Rac are required for the establishment of cadherin-dependent cell-cell contacts. *J. Cell Biol.* 137, 1421-1431 (1997).
30. Broholm, H., Laursen, H. Vascular endothelial growth factor (VEGF) receptor neuropilin-1's distribution in astrocytic tumors. *APMIS.* 112(4-5), 257-263 (2004).
31. Brooks, P.C., Silletti, S., von Schalscha, T.L., Friedlander, M., Cheresch, D.A. Disruption of angiogenesis by PEX, a noncatalytic metalloproteinase fragment with integrin binding activity. *Cell.* 92, 391-400 (1998).
32. Brose, K., et al. Slit proteins bind Robo receptors and have an evolutionary conserved role in repulsive axon guidance. *Cell* 96, 795-806 (1999).
33. Burnett, M.E., White, E.C., Sih, S., von Haken, M.S., Cogen, P.H. Chromosome arm 17p deletion analysis reveals molecular genetic heterogeneity in supratentorial and infratentorial primitive neuroectodermal tumors of the central nervous system. *Cancer Genet. Cytogenet.* 97, 25-31 (1997).
34. Chan, P., Risler, J.L., Raguenez, G., Salier, J.P. The three heavy-chain precursors for the inter-alpha-inhibitor family in mouse: new members of the multicopper

- oxidase protein group with differential transcription in liver and brain. *Biochem. J.* 306, 505-512 (1995).
35. Chandrasekar, N., et al. Downregulation of uPA inhibits migration and PI3k/Akt signaling in glioblastoma cells. *Oncogene.* 22, 392-400 (2003).
36. Chekenya, M., et al. The NG2 chondroitin sulfate proteoglycan: role in malignant progression of human brain tumors. *Int. J. Dev. Neurosci.* 17, 421-435 (1999).
37. Chen, L., Zhang, H., Powers, R.W., Russell, P.T., Larsen, W.J. Covalent linkage between proteins of the inter- α -inhibitor family and hyaluronic acid is mediated by a factor produced by granulosa cells. *J. Biol. Chem.* 271(32), 19409-19414 (1996).
38. Cheng, H.J., et al. Plexin-A3 mediates semaphoring signaling and regulates the development of hippocampal axonal projections. *Neuron.* 32(2), 249-263 (2001).
39. Chicoine, M.R., Madsen, B.S., Silbergeld, D.L. Modification of human glioma locomotion *in vitro* by cytokines EGF, bFGF, PDGFbb, NGF and TNF α . *Neurosurgery.* 36(6), 1165-1171 (1995).
40. Chicoine, M.R., Silbergeld, D.L. Invading C6 glioma cell maintaining tumorigenicity. *J. Neurosurg.* 85, 665-671 (1995).
41. Chicoine, M.R., Silbergeld, D.L. Mitogens as motogens. *J. Neurooncol.* 35, 249-257 (1997).
42. Chintala, S.K., et al. Adenovirus-mediated p16/CDKN2 gene transfer suppresses glioma invasion *in vitro*. *Oncogene.* 15, 2049-2057 (1997).
43. Chuang, Y., et al. Role of synaptotjanin 2 in glioma cell migration and invasion. *Cancer Res.* 64, 8271-8275 (2004).

44. Cirielli, C., Inyaku, K., Capogrossi, M.C., Yuan, X., Williams, J.A. Adenovirus-mediated wild-type p53 expression induces apoptosis and suppresses tumorigenesis of experimental intracranial human malignant gliomas. *J. Neurooncol.* 43, 99-108 (1999).
45. Coffey, M.C., Strong, J.E., Forsyth, P.A., Lee, P.W.K. Reovirus therapy of tumor with activated ras pathway. *Science.* 282, 1332-1334 (1998).
46. Cogen, P.H., McDonald, J.D. Tumor suppressor genes and medulloblastoma. *J. Neurooncol.* 29, 103-112 (1996).
47. Corcoran, A., Del Maestro, R.F. Testing the "Go or Grow" hypothesis in human medulloblastoma cell lines in two and three dimensions. *Neurosurgery.* 53(1), 174-184 (2003).
48. Corcoran, A., et al. Evolution of the brain tumor spheroid model: transcending current model limitations. *Acta Neurochir. (Wien)* 145(9), 819-824 (2003).
49. Dahmen, R.P., et al. Deletions of AXIN1, a component of the WNT/wingless pathway, in sporadic medulloblastomas. *Cancer Res.* 61, 7039-7043 (2001).
50. Dallol, A., et al. Frequent epigenetic inactivation of the SLIT2 gene in gliomas. *Oncogene* 22(29), 4611-4616 (2003a).
51. Dallol, A., et al. SLIT2, a human homologue of the Drosophila Slit2 gene, has tumor suppressor activity and is frequently inactivated in lung and breast cancers. *Cancer Res.* 62(20), 5874-5880 (2002).
52. Dallol, A., Morton, D., Maher, E.R., Latif, F. SLIT2 axon guidance molecule is frequently inactivated in colorectal cancer and suppresses growth of colorectal carcinoma cells. *Cancer Res.* 63(5), 1054-1058 (2003b).

53. Darquy, S., Sun, A.M. Microencapsulation of parathyroid cells as a bioartificial parathyroid: *in vitro* studies. *Trans. Am. Soc. Artif. Intern. Organs.* 33, 356-358 (1987).
54. De Angelis, L.M., Gutin, P.H., Leibel, S.A., Posner, J.B. *Intracranial tumors: diagnosis and treatment.* (Scarborough: Taylor & Francis group, 2002). 165-166.
55. Del Duca, D., Werbowetski, T., Del Maestro, R.F. Spheroid preparation from hanging drops: characterization of a model of brain tumor invasion. *J. Neurooncol.* 67(3), 295-303 (2004).
56. Del Maestro, R.F., Shivers, R.R., McDonald, W., Del Maestro, A. Dynamics of C6 astrocytoma invasion into three-dimensional collagen gels. *J. Neurooncol.* 53, 87-98 (2001).
57. Del Maestro, R.F., Tamaki, M., McDonald, W., Amberger, V. The C6 astrocytoma spheroid invasion model: evidence for the presence of a glial-repellent factor(s). *Can J Neurol Sci* 24(Suppl 1):S18 (1997).
58. Delmas, C., et al. Farnesyltransferase inhibitor, R115777, reverses the resistance of human glioma cell lines to ionizing radiation. *Int. J. Cancer.* 100, 43-48 (2002).
59. Demuth, T., Berens, M.E. Molecular mechanisms of glioma cell migration and invasion. *J. Neurooncol.* 70, 217-228 (2004).
60. Deryugina, E.I., Soroceanu, L., Strongin, A.Y. Up-regulation of vascular endothelial growth factor by membrane-type 1 matrix metalloproteinase stimulates human glioma xenograft growth and angiogenesis. *Cancer Res.* 62, 580-588 (2002).
61. Diarra-Mehrpour, M., et al. Human plasma inter-alpha trypsin inhibitor is encoded by four genes on three chromosomes. *Eur. J. Biochem.* 179(1), 147-154 (1989).

62. Dickson, B.J. Molecular mechanisms of axon guidance. *Science*. 298, 1959-1964 (2002).
63. Ding, H., et al. Astrocyte-specific expression of activated p21-ras results in malignant astrocytoma formation in a transgenic mouse model of human gliomas. *Cancer Res.* 61, 3826-3836 (2001).
64. Ebens, A., et al. Hepatocyte growth factor/scatter factor is an axonal chemoattractant and a neurotrophic factor for spinal motor neurons. *Neuron*. 17, 1157-1172 (1996).
65. Ehteshami, M., et al. The use of interleukin 12-secreting neural stem cells for the treatment of intracranial glioma. *Cancer Res.* 62, 5657-5663 (2002).
66. Ekstrand, A.J., Sugawa, N., James, C.D., Collins, V.P. Amplified and rearranged epidermal growth factor receptor genes in human glioblastomas reveal deletions of sequences encoding portions of the N- and/or C- terminal tails. *Proc. Natl. Acad. Sci. USA.* 89, 4309-4313 (1992).
67. Engebraaten, O., et al. Interaction between human brain tumor biopsies and fetal brain tissue *in vitro*. *Acta Neuropathol (Berl)* 81(2), 130-140 (1990).
68. Engebraaten, O., Bjerkvig, R., Pedersen, P., Laerum, O.D. Effects of EGF, bFGF, NGF and PDGF(bb) on cell proliferative, migratory, and invasive capacities of human brain-tumor biopsies *in vitro*. *Int. J. Cancer.* 53, 209-214 (1993).
69. Engers R., Springer E., Michiels F., Collard J.G., Gabbert H.E. Rac affects invasion of human renal cell carcinomas by upregulating TIMP-1 and TIMP-2 expression. *J. Biol. Chem.* 276(45), 41889-41897 (2001).
70. Etienne-Manneville, S., Hall, A. Integrin-mediated activation of Cdc42 controls cell polarity in migrating astrocytes through PKC ζ . *Cell*. 106, 489-498 (2001).

71. Etienne-Manneville, S., Hall, A. Cdc42 regulates GSK3 β and adenomatous polyposis coli to control cell polarity. *Nature*. 421, 753-756 (2003).
72. Fan, X., Labrado, J.P., Hing, H., Bashaw, G.J. Slit stimulation recruits dock and pak to the roundabout receptor and increases rac activity to regulate axon repulsion at the CNS midline. *Neuron* 40, 113-127 (2003)
73. Farrell, C.L., Stewart, P.A., Del Maestro, R.F. A new glioma model in rat: The C6 spheroid implantation technique permeability and vascular characterization. *J. Neurooncol.* 4, 403-415 (1987).
74. Feldkamp, M.M., Lala, P., Lau, N., Boss, G., Pawson, A. Expression of activated epidermal growth factor receptors, ras-guanosine triphosphate, and mitogen activated protein kinase in human glioblastoma multiforme specimens. *Neurosurgery*. 45, 1442-1453 (1999).
75. Friedl, P., et al. Migration of highly aggressive MV3 melanoma cells in 3-D collagen lattices results in local matrix reorganization and shedding of $\alpha 2$ and $\beta 1$ integrins and CD44. *Cancer Res.* 57, 2061-2070 (1997).
76. Georger, B., et al. Antitumor activity of the rapamycin analog CCI-779 in human primitive neuroectodermal tumor/medulloblastoma models as single agent and in combination chemotherapy. *Cancer Res.* 61(4), 1527-1532 (2001).
77. Giangaspero, F., Bigner, S.H., Kleihues, P., Pietsch, T., Trojanowski, J.Q.. In *World Health Organization Classification of Tumors: Pathology and Genetics of the Tumors of the Central Nervous System*, eds Kleihues, PC, Cavenee WK. (Int. Agency for Res. On Cancer, Lyon, France, 2000). 129-137.

78. Giese, A., et al. Dichotomy of astrocytoma migration and proliferation. *Int. J. Cancer*. 67(2), 275-282 (1996).
79. Glass, T.L., Liu, T.J., Yung, W.K. Inhibition of cell growth in human glioblastoma cell lines by farnesyltransferase inhibitor SCH66336. *Neuro-oncol.* 2, 151-158 (2000).
80. Goldberg, W.J., Levine, K.V., Laws, E.R., Bernstein, J.J. Mechanisms of C6 glioma cell and fetal astrocyte migration into hydrated collagen I gels. *Brain Res.* 581, 81-90 (1992).
81. Goldbrunner, R.H., et al. Transfection and dye premarking of human and rat glioma cell lines affects adhesion, migration and proliferation. *Anticancer Res.* 17(6D):4467-4471 (1997).
82. Gomes, E.R., Shantanu, J., Gundersen, G.G. Nuclear movement regulated by Cdc42, MRCK, myosin, and actin flow establishes MTOC polarization in migrating cells. *Cell.* 121, 451-463 (2005).
83. Goodrich, L.V., Milenkovic, L., Higgins, K.M., Scott, M.P. Altered neural cell fates and medulloblastoma in mouse patched mutants. *Science.* 277, 1109-1113 (1997).
84. Goudar, R.K., et al. Combination therapy of inhibitors of epidermal growth factor receptor/vascular endothelial growth factor receptor 2 (AEE788) and the mammalian target of rapamycin (RAD001) offers improved glioblastoma tumor growth inhibition. *Mol. Cancer Ther.* 4(1), 101-112 (2005).
85. Gratsa, A. et al. Correlation of expression of NCAM and GD3 ganglioside to motile behaviour in neoplastic glia. *Anticancer Res.* 17, 4111-4117 (1997).

86. Greenberg, J.M., Thomson, F.Y., Brooks, S.K., Shannon, J.M., Akeson, A.L. Slit and Robo expression in the developing mouse lung. *Dev. Dyn.* 230, 350-360 (2004).
87. Guha, A., Feldkamp, M.M., Lau, N., Boss, G., Pawson, A. Proliferation of human malignant astrocytomas is dependent on ras activation. *Oncogene.* 15, 2755-2765 (1997).
88. Habets, G.G., et al. Identification of an invasion-inducing gene, Tiam1 that encodes a protein with homology to GDP-GTP exchangers for Rho-like proteins. *Cell.* 77, 537-549 (1994).
89. Hahn, H., et al. Rhabdomyosarcomas and radiation hypersensitivity in a mouse model of Gorlin syndrome. *Nat. Med.* 4, 619-622 (1998).
90. Hamasuna, R., et al. Reduced expression of hepatocyte growth factor activator inhibitor type-2/placental bikunin (HAI-2/PB) in human glioblastomas: implication for anti-invasive role of HAI-2/PB in glioblastoma cells. *Int. J. Cancer.* 93, 339-345 (2001).
91. Hamasuna, R., et al. Regulation of matrix metalloproteinase-2 (MMP-2) by hepatocyte growth factor/scatter factor (HGF/SF) in human glioma cells: HGF/SF enhances MMP-2 expression and activation accompanying up-regulation of membrane type-1 MMP. *Int. J. Cancer.* 82, 274-281 (1999).
92. Hamel, W., Westphal, M. Growth factors in gliomas revisited. *Acta Neurochir. (Wien).* 142, 113-138 (2000).
93. Hamilton, S.R., et al. The molecular basis of Turcot's syndrome. *N. Engl. J. Med.* 332(13), 839-847 (1995).

94. Hara, A., Saegusa, M., Mikami, T., Okayasu, I. Loss of DCC expression in astrocytomas: relation to p53 abnormalities, cell kinetics and survival. *J. Clin. Pathol.* 54, 860-865 (2001).
95. Hermanson, M., et al. Platelet-derived growth factor and its receptors in human glioma tissue: expression of messenger RNA and protein suggest the presence of autocrine and paracrine loops. *Cancer Res.* 52(11), 3213-3219 (1992).
96. Hesselager, G., Holland, E.C. Using mice to decipher the molecular genetics of brain tumors. *Neurosurgery.* 53(3), 685-695 (2003).
97. Himmelfarb, M., et al. ITI H5, a novel member of the inter- α -trypsin inhibitor heavy chain family is downregulated in breast cancer. *Cancer Lett.* 204, 69-77 (2004).
98. Hoelzinger, D.B., et al. Gene expression profile of glioblastoma multiforme invasive phenotype points to new therapeutic targets. *Neoplasia.* 7(1), 7-16 (2005).
99. Holland, E.C., et al. Combined activation of Ras and Akt in neural progenitors induces glioblastoma formation in nude mice. *Nat. Genet.* 25(1), 55-57 (2000).
100. Hordijk, P.L., et al. Inhibition of invasion of epithelial cells by Tiam1-Rac signaling. *Science.* 278, 1464-1466 (1997).
101. Hu H. Chemorepulsion of neuronal migration by Slit2 in the developing mammalian forebrain. *Neuron* 23, 703-711 (1999).
102. Huang, H., et al. APC mutations in sporadic medulloblastoma. *Am. J. Pathol.* 156(2), 433-437 (2000).
103. Ichimua, K., Ohgaki, H., Kleihues, P., Collins, P.V. Molecular pathogenesis of astrocytic tumors. *J. Neurooncol.* 70, 137-160 (2004).

104. Jalink, K., et al. Inhibition of lysophosphatidate- and thrombin-induced neurite retraction and neuronal cell rounding by ADP ribosylation of the small GTP-binding protein Rho. *J. Cell Biol.* 126, 801-810 (1994).
105. Jarjour, A.A., et al. Netrin-1 is a chemorepellent for oligodendrocyte precursor cells in the embryonic spinal cord. *J. Neurosci.* 23(9), 3735-3744 (2003).
106. Jen, J.C., et al. Mutations in a human ROBO gene disrupt hindbrain axon pathway crossing and morphogenesis. *Science* 304, 1509-1513 (2004).
107. Joki, T. et al. Continuous release of endostatin from microencapsulated engineered cells for tumor therapy. *Nat. Biotechnol.* 19(1), 35-39 (2001).
108. Juliano, R.L. Signal transduction by cell adhesion receptors and cytoskeleton: Functions of integrins, cadherins, selectins, and immunoglobulin-superfamily members. *Annu. Rev. Pharmacol. Toxicol.* 42, 283-323 (2002).
109. Kassis, J., Lauffenburger, D.A., Turner, T., Wells, A. Tumor invasion as dysregulated cell motility. *Semin. Cancer. Biol.* 11, 105-117 (2001).
110. Keleman, K., Ribeiro, C., Dickson, B.J. Comm function in commissural axon guidance: cell-autonomous sorting of Robo *in vivo*. *Nat. Neurosci.* 8(2), 156-163 (2005).
111. Keleman, K., et al. Comm sorts robo to control axon guidance at the *Drosophila* midline. *Cell.* 110, 415-427 (2002).
112. Kennedy, T.E., Serafini, T., de la Torre, J.R., Tessier-Lavigne, M. Netrins are diffusible chemotropic factors for commissural axons in the embryonic spinal cord. *Cell* 78(3), 425-435 (1994).

113. Khoshyomn, S., Lew, S., DeMattia, J., Winger, E.B., Penar, P.L. Brain tumor invasion rate measured *in vitro* does not correlate with Ki-67 expression. *J. Neurooncol.* 45, 111-116 (1999).
114. Kidd, T., Bland, K.S., Goodman, C.S. Slit is the midline repellent for the Robo receptor for *Drosophila*. *Cell* 96, 785-794 (1999).
115. Kim, J.Y., et al. Activation of neurotrophins-3 receptor TrkC induces apoptosis in medulloblastoma. *Cancer Res.* 59(3), 711-719 (1999).
116. Kleihues, P. et al., *World Health Organization Classification of Tumors: Pathology and Genetics of Tumors of the Central Nervous System*, eds. Kleihues, PC, Cavenee WK. (Int. Agency for Research on Cancer, Lyon, France, 2000) 29-39.
117. Koochekpour, S., et al. Met and hepatocyte growth factor/scatter factor expression in human gliomas. *Cancer Res.* 57, 5391-5398 (1997).
118. Kubiowski, T., et al. Association of increased phosphatidylinositol 3-kinase signaling with increased invasiveness and gelatinase activity in malignant gliomas. *J. Neurosurg.* 95, 480-488 (2001).
119. Kuroda, S., et al. Regulation of cell-cell adhesion of MDCK cells by Cdc42 and Rac1 small GTPases. *Biochem. Biophys. Res. Commun.* 240, 430-435 (1997).
120. Ladiwala, U., et al. P75 neurotrophin receptor expression on adult human oligodendrocytes: signaling without cell death in response to NGF. *J. Neurosci.* 18(4), 1297-1304 (1998).
121. Latil, A., et al. Quantification of netrins, slits and their receptors in human prostate cancers. *Int. J. Cancer* 103(3), 306-315 (2003).

122. Lee, A., et al. Isolation of neural stem cells from the postnatal cerebellum. *Nat. Neurosci.* 8, 723-729 (2005).
123. Lefranc, F., Brotchi, J., Kiss, R. Possible future issues in the treatment of glioblastomas: special emphasis on cell migration and the resistance of migrating glioblastoma cells to apoptosis. *J. Clin. Oncol.* 23(10), 2411-2422 (2005).
124. Li, H.S., et al. Vertebrate slit, a secreted ligand for the transmembrane protein roundabout, is a repellent for olfactory bulb axons. *Cell* 96, 807-818 (1999).
125. Li, J., et al. PTEN, a putative protein tyrosine phosphatase gene mutated in human brain, breast and prostate cancer. *Science.* 275(5308), 1943-1947 (1997).
126. Li, D.M., Sun, H. TEP1, encoded by a candidate tumor suppressor locus, is a novel protein tyrosine phosphatase regulated by transforming growth factor beta. *Cancer Res.* 57(11), 2124-2129 (1997).
127. Libermann, T.A., et al. Amplification and overexpression of the EGF receptor gene in primary human glioblastoma. *J. Cell Sci. Suppl.* 3, 161-172 (1985a).
128. Libermann, T.A., et al. Amplification, enhanced expression and possible rearrangement of EGF receptor gene in primary human brain tumors of glial origin. *Nature.* 313, 144-147 (1985b).
129. Lim, F., Sun, A.M. Microencapsulated islets as bioartificial endocrine pancreas. *Science.* 210, 908-910 (1980).
130. Ling, J., Liu, Z., Wang, D., Gladson, C.L. Malignant astrocytoma cell attachment and migration to various matrix proteins is differentially sensitive to phosphoinositide 3-OH kinase inhibitors. *J. Cell. Biochem.* 73, 533-544 (1999).

131. Liotta, L.A., et al. Tumor cell autocrine motility factor. *Proc. Natl. Acad. Sci. USA.* 83, 3302-3306 (1986).
132. Lokker, N.A., Sullivan, C.M., Hollenbach, S.J., Israel, M.A., Giese, N.A. Platelet-derived growth factor (PDGF) autocrine signaling regulates survival and mitogenic pathways in glioblastoma cells: evidence that the novel PDGF-C and PDGF-D ligands may play a role in the development of brain tumors. *Cancer Res.* 62(13), 3729-3735 (2002).
133. Lopez, M.B.S., VandenBerg, S.R., Scheithauer, B.W. *Histopathology, immunochemistry and ultrastructure of brain tumors.* In: Kaye AH, Laws ER, editors. Brain tumors: an encyclopedic approach. (Edinburgh UK: Churchill Livingstone 1995) 125-162.
134. Louis, D.N., Pomeroy, S.L., Cairncross, J.G. Focus on central nervous system neoplasia. *Cancer Cell* 1, 125-128 (2002).
135. Lumsden, A.G.S., Davies, A.M. Earliest sensory nerve fibres are guided to peripheral targets by attractants other than nerve growth factor. *Nature* 306(5945), 786-788 (1983).
136. Lumsden, A.G.S., Davies, A.M. Chemotropic effect of specific target epithelium in the developing mammalian nervous system. *Nature* 323(6088), 538-539 (1986).
137. Lund-Johansen, M., et al. Effect of epidermal growth factor on glioma cell growth, migration and invasion *in vitro.* *Cancer Res.* 50, 6039-6044 (1990).
138. Lund-Johansen, M., Forsberg, K., Bjerkvig, R., Laerum, O.D. Effects of growth factors on a human glioma cell line during invasion into rat brain aggregates in culture. *Acta Neuropathol. (Berl)* 84(2), 190-197 (1992).

139. Lundstrom, A., et al. Vilese, a conserved rac/cdc42 GAP mediating robo repulsion in tracheal cells and axons. *Genes Dev.* 18, 2161-2171 (2004).
140. Luo, L. RhoGTPases in neuronal morphogenesis. *Nat. Rev. Neurosci.* 1, 173-180 (2000).
141. Luo, L., Liao, Y.J., Jan, L.Y., Jan Y.N. Distinct morphogenetic functions of similar small GTPases: *Drosophila* Drac1 is involved in axonal outgrowth and myoblast fusion. *Genes Dev.* 8, 1787-1802 (1994).
142. Maidment, S.L. An inverse correlation between expression of NCAM-A and the matrix metalloproteinases gelatinase-A and gelatinase-B in human glioma cells *in vitro*. *Cancer Lett.* 116, 71-77 (1997).
143. Mariani, L., et al. Glioma cell motility is associated with reduced transcription of proapoptotic and proliferation genes: a cDNA microarray analysis. *J. Neurooncol.* 53, 161-176 (2001).
144. Marillat, V., et al. The slit receptor rig-1/robo3 controls midline crossing of hindbrain precerebellar neurons and axons. *Neuron* 43, 69-79 (2004).
145. Marino, S., Vooijs, M., van Der Gulden, H., Jonkers, J., Berns, A. Induction of medulloblastoma in p52-null mutant mice by somatic inactivation of Rb in the external granular layer cells of the cerebellum. *Genes. Dev.* 14, 994-1004 (2000).
146. Martin-Vandeleet N., Paris S., Bourguignon J., Sesboue R., Martin J.P., Diarra-Mehrpour M. Assembly and secretion of recombinant chains of human inter- α -trypsin inhibitor in COS-7 cells. *Eur. J. Biochem.* 259, 476-484 (1999).

147. Mason, H.A., Susumu, I., Corfas, G. Extracellular signals that regulate the tangential migration of olfactory bulb neuronal precursors: inducers, inhibitors and repellents. *J. Neurosci.* 21(19), 7654-7663 (2001).
148. Matsumura, H., Ohnishi, T., Kanemura, Y., Maruno, M., Yoshimine, T. Quantitative analysis of glioma cell invasion by confocal laser scanning microscopy in a novel brain slice model. *Biochem. Biophys. Res. Commun.* 269, 513-520 (2000).
149. Matsuzaki, H., et al. Plasma bikunin as a favorable prognostic factor in ovarian cancer. *J. Clin. Oncol.* 23(7), 1463-1472 (2005).
150. Merzak, A., McCrea, S., Koocheckpour, S., Pilkington, G.J. Control of human glioma cell growth, migration and invasion *in vitro* by transforming growth factor β . *Br. J. Cancer.* 70, 199-203 (1994).
151. Michiels, F., Habets, G.G., Stam, J.C., Van der Kammen, R.A., Collard, J.G. A role for Rac in Tiam-1 induced membrane ruffling and invasion. *Nature.* 375, 338-340 (1995).
152. Miura, Y., Akimoto, T., Kanazawa, H., Yagi, K. Synthesis and secretion of protein by hepatocytes entrapped within calcium alginate. *Artific. Organs.* 10, 460-465 (1986).
153. Miyamoto, Y., Yamauchi, J., Mizuno, N., Itoh, H. The adaptor protein Nck1 mediates endothelin A receptor-regulated cell migration through the Cdc42-dependent c-Jun N-terminal kinase pathway. *J. Biol. Chem.* 279(32), 34336-34342 (2004).

154. Mizushima, S., Nii, A., Katao, K., Uemura, A. Gene expression of the two heavy chains and one light chain forming the inter-alpha-trypsin-inhibitor in human tissues. *Biol. Pharm. Bull.* 21(2), 167-169 (1998).
155. Mohanam, S. et al. Stable transfection of urokinase-type plasminogen activator antisense construct modulates invasion of human glioblastoma cells. *Clin. Cancer Res.* 7, 2519-2526 (2001).
156. Mueller, M.M., Werbowetski, T., Del Maestro, R.F. Soluble factors in glioma invasion. *Acta Neurochir. (Wien)* 145, 999-1008 (2003).
157. Myat, A., et al. *Drosophila* Nedd4, a ubiquitin ligase, is recruited by Commissureless to control cell surface levels of the roundabout receptor. *Neuron.* 35, 447-459 (2002).
158. Nakada, M., et al. The phosphorylation of EphB2 receptor regulates migration and invasion of human glioma cells. *Cancer Res.* 64(9), 3179-3185 (2004).
159. Nakagawa, T., et al. Production of matrix metalloproteinases and tissue inhibitor of metalloproteinases-1 by human brain tumors. *J Neurosurg.* 81, 69-77 (1994).
160. Nakatani, K., et al. The significance of the expression of tumor suppressor gene DCC in human gliomas. *J. Neurooncol.* 40, 237-242 (1998).
161. Nelson, A.L., et al. Magnetic resonance imaging of *patched* heterozygotes and xenografted mouse brain tumors. *J. Neurooncol.* 62, 259-267 (2003).
162. Nguyen-Ba-Charvet, K.T., et al. Multiple roles for slits in the control of cell migration in the rostral migratory stream. *J. Neurosci.* 24(6), 1497-1506 (2004).

163. Nygaard, S.J., et al. Glioma cell invasion visualized by scanning confocal laser microscopy in an *in vitro* co-culture system. *Invasion Metastasis* 15(5), 179-188 (1995).
164. Ochi, K., Mori, T., Toyama, Y., Nakamura, Y., Arakawa, H. Identification of semaphorin3B as a direct target of p53. *Neoplasia*. 4(1), 82-87 (2002).
165. ODum, L., Andersen, C.Y., Jessen, T.E. Characterization of the coupling activity for the binding of inter-alpha-trypsin inhibitor to hyaluronan in human and bovine follicular fluid. *Reproduction*. 124(2), 249-257 (2002).
166. Oliver, T.G., et al. Transcriptional profiling of the Sonic hedgehog response: a critical role for N-myc in proliferation of neuronal precursors. *Proc. Natl. Acad. Sci. USA*. 100(12), 7331-7336 (2003).
167. Ozen, P., et al. Expression of matrix metalloproteinases and their inhibitors in medulloblastomas and their prognostic relevance. *Clin. Cancer Res.* 10(14), 4746-4753 (2004).
168. Palazzo, A.F., et al. Cdc42, dynein, and dynactin regulate MTOC reorientation independent of Rho-regulated microtubule stabilization. *Curr. Biol.* 11, 1536-1541 (2001).
169. Palecek, S.P., Schmidt, C.E., Lauffenburger, D.A., Horwitz, A.F. Integrin dynamics on the uropodal region of migrating fibroblasts. *J. Cell. Sci.* 109, 941-952 (1996).
170. Paris, S., et al. Inhibition of tumor growth and metastatic spreading by overexpression of inter-alpha-trypsin inhibitor family chains. *Int. J. Cancer.* 97, 615-620 (2002).

171. Park, K.W., et al. Robo4 is a vascular-specific receptor that inhibits endothelial migration. *Dev. Biol.* 261, 251-267 (2003).
172. Paulino, A.C. Long-term survival in a child with extraneural metastasis from medulloblastoma treated with chemo-radiotherapy. *Med. Pediatr. Oncol.* 40(6), 396-397 (2003).
173. Paulus, W., Baur, I., Beutler, A.S., Reeves, S.A. Diffuse brain invasion of glioma cells requires beta 1 integrins. *Lab Invest.* 75, 819-826 (1996).
174. Paulus, W., Tonn, J.C. Basement-membrane invasion of glioma cells mediated by integrin receptors. *J. Neurosurg.* 80, 515-519 (1994).
175. Perkins, D.N., Pappin, D.J., Creasy, D.M., and Cottrell, J.S. Probability-based protein identification by searching sequence databases using mass spectrometry data. *Electrophoresis.* 20(18):3551-3567 (1999).
176. Perry, A., Gutmann, D.H., Reifenberger, G. Molecular pathogenesis of meningiomas. *J. Neurooncol.* 70, 183-202 (2004).
177. Pham, C.D., et al. Magnetic resonance imaging detects suppression of tumor vascular permeability after administration of antibody to vascular endothelial growth factor. *Cancer Invest.* 16, 225-230 (1998).
178. Pietsch, T., Taylor, M.D., Rutka, J.T. Molecular pathogenesis of childhood brain tumors. *J. Neurooncol.* 70, 203-215 (2004).
179. Pietsch, T., et al. Medulloblastomas of the desmoplastic variant carry mutations of the human homologue of *Drosophila* patched. *Cancer Res.* 57, 2085-2088 (1997).
180. Pilorget, A., et al. Medulloblastoma cell invasion is inhibited by green tea (-) epigallocatechin-3-gallate. *J. Cell. Biochem.* 90, 745-755 (2003).

181. Placzek, M., Tessier-Lavigne, M., Jessel, T., Dodd, J. Orientation of commissural axons *in vitro* in response to a floor plate-derived chemoattractant. *Development* 110, 19-30 (1990).
182. Plump A.S., et al. Slit1 and slit2 cooperate to prevent premature midline crossing of retinal axons in the mouse visual system. *Neuron* 33, 219-232 (2002).
183. Pomeroy, S., et al. Prediction of central nervous system embryonal tumor outcome based on gene expression. *Nature*. 415(6870), 436-442 (2002).
184. Prag, S., et al. NCAM regulates cell motility. *J. Cell Sci.* 115, 283-292 (2002).
185. Raffel, C. Medulloblastoma: Molecular genetics and animal models. *Neoplasia* 6(4), 310-322 (2004).
186. Raffel, C., et al. Sporadic medulloblastoma contain PTCH mutations. *Cancer Res.* 57, 842-845 (1997).
187. Raffel, C., Thomas, G.A., Tishler, D.M., Lassoﬀ, S., Allen, J.C. Absence of p53 mutations in childhood central nervous system primitive neuroectodermal tumor. *Neurosurgery.* 33, 301-305 (1993)
188. Raffel, C., Ueki, K., Harsh, 4th G.R., Louis, D.N. The multiple tumor suppressor 1/cyclin-dependent kinase inhibitor 2 gene in human central nervous system primitive neuroectodermal tumor. *Neurosurgery.* 36, 971-974 (1995).
189. Rajagopalan, S., Nicolas, E., Vivancos, V., Berger, J., Dickson, B. Crossing the midline: roles and regulations of Robo receptors. *Neuron.* 28, 767-777 (2000).
190. Raper, J.A. Semaphorins and their receptors in vertebrates and invertebrates. *Curr. Opin. Neurobiol.* 10(1), 88-94 (2000).

191. Rao, G., et al. Sonic hedgehog and insulin-like growth factor signaling synergize to induce medulloblastoma formation from nestin-expressing neural progenitors in mice. *Oncogene*. 23(36) 6156-6162 (2004).
192. Read, T.A., et al. Intravital microscopy reveals novel antivascular and antitumor effects of endostatin delivered locally by alginate-encapsulated cells. *Cancer Res*. 61, 6830-6837 (2001a).
193. Read, T.A., et al. Local endostatin treatment of gliomas administered by microencapsulated producer cells. *Nat. Biotechnol*. 19(1), 29-34 (2001b).
194. Read, T.A., et al. Cells encapsulated in alginate: a potential system for delivery of recombinant proteins to malignant brain tumors. *Int. J. Dev. Neurosci*. 17(5-6), 653-663 (1999).
195. Regen, C.M., Horwitz, A.F. Dynamics of β 1 integrin-mediated adhesive contacts in motile fibroblasts. *J. Cell. Biol*. 119, 1347-1359 (1992).
196. Reifenberger, J. et al. Missense mutations in SMOH in sporadic basal cell carcinomas of the skin and primitive neuroectodermal tumors of the central nervous system. *Cancer Res*. 58(9), 1798-1803 (1998).
197. Reilly, K.M., Loisel, D.A., Bronson, R.T., McLaughlin, M.E., Jacks, T. Nf1; Trp53 mutant mice develop glioblastoma with evidence of strain-specific effects. *Nat. Genet*. 26, 109-113 (2000).
198. Rempel, S.A., Golembieski, W.A., Fisher, J.L., Maile, M., Nakeff, A. SPARC modulates cell growth, attachment and migration of glioma cells on brain extracellular matrix proteins. *J. Neurooncol*. 53(2), 149-160 (2001).

199. Rhee, J., et al. Activation of the repulsive receptor roundabout inhibits N-cadherin mediated cell adhesion. *Nat. Cell Biol.* 4, 798-805 (2002).
200. Rieger, J., Wick, W., Weller, M. Human malignant glioma cells express semaphorins and their receptors, neuropilins and plexins. *Glia.* 42, 379-389 (2003).
201. Romer, J.T., et al. Suppression of the Shh pathway using a small molecule inhibitor eliminates medulloblastoma in Ptc +/- p53 -/- mice. *Cancer Cell.* 6, 229-240 (2004).
202. Rooprai, H.K., et al. The role of integrin receptors in aspects of glioma invasion *in vitro*. *Int. J. Dev. Neurosci.* 17, 613-623 (1999).
203. Roth, W., et al. Secreted frizzled-related proteins inhibit motility and promote growth of human malignant glioma cells. *Oncogene.* 19, 4210-4220 (2000).
204. Rugg, M. et al. Characterization of complexes formed between TSG-G and inter- α -inhibitor that acts as intermediates in the covalent transfer of heavy chains onto hyaluronan. *J. Biol. Chem.* (in press) (2005).
205. Sabatier, C. et al. The divergent Robo family protein Rig-1/Robo3 is a negative regulator of slit responsiveness required for midline crossing by commissural axons. *Cell* 117, 157-169 (2004).
206. Saleh, M., Stacker, S.A., Wilks, A.F. Inhibition of growth of C6 glioma cells *in vivo* by expression of antisense vascular endothelial growth factor sequence. *Cancer Res.* 56, 393-401 (1996).
207. Sander, E.E., ten Klooster, J.P., van Delft, S., van der Kammen, R.A., and Collard, J.G. Rac downregulates Rho activity: Reciprocal balance between both

- GTPases determines cellular morphology and migratory behavior. *J. Cell. Biol.* 147, 1009-1022 (1999).
208. Sander, E.E., et al. Matrix-dependent Tiam1/Rac signaling in epithelial cells promotes either cell-cell adhesion or cell migration and is regulated by phosphatidylinositol 3-kinase. *J. Cell Biol.* 143, 1385-1398 (1998).
209. Schmitz, A.A.P., Gove, E., Bottler, B., Van Ales, L. RhoGTPases: signaling, migration and invasion. *Exp Cell Res.* 261, 1-12 (2000).
210. Segal, R.A., Goumnerova, L.C., Kwon, Y.K., Stiles, C.D., Pomeroy, S.L. Expression of the neurotrophin receptor TRKC is linked to a favorable outcome in medulloblastoma. *Proc. Natl. Acad. Sci. USA.* 91, 12867-12871 (1994).
211. Senger, D.L. et al. Suppression of Rac activity induces apoptosis of human glioma cells but not normal human astrocytes. *Cancer Res.* 62, 2131-2140 (2002).
212. Shekarabi, M., Kennedy, T.E. The netrin-1 receptor DCC promotes filopodia formation and cell spreading by activating Cdc42 and Rac1. *Mol. Cell. Neurosci.* 19, 1-17 (2002).
213. Shu T., Richards L.J. Cortical axon guidance by the glial wedge during the development of the corpus callosum. *J. Neurosci.* 21, 2749-2758 (2001).
214. Simpson, J.H., Bland, K.S., Fetter, R.D., Goodman, C.S. Short-range and long-range guidance by Slit and its Robo receptors: a combinatorial code of Robo receptors controls lateral position. *Cell.* 103, 1019-1032 (2000).
215. Singh, S.E., et al. Identification of a cancer stem cell in human brain tumors. *Cancer Res.* 63, 5821-5828 (2003).

216. Singh, S.E., et al. Identification of human brain tumor initiating cells. *Nature*. 432, 396-401 (2004).
217. Smyth, I., et al. Isolation and characterization of human patched 2 (PTCH2), a putative tumor suppressor gene in basal cell carcinoma and medulloblastoma on chromosome 1p32. *Hum. Mol. Genet.* 8(2), 291-297 (1999).
218. Soon-Shiong, P., et al. Successful reversal of spontaneous diabetes in dogs by intraperitoneal microencapsulated islets. *Transplantation*. 54, 769-774 (1992).
219. Spassky, N., et al. Directional guidance of oligodendroglial migration by class 3 semaphorins and netrin-1. *J. Neurosci.* 22(14), 5992-6004 (2002).
220. Steck, P.A., et al. Identification of a candidate tumor suppressor gene, MMAC1, at chromosome 10q23.3 that is mutated in multiple advanced cancers. *Nat. Genet.* 15(4), 356-362 (1997).
221. Stein, E., Tessier-Lavigne, M. Hierarchical organization of guidance receptors: silencing of netrin attraction by slit through a Robo/DCC receptor complex. *Science*. 291, 1928-1938 (2001).
222. Steinsvag, S.K. Interaction between glioma cells and normal brain tissue in organ culture studied by scanning electron microscopy. *Invasion Metastasis*. 5(5), 255-269 (1985).
223. Strongin, A.Y., et al. Mechanism of cell surface activation of 72 kDa type IV collagenases: isolation of the activated form of the membrane metalloprotease. *J. Biol. Chem.* 270, 5331-5338 (1995).

224. Sugawa, N., Ekstrand, A.J., James, C.D., Collins, V.P. Identical splicing of aberrant epidermal growth factor transcripts from amplified rearranged genes in human glioblastomas. *Proc. Natl. Acad. Sci. USA.* 87, 8602-8606 (1990).
225. Sugimoto, Y., et al. Guidance of glial precursor cell migration by secreted cues in developing optic nerve. *Development.* 128, 3321-3330 (2001).
226. Sutherland, R.M., McCredie, J.A., Inch, W.R. Growth of multicell spheroids in tissue culture as a model of nodular carcinomas. *J. Natl. Cancer Inst.* 46(1), 113-120 (1971).
227. Taga, T., et al. Alpha v-integrin antagonist EMD 121974 induces apoptosis in brain tumor cells growing on vitronectin and tenascin. *Int. J. Cancer* 98, 690-698 (2002).
228. Takaishi, K., Sasaki, T., Kotani, H., Nishioka, H., Takai, Y. Regulation of cell-cell adhesion by rac and rho small GTP proteins in MDCK. *J. Cell Biol.* 139, 1047-1059 (1997).
229. Tamaki, M., McDonald, W., Amberger, V., Moore, E., Del Maestro, R.F. Implantation of C6 astrocytoma spheroids into collagen type I gels: invasive, proliferative and enzymatic characterizations. *J. Neurosurg.* 87, 602-609 (1997).
230. Tatenhorst, L., Puttman, S., Senner, V., Paulus, W. Genes associated with fast glioma cell migration *in vitro* and *in vivo*. *Brain Pathol.* 15, 46-54 (2005).
231. Taylor, M.D., Mainprize, T.G., Rutka, J.T. Molecular insight into medulloblastoma and central nervous system primitive neuroectodermal tumor biology from hereditary syndromes. *Neurosurgery.* 47(4), 888-901 (2000).

232. Tessier-Lavigne, M., Goodman, C.S. The molecular biology of axon guidance. *Science*. 274, 1123-1133 (1996).
233. Thogersen, I.B., Enghild, J.J. Biosynthesis of bikunin proteins in the human carcinoma cell line HepG2 and in primary human hepatocytes. *J. Biol. Chem.* 270, 18700-1870 (1995).
234. Thu, B.J. *Alginate polycation microcapsules: A study of some molecular and functional properties relevant to their use as a bioartificial pancreas*. Department of Biotechnology, Norwegian University of Science and Technology, Trondheim, 1996.
235. Tremont-Lukats, I.W., Gilbert, M.R. Advances in molecular therapies in patients with brain tumors. *Cancer Control*. 10(2), 125-137 (2003).
236. Uhm, J.H., Dooley, N.P., Villemure, J.G., Yong, V.W. Glioma invasion *in vitro*: regulation by matrix metalloproteinase-2 and protein kinase C. *Clin. Exp. Metast.* 14, 421-433 (1996).
237. Uhm, J.H., Dooley, N.P., Villemure, J.G., Yong, V.W. Mechanisms of glioma invasion: role of matrix metalloproteinases. *Can. J. Neurol. Sci.* 24, 3-15 (1997).
238. Uhrbom, E., Hesselager, G., Nister, M., Westermark, B. Induction of brain tumors in mice using a recombinant platelet-derived growth factor B-chain retrovirus. *Cancer Res.* 58(23), 5275-5279 (1998).
239. Unemori, E.N., Werb, Z. Reorganization of polymerized actin: a possible trigger for induction of procollagenase in fibroblasts cultured in and on collagen gels. *J. Cell Biol.* 103, 1021-1031 (1986).

240. Vachon, P., Girard, C., Theoret, Y. Effects of basic fibroblastic growth factor on the growth of human medulloblastoma xenografts. *J. Neurooncol.* 67, 139-146 (2004).
241. Vince, G.H., Bouterfa, H., Goldbrunner, R., Roosen, K., Tonn, J.C. Fast blue, a fluorescent tracer in glioma cell culture, affects proliferation and motility. *Neurosci. Lett.* 233(2-3), 148-150 (1997).
242. Von Bulow, C., et al. Endothelial capillaries chemotactically attract tumor cells. *J. Pathol.* 193, 367-376 (2001).
243. Wang, B., et al. Induction of tumor angiogenesis by slit-robo signaling and inhibition of cancer growth by blocking robo activity. *Cancer Cell* 4(1), 19-29 (2003).
244. Wang, K.H., et al. Biochemical purification of a mammalian slit protein as a positive regulator of sensory axon elongation and branching. *Cell* 96, 771-784 (1999).
245. Ward, M., McCann, C., DeWulf, M., Wu, J.Y., Rao, Y. Distinguishing between directional guidance and motility regulation in neuronal migration. *J. Neurosci.* 23(12), 5170-5177 (2003).
246. Wechsler-Reya, R., Scott, M.P. The developmental biology of brain tumors. *Annu. Rev. Neurosci.* 24, 385-428 (2001).
247. Wechsler-Reya, R.J., Scott, M.P. Control of neuronal precursor proliferation in the cerebellum by Sonic Hedgehog. *Neuron.* 22, 103-114 (1999).
248. Weiner, H.L., et al. Induction of medulloblastoma in mice by sonic hedgehog, independent of Gli1. *Cancer Res.* 62, 6385-6389 (2002).

249. Weissenberger, J., et al. Development and malignant progression of astrocytomas in GFAP-v-src transgenic mice. *Oncogene*. 14, 2005-2013 (1997).
250. Werbowetski, T., Bjerkvig, R., Del Maestro, RF. Evidence for a secreted chemorepellent that directs glioma cell invasion. *J. Neurobiol.* 60(1), 71-88 (2004).
251. Wetmore, C., Eberhart, D.E., Curran, T. The normal patched allele is expressed in medulloblastoma from mice with heterozygous germ-line mutation of patched. *Cancer Res.* 60, 2239-2256 (2000).
252. Wetmore, C., Eberhart, D.E., Curran, T. Loss of p53 but not ARF accelerates medulloblastoma in mice heterozygotes for patched. *Cancer Res.* 61, 513-516 (2001).
253. White, L., Sterling-Levis, K., Kees, U.R., Tobias, V. Medulloblastoma/primitive neuroectodermal tumor studied as a Matrigel enhanced subcutaneous xenograft model. *J. Clin. Neurosci.* 8(2), 151-156 (2001).
254. Wilkinson, D.G. Multiple roles of Eph receptors and ephrins in neural development. *Nat. Rev. Neurosci.* 2(3), 155-164 (2001).
255. Wong, A.J., et al. Structural alterations of the epidermal growth factor receptor gene in human gliomas. *Proc. Natl. Acad. Sci. USA.* 89, 2965-2969 (1992).
256. Wong, K., et al. Signal Transduction in neuronal migration: roles of GTPase activating proteins and the small GTPase Cdc42 in the slit-robo pathway. *Cell* 107, 209-221 (2001).
257. Wong, K., Park, H.T., Wu, J.Y., Rao, Y. Slit proteins: molecular guidance cues for cells ranging from neurons to leukocytes. *Curr. Opin. Genet. Dev.* 12(5), 583-591 (2002).

258. Wong, J.T., Wong, S.T., O'Connor, T.P. Ectopic semaphorin-1a functions as an attractive guidance cue for developing peripheral neurons. *Nat. Neurosci.* 2(9), 798-803 (1999).
259. Wu, J.Y., et al. The neuronal repellent slit inhibits leukocyte chemotaxis induced by chemotactic factors. *Nature* 410, 948-952 (2001).
260. Wu, W., et al. Directional guidance of neuronal migration in the olfactory system by the protein slit. *Nature.* 400, 331-336 (1999).
261. Xian, J., et al. Inadequate lung development and bronchial hyperplasia in mice with a targeted deletion in the *Dutt1/Robo1* gene. *Proc. Natl. Acad. Sci. USA.* 98(26), 15062-15066 (2001).
262. Xie, J., et al. Mutations of the *PATCHED* gene in several types of sporadic extracutaneous tumors. *Cancer Res.* 57, 2369-2372 (1997).
263. Yamauchi, J., et al. Endothelin suppresses cell migration via the JNK signaling pathway in a manner dependent upon Src kinase, Rac1 and Cdc42. *FEBS Lett.* 527, 284-288 (2002).
264. Yang, W.Q., et al. Reovirus prolongs survival and reduces the frequency of spinal and leptomeningeal metastases from medulloblastoma. *Cancer Res.* 63, 3162-3172 (2003).
265. Yee, K.T., Simon, H.H., Tessier-Lavigne, M., O'Leary, D.D.M. Extension of long leading processes and neuronal migration in the mammalian brain directed by the chemoattractant netrin-1. *Neuron* 24, 607-622 (1999).

266. Yoshida, D., et al. Anti-invasive effect of an anti-matrix metalloproteinase agent in a murine brain slice model using the serial monitoring of green fluorescent protein-labeled glioma cells. *Neurosurgery*. 52(1), 187-197 (2003).
267. Yuan, F., et al. Time-dependent vascular regression and permeability changes in established human tumor xenografts induced by an anti-vascular endothelial growth factor/vascular permeability factor antibody. *Proc. Natl. Acad. Sci. U.S.A.* 93, 14765-14770 (1996).
268. Zhang, Y., et al. Intravenous RNA interference gene therapy targeting the human epidermal growth factor receptor prolongs survival in intracranial brain cancer. *Clin. Cancer Res.* 10(11), 3667-3677 (2004).
269. Zhang, Z., et al. Three biomarkers identified from serum proteomic analysis for the detection of early stage ovarian cancer. *Cancer Res.* 64, 5882-5890 (2004).
270. Zhuo, L., Hascall, V.C., Kimata, K. Inter- α -trypsin inhibitor, a covalent protein-glycosaminoglycan-protein complex. *J. Biol. Chem.* 279(37), 38079-38082 (2004).
271. Zurawel, R.H., Chiappa, S.A., Allen, C., Raffel, C. Sporadic medulloblastoma contain oncogenic beta-catenin mutations. *Cancer Res.* 58(5), 896-899 (1998).

Evidence for a Secreted Chemorepellent That Directs Glioma Cell Invasion

Tamra Werbowetski,¹ Rolf Bjerkvig,² Rolando F. Del Maestro¹

¹ Brain Tumour Research Centre, Montreal Neurological Institute, McGill University, Montreal, Quebec, Canada

² Department of Anatomy and Cell Biology, University of Bergen, Bergen, Norway

Received 8 August 2003; accepted 8 September 2003

ABSTRACT: Secreted chemotropic cues guide the migration of neuronal and glial cell precursors during neural development. It is not known if chemotropism contributes to directing the invasion of brain tissue by glioma cells. A model system has been developed that allows quantification of invasive behavior using gliomas spheroids embedded in collagen gels. Here we provide evidence that glioma spheroids secrete a chemorepellent factor(s) that directs cells away from the spheroid and into the collagen matrix. The relationship between total invasion, cell number, and implantation distance suggests that glioma cells respond to a gradient of the chemorepellent cue(s) that is well established at 48 h. C6 astrocytoma cells normally invade the collagen at an angle perpendicular to the spheroid edge. In contrast, an adjacent spheroid causes cells to turn away from their normal trajectory and slow their rate of invasion. As-

trocytoma cells are repelled by an adjacent glioma spheroid but rapidly infiltrate astrocyte aggregates, indicating that astrocytes do not express the repellent cue. Uniform concentrations of repellent factor(s) in spheroid conditioned medium overwhelm endogenous gradients and render glioma cells less able to exhibit this chemotropic response. Concentration gradients of spheroid conditioned medium in cell migration assays also demonstrate the chemorepellent cue(s)'s tropic effect. Our findings indicate that glioma spheroids produce a secreted diffusible cue(s) that promotes glioma cell invasion. Identification of this factor(s) may advance current therapies that aim to limit tumor cell invasion.

© 2004 Wiley Periodicals, Inc. *J Neurobiol* 60: 71–88, 2004

Keywords: chemotropism; glioblastoma; invasion; spheroid; video microscopy

INTRODUCTION

Cell migration occurs during development, wound healing, and also during tumor invasion and metastasis. Secreted proteins have been shown to function as chemotropic cues that guide neuronal and glial pre-

cursors in the developing central nervous system (reviewed by Tessier-Lavigne and Goodman, 1996; Dickson, 2002). Long-range secreted chemotropic guidance cues such as the netrins, semaphorins, and hepatocyte growth factor/scatter factor guide neuronal and glial cell migration (Ebens et al., 1996; Kennedy et al., 1994; Sugimoto et al., 2001; Yee et al., 1999). The slit family of extracellular proteins not only plays a role in axon guidance (Wang et al., 1999; Brose et al., 1999; Kidd et al., 1999; Li et al., 1999) and neuronal migration (Wu et al., 1999), but also leukocyte chemotaxis (Wu et al., 2001) and tumor angiogenesis (Wang et al., 2003). Other studies have used neural stem cells to track astrocytic tumors *in vivo*, providing evidence for positive chemotropism in experimental intracranial glioma models (Aboody et al., 2000). These investigations have prompted further

Correspondence to: R. Del Maestro (rolando.delmaestro@mcgill.ca).

Contract grant sponsor: Brain Tumor Foundation of Canada.

Contract grant sponsor: Montreal Neurological Institute.

Contract grant sponsor: Alex Pavanel Family.

This article includes Supplementary Material available via the Internet at <http://www.interscience.wiley.com/jpages/0022-3034/suppmat>

© 2004 Wiley Periodicals, Inc.

Published online 7 April 2004 in Wiley InterScience (www.interscience.wiley.com).

DOI 10.1002/neu.10335

analysis of potential mechanisms for glioma chemotropism in both two- and three- dimensional *in vitro* systems.

Malignant astrocytomas are the most common primary supratentorial cerebral neoplasms in adults (Chiocine and Silbergeld, 1997). Thought to arise from astrocytes or astrocytic precursors, their morphological heterogeneity often makes conclusions about their origin difficult (Lopes et al., 1995). The hallmark of malignant astrocytic tumors lies in their ability to rapidly invade the brain and disrupt the normal tissue architecture (Uhm et al., 1996). Despite surgical removal and other available treatment modalities, diffuse infiltrative growth of the remaining invasive cells leads to recurrence and death within 1–2 years of diagnosis (Berens et al., 1990). Studies are presently focused on identification of the diffusible molecules and cell signaling cascades that result in glial tumor cell migration and invasion.

Researchers have developed several methods of producing tumor cell aggregates or “spheroids” to study tumor invasion in three-dimensions. Sutherland et al. (1971) were the first to produce spheroids from a rotating cell suspension of Chinese hamster V79 lung cells in spinner culture. We have adapted this system for glioma cells and utilized this model for quantification of invasive behavior using glioma spheroids as well as human tumor explants in collagen gels (Tamaki et al., 1997; Bauman et al., 1999a,b). This three-dimensional spheroid implantation model has been used to elucidate the dynamics of the invasive paradigm in collagen type I gels (Vitrogen 100) (Corcoran and Del Maestro, 2003; Corcoran et al., 2003; Del Maestro et al., 2001). Using this system, it is possible to evaluate both long-range and contact-mediated tropic mechanisms using cocultures of glioma spheroids and/or normal brain aggregates in a three-dimensional environment.

Studies have suggested that glioma spheroids release a factor(s) that directs cells away from the spheroid and into the three-dimensional matrix (Tamaki et al., 1997; Del Maestro et al., 1997). A direct correlation exists between the development of larger spheroids exhibiting hypoxic and necrotic centers and invasive rate (Tamaki et al., 1997). These findings led to the hypothesis that a repellent factor(s) is secreted by glioma spheroids and that a gradient of this repellent cue(s) directs cell invasion away from the spheroid. Here, we test this hypothesis using two-spheroid cocultures, time-lapse video microscopy, and cell migration assays. Our findings provide evidence for an autocrine chemorepellent cue produced by glioma cells that promotes tumor cell invasion.

MATERIALS AND METHODS

Spheroid Culture and the Three-Dimensional Collagen Type I Implantation Model

C6 (murine astrocytoma) and U251 (human glioblastoma) cells were cultured in Dulbecco's modified Eagle's medium (DMEM) supplemented with 10% fetal bovine serum (FBS), 125 U/mL penicillin G, 125 μ g/mL streptomycin sulfate, and 2.2 μ g/mL amphotericin B (Fungizone). Cultures were maintained at 37°C in a humidified atmosphere of 5% CO₂. Upon reaching confluency, cells were trypsinized using 0.05% trypsin, 0.53 mM EDTA, and 3×10^6 cells/100 mL DMEM were seeded into spinner culture flasks and spun at 180 rotations per minute for 3–8 weeks depending on the desired spheroid size (Tamaki et al., 1997). All culture reagents were obtained from Gibco BRL (Invitrogen, Burlington, ON) unless otherwise stated. Both C6 and U251 cell lines were purchased from American Type Culture Collection (ATCC) (Rockville, MD).

A collagen solution was prepared consisting of 3.2 mg/mL collagen type I in 0.012 M HCl (Vitrogen 100) (COHESION, Palo Alto, CA) and 10-fold concentrated DMEM. The pH of the solution was adjusted by the addition of 0.1 M NaOH. From this solution, 500 μ L aliquots were added to 24-well culture dishes and spheroids of defined size were implanted into each well using a Pasteur pipette. After gelling at 37°C in a humidified atmosphere of 5% CO₂ for 30–60 min, the gel was overlaid with 500 μ L DMEM + 10% FBS or 250 μ L DMEM + 250 μ L of medium conditioned by C6 spheroids, U251 spheroids, or fetal human astrocytes. Cell invasion was assessed daily using an inverted phase contrast light microscope. Total invasion distance was calculated at the same time each day from the center of the spheroid to the population of invasive cells most distant from the spheroid. The original radius was subtracted from these values, and measurements were taken after 24 h (time lapse video microscopy) and 9 days (conditioned medium experiments).

Newborn Rat Astrocytes and U251 Aggregate Culture

Astrocytes were obtained from the cortex of newborn Sprague Dawley rat cortex and maintained as a mixed glial culture for 2–3 weeks in DMEM supplemented with 10% FBS. Enriched populations of astrocytes were obtained as described (Armstrong, 1998) and hanging-drop aggregates were prepared as described (Corcoran and Del Maestro, 2003; Corcoran et al., 2003; Kennedy et al., 1994). Briefly, confluent cultures of newborn astrocytes and U251 cells were washed in phosphate buffered saline (PBS), trypsinized (0.05% trypsin/0.53 mM EDTA), and resuspended in a small volume of media. Twenty microliter drops containing an equal amount of cells (25,000 cells/drop for U251 cells and 45,000 cells/drop for astrocytes) were suspended from the lids of 100 mm Petri dishes for 2–3 days. Cell aggregates were harvested using a sterilized spatula,

and placed on 2% agar/PBS base-coated 100 mm Petri dishes for 2–3 days and then individually implanted into three-dimensional type I collagen gels adjacent to C6 astrocytoma (newborn astrocytes) or U251 glioblastoma spinner culture spheroids (U251 drop aggregates).

Human Biopsy Spheroids and Human Fetal Astrocytes

The Haukeland Hospital ethics board in Bergen, Norway approved collection of human tumor tissue. Glioblastoma tumor fragments 1 cm or smaller in size were obtained at surgery. The specimens were collected from macroscopically viable tumor regions corresponding to areas of contrast enhancement on computerized tomography (CT) and magnetic resonance (MRI) scans. The specimens were immediately transferred to test tubes containing complete growth medium consisting of DMEM, supplemented with 10% heat-inactivated newborn calf serum, 2% L-glutamine, 100 IU/mL penicillin, and 100 IU/mL streptomycin.

Human biopsy spheroids were prepared as described (Bjerkvig et al., 1990). Briefly, glioblastoma tumor tissue was cut into 300–500 μm pieces and incubated in 80 cm^2 tissue culture flasks base-coated with 10 mL 0.75% agar (Difco, Detroit, MI) in complete growth medium. The biopsy spheroids were maintained at 37°C in a humidified atmosphere of 5% CO_2 , and medium was changed once a week. After 3–4 weeks in culture, spheroids with diameters between 200–400 μm were selected for implantation as described above. Confocal scanning laser microscopy using Cell Tracker dyes was carried out using a Bio-Rad MRC 1000 (Bio-Rad, Hertfordshire, UK) microscope.

Human fetal astrocytes were prepared from fetal CNS tissue as previously described (Ladiwala et al., 1998). Briefly, human fetal CNS tissue was obtained at 12–16 weeks gestation following Canadian Institutes of Health Research (CIHR) guidelines. The tissue was mechanically dissociated using a scalpel and then treated with 0.25% trypsin and 50 $\mu\text{g}/\text{mL}$ DNase for 45 min at 37°C. Dissociated tissue was passed through a 130 μm mesh, washed twice with PBS, and plated onto tissue culture flasks in MEM supplemented with 5% FCS. Populations of proliferating fetal astrocytes were obtained after three to four passages and used to prepare hanging drop aggregates for collagen implantation as described above.

Cell Tracker Dye Labeling and Spheroid Coculture Quantification

Stock solutions of 10 mM Cell Tracker Green CMFDA (5-chloromethylfluorescein diacetate) and Cell Tracker Orange CMTMR (5-(and 6)-((4-chloromethyl) benzoylamino) tetramethylrhodamine) (Molecular Probes, Eugene, OR) were prepared in DMSO, diluted to 25 μM in DMEM + 10% FBS, and used for cell labeling. Spheroids were collected from spinner culture and allowed to settle. Conditioned media were removed and replaced with 1 mL 25 μM Cell Tracker Green or Cell Tracker Orange solution. The spheroids were placed on a rocker in a 5% CO_2 incu-

bator for 20 min and then washed twice with DMEM + 10% serum. Fluorescently labeled spheroids were implanted both alone and adjacent to unlabeled C6 and U251 spheroids (400–600 μm) at various distances, and photographed 24 and 48 h postimplantation. Cocultures were imaged using a Retiga 1300 CCD digital camera (Q Imaging, Burnaby, BC) mounted on an Axiovert 200M microscope (Carl Zeiss, Toronto, ON) and Northern Eclipse 6.0 time-lapse software (Empix Imaging Inc., Mississauga, ON). Fluorescently labeled spheroids were divided into four quadrants with respect to the position of the adjacent spheroid (quadrant A). The total cell number and invasive distance per cell in each quadrant were calculated for both single spheroids and two-spheroid cocultures.

Time-Lapse Video Microscopy

Spheroids were cultured as described, and individual astrocytoma spheroid implants between 450 and 600 μm were prepared for time-lapse video microscopy. For two-spheroid cocultures, C6 astrocytoma spheroids were implanted approximately 300 μm apart. Cultures were maintained at 37°C and 5% CO_2 using a heating microscope stage including a 37-2 digital temperature control unit (Carl Zeiss). Invading cells were imaged for 24 h using a Retiga 1300 CCD digital camera mounted on an Axiovert 25 microscope and Northern Eclipse 5.0 time-lapse software. One still image was taken every 4 min compressing 20–24 h into approximately 90 s of video (Corcoran and Del Maestro, 2003). For each video, invasion rate and deviation from the expected invasive path (angle change from perpendicular) were calculated for individual C6 cells. Randomly selected cells were followed for single spheroid controls and compared with cell measurements obtained from spheroid cocultures.

Spheroid/Glass Bead Controls

Individual C6 spheroids approximately 450–600 μm in size were prepared and implanted as stated into three-dimensional type I collagen gels. Glass beads (Sigma-Aldrich Co. Canada Ltd., Oakville, ON) 425–600 μm in size were washed in 95% ethanol followed by DMEM + 10% FBS before implanting them adjacent to C6 spheroids. Six 24 h videos were recorded, and the angle of deviation measured.

Confocal Scanning Laser Microscopy

C6-C6, C6-astrocyte, and U251-human fetal astrocyte cocultures were labeled with Cell Tracker Green CMFDA and Cell Tracker Orange CMTMR, implanted into collagen, and analyzed using a LSM 510 confocal scanning laser microscope (Carl Zeiss) and a 10X objective. Cell Trackers were detected with argon 2 (488 nm) and helium-neon (543 nm) lasers for the green and orange fluorescent probes, respectively. Samples were optically sectioned from the surface to the spheroid center with 12 μm between each slice, and images 1024 \times 1024 pixels were collected. Human biopsy

spheroids were similarly labeled and analyzed using a Bio-Rad MRC 1000 confocal scanning laser microscope (Bio-Rad). Cocultures were optically sectioned from the surface to the spheroid centers with 16 μm between each slice.

Conditioned Medium Experiments

Conditioned medium was collected from C6 and U251 spinner cultures at various time points to assess the effect of spheroid size on the quantity of the hypothesized chemorepellent cue secreted. Conditioned medium was also collected from confluent monolayer cultures of human fetal astrocytes. C6 and U251 spheroids were implanted into collagen type I gels as described above and overlaid with 500 μL DMEM + 10% FBS or 250 μL conditioned medium 250 μL DMEM + 10% FBS. Medium was changed every 3 days, and measurements were taken daily for 9 days.

Transwell Migration Assays

Migration assays were performed using 24-well transwell units with 8 μm polycarbonated filters (Corning Costar, Cambridge, MA). The lower chamber was filled with 500 μL DMEM + 10% FBS or 500 μL conditioned medium from C6 spinner culture spheroids. C6 and U251 glioblastoma cells were harvested, fluorescently labeled using 25 μM Cell Tracker Green as described above, and 2.0×10^4 cells in 100 μL DMEM + 10% FBS or C6 spheroid conditioned medium were placed in the upper chamber. Cells were left for 20 h at 37°C, and unigrated cells on the upper side were removed with a cotton tip applicator. Cells remaining in the lower chamber were counted using an Axiovert 200M microscope at 10X magnification. Each value represents the average of four individual wells.

Statistical Analysis

All tests were performed using SPSS Graduate Pack 9.0 statistical software (SPSS Inc., Chicago, IL). Descriptive statistics, including mean and standard error of the mean along with one-way ANOVAs, independent sample *t*-tests, and Tukey's test for multiple comparisons, were utilized to determine significant differences between pairs for all experiments. *p* values less than 0.05 were considered significant.

RESULTS

Glioma Cells Invade Away from Spheroids Grown in Three-Dimensional Collagen Gels

When a glioma spheroid is cultured in a three-dimensional collagen gel, cells leave the spheroid and invade at an angle nearly perpendicular to the spheroid surface where the cell detaches (see Video 1) (Fig. 1).

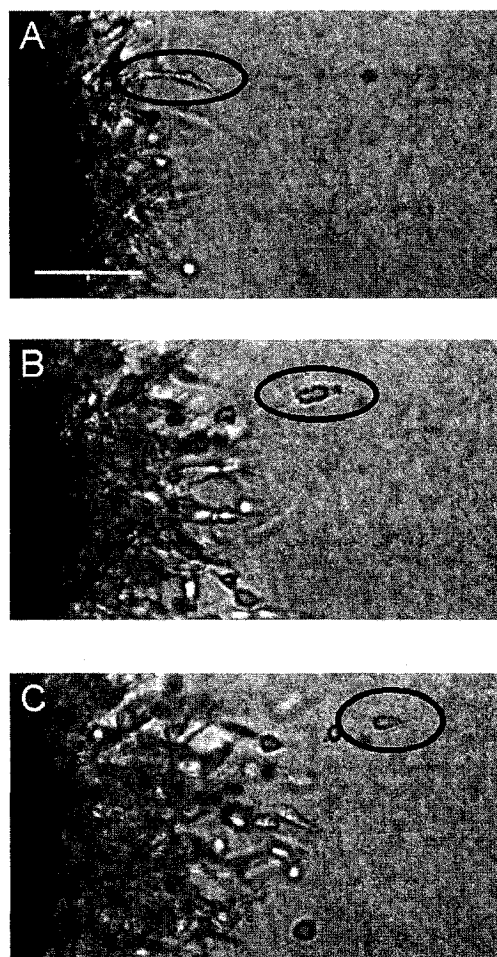


Figure 1 Single C6 astrocytoma spheroid implanted into three-dimensional type I collagen gel. (A–C) Images extracted from time-lapse video microscopy over 24 h. Objective: 20X. Scale bar = 100 μm .

Although this behavior has been well described (Tamaki et al., 1997; Del Maestro et al., 2001), the factors regulating movement of these cells as they invade the surrounding matrix are not well understood. Here, we provide evidence that a spheroid derived repellent cue directs the invasion of these cells away from the glioma cell mass.

Inhibition of Glioma Cell Invasion by the Spheroid-Derived Cue Is Distance- and Time- Dependent

We first tested the hypothesis that a spheroid derived repellent cue might direct the invasion of glioma cells in a distance- and time-dependent manner. Spheroids were cocultured and the distance and time over which this activity affected glioma cell invasion was monitored. Cocultures were labeled using different cell tracker fluorescent dyes before implanting them into

the collagen gel. This labeling allows for identification of individual cells from each spheroid during glioma cell invasion. Previous studies with fluorescent labels or cell markers have demonstrated an adverse effect on glioma cell migration in two-dimensions (Goldbrunner et al., 1997; Vince et al., 1997). Data obtained in our laboratory show that the cell trackers used in this study do not influence invasion distances in the three-dimensional implantation model (data not shown). C6 spheroids were dyed with Cell Tracker Green CMFDA and implanted at various distances apart from unlabeled spheroids C6 or U251 spheroids. After 24 and 48 h, cultures were photographed, and cell number and invasion distance quantified for each labeled spheroid quadrant [Fig. 2(A)]. Figure 2 presents the analysis of the distance traveled by individual cells in each quadrant after 24 h. There was no significant difference in the total invasion distance for all four quadrants in single spheroid controls ($n = 8$) [Fig. 2(B)]. When the cocultures were implanted a short distance apart (1–100 μm), the invasion into quadrant A was significantly less than values obtained for the remaining quadrants ($n = 5$) [Fig. 2(C)]. With distances greater than 100 μm , cell invasion into quadrant A, although lower, was not significantly different from the other quadrants for C6-C6 cocultures [Fig. 2(D)]. A similar pattern was observed when C6 spheroids were cocultured with U251 glioblastoma spheroids, although the effect was significant over greater distances of 100–400 μm [Fig. 2(E,F)]. These findings provide direct evidence for a distance dependent effect of a cue secreted by the glioma spheroid.

If the repellent cue only affected invasion but not detachment, equivalent numbers of cells would be seen in each quadrant despite decreases in total invasion. To test this hypothesis, total cell number in each quadrant was analyzed for various implantation distances. For single spheroid controls, there was no significant difference in cell number between the four quadrants ($n = 8$) [Fig. 3(B)]. Addition of the second C6 or U251 spheroid resulted in a decrease in the number of cells in the quadrant facing the adjacent spheroid [Fig. 3(C–F)]. Lower cell numbers were found in quadrant A when the C6 spheroids were cocultured 1–100 μm apart ($n = 5$) and 100–200 μm apart ($n = 7$) [Fig. 3(D)]. A significant decrease in the cell number in quadrant A was also seen for C6-U251 cocultures implanted 1–400 μm apart. In C6 cocultures implanted 100–200 μm apart, there was a non-significant increase in the number of cells in quadrant B and D; however, this was not the case for all remaining cocultures where the cell number in quadrant C was higher than B, D, or both [Fig. 3(C,E,F)]. The general failure of cells to egress into both adja-

cent B and D quadrants combined with the decrease in the cell number in quadrant A suggest that a chemorepellent(s) may also decrease cell detachment from the glioma spheroid.

To demonstrate that the effects described above are attributed to a secreted and not a contact-mediated chemorepellent cue(s), single C6 spheroids and C6-C6 cocultures were implanted further apart and analyzed at 48 h. For single C6 spheroids, there was no significant difference between total cell number and individual cell invasion distances in each quadrant [Fig. 4(A,D)]. The repulsive effect could be seen for C6-C6 cocultures at increased implantation distances with an average 59% decline in cell number compared to the remaining quadrants at 250–400 μm and 40% at 400–600 μm [Fig. 4(B,C)]. There was no significant difference between the number of cells in quadrants B–D [Fig. 4(B,C)]. Cell invasion into quadrant A was significantly less than invasion into the remaining quadrants at 48 h [Fig. 4(E,F)]. These findings demonstrate that a secreted cue(s) and not a contacted-mediated factor directs glioma cells away from the repellent source.

Glioma Cells Turn Away in Response to a Second Spheroid

The effect on glioma cell invasion could be produced by a kinetic effect of a cue that slows cell invasion, or through a tropic effect of a cue that directs cell invasion, or by a cue that exerts both kinetic and tropic effects on the invading cells. To investigate the mechanism of action of the secreted repellent cue on individual cells, glioma spheroids were implanted into collagen type I gels and imaged using time-lapse video microscopy. For single spheroid controls, C6 astrocytoma cells leave the spheroid at an angle nearly perpendicular to the spheroid surface where the cell detaches ($n = 46$; Fig. 1). In contrast, when two spheroids were cocultured adjacent to each other in the collagen gel, they changed their expected trajectory and turned away from the second spheroid when the cells reached the midpoint between the two spheroids ($n = 45$) (see Video 2) [Fig. 5(A–C)]. In addition to this evasive turning response, a subset of C6 astrocytoma cells appeared to stall and remained stationary between the two spheroids. These cells maintained a ruffled appearance throughout the time period of observation and did not extend invadopodia [Fig. 5(B,C)]. Quantification of the turning angle observed for individual cells invading toward an adjacent spheroid indicated a deviation from perpendicular invasion ($63.7 \pm 4.5^\circ$), which was significantly different from invading cells from single spheroids [Fig. 5(G)].

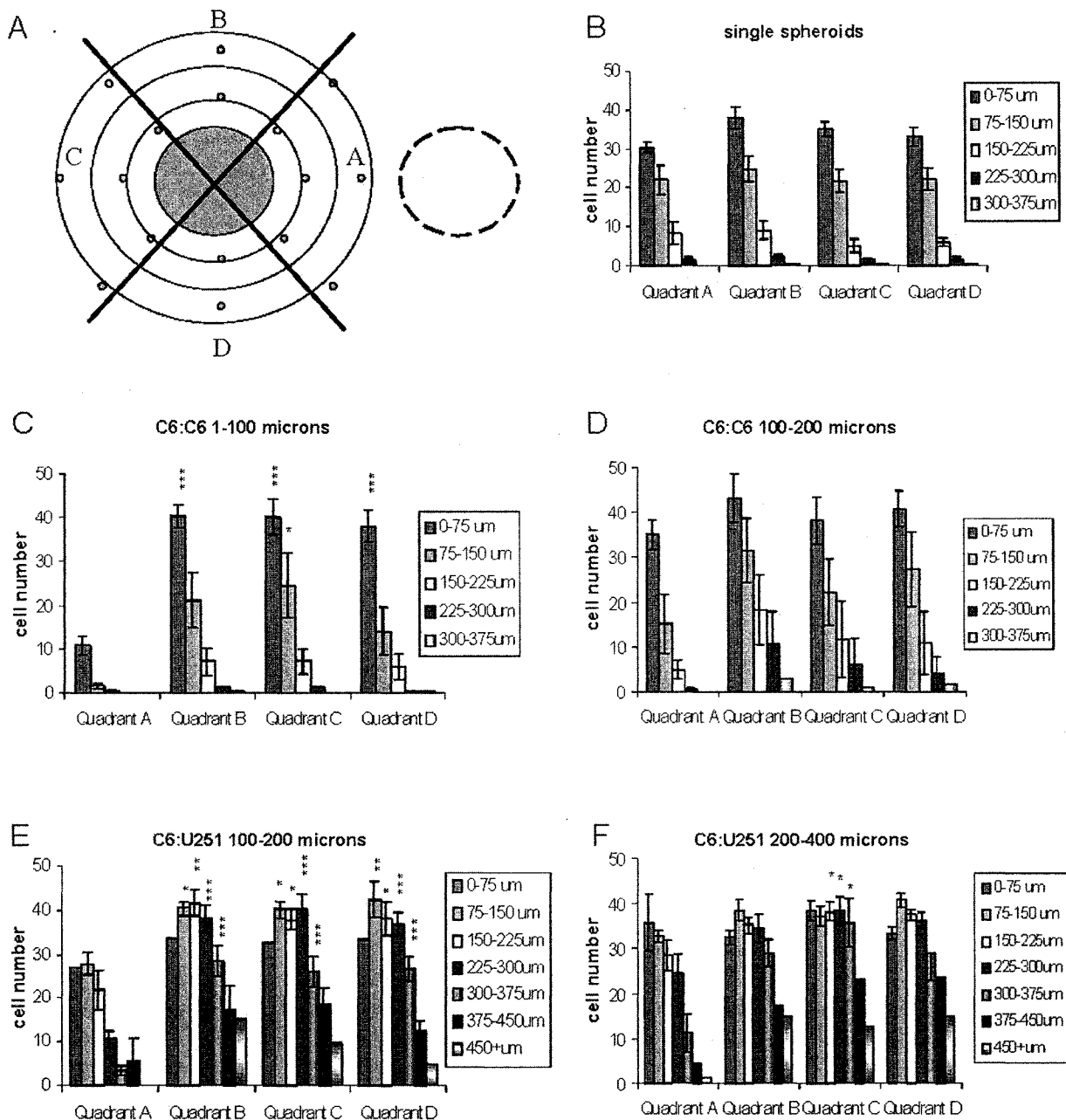


Figure 2 Quantification of glioma cell invasion after 24 h in culture by counting the number of cells invading certain invasion distances from the initial edge of the spheroid in each quadrant. Individual cells were counted 0–75, 75–150, 150–225, 225–300, 300–375, 375–450, and 450+ μm from the spheroid edge. (A) Spheroid quadrant quantification model. (B) Single C6 astrocytoma spheroids ($n = 5$). (C) C6 cocultures 1–100 μm apart ($n = 5$). (D) C6 cocultures 100–200 μm apart ($n = 6$). (E) C6-U251 cocultures 100–200 μm apart ($n = 5$). (F) C6-U251 cocultures 200–400 μm apart ($n = 4$). Asterisks indicate significant difference at $p < 0.05^*$, $p < 0.01^{**}$, and $p < 0.001^{***}$ when comparing quadrant A to other quadrants.

To determine if migratory turning is caused by a physical modification in the matrix rather than a chemical factor, we repeated the above experiments replacing one of the spheroids with a glass bead. Invading C6 cells from the spheroid followed a per-

pendicular trajectory as did cells from single spheroid controls ($n = 25$) (see Video 3) [Fig. 5(D–F)]. The mean angle of deviation from the perpendicular was $14.9 \pm 2.6^\circ$, not significantly different from data obtained for single spheroid controls ($16.7 \pm 0.8^\circ$)

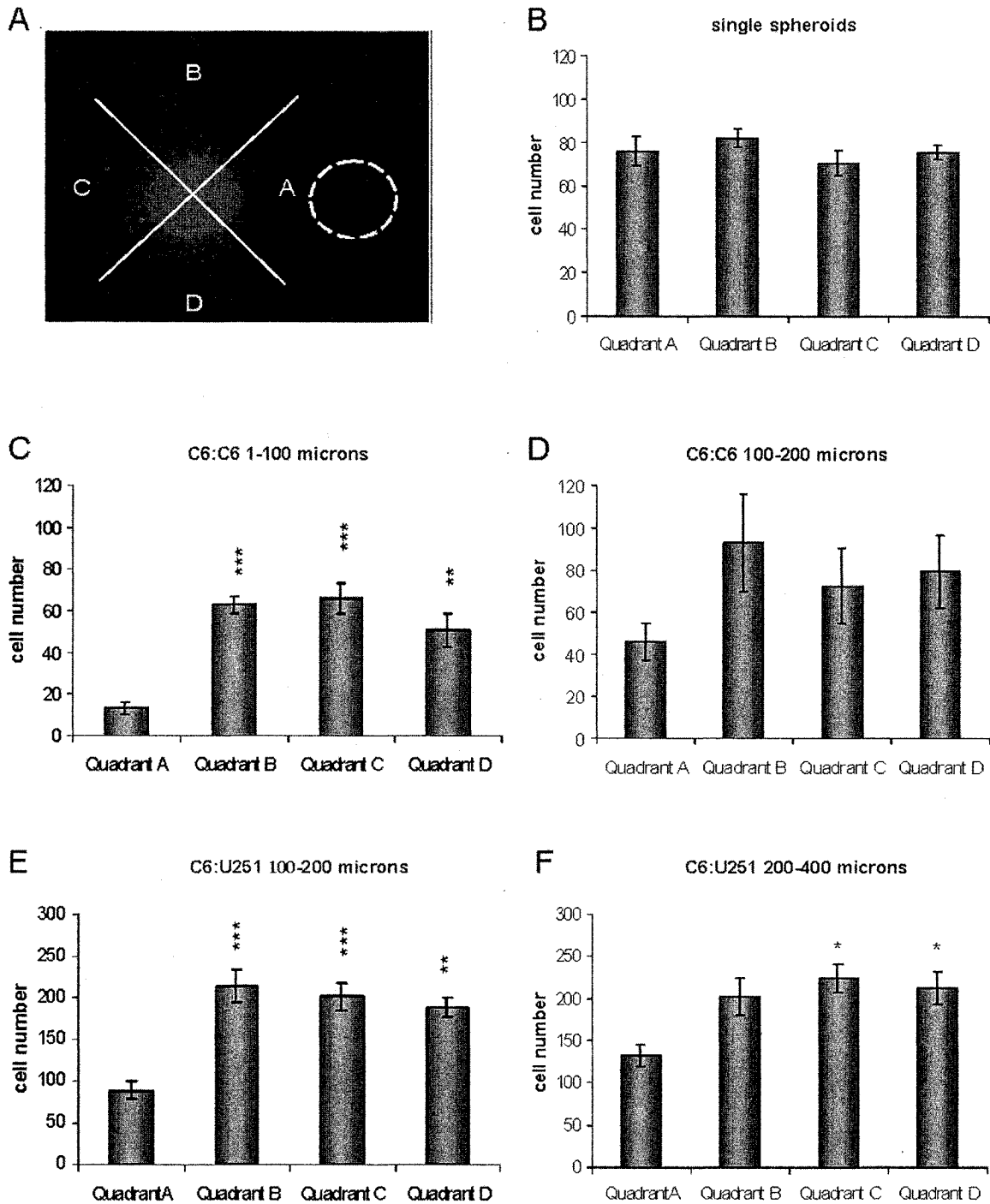


Figure 3 Quantification of glioma cell number after 24 in culture. The number of cells in each quadrant was counted for single spheroids and two-spheroid cultures at various implantation distances. (A) Spheroid quadrant quantification model. (B) Single C6 astrocytoma spheroids ($n = 5$). (C) C6 cocultures 1–100 μm apart ($n = 5$). (D) C6 cocultures 100–200 μm apart ($n = 7$). (E) C6-U251 cocultures 100–200 μm apart ($n = 5$). (F) C6-U251 cocultures 200–400 μm apart ($n = 4$). Asterisks indicate significant difference at $p < 0.05^*$, $p < 0.01^{**}$, and $p < 0.001^{***}$ when comparing quadrant A to the other quadrants.

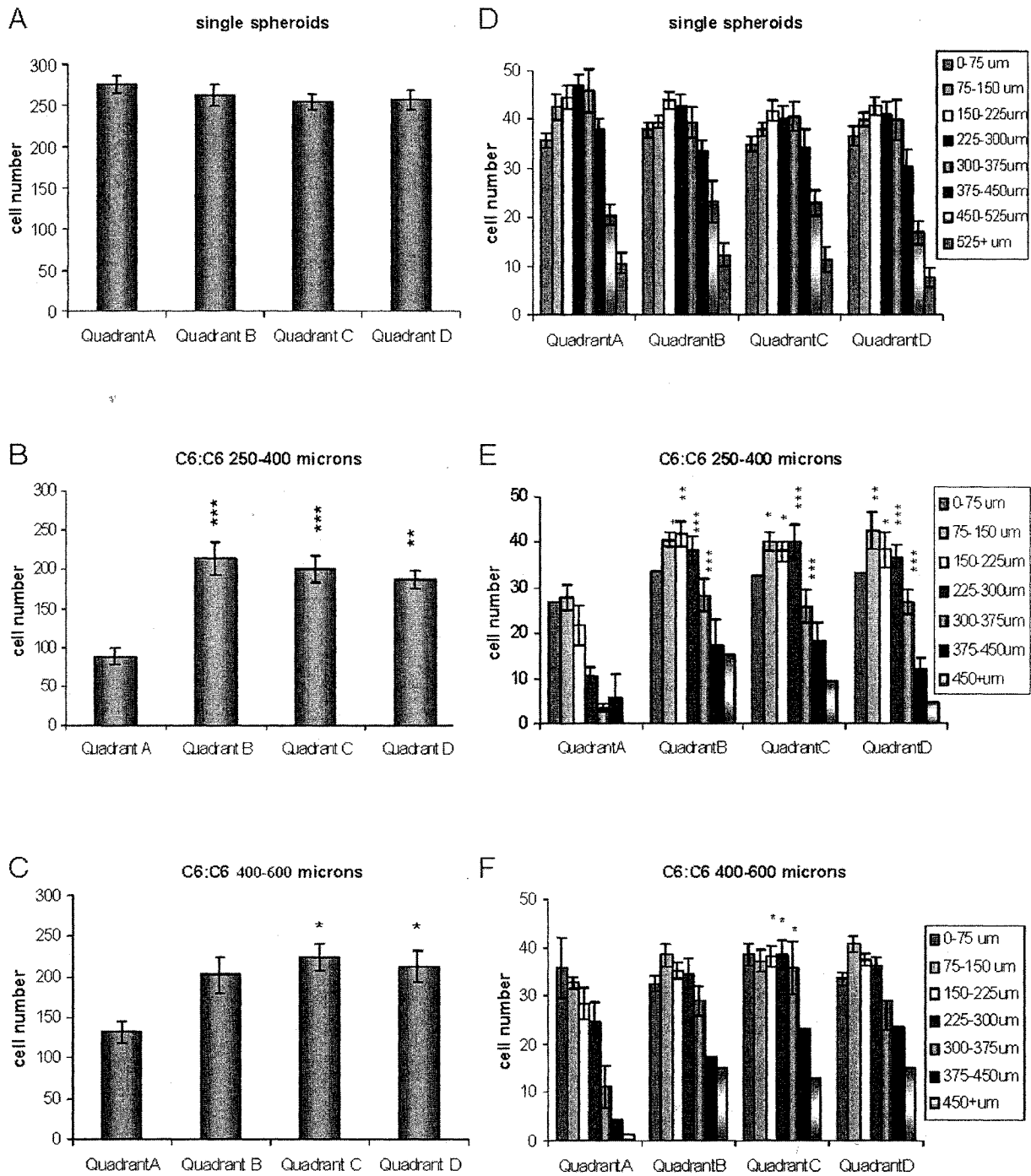


Figure 4 Quantification of glioma cell number and invasion distance after 48 h in culture. (A) Quadrant cell number for single C6 astrocytoma spheroids. (B) Cell number for C6 cocultures 250–400 μm apart ($n = 6$). (C) C6 cocultures 400–600 μm apart ($n = 4$). (D) Individual cell invasion distances for single C6 spheroids. (E) Invasion distances for C6 cocultures 250–400 μm apart ($n = 6$). (F) Invasion distances for C6 cocultures 400–600 μm apart ($n = 4$). Asterisks indicate significant difference at $p < 0.05^*$, $p < 0.01^{**}$, and $p < 0.001^{***}$ when comparing quadrant A to the other quadrants.

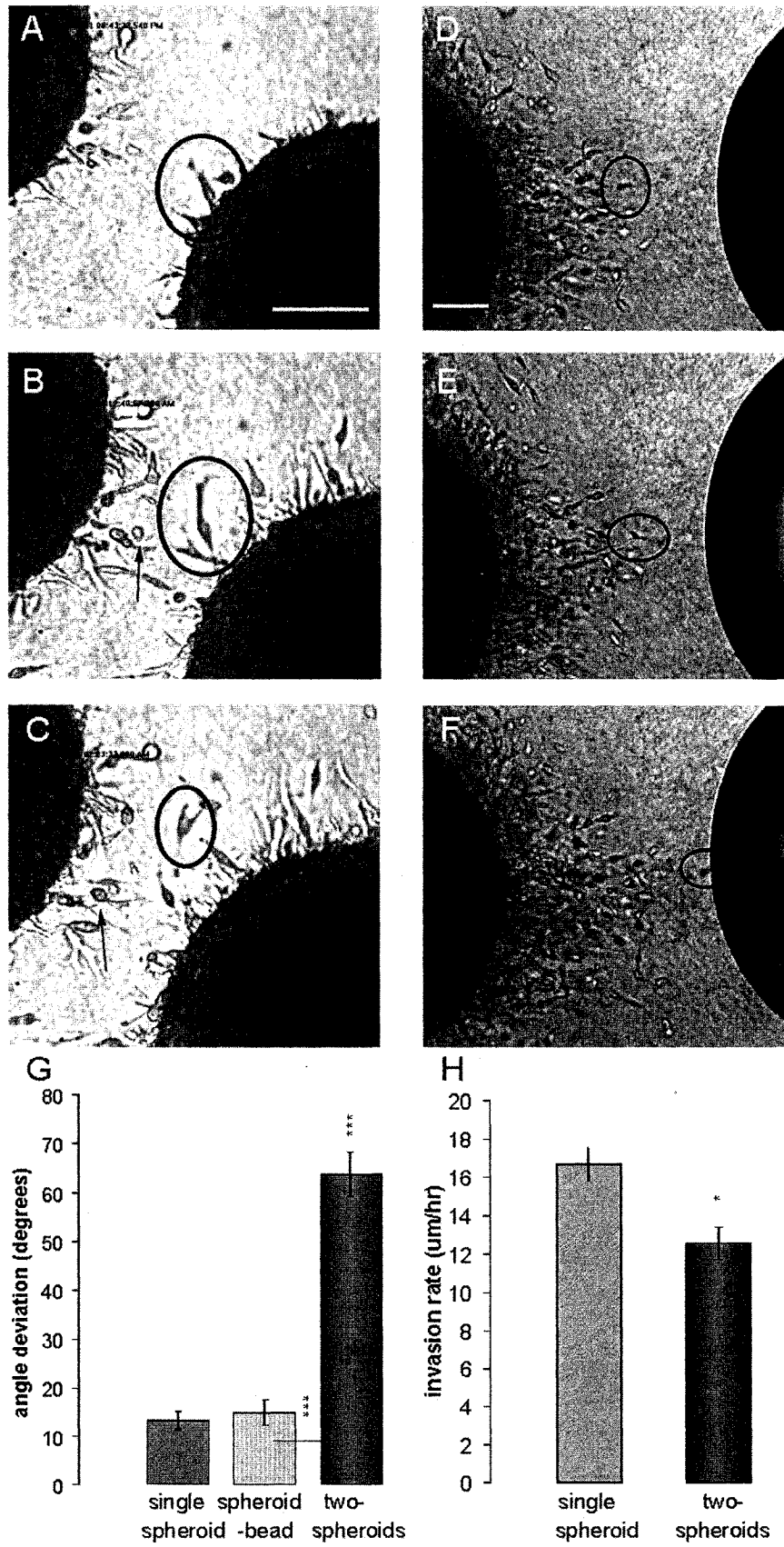


Figure 5 (see next page for legend)

[Fig. 5(G)]. Cells continued along this path until they contacted the glass bead. In some cases following contact, the cells appeared to repeatedly bounce off the bead surface (data not shown). After 48 h, the invading cells proceeded around the bead's surface (data not shown). At no point did the glioma cells change direction and migrate back toward the spheroid. To determine if the spheroid-derived cue exerts an influence on the rate of glioma cell invasion, cell invasion rate was measured in cultures containing either a single spheroid or two spheroid cocultures. Invading cells from two spheroid cocultures infiltrated the gel at rates significantly lower ($12.6 \pm 0.9 \mu\text{m/h}$) than cells derived from single spheroid controls ($16.7 \pm 0.8 \mu\text{m/h}$) ($p < 0.01$) [Fig. 5(H)].

These results provide evidence for the presence of a repellent cue secreted by glioma spheroids that directs invading glioma cells away from the spheroid mass. They indicate that the repellent cue secreted by the spheroid exerts a tropic effect by causing glioma cells to turn. The decrease in glioma cell invasion rate may be attributed to the presence of a more shallow gradient with increasing distances from the spheroids. These findings do not differentiate between the action of one or more cues.

Chemorepellent Cue Is Not Expressed by Astrocyte Aggregates

To investigate the specificity of expression of the glioma spheroid-derived repellent cue, we replaced one of the spheroids with an aggregate of primary newborn rat astrocytes. C6 spheroids implanted adjacent to newborn rat astrocyte aggregates invade in the direction of the astrocyte aggregates within the first 24–72 h (Fig. 6). The absence of an inhibitory effect on invasion was found for both cocultures in direct contact or implanted 100–200 μm apart ($n = 12$ and $n = 5$, respectively). Newborn astrocytes also appeared to invade into C6 spheroids within the first

72 h (Fig. 6). Extensive invasion is seen on the side proximal to the C6 spheroid; however, relatively little invasion is observed into the type I collagen gel around the rest of the astrocyte aggregates ($n = 12$). These findings provide evidence that astrocytes neither produce the repellent factor nor respond to it. To test the possibility that differences in the cell culture method might account for the differences observed, the hanging drop method that was used to produce the newborn rat astrocyte aggregates was also used to produce aggregates of U251 cells. U251 aggregates repelled invasion of U251 cells and C6 similar to the findings described above for U251 spheroids (not shown). These findings provide evidence that the spheroid-derived repellent cue is not ubiquitously expressed by all glial cell types, but might be a characteristic acquired by the glioma cells during their transformation process.

To determine the extent that a glioma-derived repellent cue might inhibit the infiltrative capacity of astrocytes and glioma cells, C6-C6 astrocytoma, human glioblastoma biopsy spheroids, C6-astrocyte, and U251-astrocyte aggregate cocultures were examined using scanning laser confocal microscopy to visualize the coculture centers. When two C6 spheroids were implanted 1–200 μm apart, despite spheroid growth, overlap was predominantly restricted to the fusion site with very few cells infiltrating the adjacent spheroid or invading around it after 72 h [Fig. 7(A–C)]. Similar results were obtained using C6-U251 and U251-U251 glioblastoma cocultures (data not shown). C6 spheroids implanted adjacent to fetal human astrocyte aggregates or aggregates of newborn rat astrocytes invaded the aggregates 24–72 hours after implantation [Fig. 7(D–I)]. Similar results were obtained for U251 drop aggregate-human fetal astrocyte aggregate cocultures after 48 h [Fig. 7(J)]. Confocal analysis indicated that individual astrocytes did not invade the spheroid after 72 h [Fig. 7(D–J)]. However, astrocytes invaded both over and around the adjacent spheroid

Figure 5 Two C6 spheroids and spheroid-bead cultures in a type I collagen gel. (A–C) Images extracted from time-lapse video microscopy over 24 h. Circles follow the path of an individual cell. When challenged with a second spheroid, cells deviate from their perpendicular trajectory. Arrows denote stationary ruffling cells in the microenvironment between spheroids. Objective: 20X. Scale bar = 100 μm . (D–F) Single C6 spheroid adjacent to a glass bead. Images extracted over 24 h. In both cases, invading cells move perpendicularly away from the spheroid. Objective: 10X. Scale bar = 150 μm . (G) Mean single cell angle deviation from a trajectory perpendicular to the spheroid surface for individual spheroids ($n = 45$), spheroid-glass bead cultures ($n = 25$), and two-spheroid cocultures ($n = 46$). Error bars: Standard error of the mean (SEM). Asterisks indicate a significant difference at $p < 0.001$. (H) Mean invasion rates for individual C6 cells when cultured alone ($n = 45$) and with another C6 astrocytoma spheroid ($n = 46$). Error bars: SEM. Asterisk indicates significant difference at $p < 0.05$.

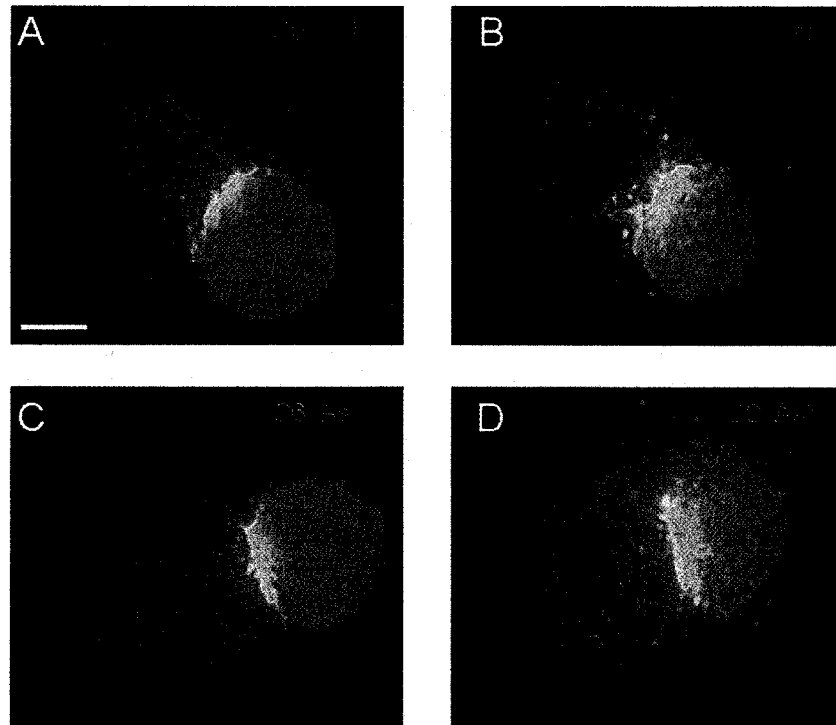


Figure 6 Cocultures of a C6 astrocytoma spheroid with an aggregate of astrocytes derived from newborn rat brain. Cells were labeled with Cell Tracker™ dyes. (A,B) Cocultures placed in contact with one another after 24 and 72 h, respectively. (C,D) Cocultures implanted 150 μm apart after 24 and 72 h, respectively. Objective: 10X. Scale bar = 250 μm .

(data not shown). Spheroids derived from different human biopsy cultures exhibited long invadopodia that extended throughout the collagen and around the adjacent spheroid [Fig. 7(K,L)]. Individual human tumor cells did not infiltrate the adjacent spheroid 48 h after implantation. These results provide further evidence for a glioma-derived repellent cue, as inhibition was restricted to glioma spheroid cocultures and was not found in glioma spheroid-astrocyte aggregate cocultures implanted together or a short distance apart.

Conditioned Medium from C6 and U251 Spheroid Culture Significantly Inhibits Glioma Invasion

If indeed glioma cells secrete and respond to a repellent factor that exerts a detachment or inhibitory effect as well as a tropic influence, then addition of this factor throughout the matrix should have a net inhibitory effect on invasion from the spheroid. We then determined if medium conditioned by C6 or U251 astrocytoma cells could influence glioma cell invasion. Medium was collected from C6 astrocytoma and U251 glioblastoma spinner cultures containing differ-

ent sized spheroids and applied to spheroids implanted in three-dimensional collagen gels (Fig. 8). For C6 astrocytoma spheroids, both U251 and C6 conditioned media had a significant inhibitory effect on invasion ($n = 4$) [Fig. 8(A)]. C6 day 33 media had the most significant effect, inhibiting invasion by 44% compared with DMEM + 10% FBS controls [Fig. 8(A)]. Similar results were obtained for U251 spheroids, as both U251 and C6 conditioned media had a significant inhibitory effect on invasion [Fig. 8(B)]. U251 day 27 and C6 day 30 conditioned media had the most significant effect on invasion at 63% and 44% inhibition, respectively ($n = 4$) [Fig. 8(B)]. For both U251 and C6 spheroids, conditioned medium collected from larger spheroids, as indicated by higher day number, generally had a more significant effect on invasion, suggesting that the quantity of the chemorepellent cue(s) secreted is related to the size of the spheroid [Fig. 8(A,B)]. Medium collected from confluent monolayer fetal astrocyte cultures had no significant effect on C6 and U251 spheroid invasion [Fig. 8(C,D)]. These results provide further evidence that glioma spheroids and not astrocytes secrete a repellent cue(s) that affects glioma cell invasion, pos-

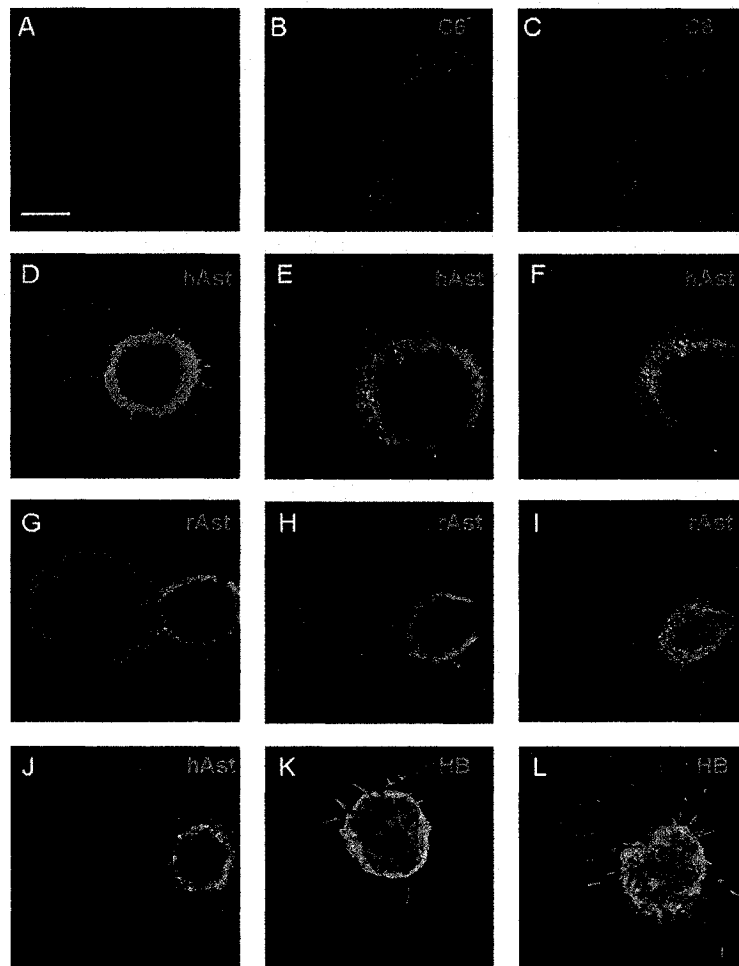


Figure 7 Confocal scanning laser microscopy images of C6 astrocytoma, C6-astrocyte, and human biopsy spheroid cocultures fluorescently labeled with Cell Trackers™ after 24–72 h. (A–C) Split images (A–B) and overlay (C) through the center of two C6 spheroids demonstrating the lack of invasion into and migration around the adjacent spheroid after 72 h. (D–I) C6 astrocytoma spheroid cocultured with fetal human (D–F) and newborn rat (G–I) astrocyte aggregates at 24, 48, and 72 h. After 48–72 h, extensive invasion of C6 glioma cells into the fetal human and newborn rat astrocyte aggregate is observed. (G–I) Coculture of C6 astrocytoma spheroid and newborn rat astrocyte aggregate after 24, 48, and 72 h, respectively. (J) Coculture of U251 glioblastoma drop aggregate spheroid with fetal human astrocyte aggregate at 48 h. Invasion into the astrocyte aggregate is similar to results obtained using C6 rat astrocytoma spheroids. (K,L) Two human biopsy spheroids implanted in contact with one another and 150 μm apart at 24 and 48 h, respectively, demonstrating no invasion into adjacent spheroids but migration of some cells around the spheroid mass. Objective: 10X. Scale bar = 250 μm .

sibly by inhibiting cell motility in addition to directing cells away from a gradient of the repellent cue(s).

Glioma Cells Are Chemotactically Repelled by a Gradient of C6 Spheroid Conditioned Medium in Cell Migration Assays

A chemorepellent cue(s) and migration inhibitor are two different phenomena. To determine the chemo-

tactic and chemokinetic properties, transwell migration assays were performed on U251 and C6 cells using medium conditioned by C6 spinner culture spheroids. Because the transwell migration assay does not involve cell detachment from a spheroid in a three-dimensional model, the repellent cue(s)'s ability to directly affect glioma cell migration can be assessed. The number of C6 and U251 cells was higher when C6 conditioned medium was placed in the upper chamber and lower when the medium was placed in

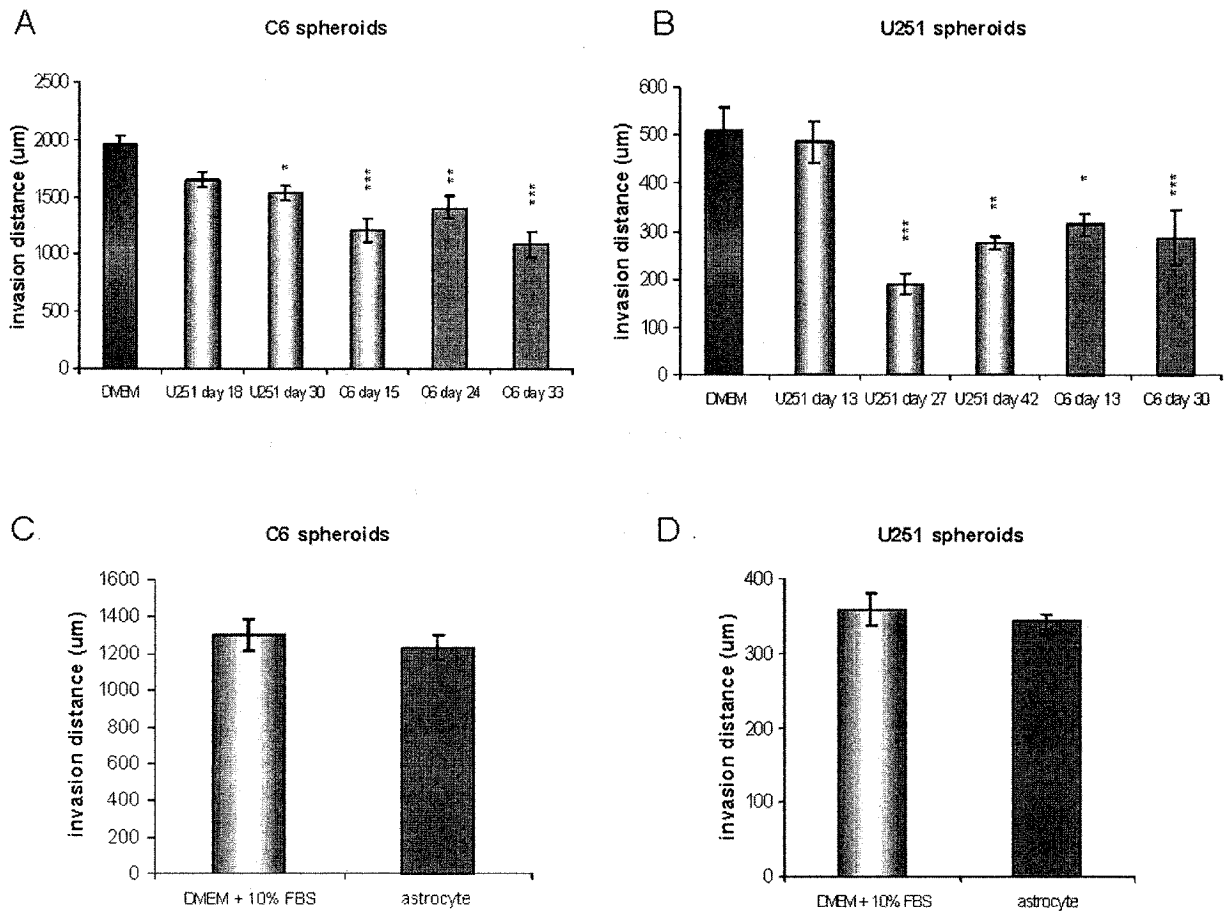


Figure 8 The effect of C6, U251, and fetal astrocyte conditioned medium on the invasion of C6 and U251 glioma spheroids. (A) C6 spheroid invasion after 9 days application of C6 and U251 conditioned medium from various-sized spheroids ($n = 4$). (B) U251 spheroid invasion after 9 days application of C6 and U251 conditioned medium from various-sized spheroids ($n = 4$). (C) C6 spheroid invasion after 9 days application of conditioned medium from confluent monolayer fetal astrocyte cultures ($n = 5$ for DMEM control and $n = 7$ for astrocyte medium). (D) U251 spheroid invasion after 9 days application of conditioned medium from confluent monolayer fetal astrocyte cultures ($n = 8$). Error bars: standard error of the mean. Asterisks indicate a significant difference at $p < 0.05^*$, $p < 0.01^{**}$, and $p < 0.001^{***}$.

the lower chamber (Table 1). Interestingly, the number of C6 and U251 cells was even lower when conditioned medium was placed in both chambers to eliminate the gradient (Table 1). These results suggest that C6 and U251 astrocytoma cells are chemotactically repelled by a secreted factor(s) from spheroid conditioned medium. However, the observation that a uniform concentration of the repellent cue(s) decreases migration indicates that it also exerts a kinetic effect on glioma cell motility.

DISCUSSION

This study provides evidence for a tumor-derived chemorepellent cue(s) that directs glioma cell inva-

sion. Previous investigations have focused on chemotropism in glial cell and neuronal precursors (Armstrong et al., 1990; Sugimoto et al., 2001; Kennedy et al., 1994; Jarjour et al., 2003). For example, the directional migration of glial precursors along the optic nerve is guided by the chemorepellent factors netrin-1 and semaphorin 3a (Sugimoto et al., 2001). These molecules, known for their directional role in neuronal and axonal migration, originate near the optic chiasm and guide glial precursors along the optic nerve (Sugimoto et al., 2001). Even polypeptide growth factors such as PDGF and extracellular matrix molecules have been shown to elicit a chemoattractive response in glial precursors and type 1 astrocytes, respectively (Armstrong et al., 1990).

Table 1 Transwell Chamber Analysis of C6 (A) and U251 (B) Cell Migration in Response to Medium Conditioned by C6 Astrocytoma Spinner Culture Spheroids

Lower Chamber	Upper Chamber	
	0%	100%
0%	182	187
100%	89***	0***

Lower Chamber	Upper Chamber	
	0%	100%
0%	75	106
100%	3*	1*

Conditioned medium was added to either the upper or lower chamber or both. Note that migration is maximal when C6 conditioned medium is added to the upper chamber and is reduced when medium is added to the lower chamber or both, indicating that C6 and U251 cells are inhibited by a secreted cue from the conditioned medium in a chemotropic and chemokinetic manner. The data represent the mean of four replicates; $p < 0.05$ *, $p < 0.001$ ***

Glioma Chemotropism and Growth Factors

Studies have examined growth and motility factors such as EGF, bFGF, autocrine motility factor, and PDGFbb that act predominantly via chemoattractant mechanisms (Chicoine and Silbergeld, 1995; Liotta et al., 1986; Engebraaten et al., 1993; Lund-Johansen et al., 1990). Two-dimensional models such as the Boyden chamber chemotaxis and modified radial dish assays have often been used to evaluate tropic effects in glioma cells (Chicoine and Silbergeld, 1995; Liotta et al., 1986; von Bulow et al., 2001). Checkerboard migration assays have demonstrated potent induction of both melanoma and glioblastoma cell migration towards endothelial cells (von Bulow et al., 2001). However, endothelium-derived chemotactic molecules have yet to be identified (von Bulow et al., 2001). Although there is some discrepancy in the literature with regards to the effect of growth factors on glioma cell motility, the differences may be attributed to the variety of model systems employed in different studies (Chicoine and Silbergeld, 1997). In contrast to previous investigations, this study provides evidence for glioma-derived chemorepellent cue in a three-dimensional collagen type I coculture model. Although the results with the chemotaxis migration assay are also indicative of a secreted repellent(s) in conditioned medium, our spheroid model allows quantification of cell-cell and cell-matrix interactions in a three-dimensional collagen type I environment where cells undergo alterations in morphology and degradative enzyme release (Tamaki et al., 1997; Un-

emori and Werb, 1986). The use of time-lapse video microscopy and still photographs to quantify cell number and total invasion in all quadrants as well as direction changes allows for evaluation of chemotropic mechanisms at various implantation distances and examination of the effect over time.

Evidence for a Glioma Chemorepellent Cue

Using the C6 rat astrocytoma spheroid implantation model, our laboratory first proposed the glioma repellent factor gradient hypothesis based on two observations (Tamaki et al., 1997). Larger spheroids, having well-established areas of hypoxia and necrosis, had higher invasive rates 1–5 days postimplantation, and after 10–13 days, invasion plateaus when cells reached approximately 2000–2500 μm from the spheroid source. We suggested that physically stressful conditions, such as decreased tissue pH, oxygen, and metabolic substrate(s) concentrations, may lead to generation of a chemotropic repellent factor(s) concentration gradient that results in increased cell invasion from the spheroid and cell invasion arrest when the gradient is no longer present. Larger spheroids, exhibiting extensive stressful microregions, may secrete more of the factor(s), and consequently further accelerate invasion. A number of scatter growth promoting factors and guidance cues have been tested for their role in the spheroid implantation model; however, none appear to exhibit the proposed repellent factor(s) properties (unpublished data). Platelet derived growth factor (PDGF) AA, BB, basic fibroblast growth factor (bFGF) at concentrations between 10 and 200 ng/mL, as well as conditioned medium from 293T overexpressing secreted slit-2 and netrin-1, have been added to medium and applied to spheroids implanted in collagen gels. Analysis of glioma spheroids cocultured with 293T cell aggregates overexpressing slit-2 and netrin-1 has also been conducted. All experiments have resulted in either an increase in glioma invasion or no effect. Studies are currently underway to assess the role of slit-2 and netrin-1 as potential repellents in other brain tumors such as medulloblastoma. Although the data presented in this study support the chemorepellent cue(s) hypothesis, the relationship of the secretion of the factor(s) to the presence of stressful microregions is unclear. Cocultures consisting of U251 or human biopsy spheroids both exhibit invasion inhibition similar to C6 astrocytoma cocultures, and these spheroids do not have established areas of necrosis and hypoxia (Corcoran et al., 2003). The apparent higher concentrations of chemorepellent cue(s) from larger spheroids may be related to total cell number.

In this study, a two-spheroid coculture system was employed using the three-dimensional spheroid implantation model. Based on the repellent factor hypothesis, invading glioma cells should be repelled by an endogenous gradient of a secreted repellent cue derived from the adjacent spheroid. Monitoring cell number and invasion in glioma cocultures confirmed this hypothesis. Fluorescently labeled glioma cells facing the adjacent spheroid invade the gel and infiltrate the other spheroid less when implantation distances are below 200–400 μm . At implantation distances exceeding 400 μm , the chemorepellent cue(s) does not have a statistically significant effect on cell number and invasion at 24 h. The effect over this distance is consistent with studies of chemotropic molecules in other systems. Localized sources of floor-plate-derived chemoattractant reoriented dorsal spinal cord axons over a mean distance of 243 μm after 40 h in culture (Placzek et al., 1990). When the cocultures are examined at 48 h, there is a significant effect between 250 and 600 μm . These results suggest that the gradient is well established at 48 h and the chemorepellent cue(s) is secreted. There is a direct correlation between tumor cell number/invasion and implantation distance on the side facing an opposing spheroid. The effect on cell number may reflect a chemorepellent cue(s)'s negative influence on proliferation or the ability to detach from the spheroid and invade the gel. Video microscopy studies showed cell division between glioma cocultures, and therefore confirmed that the chemorepellent cue(s) does not influence cell proliferation (data not shown). Data obtained from quadrant cell number analysis suggest a detachment problem. Invading glioma cells in quadrant A did not move into the adjacent B and D quadrants, as cell numbers here were not significantly different from those in the distal C quadrant. The transwell migration assay does not directly assess cell detachment, and can be used to differentiate between chemorepellent cue(s) and glioma cell migration inhibitors. Because both a gradient and a uniform concentration of the repellent cue(s) significantly inhibited glioma cell migration, it seems that the factor exerts both a tropic and a kinetic influence. The inhibitory effects seen with a uniform concentration of glioma conditioned medium on C6 and U251 spheroids also supports a role for the repellent cue(s) in inhibiting glioma cell migration.

Lumsden and Davies (1983, 1986) conducted similar quadrant experiments to demonstrate that secreted chemoattractants guide earliest sensory nerve fibers to their peripheral targets. Cocultures of trigeminal ganglion and peripheral maxillary epithelial target tissue explants were used to demonstrate the presence of a chemotactic molecule(s) guiding trigeminal sensory

neurons to their targets (Lumsden and Davies, 1983, 1986). Secreted chemotropic cues such as the netrin and semaphorin families were later identified and shown to play a major role in the neuronal guidance mechanisms seen in previous studies (reviewed by Tessier-Lavigne and Goodman, 1996).

To further investigate the specific mechanism of action of the chemorepellent cue(s), we imaged C6 rat astrocytoma cocultures using time-lapse video microscopy. Our results are consistent with the concept of a secreted repellent factor because glioma cells changed their expected invasive path in the presence of an adjacent spheroid. A significant deviation from the expected perpendicular angle was found, and this was not related to the presence of a physical object in the glioma cells' path. The decrease in cell velocity seen in coculture experiments may be related to a change in cell trajectory that renders cells less able to commit their metabolic and cytoskeletal machinery to invade the matrix at rates similar to controls. This effect may be secondary to an alteration in the concentration of the chemorepellent gradient in the microenvironment between the two spheroids. Highly concentrated chemorepellent gradients may also explain why some cells do not invade following detachment when they are in the immediate microenvironment between two adjacent spheroids. Conditioned medium placed in both chambers of the transwell migration assay prevented glioma cell migration in a similar manner.

Astrocyte Invasion and Migration

The direct relationship between cell number/invasion and implantation distance does not hold true for spheroid-astrocyte aggregate cocultures. The results obtained using fetal human and newborn rat astrocytes aggregates are consistent with data obtained for confrontation cultures of spheroid/fetal rat brain aggregates on agar (Bjerkvig et al., 1986). Invading glioma cells are not hindered by the presence of the newborn rat astrocyte aggregates and are able to infiltrate the normal fetal rat brain as demonstrated by scanning and confocal laser microscopy (Bjerkvig et al., 1986; Steinsvag, 1985; Nygaard et al., 1995; Enggebraaten et al., 1990).

In the light microscopy images, newborn rat astrocytes appear to invade adjacent C6 spheroids. This was clearly seen in both touching cocultures, and cultures implanted 100–200 μm apart. Confocal microscopy studies revealed that astrocytes are moving over the tumor surface and around the spheroid. These results suggest either the presence of a glioma spheroid secreted or contact-mediated chemoattractant molecule or perhaps a more permissive substrate pro-

vided by the spheroid surface. Similar studies using fetal astrocytes demonstrate variable results depending on the substrate employed. Bernstein et al. (1991) showed that C6 glioma cells, but not fetal astrocytes, rapidly invade artificial basement membrane substrates. However, when experiments were conducted with hydrated collagen I wafers, both cell types migrated through the entire thickness of the substrate (Goldberg et al., 1992). The invasion displayed in our coculture assays may reflect not only the substrate difference but also the three-dimensional nature of the model. The use of confocal microscopy is important to distinguish between cells invading a glioma tumor spheroid and cells migrating along its surface.

Although confrontation cultures are commonly used to study glioma invasion, most models utilize aggregates on plastic or agar, and thus do not reconstruct the brain's more complex three-dimensional architecture. A drawback to standard confrontation cocultures is the use of fetal/newborn rat brain instead of adult brain aggregates. Glioblastomas are primarily adult supratentorial cerebral neoplasms, and so adult brain aggregates would most accurately represent brain tumor invasion in three-dimensional models (Chicoine and Silbergeld, 1997). Studies with human glioma explant cocultures and multiple patient white matter tissue samples may further substantiate the chemotropic responses demonstrated here.

Glioma-Derived Chemorepellent Cue(s)

The inhibition of glioma invasion by C6 and U251 conditioned medium supports the chemorepellent factor(s) hypothesis. A uniform concentration of factor(s) may have less discernible effect on tumor invasion if the glioma cells respond to an established chemorepellent cue concentration gradient. The data obtained for both quadrant quantification and angle deviation suggest that the glioma cells are responsive to localized higher concentrations of the factor(s). However, a uniform concentration may overwhelm existing endogenous gradients, thus eliminating signaling mechanisms that deter cells away from the spheroid mass. Less able to exhibit a chemotropic response, the glioma cells decrease their overall invasive rate while others may arrest cell movement or exhibit decreased cell detachment. Previous studies using conditioned medium containing secreted chemoattractant molecules also provide evidence for uniform concentration effects (Placzek et al., 1990). When conditioned medium was collected from E13 floor plate and applied to E11 dorsal spinal cord explants, there was extensive axon outgrowth from the explant edges. This floor-plate-derived chemoattractant, later identified as netrin-1, appeared to ex-

hibit both directional and possibly outgrowth-promoting properties, as commissural axons responded to both uniform concentrations and gradients of the floor plate factor (Placzek et al., 1990; Kennedy et al., 1994).

Identification of chemotropic secretion products using the spheroid implantation model may shed light on the issue of glial cell movement in the central nervous system. The highly infiltrative nature of some human gliomas such as glioblastoma multiforme and gliomatosis cerebri may be attributed to yet unidentified chemorepellent cues that are secreted by the main tumor mass. These chemorepellent cues may help tumor cells detach and guide them from their source into normal brain architecture (DeAngelis et al., 2002). Similar chemorepellent cues may also play a role in normal brain growth. Knowledge of chemorepellent factors may enable introduction of novel therapies that force cells to change their invasive path, stop, or even return to the original resection site thus diminishing the risk of recurrence. Alternatively, chemoattractants may stimulate cells to invade towards and potentially infiltrate gliomas, thereby creating the potential to treat brain tumors from the inside-out using specific drug biodelivery approaches. Although one must proceed with caution when extrapolating *in vitro* results to the clinical situation, a thorough understanding of chemotropic cues and their influence on glioma invasion is essential, as more advanced therapies may target a combination of chemotropic factors and their downstream effectors.

CONCLUSIONS

Our study supports the chemorepellent cue(s) hypothesis. We have provided evidence for a secreted repellent factor that not only exerts a tropic influence by directing glioma cell invasion in the direction of less inhibition but also a kinetic influence by decreasing glioma cell motility. The combined effects on tumor cell invasion make the chemorepellent cue(s) an attractive target for future studies.

We wish to thank Andrew Jarjour and Cecilia Flores (Montreal Neurological Institute) for supplying the newborn astrocyte cultures, Dr. Jack Antel for supplying the fetal human astrocytes, and Per-Oyvind Enger (Haukeland Hospital, University of Bergen) for human biopsy spheroid preparation. We would also like to thank Dr. Nathalie Agar and Alexandre Angers-Loustau for technical assistance and manuscript advice as well as Carmen Sabau (Montreal Neurological Institute, Montreal, Quebec) and Audhild Drange (Haukeland Hospital, Bergen Norway) for technical assistance. R.F.D.M. is a Killam Scholar, and T.W. is a

recipient of the Natural Sciences and Engineering Research Council of Canada (NSERC) PGS-A Scholarship and a Canadian Institutes of Health Research (CIHR) Doctoral Research Award.

REFERENCES

- Aboudy KS, Brown A, Rainov NG, Bower KA, Liu S, Yang W, Small JE, Herrlinger U, Ourednik V, Black PM, et al. 2000. Neural stem cells display extensive tropism for pathology in adult brain: evidence for intracranial gliomas. *Proc Natl Acad Sci USA* 97:12846–12851.
- Armstrong RC. 1998. Isolation and Characterization of Immature Oligodendrocyte Lineage Cells. *Methods: A Companion to Methods in Enzymology* 16:282–292.
- Armstrong RC, Harvath L, Dubois-Dalcq ME. 1990. Type 1 astrocytes and oligodendrocyte-type 2 astrocyte glial progenitors migrate toward distinct molecules. *J Neurosci Res* 27:400–407.
- Bauman GS, Fisher BJ, McDonald W, Amberger VR, Moore E, Del Maestro RF. 1999a. Effects of a radiation on a three-dimensional model of malignant glioma invasion. *Int J Dev Neurosci* 17:643–651.
- Bauman GS, MacDonald W, Moore E, Ramsey DA, Fisher BJ, Amberger VR, Del Maestro RM. 1999b. Effect of radiation on a model of malignant glioma invasion. *J Neurooncol* 44:223–231.
- Berens ME, Rutka JT, Rosenblum ML. 1990. Brain tumor epidemiology, growth and invasion. *Neurosurg Clin N Am* 1:1–18.
- Bernstein JJ, Laws ER, Levine KV, Wood LR, Tadvalkar G, Goldberg W. 1991. C6 glioma-astrocytoma cell and fetal astrocyte migration into artificial basement membrane: a permissive substrate for neural tumors not fetal astrocytes. *Neurosurgery* 28:652–658.
- Bjerkvig R, Laerum OD, Mella O. 1986. Glioma cell interactions with fetal rat brain aggregates in vitro and with brain tissue in vivo. *Cancer Res* 46:4071–4079.
- Bjerkvig R, Tonnesen A, Laerum OD, Backlund E. 1990. Multicellular tumor spheroids from human glioma maintained in organ culture. *J Neurosurg* 72:463–475.
- Brose K, Bland KS, Wang KH, Arnott D, Henzel W, Goodman CS, Tessier-Lavigne M, Kidd T. 1999. Slit proteins bind Robo receptors and have an evolutionary conserved role in repulsive axon guidance. *Cell* 96:795–806.
- Chicoine MR, Silbergeld DL. 1995. Invading C6 glioma cell maintaining tumorigenicity. *J Neurosurg* 85:665–671.
- Chicoine MR, Silbergeld DL. 1997. Mitogens as motogens. *J Neurooncol* 35:249–257.
- Corcoran A, Del Maestro RF. 2003. Testing the “grow or go hypothesis” in human medulloblastoma cell lines in two and three dimensions. *Neurosurgery* 53:174–185.
- Corcoran A, de Ridder LIF, Del Duca D, Kalala OJP, Lah T, Pilkington GJ, Del Maestro RF. 2003. Evolution of the brain tumor spheroid model: transcending current model limitations. *Acta Neurochir*, to appear.
- De Angelis LM, Gutin PH, Leibel SA, Posner JB. 2002. Intracranial tumors: diagnosis and treatment. *Scarborough: Taylor & Francis Group*. p 165–166.
- Del Maestro R, Shivers R, McDonald W, Del Maestro A. 2001. Dynamics of C6 astrocytoma invasion into three-dimensional collagen gels. *J Neurooncol* 53:87–98.
- Del Maestro RF, Tamaki M, McDonald W, Amberger V. 1997. The C6 astrocytoma spheroid invasion model: evidence for the presence of a glial-repellent factor(s). *Can J Neurol Sci* 24:S18.
- Dickson BJ. 2002. Molecular mechanisms of axon guidance. *Science* 298:1959–1964.
- Ebens A, Brose K, Leonardo ED, Hanson MG, Bladt F, Birchmeier C, Barres BA, Tessier-Lavigne M. 1996. Hepatocyte growth factor/scatter factor is an axonal chemoattractant and a neurotrophic factor for spinal motor neurons. *Neuron* 17:1157–1172.
- Engebraaten O, Bjerkvig R, Lund-Johansen M, Wester K, Pedersen PH, Mork S, Backlund EO, Laerum OD. 1990. Interaction between human brain tumor biopsies and fetal brain tissue in vitro. *Acta Neuropathol (Berl)* 81:130–140.
- Engebraaten O, Bjerkvig R, Pedersen P, Laerum OD. 1993. Effects of EGF, bFGF, NGF and PDGF(bb) on cell proliferative, migratory and invasive capacities of human brain-tumor biopsies in vitro. *Int J Cancer* 53:209–214.
- Goldberg WJ, Levine KV, Laws ER, Bernstein JJ. 1992. Mechanisms of C6 glioma cell and fetal astrocyte migration into hydrated collagen I gels. *Brain Res* 581:81–90.
- Goldbrunner RH, Bouterfa H, Vince GH, Bernstein JJ, Roosen K, Tonn JC. 1997. Transfection and dye premarking of human and rat glioma cell lines affects adhesion, migration and proliferation. *Anticancer Res* 17:4467–4471.
- Jarjour AA, Manitt C, Moore SW, Thompson KM, Yuh S, Kennedy TE. 2003. Netrin-1 is a chemorepellent for oligodendrocyte precursor cells in the embryonic spinal cord. *J Neurosci* 23:3735–3744.
- Kennedy TE, Serafini T, de la Torre JR, Tessier-Lavigne M. 1994. Netrins are diffusible chemotropic factors for commissural axons in the embryonic spinal cord. *Cell* 78:425–435.
- Kidd T, Bland KS, Goodman CS. 1999. Slit is the midline repellent for the Robo receptor for *Drosophila*. *Cell* 96:785–794.
- Ladiwala U, Lachance C, Simoneau SJJ, Bhakar A, Barker PA, Antel JP. 1998. P75 neurotrophin receptor expression on adult human oligodendrocytes: signaling without cell death in response to NGF. *J Neurosci* 18:1297–1304.
- Li HS, Chen JH, Wu W, Fagaly T, Zhou LF, Yuan WL, Dupuis S, Jiang ZH, Nash W, Gick C, et al. 1999. Vertebrate Slit, a secreted ligand for the transmembrane protein Roundabout, is a repellent for olfactory bulb axons. *Cell* 96:807–818.
- Liotta LA, Mandler R, Murano G, Katz DA, Gordon RK, Chiang PK, Schiffmann E. 1986. Tumor cell autocrine motility factor. *Proc Natl Acad Sci USA* 83:3302–3306.
- Lopez MBS, VandenBerg SR, Scheithauer BW. 1995. Histopathology, immunohistochemistry and ultrastructure of brain tumors. In: Kaye AH, Laws ER, editors. *Brain*

- Tumors: An encyclopedic approach. Edinburgh UK: Churchill Livingstone, p 125–162.
- Lumsden AGS, Davies AM. 1983. Earliest sensory nerve fibres are guided to peripheral targets by attractants other than nerve growth factor. *Nature* 306:786–788.
- Lumsden AGS, Davies AM. 1986. Chemotropic effect of specific target epithelium in the developing mammalian nervous system *Nature* 323:538–539.
- Lund-Johansen M, Bjerkvig R, Humphrey PA, Bigner SH, Bigner DD, Laerum O. 1990. Effect of epidermal growth factor on glioma cell growth, migration and invasion in vitro. *Cancer Res* 50:6039–6044.
- Nygaard SJ, Pedersen PH, Mikkelsen T, Terzis AJ, Tysnes OB, Bjerkvig R. 1995. Glioma cell invasion visualized by scanning confocal laser microscopy in an in vitro co-culture system. *Invasion Metastasis* 15:179–188.
- Placzek M, Tessier-Lavigne M, Jessel T, Dodd J. 1990. Orientation of commissural axons in vitro in response to a floor plate-derived chemoattractant *Development* 110:19–30.
- Steinsvag SK. 1985. Interaction between glioma cells and normal brain tissue in organ culture studied by scanning electron microscopy. *Invasion Metastasis* 5:255–269.
- Sugimoto Y, Taniguchi M, Yagi T, Akagi Y, Nojyo Y, Tamamaki N. 2001. Guidance of glial precursor cell migration by secreted cues in developing optic nerve. *Development* 128:3321–3330.
- Sutherland RM, McCredie JA, Inch WR. 1971. Growth of multicell spheroids in tissue culture as a model of nodular carcinomas. *J Natl Cancer Inst* 46:113–120.
- Tamaki M, McDonald W, Amberger V, Moore E, Del Maestro RF. 1997. Implantation of C6 astrocytoma spheroid into collagen type I gels: invasive, proliferative, and enzymatic characterizations. *J Neurosurg* 87:602–609.
- Tessier-Lavigne M, Goodman CS. 1996. The molecular biology of axon guidance. *Science* 274:1123–1133.
- Uhm JH, Dooley NP, Villemure JG, Yong VW. 1996. Glioma invasion in vitro: regulation by matrix metallo-protease-2 and protein kinase C. *Clin Exp Metast* 14:421–433.
- Unemori EN, Werb Z. 1986. Reorganization of polymerized actin: a possible trigger for induction of procollagenase in fibroblasts cultured in and on collagen gels. *J Cell Biol* 103:1021–1031.
- Vince GH, Bouterfa H, Goldbrunner R, Roosen K, Tonn JC. 1997. Fast blue, a fluorescent tracer in glioma cell culture, affects proliferation and motility. *Neurosci Lett* 233:148–150.
- Von Bulow C, Hayen W, Hartmann A, Mueller-Klieser W, Allolio B, Nehls V. 2001. Endothelial capillaries chemotactically attract tumor cells. *J Pathol* 193:367–376.
- Wang B, Xiao Y, Ding B, Zhang N, Yuan X, Gui L, Qian K, Duan S, Xhen Z, Rao Y, et al. 2003. Induction of tumor angiogenesis by Slit-Robo signaling and inhibition of cancer growth by blocking Robo activity. *Cancer Cell* 4:19–29.
- Wang KH, Brose K, Arnott D, Kidd T, Goodman CS, Henzel W, Tessier-Lavigne M. 1999. Biochemical purification of a mammalian Slit protein as a positive regulator of sensory axon elongation and branch. *Cell* 96:771–784.
- Wu JY, Feng LL, Park HT, Havlioglu N, Wen L, Tang H, Bacon KB, Jiang ZH, Zhang XC, Rao Y. 2001. The neuronal repellent Slit inhibits leukocyte chemotaxis induced by chemotactic factors. *Nature* 410:948–952.
- Wu W, Wong K, Chen JH, Jiang ZH, Dupuis SM, Wu JY, Rao Y. 1999. Directional guidance of neuronal migration in the olfactory system by the protein Slit. *Nature* 400:331–336.
- Yee KT, Simon HH, Tessier-Lavigne M, O'Leary DDM. 1999. Extension of long leading processes and neuronal migration in the mammalian brain directed by the chemoattractant netrin-1. *Neuron* 24:607–622.

John Wiley & Sons, Inc.

Publishers Since 1807



WILEY

July 5, 2005

Tamara Werbowetski
BT 210 Brain Tumor Research Centre
Montreal Neurological Institute and Hospital
3801 University St.
Montreal QC H3A 2BA
VIA FACSIMILE: 514-398-3971

Dear Ms. Werbowetski:

RE: Your June 28, 2005 request for permission to republish pages 71-88 from *J Neurobiol*, (2004) Vol. 60 No 1, This material will appear in your forthcoming dissertation, to be published by Montreal Neurological Institute and Hospital in 2005.

1. Permission is granted for this use. No rights are granted to use content that appears in the Material or the Work with credit to another source.
2. Permitted use is limited to your edition described above, and does not include the right to grant others permission to photocopy or otherwise reproduce this material except for versions made for use by visually or physically handicapped persons. Up to five copies of the published thesis may be photocopied by a microfilm company.
3. Appropriate credit to our publication must appear on every copy of your thesis, either on the first page of the quoted text, in a separate acknowledgment page, or figure legend. The following components must be included: Title, author(s) and /or editor(s), journal title (if applicable), Copyright © 2004 Wiley-Liss, Inc., subsidiary of John Wiley & Sons, Inc. Reprinted with permission of John Wiley & Sons, Inc.
4. This license is non-transferable. This license is for non-exclusive English language print rights and microfilm storage rights by Montreal Neurological Institute and Hospital only, throughout the world. For translation rights, please reapply for a license when you have plans to translate your work into a specific language.

Sincerely,

Paulette Goldweber
Copyright & Permissions
Legal Department

Review Article

Soluble factors involved in glioma invasion

M. M. Mueller¹, T. Werbowetski², and R. F. Del Maestro²

¹ Division of Carcinogenesis and Differentiation, German Cancer Research Centre, Heidelberg, Germany

² Department of Neurology and Neurosurgery, Brain Tumour Research Centre, Montreal Neurological Institute and Hospital, Mc Gill University, Montreal, Quebec

Published online November 3, 2003

© Springer-Verlag 2003

Summary

Recent studies using molecular and cellular techniques of the factors regulating the invasion process have revealed a crucial role for a number of growth factors and cytokines. Their function lies on the one hand in the autocrine stimulation of the tumor cells themselves, resulting in the stimulation of protease expression and an enhancement of migratory potential. On the other hand, the growth factors and cytokines seem to play a major role in the paracrine activation of the tumor surrounding stroma. Through stimulation of the strong angiogenic response that is characteristic for gliomas and also of the expression of proteases in the stromal cells, they contribute critically to the generation of a stromal environment that is permissive or even inductive for tumor cell invasion. Understanding of the mechanisms by which soluble factors modulate glioma cell invasion therefore will help to determine targets for the modification of existing therapies and lead to the development of novel therapeutic strategies in the management of gliomas.

Keywords: Glioma; growth factor; invasion.

Introduction

Gliomas are the most common type of primary intracranial tumour in adults [74]. Characterized by a rapid growth rate, a high degree of neovascularization and an extremely invasive phenotype, these tumours culminate in extensive and diffuse infiltration into the contiguous brain. Consequently, gliomas prove largely resistant to established treatment modalities. Single tumour cells that invade the normal brain tissue as far as several centimetres from the macroscopic tumour border escape cytoreductive surgery and even involved-field radiotherapy with a safety margin no more than 2 cm around the

presurgical tumour volume. This usually results in tumour recurrence within a few months [75].

The mechanisms underlying migration and invasion of glioma tumour cells are complex and involve a number of sequential steps that require the adhesion of tumour cells to resident cells or matrix components, remodelling and degradation of this matrix and successful invasion of the infiltrating cells into the modified region.

During invasion, homotypic cell adhesion to other tumour cells is reduced while heterotypic adhesion to other cells or the extracellular matrix increases concomitantly. This is accompanied by an altered expression of specific cell adhesion molecules such as integrins, cadherins, or CD44. Remodelling and degradation of the extracellular matrix encompasses both secretion of altered matrix components and proteolytic modification of the existing matrix by proteases whose expression and activity is regulated by a number of interactive factors [23]. Finally, the migration and thus completed invasion of the tumour cells into the modified region is stimulated by a vast variety of soluble factors that are secreted either by the tumour cells themselves or by the surrounding stroma. These factors act in an autocrine or paracrine fashion, inducing cell migration and proteolytic activity.

In this review we will focus on growth factors, on their influence on glioma invasion and will discuss new concepts, including diffusible molecules that act as chemotropic repellent factors in gliomas.

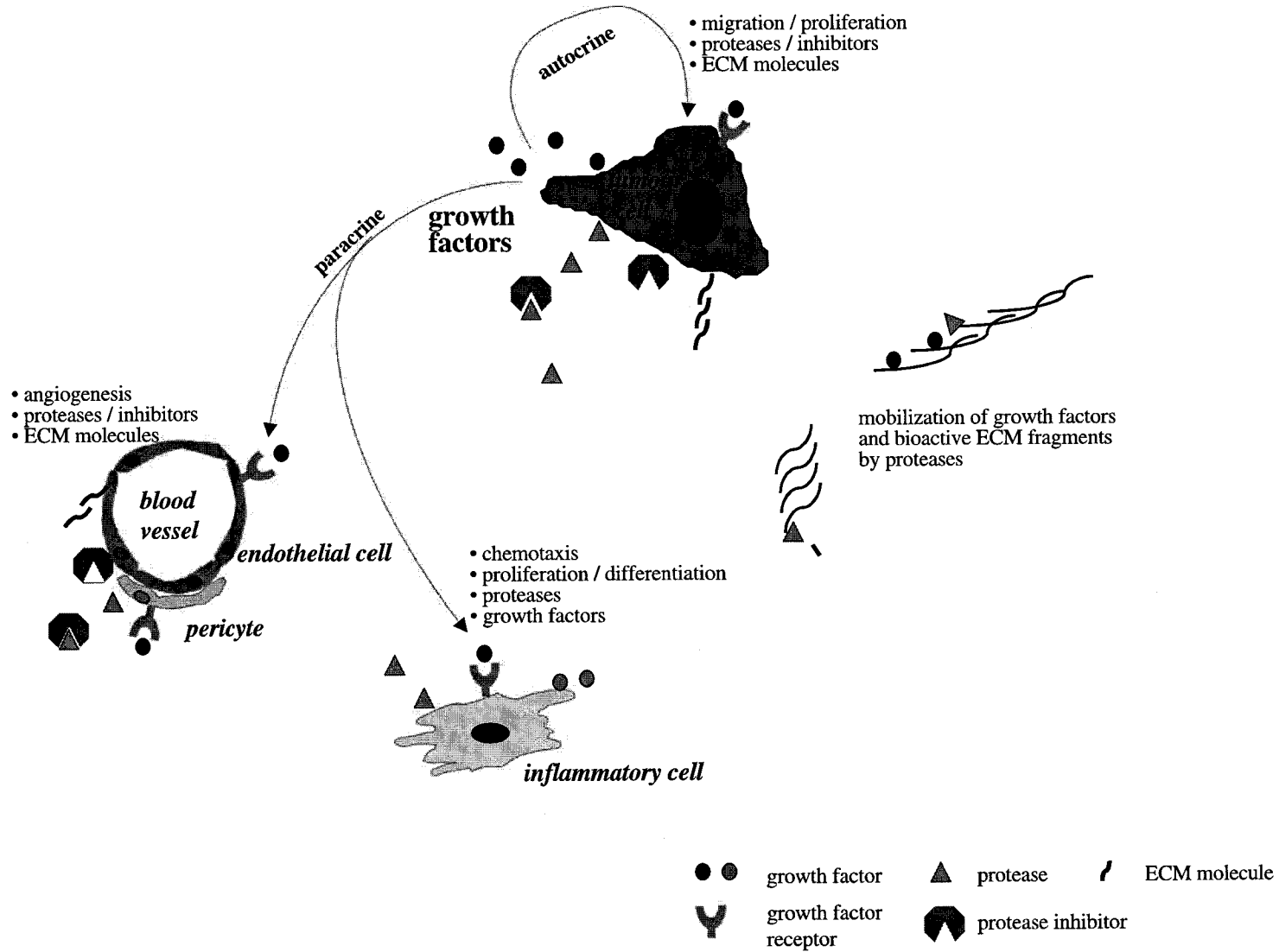


Fig. 1. Growth factors produced by the tumor cells act in an autocrine manner by stimulating tumour cell migration/invasion and proliferation. Concomitantly they induce the secretion of specific ECM molecules and the expression of proteases and reduce the expression of protease inhibitors, resulting in the mobilisation of matrix bound cytokines and the generation of bioactive ECM fragments. This allows the tumour cells to modulate their direct environment in favour of invasion. At the same time the tumour derived growth factors act in a paracrine loop on the tumour microenvironment stimulating angiogenesis by inducing endothelial cell and pericyte proliferation and migration as well as the secretion specific ECM molecules and of proteases and the reduced synthesis of protease inhibitors by these cells. Additionally, they induce chemotaxis, proliferation and differentiation of inflammatory cells and again modulate the ECM generating an invasion permissive environment by stimulating the secretion of additional paracrine acting growth factors and proteases

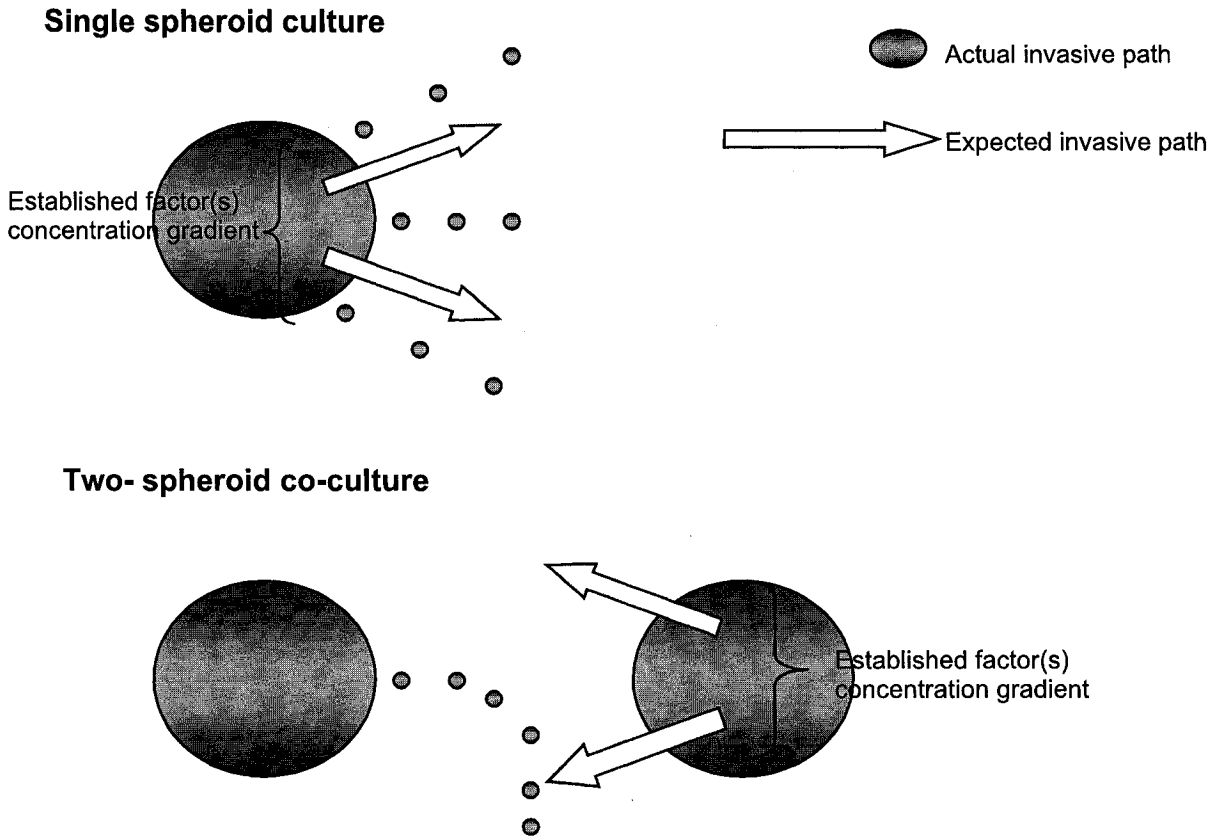


Fig. 2. The repellent factor hypothesis. Glioma cells from single spheroids implanted into a three-dimensional type I collagen gel invade the gel in a radial manner, leaving the spheroid at an angle nearly perpendicular to the spheroid surface where the cell detaches. When two spheroids are co-cultured adjacent to each other in the collagen gel, glioma cells from one spheroid will change their expected trajectory in response to an established concentration gradient of the repellent factor(s) from the adjacent spheroid. This can be demonstrated by time-lapse videomicroscopy

Growth factors in glioma invasion

The mechanisms underlying the growth factor-mediated stimulation of glioma invasion are not well understood. Generally, growth factors exert their function by binding to their cognate receptors, which can either be expressed by the tumor cells themselves or by neighbouring cells, resulting respectively in either an autocrine or a paracrine effect. In addition, membrane-anchored growth factor isoforms that are generated by alternative splicing may bind to the respective receptors on the same (juxtacrine) or neighbouring cells. Intracellular activation of growth factor receptor systems also can lead to an intracrine activation of the signaling cascades. A number of growth factors/receptor systems have been described to play a role in glioma invasion. Their activation may result in changes in tumour cell adhesion [66, 68], secretion of ECM components [60, 64] or lead to a stimulation of protease expression [73] and chemotactic effects on tumour and stromal cells [25].

VEGF

Vascular endothelial growth factor (VEGF) is considered to be the most potent factor in the stimulation of angiogenesis in gliomas [51, 67]. Its angiogenic activity is mediated by binding to 2 high affinity protein tyrosine kinase receptors VEGFR-1 (fms-like tyrosine kinase, Flt-1) and VEGFR-2 (fetal liver kinase-1/kinase insert domain-containing receptor, Flk-1) on human endothelial cells. As a consequence of the critical role of angiogenesis in tumour growth and progression, the VEGF/VEGFR-2 system has recently become one of the most prominent targets for alternative tumour therapies. Studies inhibiting either VEGF by monoclonal antibodies or antisense strategies [5, 65, 76] or the VEGFR-2 function e.g. via selective inhibition of its catalytic protein kinase activity, have shown inhibition of angiogenesis and glioma growth *in vivo* [87]. Interestingly, such inhibition of glioma angiogenesis resulted in a clearly reduced invasion of tumour cells into the surrounding brain tissue and reduced expression

of the pro-invasive molecule SPARC [88]. Angiogenesis and invasion seem to share common pathways of adhesion, proteolysis and cellular migration [7, 39], supporting the concept of a strong interdependency of both processes. The mechanistic interrelationship of the two processes has been clarified in studies that show a reciprocal regulatory network between VEGF and proteases/protease inhibitors. VEGF expression is upregulated by thrombin [96] or through the overexpression of MT-1MMP, resulting in enhanced tumor growth *in vivo* [16]. Furthermore, VEGF was shown to upregulate the expression of MMP-2 and MMP-9 [73] and to downregulate Timp-1 and Timp-2 [45]. Although the inhibition of tumour cell invasion by blocking VEGF seems to be mediated by the disruption of a paracrine pathway between tumour cells and stromal cells, recent studies have described an additional autocrine function for VEGF on the tumour cells themselves. As a result of binding to the VEGFR-1 that was shown to be expressed on glioma cells, VEGF inhibited tumour cell proliferation and migration [29], consequently also influencing tumour cell invasion. This autocrine loop is interpreted as a "rescue mechanism" for the tumour cells. Deficiencies in oxygen and nutrient supply result in an upregulation of VEGF. On the one hand this induces an angiogenic response in the stromal cells, on the other hand, tumour cell proliferation and migration are inhibited. The growth of new blood vessels then provides the necessary oxygen and nutrients leading to a downregulation of the expression of VEGF and a release of the tumour cells from the autocrine inhibition. Because the secretion of VEGF by glioma cells increases after X-ray radiation, the autocrine inhibition of cell proliferation through VEGFR-1 may result in a decreased radiosensitivity of the glioma tumour cells and thus provide a possible mechanistic explanation for the escape of tumour cells from radiation treatment in glioblastoma therapy [82].

SF/HGF

Scatter factor/hepatocyte growth factor exerts pleiotropic influences on cancer cells including the stimulation of tumour cell migration and angiogenesis [25]. SF/HGF and its receptor, encoded by the c-MET proto-oncogene, are both expressed in glioma cells *in vivo* and seem to be upregulated during transition from low (WHO grade II) to high grade (WHO grade III and IV) gliomas [56]. In *in vitro* studies, SF/HGF stimulated

glioma cell migration and invasion and to a lesser extent, tumour cell proliferation [46, 92]. Transfection of SF/HGF cDNA, into glioma cells expressing the MET receptor resulted in larger, more vascularized tumours. Antisense ribozyme targeting in glioma cells expressing both SF/HGF and the MET receptor, lead to a significant decrease in tumorigenicity and tumour growth *in vivo* [4]. This tumour-promoting effect of SF/HGF may result from a stimulation of angiogenesis through SF/HGF action on endothelial cell motility *in vitro* [47] and tube formation in a three dimensional *in vitro* angiogenesis assay [78]. In addition, SF/HGF was shown to upregulate expression and activity of MMP-2 through an enhanced expression of MT-1MMP [24, 31] and also upregulates the activity of plasmin, through the activation of urokinase-type plasminogen activator and uPA receptor [55]. These observations again underline the important interplay between angiogenesis and invasion.

EGF/TGF α /heregulin/EGFR

Amplification and overexpression of the EGF receptor (EGFR), the product of the cellular homologue of the v-erbB oncogene, is one of the most extensively studied genetic events in glioma tumorigenesis. It is found in about 40% of tumours and characterizes so called de novo glioblastomas in contrast to the progressive type of glioblastoma developing from low grade astrocytomas [38]. EGFR has a number of cognate ligands including EGF itself [12], TGF α [84], heparin-binding EGF-like growth factor (HB-EGF) [30], batimastat [79], amphiregulin [80], and epiregulin [85]. Upon binding of its ligand, EGFR dimerizes with another EGFR molecule or another homologue of the erbB tyrosine kinase receptor family [28, 43, 48, 59, 72] and activates different second messenger systems, thereby exerting a number of different effects on tumor cells. The EGFR system, activated by different ligands, may influence glioma invasion by upregulation of proteases. EGF itself was shown to enhance invasiveness in tumour spheroids prepared from glioma biopsy specimen [20] and to induce MMP-2 and MMP-9 expression in short term cultures of glioma surgical samples [73]. In U373 astrocytoma cells EGF upregulates t-PA and uPA followed by considerably slower increases in PAI-1, suggesting that EGF-signalling drastically changes the balance between proteolytic and anti-proteolytic components of the plasminogen cascade [34]. An upregulation of uPA and its receptor in a

glioma cell line was also observed in response to the EGFR ligand TGF α [54], thus confirming a functional role for TGF α in glioma invasion.

Heregulin and its cognate receptors, the EGFR homologues cerbB2/HER2, cerbB3/HER3 and cerbB4/HER4, are also expressed in human gliomas. Although the biological significance of this factor receptor coexpression for glioma growth and invasion remains to be determined [93], heregulin can induce the expression of MMP-9 in breast cancer cell lines [97], this again suggests that this ligand receptor system contributes to tumour invasion. Similarly other EGFR ligands like BTC, HB-EGF, amphiregulin and epiregulin were shown to upregulate MMPs and components of the plasminogen cascade in a number of different tumour systems [40, 62]. Nevertheless, as with heregulin, their role in gliomas still remains to be elucidated.

A number of altered forms of the EGFR – the result of gene mutations, alternative splicing or translational alterations- have been detected in human glioma tissue and cell lines. The most common mutant EGFR is the EGFRvIII, which results from an in frame deletion of exons 2–7 in the EGF receptor gene [13]. EGFRvIII is constitutively activated in a ligand-independent manner and may not require dimerization with another erbB receptor for signalling [11]. Because it is less efficiently translocated to the cell surface than wild-Type EGFR, EGFRvIII may show an altered subcellular location [19] resulting in the activation of different second messenger systems (as was shown for glioma cells) [35]. This may result in a different spectrum of biological activities compared to the wild type receptor. EGFRvIII was shown to enhance glioma cell proliferation and to reduce apoptosis *in vitro*; however, to date it is not clear whether this constitutively active mutant EGFR also contributes to glioma invasion.

NGF

NGF, like brain derived neurotrophic factor (BDNF) and neurotrophin, is a member of the family of neurotrophic factors. These factors are widely expressed in human glioma cell lines and glioma tissues [26]. They bind with different affinity to receptors of the trk family (trkA, -B and -C) that are expressed in primary glioma tissues [90]. In an autocrine manner, NGF in the presence of serum stimulates tumour cell proliferation in glioma cell lines [91]. In addition NGF may contribute to glioma invasion by stimulating MMP-9 expression in vascular smooth muscle cells [37].

bFGF

bFGF belongs to a family of heparin binding growth factors, consisting of 19 members, that bind to different high affinity receptors encoded by 4 genes (FGFR1–4) [8]. bFGF is able to exert its effect by binding to all 4 receptors, however, in glioma cells it is predominantly FGFR-1beta and FGFR-4 that are overexpressed. Ligand binding induces receptor dimerization which is required to initiate the tyrosine kinase activity of the receptor and subsequent trans-autophosphorylation activation [81]. It has been demonstrated that proteoglycans may increase the binding of FGF to their receptors [63]. bFGF contributes significantly to glioma angiogenesis by acting directly as a chemotactic factor on endothelial cells [14] inducing them to form capillary-like tubes in three dimensional collagen matrices [53]. It also acts indirectly by inducing the expression of VEGF, thereby stimulating glioma growth and invasion *in vivo* [1]. Furthermore, bFGF may exert a direct effect on glioma invasion by stimulating glioma cell migration [41] and by upregulating the expression of ECM degrading proteases like uPA and its receptor [54] as well as MMP-2 and MMP-9 [73]. An additional indirect effect of bFGF on glioma invasion may result from the induction of TGF β release by glioma cells [17], this then leads to an upregulation of MMP expression and/or an altered expression of ECM components and their cell surface integrin receptors.

TGF β

TGF β , characterized in three subtypes (TGF β 1–3), belongs to a superfamily of growth factors including activins, inhibins, bone morphogenic protein (BMP), Müllerian-inhibiting substance the Drosophila decapentaplegic (DPP) complex and veg-1. It differs from the previously mentioned growth factors in that it activates a serine/threonine-kinase receptor. TGF β protein is released from cells and stored in an inactive form associated with a dimer of its N-terminal propeptide, the latency-associated-protein, which is frequently additionally linked to latent TGF β binding proteins. Active TGF β is released from this complex by a variety of molecules like thrombospondin-1, α v β 6 integrin, and various proteases including plasmin, calpain and furin. TGF β has a wide spectrum of biological effects that differ considerably between cell and tissue types [69]. TGF β proteins as well as their functional receptors are expressed in glioblastoma and anaplastic astrocytoma but are barely detectable in low grade gliomas and

normal brain [95]. The functional significance of TGF β expression in gliomas has been extensively studied and its contribution to glioma invasion via a number of different mechanisms has been clearly established. In glioma cells TGF β promotes cell motility [49], an effect that may be mediated by an upregulation of the α 2 integrin subunit [52] or the α v β 3 integrin [68]. TGF β may further stimulate glioma cell invasion by changing the ECM composition through an increased synthesis and secretion of specific ECM molecules like collagens, fibronectin, tenascin, and laminin [60, 64]. Additionally TGF β influences the ECM remodelling during glioma invasion by stimulating the synthesis of proteases such as MMP-2 and -9 and suppressing the expression of tissue inhibitor of metalloproteinases (TIMP)-2 [73, 94].

G-CSF/GM-CSF

G-CSF and GM-CSF were originally identified as factors controlling proliferation, maturation, and functional activity of granulocytes, macrophages, and their precursors [50]. In addition to their role as growth and differentiation factors for the hematopoietic system, G-CSF and GM-CSF were reported to be expressed in a number of nonhematopoietic human tumor cells [58, 61]. This suggests a potential role for these factors in tumor growth and invasion [70, 86]. G-CSF, GM-CSF and their receptors are expressed at the mRNA and protein levels in glioma tissues and in derived cell cultures. The factors and their receptors are absent in normal brain. Expression of the receptor alone, i.e. without the respective factors, is found predominantly in low-grade gliomas. Co-expression of both G-CSF and GM-CSF together with their respective receptors is almost exclusively found in grade IV glioblastoma, thus correlating with an advanced tumour stage. The co-expression of factors and receptors indicates a shift from a paracrine to an autocrine mechanism during tumour progression. In agreement with this concept, G-CSF and GM-CSF stimulate glioma cell migration (and proliferation) in an autocrine fashion as shown by addition of exogenous growth factor and blocking of the endogenous glioma expressed growth factor via neutralising antibodies [57]. In addition to stimulation of glioma cell migration, G-CSF and GM-CSF may also contribute to glioma invasion through recruitment of inflammatory cells which are then induced to secrete MMPs [33, 98]. On the other hand, G-CSF and GM-CSF may also induce the secretion of MMPs in the tumour cells themselves [71].

Interleukins

Glioma cells secrete a number of different cytokines frequently together with their cognate receptors. Examples include interleukins IL-1, IL-6 and IL-8 [27, 77]. IL-1 may directly stimulate glioma cell proliferation and induce the secretion of other cytokines like IL-6 and IL-8 by an autocrine loop [89]. IL-1, IL-6 and IL-8 share the capacity to induce the expression and secretion of MMP-2, MMP-9 in normal and tumour cells [32, 42, 44]. In addition IL-1 induces the expression of tPA and uPA in U373-MG astrocytoma cells [34]. Thus, IL-1, IL-6 and IL-8 may contribute to invasion of glioma cells through the induction of matrix degrading proteinases.

IGF

Two insulin-like growth factors, IGF-1 and IGF-2, have been described. Together with their receptors (type 1 and type 2 IGF receptor), they play an important role in CNS development [2, 6]. Expression of IGF and its receptors in human gliomas is well established and autocrine receptor stimulation has been discussed [21]. Recent evidence suggests that in human gliomas IGFR can compensate for the loss of EGFR function e.g. in anti-EGFR therapy. As a consequence of IGF signalling mediated through Phosphoinositide 3-Kinase leads to enhanced invasion of primary glioblastoma cell lines [9].

Novel ideas/glioma repellent factor

Growth factors and cytokines are well established as almost "classical" players in the regulation of glioma invasion; recent studies have drawn attention to a different set of modulators of glioma invasion, one of which – the glioma repellent factor – will be discussed here.

In the mammalian nervous system, there are several examples of chemotropism by chemoattractant/chemorepellent factors where specific diffusible molecules guide developing axons or growth cones to peripheral targets [18, 22, 36]. Recent evidence suggests that glioblastoma spheroids secrete a chemotropic repellent factor by mechanisms that parallel those for neuronal guidance cues. Tamaki *et al.* [83] first raised this hypothesis with an analysis using the three-dimensional implantation model of C6 astrocytoma spheroid invasive paradigm. Spheroids of desired size were individually implanted into three-dimensional type I collagen gels, and invasive parameters were followed daily.

For large C6 spheroids (>700 μ m), the majority of invasive activity occurred between day 1 and day 5 with

maximum daily invasive rates occurring within the first 24 hours [83]. Compared to their smaller counterparts, invading cells derived from larger C6 spheroids reached further distances faster and eventually plateaued approximately 2000–2500 μm from the spheroid [83].

From these initial studies, two hypotheses have been proposed to explain the differences in cell invasion in this model. The first is a direct effect of physical stress on invading cells whereby cell density dictates motility from an area of high concentration to one of low concentration distant from the spheroid mass. The second hypothesis involves the influence of a proposed chemotropic repellent factor(s), released from spheroids in response to established hypoxic and necrotic central microregions, that deters invading cells from the spheroid source [83]. Larger spheroids, exhibiting extensive hypoxic and necrotic centres with decreased tissue pH, oxygen and metabolic substrate(s) concentration, may secrete more of the factor(s), and consequently further accelerate invasion. Once a sufficient distance from the stressed microenvironment is achieved and exposure to high concentrations of the proposed factor(s) has diminished, the infiltrating cells will decrease invasive rates, and eventually stop, as they are no longer able to exhibit a chemotropic response [83].

Further studies of the effects of resection of spheroid implants provide support for the repellent factor(s) hypothesis. Removal of a spheroid several days after implantation results in invasive cell rate decline. Re-implantation of a new spheroid allows remaining cells to reach normal invasive rates, thereby implicating the spheroid as the source of a secreted repellent factor(s) [15].

Current studies, using two-spheroid co-cultures and conditioned media derived from U251 (human glioblastoma) and C6 (rat astrocytoma) spheroids, add support for the existence of a tumour repellent factor(s). Compared with single spheroid controls, invading cells in two-spheroid co-cultures change their expected “radial” invasive pattern when they contact an endogenous repellent factor(s) gradient from the adjacent spheroid (unpublished data). These observations contrast those on spheroid-fetal rat brain aggregates co-cultured on agar, where invading glioma cells rapidly infiltrate and consume the rat brain [3]. It is hypothesized that the repellent factor is secreted in the form of a concentration gradient such that higher concentrations are located proximal to the spheroid. Application of this factor collected from glioma-conditioned media to an implanted spheroid in a collagen gel will then result in removal of

the endogenous gradient. In agreement with this hypothesis, invasion is inhibited, as the cells no longer exhibit a chemotropic response. Interestingly, the factor(s) is not species-specific, and its presence has been confirmed in both human and rat glioma cell lines. The effect is also not attributed to nutritional deficits and is not present in the conditioned media from confluent monolayer fetal astrocyte cultures (unpublished data). Previous studies have focused on growth and motility factors such as EGF, bFGF, and autocrine motility factors that act predominantly via chemoattractant mechanisms [10, 20] and none appear to exhibit the repellent factor(s) properties described here. The glioma cell-derived tumour repellent factor(s), thus represents a new concept and purification and identification of this glioblastoma secretion product may shed light on the mechanisms of glioma invasion in the central nervous system.

Conclusions

During the past few years, understanding of the genetics and biochemistry of glioma cell invasion has grown tremendously. This increasing knowledge of factors modulating glioma invasion invites the manipulation of ligands, receptors, and signalling or effector molecules, followed by the analysis of the consequences on glioma cell behaviour *in vitro* and glioma growth and invasion in *in vivo* animal models.

It is necessary to proceed with caution when extrapolating *in vitro* results to the clinical situation, and a thorough understanding of cytokines and soluble factors and of their influence on glioma invasion is essential for the development of more advanced therapeutic strategies. Targeting a combination of factors and their downstream effectors should lead ultimately to better therapeutic options for this rapidly lethal cancer.

References

1. Aguste P, Gürsel DB, Lemièrre S, Reimers D, Cuevas P, Carceller F, Di Santo JP, Bikfalvi A (2001) Inhibition of fibroblast growth factor/fibroblast growth factor receptor activity in glioma cells impedes tumor growth by both angiogenesis-dependent and -independent mechanisms. *Cancer Res* 61: 1717–1726
2. Baskin DG, Wilcox BJ, Figlewicz DP, Dorsa DM (1988) Insulin and insulin like growth factors in the CNS. *Trends Neurosci* 11: 107–111
3. Bjerkvig R, Laerum OD, Mella O (1986) Glioma cell interactions with fetal rat brain aggregates *in vitro* and with brain tissue *in vivo*. *Cancer Res* 46: 4071–4079
4. Bolteus AJ, Berens ME, Pilkington GJ (2001) Migration and invasion in brain neoplasms. *Curr Neurol Neurosci Reports* 1: 225–232

5. Borgstrom P, Hillan KJ, Sriramarao P, Ferrara N (1996) Complete inhibition of angiogenesis and growth of micro-tumours by anti-vascular endothelial growth factor neutralizing antibody: novel concepts of angiostatic therapy from intravital videomicroscopy. *Cancer Res* 56: 4032–4039
6. Braulke T (1999) Type-2 IGF receptor: a multi-ligand binding protein. *Horm Metab Res* 31: 242–246
7. Brooks PC, Stromblad S, Klemke R, Visscher D, Sarkar FH, Ceresch DA (1995) Antiintegrin $\alpha v \beta 3$ blocks human breast cancer growth and angiogenesis in human skin. *J Clin Invest* 96: 1815–1822
8. Burke D, Wilkes D, Blundell TL, Malcom S (1998) Fibroblast growth factor receptors: lessons from the genes. *Trends Biochem Sci* 23: 59–62
9. Chakravarti A, Loeffler JS, Dyson NJ (2002) Insulin-like growth factor receptor mediates resistance to anti-epidermal growth factor therapy in primary human glioblastoma cells through continued activation of phosphoinositide 3-kinase signalling. *Cancer Res* 62: 200–207
10. Chicoine MR, Madsen C, Silbergeld DL (1995) Modification of human glioma locomotion in vitro by cytokines EGF, bFGF, PDGFbb, NGF, and TNF α . *Neurosurgery* 36(6): 1165–1171
11. Chu CT, Everiss KD, Wikstrand CJ, Batra SK, Kung HJ, Bigner D (1997) Receptor dimerization is not a factor in the signalling activity of a transforming variant epidermal growth factor receptor (EGFRvIII). *Biochem J* 324: 855–861
12. Cohen S (1962) Isolation of a mouse submaxillary gland protein accelerating incisor eruption and eyelid opening in the newborn animal. *J Biol Chem* 237: 1555–1562
13. Collins VP (1995) Gene amplification in human gliomas. *Glia* 15: 289–296
14. Connolly DT, Stoddard BL, Harakas NK, Feder J (1987) Human fibroblast-derived growth factor is a mitogen and chemoattractant for endothelial cells. *Biochem Biophys Res Commun* 144: 705–712
15. Del Maestro RF, Tamaki M, McDonald W, Amberger VR (1997) The C6 astrocytoma spheroid invasion model: evidence for the presence of a glial-repellent factor(s). *Can J Neurol Sci [Suppl]* 24: S18 (abstract)
16. Deryugina EI, Soroceanu L, Strongin AY (2002) Up-regulation of vascular endothelial growth factor by membrane-type-1 matrix metalloproteinase stimulates human glioma xenograft growth and angiogenesis. *Cancer Res* 62: 580–588
17. Dhandapani KM, Wade MF, Mahesh VB, Brann DW (2002) Basic fibroblast growth factor induces TGF- β release in an isoform and glioma-specific manner. *Neuroreport* 13: 239–241
18. Dodd J, Jessell TM (1988) Axon guidance and the patterning of neural projections in vertebrates. *Science* 242: 692–699
19. Ekstrand AJ, Liu L, He J, Hamid ML, Longo N, Collins VP, James CD (1995) Altered subcellular location of an activated and tumour-associated epidermal growth factor receptor. *Oncogene* 10: 1455–1460
20. Engebraaten O, Bjerkvig R, Pedersen PH, Laerum OD (1993) Effects of EGF, bFGF, NGF and PDGF(bb) on cell proliferative, migratory and invasive capacities of human brain tumour biopsies in vitro. *Int J Cancer* 53: 209–214
21. Glick RP, Lichtor T, Unterman TG (1997) Insulin-like growth factors in central nervous system tumors. *J Neuro-Oncol* 35: 315–325
22. Goodman C, Shatz C (1993) Developmental mechanisms that generate precise patterns of neuronal connectivity. *Cell* 72/Neuron [Suppl] 10: 65–75
23. Goldbrunner RH, Berstein JJ, Tonn J-C (1999) Cell-extracellular matrix interaction in glioma invasion. *Acta Neurochir (Wien)* 141: 295–305
24. Hamasuna R, Kataoka H, Moriyama T, Itoh H, Seiki M, Koono M (1999) Regulation of matrix metalloproteinase-2 (MMP-2) by hepatocyte growth factor/scatter factor (HGF/SF) in human glioma cells: HGF/SF enhances MMP-2 expression and activation accompanying up-regulation of membrane type-1 MMP. *Int J Cancer* 82: 274–281
25. Hamel W, Westphal M (2000) Growth factors in gliomas revisited. *Acta Neurochir* 142: 113–138
26. Hamel W, Westphal M, Szonyi E, Escandon E, Nikolics K (1993) Neurotrophin gene expression by cell lines derived from human gliomas. *J Neurosci Res* 34: 147–157
27. Hao C, Parney IF, Roa WH, Turner J, Petruk KC, Ramsay DA (2002) Cytokine and cytokine receptor mRNA expression in human glioblastomas: evidence of Th1, Th2 and Th3 cytokine dysregulation. *Acta Neuropathol* 103: 171–178
28. Heldin CH (1995) Dimerization of cell surface receptors in signal transduction. *Cell* 80: 213–223
29. Herold-Mende C, Steiner H-H, Andl T, Riede D, Buttler A, Reisser C, Fusenig NE, Mueller MM (1999) Expression and functional role of VEGF receptors in human tumor cells. *Lab Invest* 79: 1573–1582
30. Higashiyama S, Abraham JA, Miller JL, Fiddes JC, Klagsbrun M (1991) A heparin-binding growth factor secreted by macrophage-like cell that is related to EGF. *Science* 251: 936–939
31. Hirohito Y, Hara A, Murase S, Hayashi K, Ando H, Shinoda J, Shimokawa K, Noboru S (2001) Expression of hepatocyte growth factor and matrix metalloproteinase-2 in human glioma. *Brain Tumor Pathol* 18: 7–12
32. Inoue K, Slaton JW, Eve BY, Kim SJ, Perrotte P, Balbay MD, Yano S, Bar-Eli M, Radinsky R, Pettaway CA, Dinney CP (2000) Interleukin 8 expression regulates tumorigenicity and metastases in androgen-independent prostate cancer. *Clin Cancer Res* 6: 2104–2119
33. Janowska-Wieczorek A, Marquez LA, Nabholz J-M, Cabuhat ML, Montaño J, Chang H, Rozmus J, Russell JA, Edwards DR, Turner AR (1999) Growth factors and cytokines upregulate gelatinase expression in bone marrow CD34+ cells and their transmigration through reconstituted basement membrane. *Blood* 93: 3379–3390
34. Kasza A, Kowanetz M, Poslednik K, Witek B, Kordula T, Koj A (2001) Epidermal growth factor and pro-inflammatory cytokines regulate the expression of components of the plasminogen activation system in U373-MG astrocytoma cells. *Cytokine* 16: 187–190
35. Kaufmann K, Thiel G (2001) Epidermal growth factor and platelet-derived growth factor induce expression of Egr-1, a zinc finger transcription factor, in human malignant glioma cells. *J Neurol Sci* 189: 83–91
36. Kennedy TE, Serafini T, de la Torre JR, Tessier-Lavigne M (1994) Netrins are diffusible chemotropic factors for commissural axons in the embryonic spinal cord. *Cell* 78(3): 425–435
37. Khan KM, Falcone DJ, Kraemer R (2002) Nerve growth factor activation of Erk-1 and Erk-2 induces matrix metalloproteinase-9 expression in vascular smooth muscle cells. *J Biol Chem* 277: 2353–2359
38. Kleihues P, Ohgaki H (1997) Genetics of glioma progression and the definition of primary and secondary glioblastomas. *Brain Pathol* 7: 1131–1136
39. Kohn EC, Liotta LA (1995) Molecular insights into cancer invasion: Strategies for prevention and intervention. *Cancer Res* 55: 1856–1862
40. Kondapaka SB, Fridman R, Reddy KB (1997) Epidermal growth factor and amphiregulin up-regulated matrix metalloproteinase-9 (MMP-9) in human breast cancer cells. *Int J Cancer* 70: 722–726
41. Koocheckpour S, Merzak A, Pilkington GJ (1995) Extracellular matrix proteins inhibit proliferation, upregulate migration and induce morphological changes in human glioma cell lines. *Eur J Cancer* 31: 375–380

42. Kossakowska AE, Edwards DR, Prusinkiewicz C, Zhang MC, Guo D, Urbanski SJ, Grogan T, Marquez LA, Janowska-Wieczorek A (1999) Interleukin-6 regulation of matrix metalloproteinase (MMP-2 and MMP-9) and tissue inhibitor of metalloproteinase (TIMP-1) expression in malignant non-Hodgkin's lymphomas. *Blood* 94: 2080–2089
43. Kraus MH, Issing W, Miki T, Popescu NC, Aaronson SA (1989) Isolation and characterization of ERBB3, a third member of the ERBB/epidermal growth factor receptor family: evidence for overexpression in a subset of human mammary tumors. *Proc Natl Acad Sci USA* 86: 9193–9197
44. Kubota Y, Oka S, Nakagawa S, Shirasuna K (2002) Interleukin-1 α enhances type I collagen-induced activation of matrix metalloproteinase-2 in odontogenic keratocyst fibroblasts. *J Dent Res* 81: 23–27
45. Lamoreaux WJ, Fitzgerald MEC, Reiner A, Hasty KA, Charles ST (1998) Vascular endothelial growth factor increases release of gelatinase A and decreases release of tissue inhibitors of metalloproteinases by microvascular endothelial cells *in vitro*. *Microvascular Res* 55: 29–42
46. Lamszus K, Laterra J, Westphal M, Rosen EM (1999) Scatter factor/hepatocyte growth factor (SF/HGF) content and function in human gliomas. *Int J Dev Neurosci* 17: 517–530
47. Lamszus K, Schmidt NO, Jin L, Laterra J, Zagzag D, Way D, Witte M, Weinand M, Goldberg ID, Westphal M, Rosen EM (1998) Scatter factor promotes motility of human glioma and neuromicrovascular endothelial cells. *Int J Cancer* 75: 19–28
48. Lemmon MA, Schlessinger J (1994) Regulation of signal transduction and signal diversity by receptor oligomerization. *Trends Biochem Sci* 19: 459–463
49. Merzak A, McCrear S, Koocheckpour S, Pilkington GJ (1994) Control of human glioma cell growth, migration and invasion *in vitro* by transforming growth factor beta 1. *Br J Cancer* 70: 199–203
50. Metcalf D (1985) The granulocyte-macrophage colony-stimulating factors. *Science* 229: 16–22
51. Millauer B, Shawver LK, Plate KH, Risau W, Ullrich A (1994) Glioblastoma growth inhibited *in vivo* by a dominant-negative Flk-1 mutant. *Nature* 367: 576–579
52. Miyake K, Kimura S, Nakanishi M, Hisada A, Hasegawa M, Nagao S, Abe Y (2000) Transforming growth factor beta-1 stimulates contraction of human glioblastoma cell-mediated collagen lattice through enhanced alpha2 integrin expression. *J Neuropathol Exp Neurol* 59: 18–28
53. Montesano R, Vassalli JD, Baird A, Guillemin R, Orci L (1986) Basic fibroblast growth factor induces angiogenesis *in vitro*. *Proc Natl Acad Sci USA* 83: 7297–7301
54. Mori T, Tatsuya A, Wakabayashi Y, Hikawa T, Matsuo K-I, Yamada Y, Kuwano M, Hori S (2000) Up-regulation of urokinase-type plasminogen activator and its receptor correlates with enhanced invasion activity of human glioma cells mediated by transforming growth factor- α or basic fibroblast growth factor. *J Neuro-Oncol* 46: 115–123
55. Moriyama T, Kataoka H, Hamasuna R, Nakano S, Koono M, Wakisak S (1999b) Up-regulation of urokinase type plasminogen activator and u-PA receptor by hepatocyte growth factor/scatter factor stimulation in human glioma cells. *Clin Exp Metast* 17: 873–879
56. Moriyama T, Kataoka H, Koono M, Wakisaka S (1999) Expression of hepatocyte growth factor/scatter factor and its receptor c-Met in brain tumors: evidence for a role in progression of astrocytic tumors (review). *Int J Mol Med* 3: 531–536
57. Mueller MM, Herold-Mende CC, Riede D, Lange M, Steiner H-H, Fusenig NE (1999) Autocrine growth regulation by G-CSF and GM-CSF in human gliomas with tumor progression. *Am J Pathol* 155: 1557–1567
58. Mueller MM, Peter W, Mappes M, Huelsen A, Steinbauer H, Boukamp P, Vaccariello M, Garlick J, Fusenig NE (2001) *In vivo* microenvironment promotes tumor progression of skin carcinomas by clonal selection and mutagenesis. *Am J Pathol* 159: 1567–1579
59. Murali R, Brennan PJ, Kieber-Emmons T, Greene MI (1996) Structural analysis of p185c-neu an epidermal growth factor receptor tyrosine kinase: oligomerization of kinase domains. *Proc Natl Acad Sci USA* 93: 6252–6257
60. Neubauer K, Krüger M, Qondamatteo F, Knittel T, Siale B, Ramadori G (1999) Transforming growth factor- β 1 stimulates the synthesis of basement membrane protein laminin, collagen type IV and entactin in rat liver sinusoidal endothelial cells. *J Hepathol* 31: 692–702
61. Nitta T, Sato K, Allegretta M, Brocke S, Lim M, Mitchell DJ, Steinman L (1992) Expression of granulocyte colony stimulating factor and granulocyte-macrophage colony stimulating factor genes in human astrocytoma cell lines and in glioma specimens. *Brain Res* 571: 19–25
62. O-charoenrat P, Modjtahedi H, Rhys-Evans P, Court WJ, Box GM, Eccles SA (2000) Epidermal growth factor-like ligands differentially up-regulate matrix metalloproteinase 9 in head and neck squamous Carcinoma Cells. *Cancer Res* 60: 1121–1128
63. Ostrovsky O, Berman B, Gallagher J, Mulloy B, Fernig DG, Delchède M, Ron D (2002) Differential effects of heparin saccharides on the formation of specific fibroblast growth factor (FGF) and FGF receptor complexes. *J Biol Chem* 277: 2444–2453
64. Paulus W, Baur I, Huettner C, Schmauß B, Roggendorf W, Schlingensiepen H, Brysch W (1995) Effects of transforming growth factor-beta 1 on collagen synthesis, integrin expression, adhesion and invasion of glioma cells. *J Neuropathol Exp Neurol* 54: 236–244
65. Pham CD, Roberts TP, van Bruggen N, Melnyk O, Mann J, Ferrara N, Cohen RL, Brasch RC (1998) Magnetic resonance imaging detects suppression of tumour vascular permeability after administration of antibody to vascular endothelial growth factor. *Cancer Invest* 16: 225–230
66. Pilkington GJ, Dunan JR, Rogers JP, Clarke TM, Knott JCA (1993) Growth factor modulation of surface ganglioside expression in cloned neoplastic glia. *Neurosci Lett* 149: 1–5
67. Plate KH, Breier G, Millauer B, Ullrich A, Risau W (1993) Upregulation of vascular endothelial growth factor and its cognate receptor in a rat glioma model of angiogenesis. *Cancer Res* 53: 5822–5827
68. Platten M, Wick W, Wild-Bode C, Aulwurm S, Dichgans J, Weller M (2000) Transforming growth factor beta 1 (TGF- β 1) and TGF- β 2 promote glioma cell migration via upregulation of alphaV-beta3 integrin expression. *Biochem Biophys Res Commun* 268: 607–611
69. Platten M, Wick W, Weller M (2001) Malignant glioma biology: role for TGF β in growth, motility, angiogenesis and immune escape. *Microscopy Res Tech* 52: 401–410
70. Pei X-H, Nakanishi Y, Takayama K, Yatsunami J, Bai F, Kawasaki M, Wakamatsu K, Tsuruta N, Mizuno K, Hara N (1996) Granulocyte-colony stimulating factor promotes invasion by human lung cancer cell lines *in vitro*. *Clin Exp Metastasis* 14: 351–357
71. Pei X-H, Nakanishi Y, Takayama K, Bai F, Hara N (1999) Granulocyte, granulocyte-macrophage, and macrophage colony-stimulating factors can stimulate the invasive capacity of human lung cancer cells. *Br J Cancer* 79: 40–46
72. Plowman GD, Green JM, Culouscou JM, Carlton GW, Rothwell VM, Buckley S (1993) Heregulin induces tyrosine phosphorylation of HER4/p180erbB4. *Nature* 366: 473–475
73. Rooprai HK, Rucklidge GJ, Panou C, Pilkington GJ (2000) The effect of exogenous growth factors on matrix metalloproteinase secretion by human brain tumour cells. *Br J Cancer* 82: 52–55

74. Russel DS, Rubenstein LJ (1989) Pathology of tumours of the nervous system, 5th edn. Williams & Wilkins, Baltimore, pp 83–289
75. Roth W, Weller M (1999) Chemotherapy and immunotherapy of malignant glioma: molecular mechanisms and clinical perspectives. *Cell Mol Life Sci* 56: 481–506
76. Saleh M, Stacker SA, Wilks AF (1996) Inhibition of growth of C6 glioma cell in vivo by expression of antisense vascular endothelial growth factor sequence. *Cancer Res* 56: 393–401
77. Sasaki A, Ishiuchi S, Kanda T, Hasegawa M, Nakazato Y (2001) Analysis of interleukin-6 gene expression in primary human gliomas, glioblastoma xenografts, and glioblastoma cell lines. *Brain Tumor Pathol* 18: 13–21
78. Schmidt NO, Westphal M, Hagel C, Ergün S, Stavrou D, Rosen EM, Lamszus K (1999) Level of vascular endothelial growth factor, hepatocyte growth factor/scatter factor and basic fibroblast growth factor in human gliomas and their relation to angiogenesis. *Int J Cancer* 84: 10–18
79. Shing Y, Cristofori G, Hanahan D, Ono Y, Sasada R, Igarashi K, Folkman J (1993) Betacellulin: a mitogen from pancreatic β cell tumors. *Science* 259: 1604–1607
80. Shoyab M, McDonald VL, Bradley G, Todaro GT (1988) Amphiregulin: a bifunctional growth-modulating glycoprotein produced by the phorbol 12-myristate-treated human breast adenocarcinoma cell line MCF-7. *Proc Natl Acad Sci USA* 85: 6528–6532
81. Stefanik DF, Rizkalla LR, Soi A, Goldblatt SA, Rizkalla WM (1991) Acidic and basic fibroblast growth factor are present in glioblastoma multiforme. *Cancer Res* 52: 5760–5765
82. Steiner H-H, Karcher S, Mueller MM, Nalbantis E, Kunze S, Herold-Mende C (2003) Autocrine pathways of the Vascular Endothelial Growth Factor (VEGF) in glioblastoma multiforme: Clinical relevance of radiation-induced increase of VEGF levels. *J Neuro-Oncol* (in press)
83. Tamaki M, McDonald W, Amberger V, Moore E, Del Maestro RF (1997) Implantation of C6 astrocytoma spheroid into collagen type I gels: invasive, proliferative, and enzymatic characterizations. *J Neurosurg* 87: 602–609
84. Todaro GJ, De Larco JE, Cohen S (1976) Transformation by murine and feline sarcoma viruses specifically blocks binding of epidermal growth factor to cells. *Nature* 264: 26–31
85. Toyoda H, Komurasaki T, Ikeda Y, Yoshimoto M, Morimoto S (1995) Molecular cloning of mouse epi-regulin, a novel epidermal growth factor-related protein, expressed in the early stage of development. *FEBS Lett* 377: 403–407
86. Tsuzuki H, Fujieda S, Sunaga H, Noda I, Saito H (1998) Expression of granulocyte colony stimulating factor receptor correlates with prognosis in oral and mesopharyngeal carcinoma. *Cancer Res* 58: 794–800
87. Vajkoczy P, Menger MD, Vollmar B, Schilling L, Schmiedeck P, Hirth KP, Ullrich A (1999) Inhibition of tumor growth, angiogenesis, and microcirculation by the novel Flk-1 inhibitor SU5416 as assessed by intravital multi-fluorescence videomicroscopy. *Neoplasia* 1: 31–41
88. Vajkoczy P, Menger MD, Goldbrunner R, Ge S, Fong AT, Vollmar B, Schilling L, Ullrich A, Hirth KP, Tonn JC, Schmiedeck P, Rempel SA (2000) Targeting angiogenesis inhibits tumor infiltration and expression of the pro-invasive protein SPARC. *Int J Cancer* 87: 261–268
89. Van Meir E, Sawamura Y, Diserens AC, Hamou MF, de Tribolet N (1990) Human glioblastoma cells release interleukin 6 in vivo and in vitro. *Cancer Res* 50: 6683–6688
90. Wang Y, Hagel C, Hamel W, Muller S, Kluwe L, Westphal M (1998) Trk A, B, and C are commonly expressed in human oligodendrocytes and oligodendroglioma. *Acta Neuropathol* 96: 357–364
91. Weiss C, Wiesenhofer B, Humpel C (2002) Nerve growth factor plays a divergent role in mediating growth of C6 rat glioma cells via binding to the p75 neurotrophin receptor. *J Neuro-Oncol* 56: 59–67
92. Welch WC, Kornblith PL, Michalopoulos GK, Petersen BE, Beedle A, Gollin SM, Goldfarb RH (1999) Hepatocyte growth factor (HGF) and receptor (c-met) in normal and malignant astrocytic cells. *Anticancer Res* 19: 1635–1640
93. Westphal M, Meima L, Szonyi E, Lofgren J, Meissner H, Hamel W, Nikolics K, Sliwkowski MX (1997) Heregulins and the ErbB2/3/4 receptors in gliomas. *J Neuro-Oncol* 35: 335–346
94. Wick W, Platten M, Weller M (2001) Glioma cell invasion: regulation of metalloproteinase activity by TGF- β . *J Neuro-Oncol* 53: 177–185
95. Yamada N, Kato M, Yamashita H, Nister N, Miyazono K, Heldin CH, Funo K (1995) Enhanced expression of transforming growth factor-beta and its type-I and type-II receptors in human glioblastoma. *Int J Cancer* 62: 386–392
96. Yamahata H, Takeshima H, Kuratsu J-I, Sarker KP, Tanioka K, Waikimaru N, Nakata M, Kitajima I, Maruyama I (2002) The role of thrombin in the neo-vascularization of malignant gliomas: An intrinsic modulator for the up-regulation of vascular endothelial growth factor. *Int J Oncol* 20: 921–928
97. Yao J, Xiong S, Klos K, Nguyen N, Grijalva R, Li P, Yu D (2001) Multiple signalling pathways involved in activation of matrix metalloproteinase-9 (MMP-9) by heregulin-beta 1 in human breast cancer cells. *Oncogene* 20: 8066–8074
98. Zhang Y, McCluskey K, Fujii K, Wahl LM (1998) Differential regulation of monocyte matrix metalloproteinase and TIMP-1 production by TNF- α , granulocyte-macrophage CSF, and IL-1 β through prostaglandin-dependent and -independent mechanisms. *J Immunol* 161: 3071–3076

Correspondence: Margareta M. Mueller Ph.D., Division of Carcinogenesis and Differentiation, German Cancer Research Centre, Im Neuenheimer Feld 280, D-69120 Heidelberg, Germany. e-mail: ma.mueller@dkfz-heidelberg.de